

PLASMA ACTIVATED WATER FOR FRESH FOOD DISINFECTION

Presented by
Sellam Perinban



Department of Bioresource Engineering
McGill University
(Montréal, Canada)

April 2022

A thesis submitted to McGill University in
partial fulfillment of the requirements of the degree of Doctor of Philosophy

Copyright © 2022 by Sellam Perinban. All rights reserved.

ABSTRACT

Fresh-cut fruits and vegetables consumption has increased globally in recent decades due to healthier food preferences and convenience. On the other hand, the foodborne outbreaks associated with fresh produce have also shown a raising trend globally. The conventional disinfectants such as chlorine and organic acids are used to reduce bacterial populations on fresh-cut fruits and vegetables. However, besides their potential toxicity, they have proved incapable of completely removing or inactivating microorganisms on fresh produce due to their variability in response and surface properties. In recent time Plasma Activated Water (PAW) has been explored for its suitability for fresh food disinfection. Plasma activated water is produced by exposing water to nonthermal plasma and the subsequent transfer of reactive species from the gas phase plasma to the water. Though PAW has been reported to be an effective disinfectant against various food pathogenic microorganisms, information on its stability, process optimization and reactivity with food components is still largely unexplored.

This thesis presents the design and development of a continuous flow dielectric barrier discharge PAW generation system and the evaluation of the produced PAW and its reactive species on fresh-cut food quality and shelf life. From the literature review it was found that dielectric barrier discharge (DBD) is the simplest method of producing nonthermal plasma at atmospheric pressure and with minimum voltage requirements. Accordingly, a DBD system was constructed, and the PAW characteristics were evaluated in terms of hydrogen peroxide concentration, ozone concentration, pH, and *Escherichia coli* disinfection efficiency. Further, the PAW process conditions were optimized for gas flow rate, water flow rate and treatment time. The treatment time had a significant positive correlation with the hydrogen peroxide concentration, ozone concentration, pH and the oxygen reactive species (ORP) of the produced PAW. The operating conditions of 104.6 ml/min water flow rate, 20 min treatment time and 4 slm gas flow rate were found as optimal for the maximum production of hydrogen peroxide and ozone in PAW.

To assess the effect of PAW and its reactive species on food proteins, whey protein isolate was chosen as a model food system for proteins. Mild oxidation of whey protein isolate and an increase in its solubility was observed upon PAW treatment. Increase in the foaming properties was also observed after PAW treatment. However, there was no new functional groups formed in the protein samples by the reactive species in PAW.

The effectiveness of PAW as a disinfectant for fresh-cut produce washing was then evaluated using kale and spinach samples. For this study, the leaf samples were inoculated with *E. coli* cells and then washed with PAW activated for 10 to 60 minutes. The differences between kale and spinach samples in terms of their quality, and surface morphology upon PAW treatment was investigated. Efficient disinfection of up to 6 log cfu/g of *E. coli* cells on both kale and spinach was observed after PAW treatment. However, degradation of chlorophyll and antioxidant properties of the leaf samples were observed at higher PAW activation times. Further, kale and spinach behaved differently in terms of antioxidant activity and membrane electrolytic leakage values upon PAW treatment due to the inherent differences in the cuticular layer and surface morphological characteristics of kale and spinach leaves.

Finally, the ultimate application of PAW in enhancing the shelf life of fresh-cut produce was explored using fresh-cut apples. The PAW treated fresh-cut apple samples were stored under refrigerated condition for 12 days and the quality parameters and enzyme activity of the samples were assessed during storage. Significant reduction in the polyphenol oxidase activity of the samples was observed after PAW treatment. However, at higher PAW activation times, the reactive species in the PAW caused undesirable changes in the apple quality. The results suggest that PAW could maintain the quality of the fresh-cut apples during storage for plasma activation times of 20 min and 30 min for up to 9 days of storage.

RÉSUMÉ

La consommation de fruits et légumes frais a augmenté au niveau mondial au cours des dernières décennies en raison des préférences alimentaires et pour des raisons pratiques. D'autre part, les éclosions de maladies d'origine alimentaire associées aux produits frais ont également montré une tendance à la hausse à l'échelle mondiale. Les désinfectants conventionnels tels que le chlore et les acides organiques sont utilisés pour réduire les populations bactériennes sur les fruits et légumes frais coupés. Cependant, outre leur toxicité potentielle, ils se sont révélés incapables à éliminer ou inactiver complètement les microorganismes présents sur les produits frais en raison de la variabilité et la sensibilité de la matière organique. Nous avons étudié la possibilité d'utiliser l'eau activée par le plasma (PAW) pour désinfecter la surface d'aliments frais. L'eau activée par le plasma est produite par exposition de l'eau au plasma non thermique et par transfert d'espèces réactives du plasma en phase gazeuse vers l'eau. Bien que le PAW ait été signalé comme un désinfectant efficace contre divers microorganismes pathogènes pour les aliments, on peu d'information est disponible sur sa stabilité, l'optimisation des procédés et la réactivité avec les composants alimentaires.

Cette thèse présente la conception et le développement d'un système de production de PAW à débit continu à décharge de barrière diélectrique et l'évaluation des espèces réactives de cette eau PAW sur la qualité des aliments frais coupés et leur durée de conservation. D'après l'examen de la littérature, il a été constaté que la décharge de barrière diélectrique (DBD) est la méthode la plus simple pour produire un plasma non thermique à pression atmosphérique et avec des exigences minimales de tension. En conséquence, un système plasma préliminaire a été mis en place et les caractéristiques de l'eau plasmolysée ont été étudiées. D'après les études préliminaires, il a été observé que le système était fragile pour des temps de traitement plus élevés et que le débit n'était pas uniforme sur la plaque. Par conséquent, le réacteur a été modifié à l'aide d'un nouveau tube de verre et les caractéristiques de l'eau PAW ont été évaluées en fonction de la concentration de peroxyde d'hydrogène, de la concentration d'ozone, du pH et de l'efficacité de désinfection d'*Escherichia coli*. De plus, les conditions d'opération du procédé PAW ont été optimisées pour le débit de gaz, le débit d'eau et le temps de traitement. Le temps de traitement avait une corrélation positive significative avec la concentration de peroxyde d'hydrogène, la concentration d'ozone, le

pH et les composés réactifs à l'oxygène de l'eau PAW. La condition de fonctionnement optimale de 104,6 ml/min de débit d'eau, de 20 min de temps de traitement et de 4 slm de débit de gaz a été trouvée comme points optimaux pour la production maximale de peroxyde d'hydrogène et d'ozone dans l'eau PAW.

Afin d'évaluer l'effet des espèces réactives aux PAW sur les protéines alimentaires, l'isolat de protéines de lactosérum a été choisi comme système alimentaire modèle pour les protéines. Une légère oxydation de l'isolat de protéine de lactosérum et une augmentation de sa solubilité ont été observées lors du traitement par PAW. Une augmentation des propriétés de mousse a également été observée après le traitement par PAW. Cependant, il n'y a pas de nouveaux groupes fonctionnels formés dans les échantillons de protéines par les espèces réactives de l'eau PAW.

L'efficacité de l'eau PAW comme désinfectant pour le lavage des produits frais coupés a ensuite été évaluée à l'aide d'échantillons de chou frisé et d'épinards. Pour cette étude, les échantillons de légumes verts ont été inoculés avec des cellules d'*E. coli*, puis lavés avec de l'eau PAW activé pendant 10 min à 60 min. Les différences entre les échantillons de chou frisé et d'épinard en ce qui concerne la qualité du produit, les caractéristiques nutritionnelles et la morphologie de la surface lors du traitement par PAW ont également été étudiées en détail. On a observé une désinfection efficace jusqu'à 6 log cfu/g de cellules d'*E. coli* sur le chou frisé et les épinards après le traitement à l'eau PAW. Cependant, la dégradation des propriétés de la chlorophylle et des propriétés antioxydantes des échantillons a été observée à des temps d'activation des PAW plus élevés. De plus, le chou frisé et les épinards se sont comportés différemment en termes d'activité antioxydante et de valeurs de fuite électrolytique membranaire lors du traitement par eau PAW en raison des changements dans la couche cuticulaire et les caractéristiques morphologiques de surface des feuilles de chou frisé et d'épinard.

Enfin, l'application ultime de l'eau PAW dans l'amélioration de la durée de conservation d'un produit frais coupé a été explorée en utilisant des pommes fraîches tranchées. Les échantillons de pommes fraîches coupées traitées à l'eau PAW ont été entreposés au réfrigérateur pendant 12 jours et les paramètres de qualité et l'activité enzymatique des échantillons ont été évalués pendant l'entreposage. Une réduction significative de l'activité de la polyphénol oxydase des échantillons a été observée après le traitement à l'eau PAW. Cependant, à des temps d'activation plus élevés,

les espèces réactives dans l'eau PAW ont causé des changements indésirables dans la qualité des aliments. Les résultats suggèrent que l'eau PAW pourrait maintenir la qualité des pommes fraîchement coupées pendant leur entreposage pour des temps d'activation plasmatique de 20 min et 30 min jusqu'à 12 jours.

ACKNOWLEDGEMENTS

I would like to express my sincere thanks to my supervisor Professor Valérie Orsat for all the unwavering support, guidance, and encouragement throughout the course of my study. I am indebted to her for believing in me and giving me the freedom to pursue a new research field under her supervision. The trust she placed on me has allowed me to persevere through this five year long journey.

I am deeply grateful to Professor Vijaya Raghavan for his mentorship, encouragement, and support in completing this study. He has been the inspiration since my undergraduate studies to pursue my career in food engineering. I thank him for all the unconditional support and the professional development opportunities which greatly enriched my experience at McGill.

I gratefully acknowledge the generous financial support from Netaji Subhas international fellowship from Indian Council of Agricultural Research and Schulich graduate fellowship. I would also like to thank the Natural Sciences and Engineering Research Council of Canada (NSERC) and the Réseau précompétitif de cocréation RITA-CTAQ for supporting this research work.

I am indebted to Mr Yvan Gariepy for all his technical support and guidance for the successful completion of this project. I am thankful to him for patiently answering my relentless questions and always helping me during the ups and downs of this project work. I would like to thank Dr. Darwin Lyew for his valuable inputs and support in conducting the microbiological analysis. I always enjoyed working with him and cherish the conversations we had.

I would like to thank Dr Marie-Josée Dumont for providing me access to the HPLC and thermogravimetric analyzer. My sincere thanks to Dr Mark Lefsrud for giving access to his lab to carry out the microbiology work and to use the microplate reader. I would like to thank Prof. Sylvain Coulombe, Department of Chemical Engineering, McGill University for facilitating a visit to his lab at the initial stages of the research work.

I would like to thank all my research committee members for their valuable suggestions and feedback to improve the research project.

I am grateful to Professor R Visvanathan for his endless support and guidance in pursuing this doctoral study. My sincere thanks to Dr KV Prabhu, Dr Ramesh Kumar, Dr IM Misra, Dr Neelam Patel and Dr Mathala Juliet for all the support and encouragement.

I would like to thank all my lab and office mates for the stimulating discussions and making this journey memorable. I am thankful to all my friends both in India and Canada for bringing hope, cheer, and inspiration at difficult times.

Finally, this PhD journey would have not been possible without the unconditional support and encouragement from my family. Their love and blessings made this endeavor possible.

CONTRIBUTION OF AUTHORS

This thesis is submitted in the form of manuscripts, prepared according to the guidelines provided by the Faculty of Graduate and Postdoctoral Studies, McGill University. It is comprised of eight chapters. Chapter I provides an introduction and the thesis objectives which is followed by Chapter II, in which the literature review on the background of this thesis is presented. This includes the overview on methods of plasma activated water generation, plasma-liquid interaction chemistry, microbial inactivation mechanism by plasma reactive species and the available literature on nonthermal plasma and PAW applications in food. Chapter III presents the preliminary studies conducted in the design and development of the dielectric barrier discharge PAW generation system. Chapters IV to VII consist of manuscripts submitted or in preparation for submission in peer-reviewed scientific journals. Chapter IV gives the details on the dielectric barrier discharge and continuous flow PAW generation system developed in this study along with the PAW time stability analysis and optimization of the PAW process parameters. In Chapter V, the effects of PAW reactive species on whey protein isolate physicochemical and functional properties are presented. Chapters VI and VII provide information on applications of PAW for the disinfection and quality evaluation of kale, spinach and fresh-cut apples. Chapter VIII is a closing chapter, summarizing the overall conclusions, contributions to knowledge of this thesis and the recommendations for future work. The following manuscripts have been produced out of this thesis.

1. Perinban, S., Orsat, V., & Raghavan, V. (2019). Nonthermal Plasma–Liquid Interactions in Food Processing: A Review. *Comprehensive Reviews in Food Science and Food Safety*, 18(6), 1985-2008. doi:10.1111/1541-4337.12503 (Chapter II)
2. Perinban, S., Orsat, V., Garipey Y., Lyew D., & Raghavan, V. Evaluation of plasma activated water characteristics, antimicrobial property, time stability and process optimization (Chapter IV)
3. Perinban, S., Orsat, V., & Raghavan, V. Assessment of changes in whey protein isolate after plasma activated water treatment (Chapter V)
4. Perinban, S., Orsat, V., Lyew D., & Raghavan, V. Effect of plasma activated water on *Escherichia coli* disinfection and quality of kale and spinach (Chapter VI)

5. Perinban, S., Orsat, V., & Raghavan, V. Influence of plasma activated water on enzyme activity and storage quality of fresh-cut apples (Chapter VII)

The research work reported here, including review of literature, design of experiments, experimental work, data analysis and manuscript preparation was performed by Sellam Perinban under the supervision and guidance of Prof. Valérie Orsat (Supervisor) and Prof. Vijaya Raghavan (Co-supervisor). Prof. Valérie Orsat provided the scientific advice and guidance, supported in project planning, and was directly involved in reviewing and editing the manuscripts. Prof. Vijaya Raghavan provided scientific advice and was directly involved in editing and reviewing the manuscripts. Mr. Yvan Gariépy provided the technical support and expert guidance in the design and construction of the PAW system and assisted in the laboratory manipulations for performing the analytical studies. Dr. Darwin Lyew provided the technical support and guidance in conducting the microbiological experiments with *Escherichia coli*. All authors are from the Department of Bioresource Engineering, McGill University, Quebec. The research work was conducted at the technical services building lab, post-harvest technology lab and Prof. Valérie Orsat's lab. The thermogravimetric analysis was conducted in Dr. Dumont's lab and part of the microbiology work was conducted at Dr. Lefsrud's lab in the Department of Bioresource Engineering, McGill University.

TABLE OF CONTENTS

ABSTRACT.....	II
RÉSUMÉ	IV
ACKNOWLEDGEMENTS	VII
CONTRIBUTION OF AUTHORS.....	IX
TABLE OF CONTENTS.....	XI
List of tables.....	XVIII
List of figures	XIX
Nomenclature	XXI
CHAPTER I INTRODUCTION.....	1
1.1 Problem Statement and Research Hypothesis.....	3
1.2 General Objective	4
1.3 Specific Objectives	4
1.4 Organization of the Thesis	4
CHAPTER II NONTHERMAL PLASMA–LIQUID INTERACTIONS IN FOOD PROCESSING: A REVIEW.....	5
2.1 Introduction.....	5
2.2. Nonthermal Plasma Liquid Interactions	6
2.2.1 System configuration	10
2.2.2 Gas composition	14
2.2.2.1 <i>Reactive Oxygen Species (ROS)</i> :	14
2.2.2.2 <i>Reactive Nitrogen Species (RNS)</i> :	15
2.3. Microbial Inactivation Mechanism	17
2.3.1 Influence of reactive species and substrate on antimicrobial properties	25
2.3.2 Influence of microbial strain on antimicrobial properties	27
2.3.3 Influence of PAW storage time on antimicrobial properties	29
2.4 NTP and PAW Interactions with food components.....	30
2.4.1 Decontamination properties of PAW in food	31
2.4.2 Changes in food quality	31
2.4.2.1 <i>Changes in Lipids</i>	34

2.4.2.2 <i>Changes in Protein</i>	34
2.4.2.3 <i>Changes in antioxidants</i>	35
2.4.2.4 <i>Changes in sensory characteristics</i>	36
2.4.2.5 <i>Changes in shelf life</i>	37
2.5 Conclusion	38
Connecting Text.....	39
CHAPTER III PRELIMINARY DESIGN AND DEVELOPMENT OF A DIELECTRIC BARRIER DISCHARGE PLASMA ACTIVATED WATER GENERATION SYSTEM	40
3.1 Introduction.....	40
3.2 Design considerations	41
3.3 Preliminary Configuration	41
3.3.1 Reactor design.....	41
3.3.2 Electrical system	44
3.3.3 PAW preparation	44
3.4 Methods.....	45
3.4.1 Evaluation of PAW physicochemical properties	45
3.4.2 NTP gas analysis using FTIR	46
3.4.3 UV Absorption spectroscopy measurement of PAW reactive species	46
3.4.4 Determination of pH, ORP and electrical conductivity	46
3.4.5 Determination of hydrogen peroxide	46
3.5 Characterization of preliminary PAW reactor	47
3.5.1 Electrical characteristics	47
3.5.2 NTP gas phase analysis	48
3.5.3 UV absorption spectra of PAW	48
3.5.4 Optimization of PAW parameters.....	50
3.6 Remodeling the Preliminary System	55
3.6.1 Design of an improved PAW reactor.....	55
3.7 Summary	57
Connecting Text.....	58
CHAPTER IV EVALUATION OF PLASMA ACTIVATED WATER CHARACTERISTICS, ANTIMICROBIAL PROPERTY, TIME STABILITY AND PROCESS OPTIMIZATION	59

4.1 Abstract.....	59
4.2. Introduction.....	59
4.3. Materials and Methods.....	61
4.3.1 PAW generation system.....	61
4.3.2 Nonthermal plasma (NTP) gas analysis using FTIR	62
4.3.3 PAW time stability.....	62
4.3.4 Hydrogen peroxide concentration, pH and ORP	63
4.3.5 Ozone analysis	63
4.3.6 Microbiological analysis.....	64
4.3.7 Experimental design for optimization.....	64
4.3.8 Statistical Analysis.....	65
4.4. Results and Discussion	67
4.4.1 Voltage-Current Characteristics	67
4.4.2 FTIR analysis of gas phase species.....	67
4.4.3. Effect of NTP treatment time and post-treatment time on PAW characteristics.....	69
4.4.4. Effect of NTP treatment time and post-treatment time of PAW on <i>E. coli</i> inactivation	73
4.4.5 Response surface optimization of PAW treatment conditions	76
4.4.5.1 <i>Fitting the model</i>	76
4.4.5.2 <i>Effect on hydrogen peroxide</i>	77
4.4.5.3 <i>Effect on ozone concentration</i>	78
4.4.5.4 <i>Effect of pH and ORP</i>	80
4.4.5.5 <i>Optimum condition</i>	81
4.5. Conclusion	81
Connecting Text.....	83
CHAPTER V ASSESSMENT OF CHANGES IN WHEY PROTEIN ISOLATE AFTER PLASMA ACTIVATED WATER TREATMENT	84
5.1 Abstract.....	84
5.1 Introduction.....	84
5.2 Materials and Methods.....	86
5.2.1 Materials	86
5.2.2 Experimental setup for PAW production and sample preparation	87

5.2.3 PAW properties measurement	87
5.2.3.1 Hydrogen peroxide and ozone concentrations	87
5.2.3.2 pH and temperature	88
5.2.4 Turbidity measurement	88
5.2.5 Color measurement	88
5.2.6 Determination of total soluble protein content	89
5.2.7 Determination of sulfhydryl group (SH) content.....	89
5.2.8 Determination of surface hydrophobicity	89
5.2.9 Determination of foaming properties.....	90
5.2.10 Thermogravimetric analysis (TGA).....	90
5.2.11 Fourier transform infrared (FTIR) spectroscopy	91
5.2.12 Sodium dodecyl sulfate polyacrylamide gel electrophoresis (SDS-PAGE) analysis ...	91
5.2.13 Statistical analysis.....	91
5.3. Results.....	92
5.3.1 PAW properties.....	92
5.3.2 Turbidimetric analysis & color analysis of WPI	92
5.3.3 Total soluble protein content	95
5.3.4 Sulfhydryl (SH) group content	95
5.3.5 Foaming properties	96
5.3.6 Surface hydrophobicity.....	97
5.3.7 TGA analysis	98
5.3.8 FTIR spectroscopy	101
5.3.9 SDS-PAGE analysis	104
5.4. Discussion	105
5.5. Conclusion	107
Connecting text	108
CHAPTER VI EFFECT OF PLASMA ACTIVATED WATER ON <i>ESCHERICHIA COLI</i> DISINFECTION AND QUALITY OF KALE AND SPINACH	109
6.1 Abstract.....	109
6.2. Introduction.....	109
6.3. Materials and Methods.....	111

6.3.1 Materials	111
6.3.2 Nonthermal plasma system and PAW generation	112
6.3.3 PAW properties.....	112
6.3.4 PAW treatment of kale and spinach leaves	113
6.3.5 <i>Escherichia coli</i> disinfection procedure	113
6.3.6 Color, pH and TSS measurement	114
6.3.7 Total chlorophyll and carotenoid contents.....	114
6.3.8 Determination of ascorbic acid (AA) content.....	115
6.3.9 Antioxidant properties	115
6.3.9.1 <i>Methanolic extract preparation</i>	115
6.3.9.2 <i>Total phenolic content</i>	115
6.3.9.3 <i>Total flavonoid content</i>	115
6.3.9.4 <i>Total antioxidant capacity</i>	116
6.3.10 Electrolytic leakage.....	116
6.3.11 FTIR cuticle analysis	117
6.3.12 SEM imaging of leaf surfaces.....	117
6.3.13 Statistical analysis.....	117
6.4. Results and Discussion	118
6.4.1 PAW properties.....	118
6.4.2 Impact of PAW treatment on <i>E. coli</i> disinfection.....	118
6.4.3 Color analysis	121
6.4.4 Chlorophyll and carotenoid contents	122
6.4.5 Antioxidant properties and antioxidant activity of kale and spinach samples after PAW treatment.....	124
6.4.5.1 <i>Ascorbic acid, TPC and TFC contents</i>	124
6.4.5.2 <i>Antioxidant activity</i>	125
6.4.6 Electrolytic leakage.....	127
6.4.7 FTIR cuticle analysis	128
6.4.8 SEM imaging of PAW treated kale and spinach leaf surfaces	132
6.5. Conclusion	134
Connecting Text.....	135

CHAPTER VII INFLUENCE OF PLASMA ACTIVATED WATER ON ENZYME ACTIVITY AND STORAGE QUALITY OF FRESH-CUT APPLES	136
7.1 Abstract.....	136
7.2. Introduction.....	136
7.3. Materials and Methods.....	138
7.3.1 Materials	138
7.3.2 Plasma device and PAW treatment.....	138
7.3.3 Weight loss and soluble solid content.....	140
7.3.4 Color measurement	140
7.3.5 Membrane permeability	141
7.3.6 Respiration rate measurement.....	141
7.3.7 Firmness.....	142
7.3.8 Antioxidant properties	142
7.3.8.1 <i>Total phenolic content</i>	142
7.3.8.2 <i>DPPH radical scavenging activity</i>	142
7.3.8.3 <i>Ferric-reducing antioxidant power (FRAP) assay</i>	143
7.3.9 Enzyme activity assay.....	143
7.3.10 Malondialdehyde (MDA) content.....	144
7.3.11 Microbiological analysis.....	144
7.3.12 Scanning electron microscopy	145
7.3.13 Statistical Analysis.....	145
7.4. Results and Discussion	145
7.4.1 Weight loss, and soluble solids content	145
7.4.2 Color	146
7.4.3 Membrane permeability and MDA content	148
7.4.4 Respiration rate	150
7.4.5 Firmness.....	152
7.4.6 Antioxidant properties	153
7.4.6.1 <i>Total phenolics content</i>	153
7.4.6.2 <i>Antioxidant activity</i>	155
7.4.7 PPO and POD enzyme activity	155

7.4.8 Microbial quality.....	157
7.4.9 SEM image analysis.....	159
7.5 Conclusion	160
CHAPTER VIII CONCLUSIONS AND RECOMMENDATIONS	162
8.1 General summary and conclusion.....	162
8.2 Contribution to knowledge	164
8.3 Recommendations for future work	165
BIBLIGRAPHY	167

LIST OF TABLES

Table 2.1 Diffusion coefficients of NTP reactive species in water.....	8
Table 2.2 Microbial inactivation by NTP activated liquids and liquid foods	18
Table 2.3 Effect of NTP and PAW treatment on food quality	32
Table 3.1 Experimental design for process optimization of preliminary setup.....	46
Table 3.2 Coded factors and the corresponding experimental results of response variables	51
Table 4.2 Fitted second-order polynomial model with ANOVA details	77
Table 5.1: Effect of PAW treatment on color, turbidity, and soluble protein content of WPI.....	94
Table 5.2 Effect of PAW on SH group content of WPI.....	96
Table 5.3. Thermogravimetric characteristics of PAW treated WPI	99
Table 5.4 Secondary structural components of PAW treated WPI.....	104
Table 6.1 Changes in the color values and soluble solid content of kale and spinach after PAW treatment.....	122
Table 6.2 AA, TPC, TFC contents, DPPH inhibition and FRAP of kale and spinach following PAW treatments..	126
Table 6.3 Assignments of main absorption bands and their corresponding cell wall component	131
Table 7.1 Properties of PAW at different activation times.	139
Table 7.2 Changes in the color parameters of PAW treated fresh-cut apple samples during storage.....	148
Table 7.3 MDA content of PAW treated fresh-cut apple samples during storage.....	149

LIST OF FIGURES

Figure 2.1 Overview of Nonthermal Plasma-Liquid Interactions (Bruggeman et al., 2016; Chen et al., 2014a; Jiang et al., 2016; Zhou et al., 2018).....	7
Figure 2.2 NTP-liquid reactions – formation of reactive species at different sections (Liu et al., 2016; Verlackt et al., 2018).....	9
Figure 2.3 - Schematics of NTP-liquid reaction systems.....	11
Figure 2.4 Microbial inactivation mechanism by PAW reactive species (Ma et al., 2013; Thirumdas et al., 2018; Zhang et al., 2016).....	17
Figure 3.1 Design of dielectric barrier discharge PAW generator.....	42
Figure 3.2a: Schematic representation of experimental setup	43
Figure 3.2b: Picture of Dielectric Barrier Discharge	43
Figure 3.3: Experimental set-up of preliminary continuous flow DBD PAW generation system	43
Figure 3.4. Voltage current characteristics measures at 9 slm gas flow rate, for (a) gas phase plasma (b) PAW	48
Figure 3.5. NTP gas species – FTIR spectrum (After 20 min treatment at 9slm gas flow rate)	49
Figure 3.6. PAW UV absorption spectrum (a) at different treatment times and 6 slm gas flow rate and 100 ml/min water flow rate (b) at different gas flow rate and 30 min treatment time and 100 ml/min water flow rate	50
Figure 3.7. Predicted Vs experimental values of PAW (a) pH (b) H ₂ O ₂ (c) ORP (d) Electrical Conductivity (EC).....	52
Figure 3.8 Response profiles of treatment factors on PAW (a) Hydrogen peroxide concentration (μM), (b) electrical conductivity (μS/cm), (c) ORP (mV) and (d) post-treatment pH (e) desirability function.....	54
Figure 3.9 Design of remodeled DBD-PAW system (All dimensions are in mm).....	56
Figure 3.10 Remodeled PAW generation system (a) experimental set up (b) reactor section and (c) discharge inside the glass section; (1) High voltage generator, 2. Voltage probe, 3. Current probe, 4. Pump, 5. Gas inlet, 6. Water inlet, 7. Reactor glass section, 8. High voltage electrode, 9. DBD discharge.....	56
Figure 4.1 Schematic diagram of the remodeled PAW generation system.....	62
Figure 4.2 V-I characteristics of Ar/O ₂ NTP.....	68
Figure 4.3 Ar/O ₂ NTP gas phase FTIR spectrum acquired at (a)10 min, (b) 20 min and (c) 30 min.....	69
Figure 4.4 Properties of PAW produced at 10 min (PAW 10), 20 min (PAW 20) and 30 min (PAW 30); (a) hydrogen peroxide concentration (mM); (b) ozone concentration mg/l; (c) pH.....	71
Figure 4.5. Effect of treatment time and post-treatment time on <i>E. coli</i> population.....	74
Figure 4.6 Correlation heat map on the relationship between the <i>E. coli</i> inactivation percentage with PAW process conditions and properties.....	75
Figure 4.7 Response surface plots on PAW hydrogen peroxide concentration	78
Figure 4.8 Response surface plots on PAW ozone concentration	79
Figure 4.9 Response surface plots of the pH of PAW	80
Figure 5.1. Schematic diagram of plasma activated water system	87
Figure 5.2 Plasma activated water properties: (A) changes in hydrogen peroxide concentration, ozone concentration and temperature (B) Changes in pH of PAW. (Values that are not connected by same letter are significantly different at p<0.05)	93
Figure 5.3 Effect of PAW treatment on foaming properties (A) and surface hydrophobicity (B) of WPI	97

Figure 5.4. Thermogravimetric profiles of PAW treated WPI samples: Profiles (a) (c) (e) are Weight loss % vs temperature ($^{\circ}\text{C}$) and profiles (b) (d) (f) are Derived weight ($\%/^{\circ}\text{C}$) vs temperature ($^{\circ}\text{C}$).....	100
Figure 5.5 FTIR Spectrum of PAW treated WPI samples : (a) 5 mg/ml (b) 10 mg/ml (c) 50 mg/ml	103
Figure 5.6 SDS-PAGE band profile of PAW treated WPI	105
Figure 6.1 Schematic diagram of the PAW generation system	112
Figure 6.2 Properties of PAW with respect to plasma activation time (i) hydrogen peroxide and ozone concentrations (ii) pH and temperature.....	119
Figure 6.3 Effect of PAW treatment, at different activation times, on <i>E. coli</i> population.....	120
Figure 6.4 Effect of paw treatment on (i) kale chlorophyll content (mg/g); (ii) kale carotenoid content (mg/g); (iii) spinach chlorophyll content (mg/g); (iv) spinach carotenoid content (mg/g).....	123
Figure 6.5 Electrolytic leakage (%) in kale and spinach after PAW treatment.....	128
Figure 6.6 ATR-FTIR spectrum of kale (a) and spinach (b)	130
Figure 6.7 SEM surface images of fresh and PAW treated kale leaves (a) control (b) P10 (c) P20 (d) P30 (e) P45 and (f) P60.....	133
Figure 6.8 SEM surface images of fresh and PAW treated spinach leaves (a) control (b) P10 (c) P20 (d) P30 (e) P45 and (f) P60.....	133
Figure 7.1 Schematic diagram of plasma activated water system.	139
Figure 7.2 Effect of PAW treatment on (i) weight loss % and (ii) soluble solid content ($^{\circ}\text{Bx}$) of fresh-cut apples during storage. (Means connected with the same letter are not significant at $P < 0.05$).....	146
Figure 7.3 Changes in the membrane permeability of fresh-cut apple samples upon PAW treatment ((Means connected with the same letter are not significant at $p < 0.05$)).	149
Figure 7.4 Respiration rate of PAW treated fresh-cut apple samples during 12 days of refrigerated storage in mg/h/kg of sample. (Means connected with the same letter are not significant at $p < 0.05$)	151
Figure 7.5 Firmness (N) of the fresh-cut apple samples after PAW treatment and 12 days of storage. (Means connected with the same letter are not significant at $p < 0.05$).....	153
Figure 7.6 Changes in the antioxidant properties of the PAW treated fresh-cut apples for 12 days of storage (Means connected with the same letter are not significant at $p < 0.05$).....	154
Figure 7.7 Effect of PAW treatment on fresh-cut apple (i) PPO enzyme activity (ii) POD enzyme activity (Means connected with the same letter are not significant at $p < 0.05$).....	156
Figure 7.8 Microbial quality of PAW treated fresh-cut apples during storage (i) Total aerobic count (log CFU/g) (ii) Total yeast and molds count (log CFU/g) (Means connected with the same letter are not significant at $p < 0.05$)....	158
Figure 7.9 SEM microstructure images of PAW treated apple samples (a) control, (b) P10, (c) P20, (d) P30, (e) P45, and (f) P60.	160

NOMENCLATURE

$\Delta\Psi$	Membrane Potential
AA	Ascorbic acid
AC	Alternating Current
ANOVA	analysis of variance
BBD	Box Behnken Design
BSA	Bovine Serum Albumin
CBBG	Coomassie Brilliant Blue (G250) dye
CFU	Colony Forming Units
CIRG	Color Index of Red Grapes
DBD	Dielectric barrier discharge
DC	Direct current
DNA	Deoxyribonucleic acid
EDTA	Ethylenediaminetetraacetic acid
FAO	Food and agricultural organization
FTIR	Fourier transform infrared spectroscopy
GFR	gas flow rate
HDPE	High Density Polyethylene
HEDBS	Hollow Electrode Dielectric Barrier System
HV	High Voltage
MDA	Malondialdehyde
MW	Microwave
NTP	Nonthermal Plasma
ORP	Oxidation Reduction Potential
PAAS	Plasma Activated Acidified Solution
PAM	Plasma activated Media
PAS	Plasma Activated Solution
PAW	Plasma Activated Water
PBS	Phosphate Buffered Solution
PFU	Plaque forming unit
PMJ	Plasma Micro Jet
PTT	Post treatment time
PUFA	Polyunsaturated fatty acid
RF	Radio frequency
RNS	Reactive Nitrogen Species
RONS	Reactive Oxygen Nitrogen Species
ROS	Reactive Oxygen Species
SDS- PAGE	Sodium dodecyl sulfate polyacrylamide gel electrophoresis

SEM	Scanning Electron Microscope
SH	sulfhydryl group
slm	standard liters per minute
TFC	Total flavonoid content
TGA	Thermogravimetric analysis
TNF	α – tumor necrosis factor
TPC	Total phenolics content
TSS	Total Soluble Solids
UV radiation	Ultraviolet Radiation
WFR	water flow rate
WHO	World health organization
WPI	Whey protein isolate

CHAPTER I

INTRODUCTION

In recent decades, consumption of fresh fruits and vegetables has increased substantially due to the increased awareness among the consumers on healthy eating habits. Fresh-cut products provide convenience to the consumers for increased fresh food consumption. According to the FDA, fresh cut-products are defined as fruits and vegetables (FV) which are slightly/ minimally altered in their physical state to make them ready for consumption (FDA, 2008). This process involves simple unit operations like peeling, trimming, cutting, and washing. However, the fresh produce industry continues to be associated with a series of foodborne illness outbreaks across the globe. The World Health Organization (WHO) has reported that globally 600 million foodborne illnesses and 420,000 deaths occur annually (Organization, 2015). In Canada alone, there are 4 million domestically developed foodborne illnesses which are reported each year (Thomas et al., 2013). The fresh-cut produce industry is one of the major contributors of these food borne illness outbreaks (Carstens et al., 2019). Fresh-cut produce gets contaminated with pathogenic organisms from various sources like soil, water, handling containers, etc., through the post-harvest minimal processing and handling operations. These processes increase the surface area of the fruits and expose their cellular contents to the atmosphere, making them highly prone to microbial contamination and microbial proliferation. Increase in the consumption of fruits and vegetables, increasing pathogen diversity on fresh produce, globalization of trade, and increase in the resistance of pathogens to stress conditions are believed to be the major causes of fresh produce related food borne illnesses (Bhunja, 2018; Lynch et al., 2009; Murray et al., 2017).

Presently, chemical compounds like quaternary ammonium salts, chlorine and organic acids are being used to protect fresh fruits and vegetables from microbial spoilage and to increase their shelf life. However, many pathogens are becoming resistant to these conventional disinfecting compounds (Rodríguez-López et al., 2018; Tomat et al., 2018). Further, the efficiency of these chemical disinfection agents depends on the availability of free chlorine, wash water quality, microbial load, washing time and presence of other organic and inorganic matter (Murray et al., 2017; Xiang et al., 2019a). It is also speculated that these washing processes could lead to the cross-contamination of fresh products (Gombas et al., 2017; Murray et al., 2017). In addition, the

by-products of some of these chemical disinfectants, like the chlorine-based sanitizers, are reported to leave carcinogenic residues on foods (Lee et al., 2018; Ma et al., 2015). Consequently, there is a need for an effective disinfection method in the food industry which can protect the food material from spoilage microorganisms while preserving its nutritional quality.

Atmospheric pressure non-thermal plasma (NTP) or cold plasma is a new technology which has been the focus of many researchers in recent time as it showed promising results for the inactivation of many pathogenic microorganisms (Herianto et al., 2021). It is an emerging nonthermal, chemically benign and eco-friendly disinfection technology (Zhou et al., 2018). Effective inactivation of food pathogenic organisms in a wide range of foods such as meat (Patange et al., 2017), egg shell (Chen et al., 2015), fruits (Misra et al., 2014b), flour (Misra et al., 2015) and juices (Surowsky et al., 2014) have been reported. Apart from successful inactivation of microorganisms, it is also reported that cold plasma can degrade toxins and pesticide residues from food material (Misra et al., 2014a; Sarangapani et al., 2016). Magureanu et al. (2015) reported that the pharmaceutical pollutants present in the water were effectively destroyed or mineralized by cold plasma treatment.

In most of the food applications, nonthermal plasma is produced by partial ionization of gases at atmospheric pressure and temperature. At atmospheric pressure, the initial breakdown of the feed gas needs higher voltage to produce gas discharges. Mixing gases like argon and helium with low breakdown voltage and reducing the distance between the electrodes can decrease the voltage requirement for gas discharge (Lu et al., 2016). Different discharges such as corona discharge, dielectric barrier discharge (DBD), micro hollow cathode discharge, gliding arc discharge, and plasma jets are generally used for NTP generation. However, the gas discharge NTP applications have some disadvantages in food applications, such as surface application, difficulty in treating irregularly shaped foods and larger size foods (Herianto et al., 2021). Further, some of the strong reactive components produced in gas plasma, like UV rays, free ions and electrons, can adversely affect the quality of the treated food materials (Matthew et al., 2011). Plasma activated water could potentially be used as an alternative to gas phase NTP to overcome these issues.

Plasma activated water (PAW) is produced by exposing water directly or indirectly to the gas phase NTP. By doing so, the reactive species are transferred into the water and through post-discharge reactions in water, reactive species are produced in the water. These reactive species are

comparatively stable in water and effective disinfection of many pathogenic organisms has been reported in various food materials (Xiang et al., 2020; Xu et al., 2016). Further, once PAW has been produced, it can be stored before use, providing operational flexibility (Herianto et al., 2021), and due to the self-quenching nature of the reactive species present in PAW, it is considered environmentally benign (Cullen et al., 2018).

Washing is an inevitable process in fresh-cut produce processing. By using PAW in the fresh-cut produce washing process will not only help in ensuring food safety and it will also reduce the effluent produced in the washing process as the reactive species in PAW degrade with time. Nevertheless, PAW application in fresh-food sanitation is at the early stage of research and the impact of PAW reactive species on food material is not yet completely understood. This study will provide an alternate disinfection method for the fresh-cut produce industry, with better understanding on the effect of PAW on fresh produce quality and shelf life.

1.1 Problem Statement and Research Hypothesis

The present global demand for convenient fresh foods that are free from chemical additives and residues has led to the development of new technologies for fresh-cut produce disinfection. To address the gaps in existing fresh-cut produce cleaning and disinfection methods, there is a need for an alternate solution to ensure food safety without compromising the fresh-cut produce quality such as plasma activated water (PAW). PAW is a promising technology for fresh produce disinfection, however apart from fresh produce disinfection, more information on its effect on food components and produce quality is needed to exploit this technology at the commercial scale.

This project is based on the hypothesis that plasma activated water is a potential technology to ensure food safety in the fresh-cut food industry without any chemical additives. The results from this study will be useful in understanding the effect of PAW reactive species on food components and their quality. The effect of this technology on fresh-cut food enzyme inactivation and product shelf-life is also assessed.

1.2 General Objective

The primary objective of the project is to design, develop and optimize PAW generation system and to assess the effect of PAW reactive species on food components, fresh food quality and shelf-life.

1.3 Specific Objectives

1. To design and develop a continuous flow plasma activated water generation system
2. To evaluate the physicochemical properties and *Escherichia coli* decontamination properties of PAW and process optimization
3. To assess the effect of PAW on basic food components such as proteins that are susceptible to oxidation
4. To evaluate the effect of PAW on *Escherichia coli* disinfection on fresh-cut spinach and kale leaves and its quality assessment
5. To investigate the effect of PAW on fresh-cut apple enzyme activity and quality during storage

1.4 Organization of the Thesis

This introduction chapter is followed by Chapter II presenting a literature review in which comprehensive and detailed review on various PAW production methods and overview on fundamental PAW chemistry are discussed. This chapter also summarizes different studies on using PAW for various food disinfection applications, the mechanism of microbial disinfection by the reactive species and changes in food quality upon PAW treatment. Chapter III presents the details pertaining to the design and development of a dielectric barrier PAW generation system. In Chapters IV to VII, the experimental results of specific research objectives are presented. Finally, Chapter VIII summarizes the overall conclusions and contributions to knowledge that can be drawn from this work, along with recommendations for future work.

CHAPTER II

NONTHERMAL PLASMA–LIQUID INTERACTIONS IN FOOD PROCESSING: A REVIEW

2.1 Introduction

Increasing population and climate change are imposing great pressure on our food systems requiring sustainable technologies to improve global food and nutritional security (Porat et al., 2018). With improved agricultural production technologies, productivity has increased. However due to inadequate postharvest operations, one-third of the food production is wasted both in developed and developing countries (Bradford et al., 2018). Fresh fruits and vegetables are the major contributors to food wastage during various postharvest operations both at retail and consumer levels (Porat et al., 2018). It has also been the major source of foodborne illnesses in recent times (Murray et al., 2017). Increase in the consumption of fruits and vegetables, increasing pathogen diversity on fresh produce, globalization of trade, and increase in the resistance of pathogens to stress conditions are believed to be the major causes of fresh produce related food borne illnesses (Bhunia, 2018; Lynch et al., 2009; Murray et al., 2017) .

The efficiency of the commercial chemical disinfecting agents such as quaternary ammonium salts, chlorine and acids depends on the availability of free chlorine, wash water quality, microbial load, washing time and presence of other organic and inorganic matter (Murray et al., 2017; Xiang et al., 2019a). The by-products of some of these chemical sanitizers like the chlorine-based sanitizers, are reported to leave carcinogenic residues on food (Ma et al., 2015).

Nonthermal plasma (NTP) processing techniques have gained importance among researchers during the last decade particularly for their applications in food (Surowsky et al., 2015). Due to their high reactivity and the self-quenching characteristic, NTP reactive species have great potential to address issues related to food safety, nutritional quality, and environmental safety (Bourke et al., 2018; Misra et al., 2016; Pankaj & Keener, 2017). Apart from its bactericidal properties, NTP can also be used for the removal of pesticides residues (Misra et al., 2014a; Misra, 2015), antibiotic residue in water (Magureanu et al., 2015), while it can alter the functional properties of food (Jampala et al., 2005; Misra et al., 2015; Thirumdas et al., 2017b) and packaging materials (Pankaj et al., 2014). Ekezie et al. (2017) also proposed the potential use of NTP in

hydrogenation of oils, removal of allergens and antinutrients in food. However, the physical species present in the gas plasma such as charged particles, ultraviolet rays, and electrons, along with the high electrical field can cause detrimental changes in delicate biological materials (Cooper et al., 2010; Ercan et al., 2013; Ma et al., 2015), such as surface erosion (Grzegorzewski et al., 2011). Using water activated by NTP, known as Plasma Activated Water (PAW) could provide a potential solution to substitute the chemical sanitizing agents like chlorine in fresh food cleaning processes (Ma et al., 2015). Shen et al. (2016) called PAW as a “green disinfectant” because it has a less adverse impact on the environment than chemical agents and proposed it as a promising food sanitizer.

Plasma interactions with water are highly complex and the presence of moisture significantly affects the microbial inactivation efficiency of NTP (Cooper et al., 2010; Dobrynin et al., 2009). A complete understanding of the interactions between the NTP and water is crucial to advance this technology to a commercially viable processing method. Hence the focus of this review gives a comprehensive insight on the NTP-liquid interaction processes and their implications in food processing.

2.2. Nonthermal Plasma Liquid Interactions

Since water is a polar liquid, its conductivity changes when exposed to high voltage (Šunka, 2001), thus making the application of NTP to a wet surface or a liquid substrate, a more complicated process (Bruggeman et al., 2016; Liu et al., 2016). It has been reported that the inactivation of microorganisms by plasma in a liquid substrate is mediated by the liquid phase and it is important to understand the complete NTP-liquid interactions to optimize food and medical applications (Bruggeman et al., 2016; Liu et al., 2016). Presence of humidity in the carrier gas also leads to modifications in the reactive species of the NTP system and acts as a barrier for the NTP reactive species to penetrate within the liquid substrate (Gorbanev et al., 2016; Krohmann et al., 2018). When the NTP is targeted over a liquid substrate, the system can be divided into three regions (i) gas phase plasma ; (ii) plasma-liquid interface; (iii) bulk liquid region (Bruggeman et al., 2016) (Figure 2.1). Though many authors have studied the reactions and resultant reactive species in the gas phase region (Du et al., 2008; Misra et al., 2016; Moreau et al., 2008) and liquid phase (Lukes et al., 2012; Sun et al., 2012; Tian & Kushner, 2014), the distribution of these reactive species in liquid phase is still not clearly understood (Jiang et al., 2016).

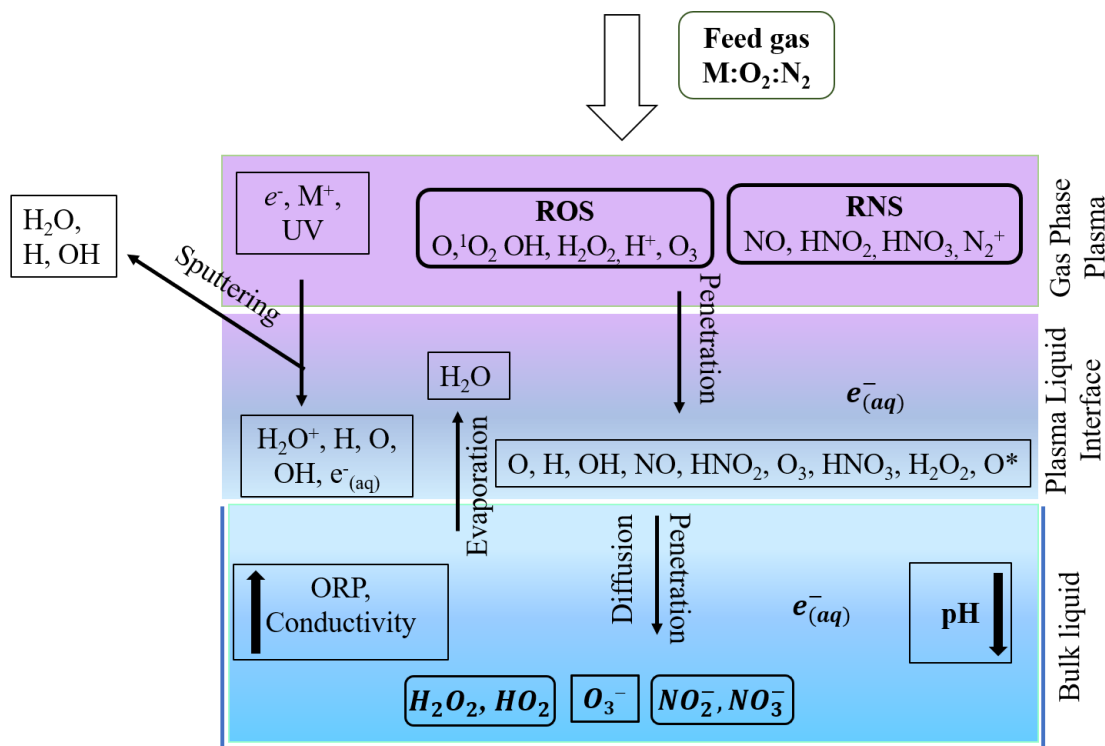


Figure 2.1 Overview of Nonthermal Plasma-Liquid Interactions (Bruggeman et al., 2016; Chen et al., 2014a; Jiang et al., 2016; Zhou et al., 2018)

In the gas-liquid interface region, the NTP species produced in the gas phase contact the water vapor present above the liquid surface. The processes governing the reaction between these two phases are either direct penetration of reactive species from the gas phase to the liquid phase or by various transfer processes such as gas phase kinetic collisions among the species, diffusion, solvation, absorption, desorption and chemical transfer (Bruggeman et al., 2016; Zhou et al., 2018; Zhou et al., 2016a) (Figure 2.1). After exposing water to gas plasma, the reactive species in the liquid initiate many post-discharge reactions within the liquid. The liquid chemical reaction pathways and the diffusion coefficients of NTP reactive species in the liquid phase are presented in Figure 2.2 (Liu et al., 2016; Verlackt et al., 2018) and Table 2.1, respectively.

Table 2.1 Diffusion coefficients of NTP reactive species in water

Reactive species	Diffusion coefficient (cm ² s ⁻¹)	Reference
e	1.0×10^{-1}	(Jiang et al., 2016)
O	2.0×10^{-5}	(Jiang et al., 2016)
O⁻	2.0×10^{-5}	(Jiang et al., 2016)
O₂⁻	1.97×10^{-5}	(Jiang et al., 2016)
O₃⁻	1.75×10^{-5}	(Jiang et al., 2016)
O₃	1.75×10^{-5}	(Jiang et al., 2016)
H⁺	9.31×10^{-5}	(Jiang et al., 2016)
H⁻	1.10×10^{-4}	(Jiang et al., 2016)
H	4.5×10^{-5}	(Jiang et al., 2016)
H₂	4.5×10^{-5}	(Jiang et al., 2016)
OH	$7.1 - 8.4 \times 10^{-5}$	(Campo & Grigera, 2005; Yusupov et al., 2013b)
OH⁻	5.26×10^{-5}	(Campo & Grigera, 2005; Yusupov et al., 2013b)
HO₂	6.5×10^{-6}	(Yusupov et al., 2013b)
H₂O₂	$1.3-1.5 \times 10^{-5}$	(Yusupov et al., 2013b)
NO	2.05×10^{-5}	(Brisset & Pawlat, 2016)
NO₂	1.85×10^{-5}	(Anderson, 2016)
O=NOOH	2.5×10^{-5}	(Anderson, 2016)
NO₃⁻	1.7×10^{-5}	(Anderson, 2016)
NO₂⁻	1.7×10^{-5}	(Anderson, 2016)
HNO₂ and HNO₃	2.5×10^{-5}	(Anderson, 2016)

In Figure 2.2, the blue lines indicate the diffusion process while the black lines represent the chemical reactions. Further, the thickness of the lines and size of letters indicate the relative concentration of the reaction species. From Figure 2.2, it can be inferred that all the stable high concentration reactive species in liquid are mainly produced by the diffusion process. As the experimental validation of the distribution and penetration characteristics of reactive species is difficult to measure, these parameters and mass transfer kinetics are mostly evaluated using numerical simulation techniques (Bie et al., 2016; Chen et al., 2014b; Jiang et al., 2016; Thagard et al., 2016; Yusupov et al., 2013b).

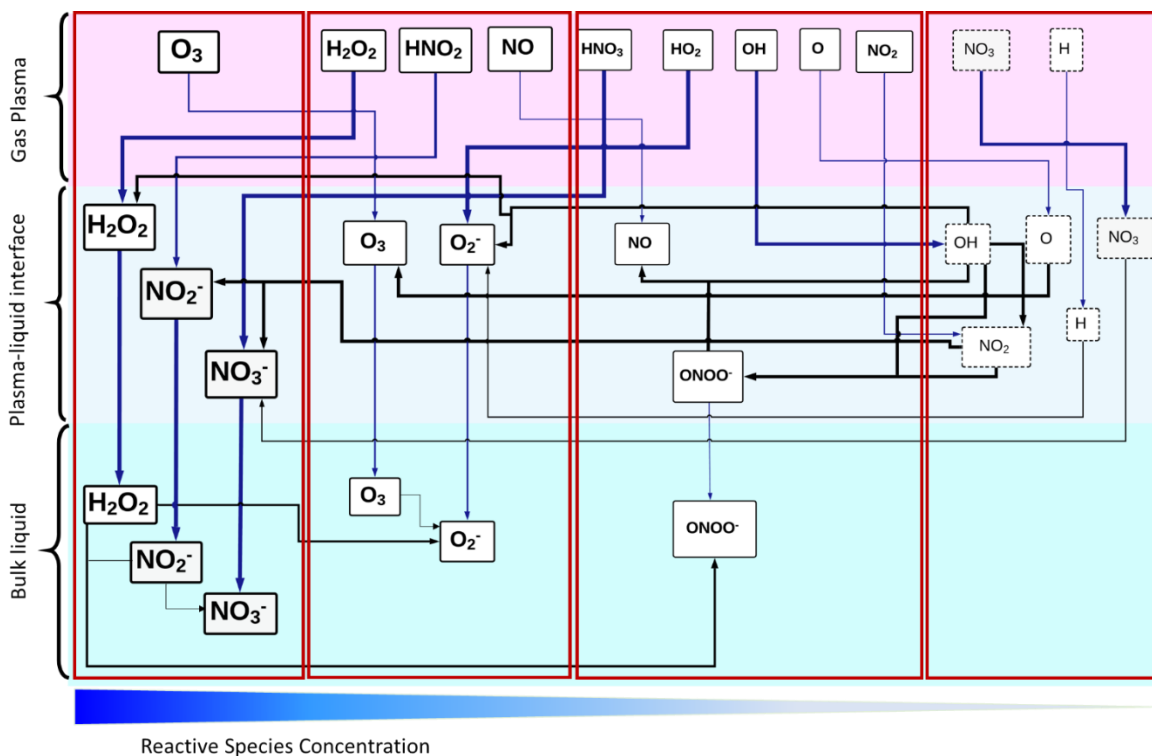


Figure 2.2 NTP-liquid reactions – formation of reactive species at different sections (Liu et al., 2016; Verlackt et al., 2018)

According to the treatment time and solution volume, the pH of the solution is reduced during NTP treatment. In the presence of nitrates, this acidic environment enhances the antimicrobial property of the solution (Oehmigen et al., 2011a). The pH of PAW did not reduce below 3.5-3 in most of the reported cases irrespective of the treatment conditions (Liu et al., 2010; Moreau et al., 2007;

Shi et al., 2011). Ikawa et al. (2010) reported that they achieved the critical pH of 4.5-4.7 during NTP treatment and claimed that only below this pH there was effective microbial inactivation. However, Tian et al. (2015) observed only a slight change in the pH of water from the initial pH of 7 to 6 after plasma activation for 20 min, irrespective of the generation mode. Zhang et al. (2012) also reported a similar change in the pH value of water from the initial pH of 6 to pH 5.

The concentration of reactive species in the liquid phase depends on several factors like the system configuration, treatment time, discharge gap, carrier gas, applied voltage and the electron energy (Gurol et al., 2012; Jiang et al., 2016; Pavlovich et al., 2013; Tian et al., 2015). Among these factors, the two most influencing ones, system configuration and gas composition are discussed below in more details.

2.2.1 System configuration

There are various system configurations (Figure 2.3) used to produce NTP at atmospheric pressure (Ajo et al., 2017; Conrads & Schmidt, 2000; Ehlbeck et al., 2010; Lu et al., 2016; Nehra et al., 2008; Tendero et al., 2006). The classification of NTP systems based on their configuration is given in Figure 2.3. Corona discharge, dielectric barrier discharge (DBD) and hollow electrode DBD (HEDBD) are the important systems used for the NTP-liquid processes and a summary of the reported studies is given in Table 2.2. Most of the food-related applications were conducted using a batch type system in which the plasma is exposed to a fixed quantity of liquid substrate.

DBD discharges (Figure 2.3a) produce negligible thermal effects in water when sinusoidal high frequency or nanosecond pulsed voltage waveforms are used. However sinusoidal waves produce filamentary discharges while nanosecond pulsed waveform produces stable glow discharges which are widely preferred over the other due to their energy efficiency (Neretti et al., 2016). Keeping the high voltage electrode covered by a dielectric material above the water surface reduces the initial discharge voltage and increases the efficiency of the system (Wenzheng & Chuanhui, 2014). Among the various configurations, DBD is preferred due to its simple electrode configuration and its ability to produce a stable plasma discharge (Tang et al., 2018). Due to the larger surface area, the reactive species concentration produced by the DBD discharge were higher than that of plasma torches glow discharges (Leduc et al., 2010).

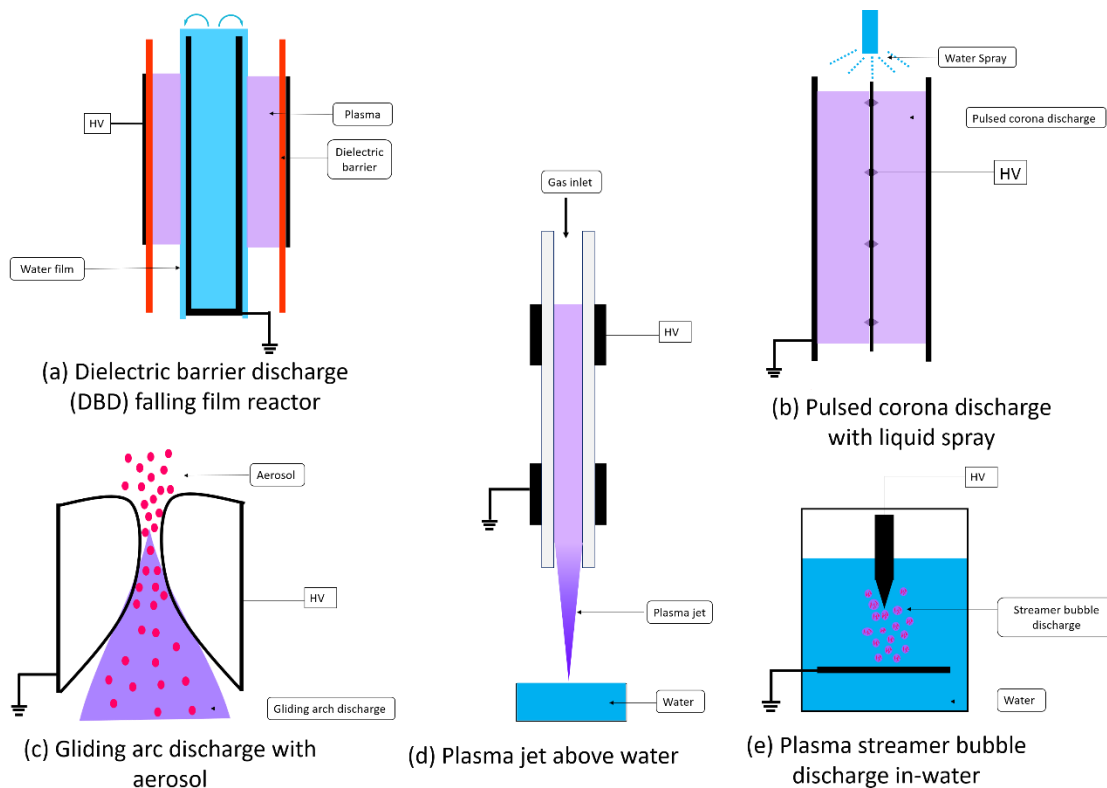


Figure 2.3 - Schematics of NTP-liquid reaction systems

Corona discharges (Figure 2.3b) are one of the highly researched NTP discharge methods. Pulsed corona discharge is a potential alternative to the existing advanced oxidation processes in water treatment (Gupta & Bluhm, 2007) and it has been widely reported for its microbial inactivation efficiency in water (Abou-Ghazala et al., 2002; Sato et al., 1996; Soušková et al., 2011; Šunka, 2001). Corona discharge could be produced by applying high voltage to a thin electrode or wire. When this streamer discharge is produced inside the water along with the reactive species, it produces shock waves, UV radiation and bubbling (Locke et al., 2006). The in-water production of pulsed-corona streamer discharge (Figure 2.3e) has better reactive species diffusion and energy efficiency (Banaschik et al., 2015). The targeted application of corona discharge creates an ion wind which facilitates mixing of liquid, subsequently increasing the diffusion of reactive species and bactericidal property of Plasma Activated Water (PAW) (Julák et al., 2018a). The major disadvantage of corona discharge systems is their unstable discharges and electrode corrosion (Baroch et al., 2008). The long-time exposure of the sharp needle to high electric field results in the corrosion of electrodes (Sunka et al., 1999).

Hamdan et al. (2018) observed electrode corrosion during in-liquid spark or streamer discharges generated by nano-pulsed corona discharges. Wu et al. (2012) and Wu et al. (2017) reported the presence of Cu^+ and Cu^{2+} ions in the activated water while using a copper electrode in plasma microjet (Figure 2.3d) powered by either a DC negative-polarity high-voltage power supply or by a 0.35 A and 100 kV power supply. These metal ions act as metal-catalysts and induce an oxidation process (Fenton reaction) which is preferred for the oxidation and mineralization of pollutants in water (Marković et al., 2015; Wu et al., 2012). Still, the erosion of metal electrodes and electrolysis of metal electrodes due to the plasma is not preferred in food and medical applications as it could contaminate the liquid phase and reduce the efficiency and life of the system (Hamdan et al., 2018; Satoh et al., 2007).

Apart from AC/DC electrical sources, microwaves (MW) and radio frequencies (RF) are also used to produce NTP (Tendero et al., 2006). Submerged Microwave Plasma Jet (MWPJ) can prevent electrode corrosion and increase the conversion of plasma species into water. Niquet et al. (2018) compared the PAW produced by DBD plasma and MW plasma. In MW NTP treated water, nitrous acid was the main species which further decomposed into nitrates while no ROS was detected due to higher plasma temperature. In DBD PAW, hydrogen peroxide was the most important and most stable reactive species. Though the bactericidal property of DBD PAW was much lower than that of MW PAW, it was stable during 24 h storage whereas the reactive species concentration in MW PAW degraded rapidly.

In gliding arc discharge (Figure 2.3c), the plasma is formed in the gap between two or more diverging electrodes by high voltage, which then gets cooled as it is moved towards the wider edge of the electrode (Burlica et al., 2006; Lu et al., 2016). Gliding arc discharges are used to activate water either indirectly by exposing the plasma over water (Benstaali et al., 2002; Burlica et al., 2004; Burlica et al., 2006) or directly by spraying water along with air (Figure 2.3c). Aerosol of water and gas (argon or oxygen) has been successfully activated by the gliding arc and used for inactivation of microorganisms (Burlica et al., 2010). In any system configuration, indirect exposure of liquid is favored over water electrodes and direct exposure, as the later may produce undesirable and unaccountable reactive species in the water (Oehmigen et al., 2010; Satoh et al., 2007).

The contact mode of gas-liquid interface significantly influences the concentrations of reactive species in the activated liquid (Aoki et al., 2008; Tian et al., 2015). Accordingly, the mode of generation can be broadly classified as (1) In-water (Figure 2.3c) (2) Above water (Figure 2.3d) (3) Aerosol (Figure 2.3c) and (4) Bubble (Figure 2.3e) (Bruggeman et al., 2016).

When the plasma is created directly inside water or a liquid substrate, the reaction efficiency is very high. The short-lived reactive species and electric current also transferred to the liquid during in-water discharge which is not possible in above-liquid application (Bruggeman & Leys, 2009; Van et al., 2013). Due to this rich reactive species transfer (content), the in-water method produces highly reactive PAW and sterilizes the contaminated liquid very effectively (Stoffels et al., 2008). However, the in-water reaction kinetics are very complex, and not yet completely understood (Bruggeman et al., 2016; Oehmigen et al., 2011a). Further, while treating living cells in medical and food applications, this method is not preferred due to drastic cell damage (Stoffels et al., 2008).

While, in above-water or indirect applications, gas-phase plasma is generated in the plasma-liquid interface, where the reactive species are transferred into the liquid by diffusion process alone. The species transfer rate can be improved by increasing the gas flow rate or by having forced convection through liquid mixing (Bruggeman et al., 2016). Hence, only the neutral species and radicals are able to reach the liquid due to the low mass transfer of long-lived reactive species from the gas phase to the liquid phase in plasma above-water systems (Tian et al., 2015). This leads to richer concentrations of nitrogen species in the liquid substrate than oxygen species when oxygen and nitrogen gas mixture is used (Thiyagarajan et al., 2013). Despite low mass transfer and energy efficiency, in-direct exposure is preferred over direct in-water exposure in biological applications due to better control of reactive species and milder reactions (Stoffels et al., 2008).

In the case of multiphase systems like aerosols, bubbles and spray systems, either of the water or gas phases will disperse into another to increase the reaction rate. Due to higher surface area and smaller droplet size, the heterogeneous mass transfer rate of reactive species is accelerated in these systems. They have better reaction kinetics and energy efficiency than in-liquid systems (Jiang et al., 2011). Burlica et al. (2006) proposed that when water was sprayed over the plasma along with oxygen gas, a larger amount of H₂O₂ was produced in PAW when compared to the indirect treatment method. In aerosol systems, the interactions between plasma and liquid droplets are not

completely understood, due to evaporation of liquid droplets and subsequent lower residence time in the plasma region (Maguire et al., 2015).

2.2.2 Gas composition

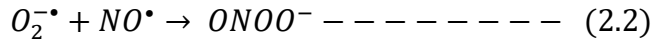
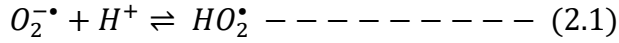
The feed gas or carrier gas composition is another important factor which affects the composition of NTP activated liquid (Thirumdas et al., 2018; Zhang et al., 2013). Noble gases like helium and argon are used in combination with oxygen and nitrogen to produce stable glow discharges, due to their low breakdown voltage at atmospheric pressure. Based on the feed gas composition, the two main NTP reactive species are Reactive Oxygen Species (ROS) and Reactive Nitrogen Species (RNS).

2.2.2.1 Reactive Oxygen Species (ROS):

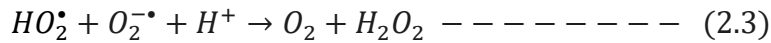
Reactive oxygen species are generated whenever there are oxygen molecules present in the carrier gas or if the substrate contains water molecules. The reactive oxygen species play an important role in the microbial inactivation efficiency of PAW (Liu et al., 2010; Satoh et al., 2007; Tian et al., 2015). The major reactive oxygen species produced in the NTP are hydroxyl radicals ($\cdot\text{OH}$), singlet oxygen ($\cdot\text{O}$), super dioxides ($^1\text{O}_2$), hydrogen peroxide (H_2O_2), and ozone (O_3) (Pankaj et al., 2018; Satoh et al., 2007).

The hydroxyl radicals ($\cdot\text{OH}$) in the gas phase are produced mainly due to the presence of water either as a main product of electron dissociation of water molecule by UV or free electrons, or as a by-product of recombination and dissociation of other reactive species and ions in the plasma (Bruggeman et al., 2016; Pankaj et al., 2018). With 2.8 eV oxidation potential, it is the most reactive and toxic species among the ROS (Jiang et al., 2016). It acts as a precursor to produce H_2O_2 in PAW and the concentration of H_2O_2 in PAW depends on the concentration of ($\cdot\text{OH}$) (Pankaj et al., 2018). The $\cdot\text{OH}$ radical density decreases with the depth of NTP application in liquid leading to the increase in the lifetime of these $\cdot\text{OH}$ radicals to 3.92 μs at the discharge depth of 6 mm when compared to the 2.7 μs lifetime on the surface discharge over water (Attri et al., 2015).

These super dioxide ions have a longer lifetime (5s) in aqueous solution and in low pH conditions are converted to hydroperoxyl radicals (HO_2^{\bullet}) through pathway (2.1). In the presence of nitrogen, $O_2^{\bullet-}$ forms peroxyxynitrite anion ($ONOO^-$) by pathway (2.2) which is a strong antimicrobial agent.



The increase in the H^+ ions in water, due to the dissociation of water molecules by NTP, increases the electrical conductivity and decreases the pH of the liquid medium (Korachi & Aslan, 2011). When the pH of the solution is reduced to the critical value of ~4.5 the HO_2^{\bullet} and O_2 reduces the hydroxyls to hydrogen peroxide (pathway 2.3) (Ikawa et al., 2010).

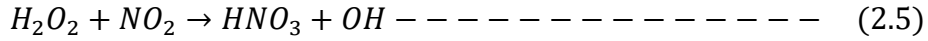
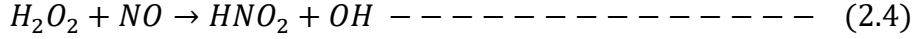


Presence of metal ions like Cu^{2+} or Fe^{3+} leads to the Fenton reaction accelerating the conversion of H_2O_2 to $\bullet OH$ (Wu et al., 2012). Further Wu et al. (2012) reported that $O_2^{\bullet-}$ is the precursor for the production $\bullet OH$ in water and singlet oxygen by $O_2^{\bullet-}$ in reaction with H_2O_2 through Haber–Weiss reaction. They quantified the amount of singlet oxygen and $\bullet OH$ in 20 s treated water as 6×10^4 M and 1.2×10^{-5} M respectively using electron spin resonance spectroscopy.

H_2O_2 is one of the important long-lived reactive species produced in the plasma treated liquid. H_2O_2 is a strong oxidizer and its oxidizing potential increases in the acidic environment (Brisset et al., 2011; Shen et al., 2016). The Henry’s constant for H_2O_2 is 0.83 mol/l/Pa which is higher than that of argon and oxygen. Thus, the solubility of gas phase H_2O_2 plays an important role in the generation of liquid phase H_2O_2 (Winter et al., 2014). Gorbanev et al. (2016) suggested that the formation of H_2O_2 was not by the dissociation of water molecules instead it was formed by the diffusion of gas phase H_2O_2 into the liquid phase. They described that the precursor species for H_2O_2 are formed in the plasma tube while $\bullet H$, $\bullet OH$ and superoxide radicals are formed in the plasma-liquid interface.

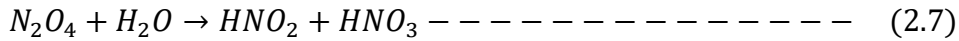
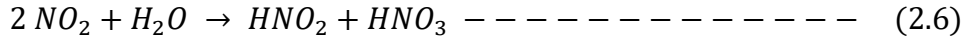
2.2.2.2 *Reactive Nitrogen Species (RNS):*

RNS species are produced in the water only when the feed gas contains nitrogen gas (Attri et al., 2015). In the absence of nitrogen, the $\bullet OH$ radicals combine with the water molecules and forms H_2O_2 . In the presence of nitrogen, NO and NO_2 are formed which inhibits the consumption of OH radicals to form H_2O_2 . Instead, it reacts with H_2O_2 through the backward reactions (pathway 2.4, 2.5) and produces $\bullet OH$ which increases the redox potential of PAW (Hamdan et al., 2018).

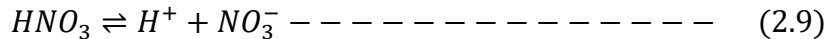
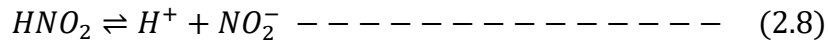


Nitrogen in the feed gas reduces the scavenging activity of O₂ ions by the formation of NO₂⁻ and reduces the depletion rate of free electrons (Rumbach et al., 2015). •OH and nitric acid radicals (NO•) are precursors for the production of nitrites, nitrates and hydrogen peroxide in PAW (Naïtali et al., 2010). The long-lived nitrates and nitrites along with H₂O₂ prolong the bactericidal activity of PASs (Su et al., 2018). The concentration of NO• in the PASs can be altered by using different discharge power levels and activation time (Tian et al., 2017).

The neutral species such as ozone, nitrogen oxides and nitric acid are produced by the dissociation of nitrogen and oxygen by the electrons. These neutral species, with relatively longer lifetime, react with water and produce nitrite and nitrate components in water through pathways (2.6, 2.7) (Jung et al., 2015a).



Then the nitric (HNO₂) and /nitrous oxides (HNO₃) decompose into protons, nitrites and nitrates through pathways (2.8, 2.9) thus reducing the pH of the solution (Hamdan et al., 2018; Oehmigen et al., 2011a; Oehmigen et al., 2011b; von Woedtke et al., 2012).



Satoh et al. (2007) claimed that the reduction in pH of the liquid substrate was observed only when the feed gas contains nitrogen gas. In the absence of nitrogen, and if oxygen was the only working gas, there was no reduction in the pH of the solution. This reduction in the pH of the solution further decomposes nitrous acid into nitrogen dioxide, causing an increase in the nitrate concentration (pathway 2.10, 2.11).



2.3. Microbial Inactivation Mechanism

Bactericidal properties are one of the key sought-after benefits of plasma activated liquids. Depending on the process parameters, exposure time, liquid substrate composition, microbial strain and target surface, plasma activated liquid may cause lethal or sublethal changes in microorganisms (Attri et al., 2015). In NTP treatment, the microorganisms are either suspended in a liquid substrate (direct) or the activated liquid is used over the microbial cell (remote application) (Table 2.2). The inactivation efficiency varies with this mode of application. Different inactivation mechanisms are proposed by the authors based on reactive species and microbial strains. Accordingly, a summary of the inactivation mechanism is given in Figure 2.4 and the factors influencing the antimicrobial properties are summarized in Table 2.2. Some of the important findings are discussed below.

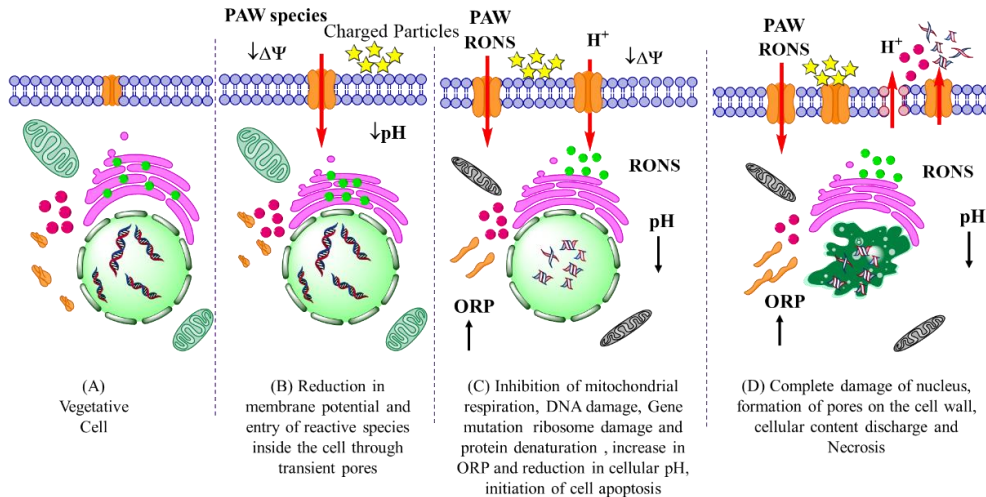


Figure 2.4 Microbial inactivation mechanism by PAW reactive species (Ma et al., 2013; Thirumdas et al., 2018; Zhang et al., 2016)

Table 2.2 Microbial inactivation by NTP activated liquids and liquid foods

Liquid substrate	Discharge type	Gas	Microorganism	Inactivation efficiency	Reactive species and inactivation kinetics	Reference
Water	AC arc discharges	Air	<i>Escherichia coli</i> , <i>Staphylococcus aureus</i> and Yeast	5 log reduction in 40-60 min treatment	Cell Mutation by electric discharges and membrane disruption by low pH	(Chen et al., 2008)
Water	Atmospheric pressure plasma microjet	Air	<i>Staphylococcus aureus</i>	98% reduction in 6 min	Peroxidation of cell membrane lipids by HO ₂ [•] and low pH (<4.5)	(Liu et al., 2010)
Distilled water and tap water	MW driven plasma device	Air	<i>Escherichia coli</i> , <i>Pseudomonas marginalis</i> , <i>Pseudomonas fluorescens</i> , <i>Pectobacterium carotovorum</i> and <i>Listeria innocua</i>	All microorganism was inactivated below detection limit (<1 CFU/ml) after 50s treatment with PAW	ROS and RNS	(Schnabel et al., 2015)
Distilled water, phosphate buffered	Indirect Surface DBD	Air	<i>Escherichia coli</i> , <i>Staphylococcus aureus</i> cells and	Complete inactivation of cells from 10 ⁶ –10 ⁸ CFU/ml after 5-	Synergic effect of RONS	(Oehmigen et al., 2010)

saline and saline water			<i>Bacillus atrophaeus</i> spores	15 min; 2.5-log reduction of spores after 30 min		
Distilled water and NaCl solution	Surface DBD	I. Ar	<i>Escherichia coli</i>	No significant reduction in population	-	(von Woedtke et al., 2012)
		II. Air	<i>Escherichia coli</i>	~ 10 ⁷ CFU/ml in 10 min	Cytotoxic effect by HNO ₂ , H ₂ O ₂ and low pH	
I. Deionized water alone and II. Deionized water with fresh-cut celery and radicchio	DBD	Air	<i>Listeria monocytogenes</i> , <i>Escherichia coli</i> serogroups O157 and O26	I. 40 min for > 6 log CFU/ml reduction II. 0.5 to -3.7 Log CFU/cm in 260 min	-	(Berardinelli et al., 2016)
PAS (H ₂ O), PAS (NaCl), and PAS (H ₂ O ₂)	HEDBS	Air	<i>Newcastle Disease Virus</i>	More than 3:1 ratio inactivation of virus	short-lived OH [•] and NO [•] and long-lived H ₂ O ₂ , changed the morphology, destroyed the RNA structure, and degraded the	(Su et al., 2018)

					protein of the virus, consequently resulting in virus inactivation	
Bacterial suspension in distilled water	Low frequency plasma jet	Helium and air	<i>Escherichia coli</i> and <i>Leuconostoc citreum</i>	~ 10 ⁵ CFU/ml 60 s in pH 3.7	Low pH and peroxidation of fatty acids in the cell membrane by hydroperoxyl radical (HO ₂ [•]). No inactivation in He gas only treatments	(Ikawa et al., 2010)
Water -spore suspension	DC PMJ -direct	Compressed air	<i>Bacillus subtilis</i> spores	97% inactivation in 6 min	short lived reactive species such as single oxygen, [•] OH, super oxide anion rupture, distortion and shrinking of the outer layer, leading to the leakage of spore inclusion	(Sun et al., 2012)
Culture broth	Gliding arc Above water	Ambient air	<i>Erwinia carotovora</i> subsp. <i>atroseptica</i>	10 log reduction in 5 min	Acid effects by NO [•] and oxidative stress by OH [•] caused structural damage and release of chromosomal DNA	(Moreau et al., 2007)

Aqueous culture media	DBD indirect discharge	Air	Eukaryotic microalgae	80 – 640 s depending on the strain	Cell morphological damage by low pH	(Tang et al., 2008)
Apple juice	Atmospheric pressure plasma jet- Indirect	Argon/O ₂ plasma	<i>Citrobacter freundii</i>	5 log cycles in 480 s and 24h storage	Cell permeabilization and RNA damage by OH and O radicals.	(Surowsky et al., 2014)
Apple Juice	DBD ACP above liquid	Air	<i>Escherichia coli</i>	4.34 log CFU/ml reduction after 30 s NTP treatment	Cell membrane damage, reduction in membrane potential by charged particles and NTP radicals	(Liao et al., 2018a)
Orange juice	DBD above surface	Air	<i>Staphylococcus aureus</i> , <i>Escherichia coli</i> , <i>Candida albicans</i>	Reduced below detection limit (<1 CFU/50 µl) after 12, 8, and 25 s respectively > 5 log reduction in 8-25s	Reaction of ROS and RNS on membrane lipids, protein, nucleic acids. pH	(Shi et al., 2011)
White grape juice	High voltage atmospheric cold plasma	Dry air	<i>Saccharomyces cerevisiae</i>	7.4 log CFU/ml inactivation in 4 min	reactive gas species resulting cell leakage by electroporation, lipid peroxidation, enzyme inactivation and DNA	(Pankaj et al., 2017)

					cleavage leading to cell death	
Milk	Encapsulated DBD	Ambient air	<i>Escherichia coli</i> , <i>Listeria monocytogenes</i> , and <i>Salmonella typhimurium</i>	~2.4 CFU/ ml reduction in 10 min	Oxidative stress and cell wall damage by ROS	(Kim et al., 2015)
PAW	DBD Batch Indirect	Argon +1% Artificial air with Nitrogen	<i>Bacteriophages T4, 174, and MS2</i>	~ up to 9 log PFU/ml reduction in survival infectivity in time dependent manner	Protein and nucleic acid damage by singlet oxygen species	(Guo et al., 2018)
PAW	HEDBS	Air	<i>Saccharomyces cerevisiae</i>	0.03% survival rate after 120 s treatment	High NO concentration, high power and long reaction time leads to cell death	(Tian et al., 2017)
PAW	HEDBS PMJ	Air	<i>Staphylococcus aureus</i>	2.5 log reduction after 5 min of PAW	OH and NO radicals react with <i>S. aureus</i> cell membrane, damages the cellular structure and reduces the cellular pH s	(Wu et al., 2017)

PAW	HEDBS PMJ	Air	<i>Enterococcus faecalis</i>	10 ⁷ CFU reduction after 5 min of treatment	Cell wall lipid oxidation and cellular protein denaturation by ROS	(Pan et al., 2017)
PAW	HEDBS PMJ	Air	Total fungal and total bacterial count	1.1 log CFU/g reduction of bacteria and fungi after 8 days of storage	Combined action of high ORP. Low pH and ROS induced oxidative stress caused cellular structure and component degradation	(Ma et al., 2016)
PAW	Single electrode plasma jet – above water – remote application	Argon+ 2% O ₂ mix	<i>Staphylococcus aureus</i> on strawberry	2.3 log reduction after 20 min activation and 3.5 log reduction during 4-day storage	ROS, pH and high ORP induced cell wall and protein oxidation	(Ma et al., 2015)
PAW	APPJ	Air	<i>Pseudomonas deceptionensis</i> CM2	5 log reduction with 10 min exposure to PAW	Disruption of outer and cytoplasmic membranes and leakage of intracellular components by high ORP, low pH and RONS	(Xiang et al., 2018)

PAW	DBD Plasma jet – In-water	Air	<i>Saccharomyces cerevisiae</i> on Grapes	0.5-log reduction on grapes and >2 log reduction in sterile water after 30min of PAW treatment	Damage to the membrane and cell structure by ROS	(Guo et al., 2017)
PAW Ice	DBD ACP	Air	<i>Total viable count of bacteria</i>	< 6 log ₁₀ CFU/g until day 8	Oxidation of cell wall and cellular components by ROS and RNS	(Liao et al., 2018b)
Plasma treated water	APPJ	N ₂ gas with H ₂ O or HNO ₃ vapour	<i>Escherichia coli</i>	5 log reduction of bacteria with N ₂ + 0.5% HNO ₃ vapour treatment	NO ₂ ⁻ and H ₂ O ₂ inactivated the bacterial cell by inhibiting the antioxidant machinery and membrane protein and DNA damage	(Shaw et al., 2018)

Chen et al. (2008) described the mutation and carcinogenesis of *Escherichia coli* cells in water suspension by direct plasma treatment and speculated on the effect of UV or H₂O₂ for cell damage. In a detailed study, Korachi and Aslan (2011) stated that the decrease in microbial population was caused by DNA damage rather than cell membrane lipid peroxidation. They proved this by performing the fatty acid profiling of *Escherichia coli* cells before and after plasma treatment and reported that there was no significant qualitative change in cell membrane fatty acids. According to Guo et al. (2018), the singlet oxygen present in PAW damages the nucleic acid and proteins in all double-stranded DNA, single-stranded DNA and the RNA bacteriophages by aggregation. Zhang et al. (2013) used Ar/O₂ PAW to inactivate *Staphylococcus aureus* and concluded that the main inactivation mechanism was damage of cell membrane by oxidative stress induced by the reactive species in PAW. They stated that when the cell membrane is damaged, ions like potassium and phosphate leach out first followed by the larger molecules like DNA/RNA and proteins (Zhang et al., 2013). Besides that, oxidative stress alters the bacterial surface structure, its chemical state and integrity of cell membrane. Severe deformation of the cell surface, cleavage of peptide bonds, and oxidation of amino acid side chains by the ROS in PAW were reported in *Enterococcus faecalis* after a 5 min treatment (Pan et al., 2017). The SEM images of microbial cells after PAW treatment shows the transformation from a smooth surface to a distorted, shrunk and ruptured surface (Ma et al., 2016; Shen et al., 2016).

2.3.1 Influence of reactive species and substrate on antimicrobial properties

The bactericidal property of PAW is not contributed by a single component and many authors emphasized the synergistic effect of plasma activated species like pH, RONS, UV radiation and oxidation-reduction potential (ORP) (Burlica et al., 2006; Kamgang-Youbi et al., 2009) (Table 2.3).

The pH of the solution plays an important role in PAW bactericidal properties (Ikawa et al., 2010; Traylor et al., 2011). Though the reduction in pH is not enough to be the sole cause for microbial inactivation (Korachi & Aslan, 2011), it acts as a catalyst for post-discharge reactions and facilitates the bactericidal properties of PAW (Liao et al., 2007). As stated in the earlier section, when there was no oxygen or nitrogen present in the feed gas, there was no reduction in the pH and the activated liquid did not have any effect on microbial cells (Surowsky et al., 2014; von

Woedtke et al., 2012; Zhang et al., 2016). Ikawa et al. (2010) claimed that PAS must be maintained at or below the critical pH of 4.7 for the bactericidal property. When the pH was below this critical value they observed a rapid reduction in the *Escherichia coli* and acidophilic *Leuconostoc citreum* population. Naïtali et al. (2010) stated that nitrites, nitrates and H₂O₂ in acidic condition, contributed to a 50% reduction in microbial population while no decontamination was observed when PAW was neutralized or buffered. However, Joshi et al. (2018) compared the *Enterobacter aerogenes* inactivation effectiveness of PAW and plasma activated acidified buffer (PAAB) solution and claimed that the PAAB had better inactivation efficiency than PAW not because of lower pH but due to the higher ORP and reactive species concentration.

The RONS like HNO₂ and HNO₃ cause the acidification of NTP activated liquid. Under this acidic environment, NO₂⁻ in combination with H₂O₂ act as antimicrobial agents (Chen et al., 2008; Wu et al., 2017). An acidic condition also promotes the oxidation by hydroperoxyl radicals and initiates the lipid peroxidation of cell membranes. The damaged cell membranes allow the flux of protons inside the cell. Further, the non-charged ONOOH produced by the nitrogen species penetrate inside the bacterial cell and break down into the highly oxidative NO₂[•] and HO[•] and destroy the microbial cells from within. The detailed reaction kinetics and equations can be found in Oehmigen et al. (2011b). Patil et al. (2016) stated that the presence of water molecules enhanced the inactivation of *Bacillus atrophaeus* spores by the formation of OH, peroxide, and nitrogen oxide (NO[•]). Interestingly, Tian et al. (2017) observed the proliferation of *Saccharomyces cerevisiae* when PAW contained low concentrations NO[•] (300 nM) and PAW inhibited the growth when the NO[•] concentration was greater than 3 mM. Zhang et al. (2016) proposed that OH[•] affect the cells by oxidation of cell membrane unsaturated fatty acids, denaturation of intracellular proteins and DNA, while NO[•] restricts the replication of cell by thymine dimerization of DNA strands.

According to Burlica et al. (2010), H₂O₂ even at low concentrations (2×10^{-3} M) could effectively inactivate planktonic bacterial cells. Conversely, Ikawa et al. (2010) and Liu et al. (2010) claimed that hydrogen peroxide alone did not contribute to the inactivation of bacterial cells. They also explained that 800 mg/l concentration of H₂O₂ is required for microbial inactivation whereas only 50 mg/l is formed in water by plasma microjet (Ikawa et al., 2010). Tian et al. (2015) also ruled out the involvement of H₂O₂ in PAW bactericidal properties due to its low concentration and considered that other ROS play an important role in *Staphylococcus aureus* inactivation. Winter

et al. (2014) proposed that H_2O_2 does not affect the microbial cell directly, instead it forms other reactive radicals such as hydroxyl radical ($\cdot OH$) and hydroperoxyl radical ($HO_2\cdot$).

Though UV radiation produced by NTP seems to cause cytotoxic effects in the liquid substrate, it does not contribute to the inactivation of microorganisms (Boudam et al., 2006; Liu et al., 2010; Shi et al., 2011). Further, Laroussi (2002) stated that at atmospheric pressure, NTP systems do not produce enough UV radiation to inactivate microorganisms. While dealing with the liquid substrates the effect of UV radiation is further diminished and its effect on microbial inactivation is negligible (Shi et al., 2011).

2.3.2 Influence of microbial strain on antimicrobial properties

The type of microorganism, its growth stage, state and substrate conditions affect the inactivation efficiency of plasma activated liquid (Burlica et al., 2010). Adherent cells are more resistive to PAW treatment than planktonic cells (Kamgang-Youbi et al., 2009). In adherent phase, the bacterial cells secrete a protective outer layer which inhibits the bactericidal effectiveness of PAW reactive species. In planktonic state, this layer is not present hence H_2O_2 alone is able to make a reduction in the microbial population (Burlica et al., 2010). Burlica et al. (2010) reported that low concentrations of H_2O_2 were enough to inactivate planktonic bacteria while concentration up to $10 \times 10^{-3} M$ was not sufficient to inactivate the adherent bacterial cells. Ercan et al. (2013) reported that the plasma activated N-acetyl-cysteine (NAC) solution can inactivate a wide range of multidrug resistant pathogens (both bacteria and fungi) in both planktonic forms and on biofilms. Its inactivation efficiency was comparable to 70% ethanol and bleach (3.8% sodium hypochlorite) solutions. In another study, Dobrynin et al. (2009) stated that a higher NTP dosage ($16-20 J/cm^2$) was required to inactivate the dried *Escherichia coli* cells, while moist *Escherichia coli* cells were inactivated at lower dose ($1-8 J/cm^2$) followed by wet bacterial cells ($11-17 J/cm^2$). In contrary to these findings, Ikawa et al. (2010) stated that if the substrate is dry, direct interaction of plasma reactive species and microorganisms leads to efficient and faster decontamination. They claimed that, when the substrate is wet, water molecules act as a barrier and reduces the decontamination efficiency.

Chen et al. (2008) found that gram-positive bacteria had more resistance to plasma inactivation than the thin-walled gram-negative bacteria while using AC corona discharges directly in water. Generally, the higher-order organisms and spores require more exposure time than the vegetative bacterial cells for inactivation (Scholtz et al., 2010; Shi et al., 2011). Yeasts and molds are more resistant to the PAW treatment than bacterial cells (Julák et al., 2018b; Kamgang-Youbi et al., 2009).

Many studies report on the effect of PAS on prokaryotic cells, however, only limited studies have been conducted for eukaryotic cells. Most of these reports are on the treatment of human cancer cells. Ahn et al. (2011) evaluated the effect of air or nitrogen plasma jet on the cervical HeLa cancer cells and concluded that the ROS present in the plasma microjet was responsible for the reduction in mitochondrial membrane potential. Leduc et al. (2010) reported that NTP significantly affected the mammalian cells and altered the DNA structure. Though they did not find any mutation effects, cell death and DNA damage were observed when the treatment time was increased. Changes to eukaryotic cells and tissues, specific to medical applications by NTP, have been reviewed in detail by Stoffels et al. (2008). However only limited reports are available for NTP induced changes in plant tissues (Stoffels et al., 2008).

In a related study, Tang et al. (2008) evaluated the effect of NTP on eukaryotic microalgae aqueous media. They reported severe morphological changes in the eukaryotic algal cells depending on the dosage and species. In prokaryotic cells, PAS causes the cellular damage and agglomeration of cells while in eukaryotic cells it causes cellular damage similar to the damages caused by low pH (2-3).

Recently, Su et al. (2018) evaluated the effectiveness of PAS against Newcastle Disease Virus (NDV). They proposed, high ORP along with OH^\bullet , NO^\bullet and H_2O_2 altered the morphology and RNA structure of the virus. In another study, Guo et al. (2018) reported that both DBD surface discharges and PAW had strong antiviral properties and effectively inactivated the T4, 174, and MS2 bacteriophages in a time-dependent manner. The PAW exhibited antiviral properties even after 10 days of storage at 22°C. They reported that singlet oxygen played an important role in the denaturation and aggregation of bacteriophages.

2.3.3 Influence of PAW storage time on antimicrobial properties

One of the main advantages of using PAS against nonthermal gas plasma is its storability. However, there is only limited literature available on the storage stability of PAW and some of these reports are contradictory to each other. Traylor et al. (2011) claimed that the solvated H_2O_2 and nitrites in the plasma activated saline solution remain stable for several days making it as a potential disinfectant solution for fruits and vegetable washing. Vlad and Anghel (2017) also observed no change in pH, conductivity, nitrate and H_2O_2 of PAW during 21 days of storage under dark conditions irrespective of the feed gas composition and initial reactive species concentration. Interestingly, three minutes of plasma activation of NAC solution using DBD plasma retained its *Escherichia coli* inactivation efficiency for up to 2 years according to the accelerated ageing time evaluation studies by Ercan et al. (2013). Based on antibacterial properties they reported that the plasma activated NAC was stable for 3 months both under refrigerated storage and room temperature. They claimed that the decrease in the discharge gap, small liquid volume and the stability of reactive species in the PAS could be the reason for the extended cytotoxic properties. Pavlovich et al. (2013) observed a stable antimicrobial property of PAW for seven days when the water was treated for 20 min by indirect DBD discharge. Joshi et al. (2018) reported no change in pH of PAW and PAAB for 7 days when stored at room temperature. However, there was a significant reduction in ORP and bactericidal property of the liquid after storage, indicating that the stability of reactive species during storage is important to maintain the bactericidal properties. On the other hand, in a detailed study, Shen et al. (2016) analyzed the germicidal activity, ORP, H_2O_2 , and NO_3^- concentrations of PAW at different storage temperatures. They reported that all these properties were decreasing with storage time when stored at 25°C , 4°C and even at -20°C and PAW stored at -80°C retained its reactivity for 30 days. When PAW was stored at higher temperatures (25°C , 4°C and -20°C) there was a reduction in the bactericidal activity against *Staphylococcus aureus*. This reduction was mainly due to the reduction in ORP, concentrations of NO_3^- and H_2O_2 . Further, in PAW stored at -80°C the retention of bactericidal activity after 30 days of storage was mainly contributed by NO_2^- in association with H_2O_2 . The pH of PAW did not change during storage irrespective of the storage temperature and H_2O_2 was not stable during storage and it was maintained only when stored at -80°C . Nitrate concentration was decreased irrespective of the storage condition while nitrite concentration was maintained when

PAW was stored at -80°C. Oehmigen et al. (2011b) treated sodium chloride solution with surface DBD and reported that the bactericidal effect was significantly reduced after 30 min of storage at room temperature. According to Traylor et al. (2011), the reactivity of the PAW reduced within 30 min of its production while the H₂O₂ concentration in plasma activated saline water did not change with storage time. Zhang et al. (2013) observed that exposing bacterial cells immediately after PAW activation, took 10 min to have 6-log reductions in the microbial population whereas, after 24 hours of storage it took 40 min to have the same level of reduction. The ORP of PAW also decreased from 490 mV to 450 mV after 24 hours of storage at 4°C. It was claimed that the decay of short-lived ROS such as [•]OH and [•]O₂ during storage led to a change in conductivity and the reduction in the inactivation efficiency (Zhang et al., 2013).

2.4 NTP and PAW Interactions with food components

When a liquid food is exposed to NTP, many chemically reactive species could be developed in liquid food. Due to the presence of nutrients like proteins and lipids, the reaction kinetics will be different from one food to another. The antioxidants present in the food also act as scavengers of reactive species and reduce their bactericidal properties. In a recent study, Xiang et al. (2019a) proved the negative impact of organic matter on the bactericidal properties of PAW in *Escherichia coli* and *Staphylococcus aureus*. They also stressed on the importance of considering the presence of organic matter including food constituents while using PAW for food-related applications. Berardinelli et al. (2016) also stated that the inactivation efficiency of PAW varies with respect to the kind of vegetables. Ma et al. (2016) observed acceleration in fruit ripening due to the oxidative species in PAW for Chinese bayberries causing a faster fruit decay with higher treatment times. They claimed that the prevention of fruit decay by PAW was not a dose dependent effect, in contrary to the findings by others (Berardinelli et al., 2016; Herceg et al., 2016; Ma et al., 2015; Scholtz et al., 2010; Tang et al., 2008). Therefore, PAW treatment conditions and the resulting bactericidal properties in non-food substrates could be completely different from food materials. The physical and chemical properties of the food material will significantly change the PAW reactive species interactions and the species concentration must be optimized according to the food material.

2.4.1 Decontamination properties of PAW in food

Using PAW for fresh foods to eliminate microorganisms could pose some challenges due to the irregularity of shape, surface texture etc. (Berardinelli et al., 2016; Joshi et al., 2018). Guo et al. (2017) speculated that the rough skin surface and fruit surface components could prevent the penetration of reactive species from PAW. Joshi et al. (2018) used PAW and plasma activated acidified buffer (PAAB) to inactivate *Enterobacter aerogenes* on various fruit surfaces. They reported that the inactivation efficiency of PAW was not dependent on the texture of the fruit surface while it was different in case of PAAB after 3 min treatment. The smoothest surface (glass) showed the highest reduction (6.32 ± 0.43 log CFU per surface), while the roughest surface (spiny gourd) showed a significantly lower reduction (2.52 ± 0.46 log CFU per surface) when treated with PAAB. They speculated that the surface properties like surface hydrophobicity and presence of cuticular waxes may affect the bacterial adhesion to produce surface and alters the performance of PAW and PAAB. Nevertheless, Joshi et al. (2018) recommended the use of PAW for dump tank washing of fruits and vegetables.

Xu et al. (2016) observed that PAW washing was effective in retarding the microbial growth on button mushrooms for 7 days at 20°C. PAW produced with 5 min and 10 min plasma exposure had better microbial disinfection than PAW produced by 15 min plasma exposure during storage. They speculated the decay of mushrooms induced by the oxidative stress caused by the rich concentrations of ROS species. In a recent study, Choi et al. (2019) reported the sequential use of PAW washing and mild heating of ready-to-eat salted and shredded cabbage. They claimed that mild heating of cabbage after PAW washing significantly reduced the microbial load without affecting the quality.

2.4.2 Changes in food quality

NTP is considered as an advanced oxidation technique (Vandamme et al., 2016) and the microbial inactivation in a liquid substrate is mainly due to oxidative stresses induced by the reactive species. However, some of these reactions are not favored in food materials as they could cause undesirable changes in the food nutritional quality by denaturation of proteins, lipids and other micronutrients (Sarangapani et al., 2017b). Further, the genotoxicity of reactive species requires to be studied in detailed while using this technology for food applications. Kim et al. (2016) evaluated the mutagenicity

and immunotoxicity of PAW cured meat. The results indicated no mutagenicity in the sausages based on the Ames test. In the immune toxicity test, the serum TNF- α values were less in mice after feeding treated samples for 32 days, indicating that no inflammatory response had occurred by feeding the sausages made by PAW. Based on these results they recommended using plasma-treated water as a nitrite source for meat curing. Similar results were presented by Yong et al. (2018) in PAW cured ham. The changes in food quality by PAW in foods are summarized in Table 2.3.

Table 2.3 Effect of NTP and PAW treatment on food quality

Food substrate	System details	Objective	Changes in food quality	Reference
PAW-Mung bean sprouts	Gliding arc, air plasma jet, 30 s activation and 10-30 min PAW treatment	Microbial and physicochemical quality	<ul style="list-style-type: none"> - 2.32- and 2.84- log CFU/g reduction in total aerobic bacteria and total yeasts and moulds respectively - No change in total phenolic content, total flavonoid content and sensory characteristics 	(Xiang et al., 2019b)
PAW-Barley	Air plasma jet, 20 min activation and 0-20min PAW treatment	Deoxynivalenol decontamination	<ul style="list-style-type: none"> - 34% reduction in Deoxynivalenol after 5 min in germinating barley - 80-90% germination after treatment - PAW better than intense pulsed light treatment 	(Chen et al., 2019)

PAW- Chinese bay berries	HEDBS PMJ in liquid PAW 0.5 to 5 min PAW treatment and 8 days storage	Effect on quality during storage	- 50% reduction in fruit decay - Firmness of the fruits were maintained - CIRG values increased - Decrease in Total soluble solids	(Ma et al., 2016)
PAW- Ham	DBD PAW; 2 h activation of water and 2 weeks storage	For curing	- Better color development than sodium nitrate - Less residual nitrite content - No difference in lipid oxidation compared to sodium nitrate treatment - Genotoxicologically safe based on Ames test	(Yong et al., 2018)
PAW- Shredded salted cabbage	DBD PAW – 30 to 120 min activation; 10 min treatment in combination with mild heating	Evaluation of microbial quality	- No change in acidity - Decrease in salinity - No change in hardness - No negative effect on color retention - 50% reduction in peroxidase activity	(Choi et al., 2019)
Water	DBD APCP; Atmospheric air; 2- 8 min exposure	Pesticide degradation	- ~ 55-80% reduction in pesticides - change in pH was not reported	(Sarangapani et al., 2016)

2.4.2.1 Changes in Lipids

When food containing fats and oils is exposed to plasma activated water, the oxidative species accelerate lipid oxidation (Yong et al., 2018). The detailed parametric study of accelerated oleic acid oxidation by NTP revealed that the presence of oxygen in the feed gas significantly increased the oxidation (Vandamme et al., 2016). The lipid oxidation was mainly caused by the singlet oxygen and atomic oxygen and by doping the feed gas with water reduced the oxidation of lipids by scavenging these ROS (Vandamme et al., 2016). The oxidation of food fatty acids during NTP treatment follows the Criegee mechanism and produces ozonides, aldehydes, carboxylic acids and hydroperoxides (Sarangapani et al., 2017a). There was an increase in the peroxide value of sausages treated with PAW, and the lipid oxidation by PAW was similar to other conventional nitrate sources like sodium nitrate and celery powder (Jung et al., 2015a). In ham curing, PAW treatment increased the peroxide value, equal to that of sodium nitrate curing after one-week storage (Yong et al., 2018). A strong increase in the Malondialdehyde (MDA) levels in PAW treated button mushroom during storage was observed due to lipid peroxidation induced by the stable PAW reactive species (Xu et al., 2016). Liao et al. (2018b) also claimed that the increase in thiobarbituric acid (TBA) content due to lipid peroxidation in shrimps was induced by the oxidative reactive species in PAW rather than enzyme or microbial activity.

2.4.2.2 Changes in Protein

In food materials, the reactive species from the gas phase NTP are transported through the liquid interface by successive reactions. The hydroxyl radical and other reactive oxygen species produced by these reactions initiate the denaturation of proteins or inactivation of enzymes by amino acid oxidation, peptide bond cleavage, and protein-protein cross-links (Misra & Jo, 2017; Surowsky et al., 2013; Surowsky et al., 2015). Takai et al. (2014) studied the effect of NTP on 20 naturally occurring amino acids in solution. They used low frequency high voltage plasma jet of helium gas to treat 1 ml of 1.0 mM amino acid solutions for 0-10 min. Based on the high-resolution mass spectroscopy results obtained, they stated that 14 amino acids were oxidized by plasma treatment. When all the 20 amino acids in combination were treated by plasma, L-methionine was completely degraded by oxidation after 10 min of plasma treatment followed by L-cysteine and L-tryptophan. The ROS in NTP lead to the irreversible sulfonation of disulfide-bond in sulfur containing amino acids like cystines and increased the concentrations of sulfonated cystine in the solution. Among

the essential amino acids, Tryptophan was rapidly degraded by hydroxylation but it has low reactivity to RNS while L-phenylalanine was sensitive to RNS and it was degraded by nitration. There was no oxidation or nitration observed in threonine and it is one of the stable amino acids under NTP treatment.

Takai et al. (2012) stated a 40% reduction in lysozyme activity after 30 min He-O₂ plasma. The hydroxyl radicals ([•]OH), superoxide anion radicals (O₂^{-•}), hydroperoxy radicals (HO₂[•]) and nitric oxide (NO[•]) induced chemical modifications in the lysozyme sidechain amino acids such as cysteine, aromatic rings of phenylalanine, tyrosine, and tryptophan. Liao et al. (2018b) reported that the protein integrity was maintained during storage based on Ca²⁺-ATPase activity and total sulfhydryl group levels and confirmed the inhibition of natural actomyosin degradation in shrimps by PAW ice.

Zhang et al. (2016) evaluated the influence of proteins on the *Staphylococcus aureus* inactivation efficiency of PAW. Bovine serum albumin (BSA) was used as a protein source, and it significantly reduced the inactivation efficiency of PAW. The single sulfhydryl (SH) group amino acid residues of BSA reacts with OH[•], HO₂[•], O₂^{-•}, and peroxynitrites (ONOOH) radicals and scavenges the RONS present in the PAW. BSA acts as a nonspecific antioxidant during PAW disinfection, and it also provides a physical barrier for the bacteria. However, no such protective effect of proteins against bacterial inactivation was reported in protein containing liquid foods (Gurol et al., 2012; Jung et al., 2015a; Kim et al., 2015).

2.4.2.3 Changes in antioxidants

Antioxidants and the other secondary food metabolites such as polyphenols protect the cells against the deteriorative effects of ROS and RNS in the NTP (Elez et al., 2015). Antioxidants like ascorbic acid and vitamin E could protect *Escherichia coli* from oxidation-mediated death by scavenging reactive oxygen species (ROS) (Joshi et al., 2011).

An increase in Vitamin C and superoxide dismutase (SOD) level was observed in PAW treated mushrooms due to the natural cell defense mechanism against the oxidative stress caused by PAW (Xu et al., 2016). A similar increase in the anthocyanin content of Chinese bayberries and pomegranate juice as a defense mechanism against ROS species was reported by Ma et al. (2016) and Bursać et al. (2016b) respectively. Phenolic content particularly ellagic acid in pomegranate

juice increased after NTP treatment irrespective of the treatment time due to the breakage of cell membrane, hydrolysis and depolymerization of ellagitannins (Herceg et al., 2016). Elez et al. (2015) also stated an increase in the total phenolic content and total anthocyanin content in sour cherry juice due to the cell rupture which led to better extraction of these components. The phenol stability after NTP treatment was comparable to pasteurization in pomegranate juice, chokeberry juice and grape juice (Bursać et al., 2016a; Herceg et al., 2016; Pankaj et al., 2017).

On the other hand, Almeida et al. (2015) stated a 50% reduction in the antioxidant capacity of prebiotic orange juice upon 60 s direct exposure of NTP whereas, in indirect exposure, there was no significant difference in the antioxidant activity. The antioxidant content and total phenolic activity of apple juice reduced with an increase in input power and treatment time (Liao et al., 2018a). Grzegorzewski et al. (2011) and Elez et al. (2015) also reported the reduction in phenolic acid content, anthocyanin content and flavonoid content in lamb's lettuce and sour cherry juice respectively after NTP. The reduction in DPPH free radical scavenging and antioxidant capacity of the grape juice due to a loss of total phenolic and flavonoid content was reported by Pankaj et al. (2017). Loss of individual anthocyanin and phenolic acids was increased in sour cherry juice with an increase in treatment time and less degradation of anthocyanins and phenolic acids was observed when larger volumes of juice were treated by NTP (Elez et al., 2015). The ability of phenolic compounds to scavenge free radicals was speculated as the cause for the reduction in its content (Elez et al., 2015; Pankaj et al., 2017). NTP treatment of chokeberry juice resulted in lower stability of flavonols and anthocyanins, and improved stability of hydroxycinnamic acids and up to 23% loss of anthocyanins (Bursać et al., 2016a).

2.4.2.4 Changes in sensory characteristics

No change in milk color was observed after 15 min of corona discharge NTP treatment and a slight change in the perceivable color difference (ΔE) value was observed (0.52) after 20 min treatment (Gurol et al., 2012). In another study, Kim et al. (2015) reported an increase in L and b values of the milk and a slight difference (non-significant) in sensory quality of DBD plasma treated milk in comparison to non-treated milk. Bursać et al. (2016b) reported a slight, positive increase in the color of cloudy pomegranate juice after NTP treatment with respect to the gas flow rate. Almeida et al. (2015) observed a slight change in the chroma and lightness of prebiotic orange juice making it more vivid upon both direct and indirect exposure of DBD NTP. Dose dependent

degradation of color values was reported by Liao et al. (2018a) in apple juice. The total color difference was increased to 14.94 after 30 s NTP. They claimed that the polymerization of phenolic compounds and oxidation of pigments by the reactive species in NTP could be the cause of color change. Alves et al. (2016) compared the effect of ozone treatment and NTP treatment of orange juice using NMR and chemometric analysis. They stated that the ozone processing affects the aromatic compounds while NTP treatment affects the aliphatic compounds.

Jung et al. (2015b) used PAW to make meat batter, and the color development was comparable with the sodium nitrate treated meat batter samples based on a^* values and they recommended the use of PAW as an alternative to sodium nitrite in meat batter curing. In a similar study, Jung et al. (2015a) used alkalized PAW, in which the color development in meat sausages was equal to that of sodium nitrate and celery powder. The sensory qualities and texture of meat sausages cured by PAW had better results than the conventional sodium nitrate and celery powder cured sausages. In the case of shrimp, PAW-ice maintained the color better than that of tap water ice during 9 days of storage. PAW ice also reduced the melanosis in shrimps and the reduction in L^* value was less in PAW ice when compared to tap water ice (Liao et al., 2018b). PAW treatment maintained the L^* value in mushrooms, with a slight increase in b^* , a^* and ΔE values after 7 days storage. The firmness of PAW treated button mushrooms were ~10% and 17% better than untreated and water treated samples respectively, after storage (Xu et al., 2016). The color values of strawberry and grapes were not affected by PAW treatment (Guo et al., 2017; Ma et al., 2015) while there was an increase in the color values of Chinese bayberries and the color changed from red or violet to dark violet during storage after PAW treatment (Ma et al., 2016). The firmness of Chinese bayberries and strawberries was also maintained during storage due to less microbial spoilage (Ma et al., 2015; Ma et al., 2016). Increase in TSS of Chinese bayberries during storage after PAW treatment was observed by Ma et al. (2016) and they proposed that the decrease respiration rate in bayberries and subsequent sugar and acid consumption caused the increase in TSS.

2.4.2.5 *Changes in shelf life*

There was no increase in the microbial population in whole milk sample stored at 4°C for 6 weeks after NTP treatment for 9 min and 20 min (Gurol et al., 2012). The microbial population in 9 min treated milk samples were reduced during the storage and reached an undetectable level after 4 days of storage while for 20 min treated milk samples there was ~4 log CFU/ml reduction observed

within one day. They speculated on the stability of reactive species present in milk during storage for the reduction in the microbial population. PAW achieved 0.4 log reduction of fungi and a 0.8 log reduction of bacteria at day 0 and it could effectively inhibit the microbial contamination on Chinese bayberries for 8 days in storage (Ma et al., 2016). PAW could efficiently inhibit the growth of *Staphylococcus aureus* and fungal growth in strawberries during 6 days of storage while preserving other physicochemical quality parameters (Ma et al., 2015). Based on the storage stability of shrimps with PAW ice, Liao et al. (2018b) concluded that PAW can significantly improve the microbial safety and quality of foods and recommended PAW ice as an alternative preservation method for fresh produce.

2.5 Conclusion

Applications of PAW in food processing is a relatively new and fast-emerging field of study. Presence of water molecules during NTP treatment affects the chemistry of reactive species and interaction with target microorganisms. This review provides information on the different methods of treating liquids with NTP, the plasma-water chemistry, and the pathogen inactivation mechanism by the reactive species in NTP and PAW. Besides, the effect of PAW and NTP reactive species on food quality is also discussed in detail. The sparse and varying research outputs show the intricacies in the optimization of this technology for food disinfection. It is also evident from the review of the literature, that no continuous flow systems are being studied or developed for PAW generation. Research work on such continuous flow systems will increase their suitability in industrial application and detailed studies on PAW interactions with specific food materials is required to further develop this technology.

CONNECTING TEXT

It can be inferred from the literature review that PAW has the potential to be used as a disinfectant for fresh food disinfection. Dielectric barrier discharge is the commonly used method to produce NTP in food related studies as there is no direct contact of the electrodes in this case. Many research studies have focused on evaluating PAW and NTP treated solutions on disinfecting various food pathogenic microorganisms. Only limited studies have focused on exploring the effects of PAW and NTP reactive species on food components and food quality in detail. In Chapter 3, an attempt will be made to develop a continuous flow DBD PAW generation system. First, a preliminary DBD system was developed, and trial runs were made with the system. From the observations made from the preliminary system, changes were made to a modified DBD PAW generation system designed to operate with Argon/oxygen feed gas.

CHAPTER III

PRELIMINARY DESIGN AND DEVELOPMENT OF A DIELECTRIC BARRIER DISCHARGE PLASMA ACTIVATED WATER GENERATION SYSTEM

Abstract

The Plasma Activated Water (PAW) contains all the reactive species of gas plasma which makes PAW a strong disinfectant. In this study, a preliminary, plate type dielectric barrier discharge reactor was designed to produce plasma activated water. Argon and oxygen gases were used as carrier gas to produce the NTP. To analyse the effects of the process factors on PAW properties, and to optimize the process conditions, Response Surface Methodology (RSM) with face-centered central composite design (CCD) ($\alpha=1$) was used for this study. The factors used for the optimization of PAW were treatment time, gas flow rate and water flow rate. The response variables used for the optimization of PAW process conditions were pH, oxidation reduction potential (ORP), electrical conductivity and hydrogen peroxide. The results indicated that the hydrogen peroxide concentration in PAW is affected by time by linear effect. pH and gas flow rate did not have any linear effect on H₂O₂ concentration, however there was a significant interaction effect of pH and treatment time.

3.1 Introduction

Nonthermal plasma (NTP) is a partially ionized gas produced through a high voltage electrical discharge. Based on the electrical discharge type, NTP can be produced by various discharge types such as corona discharge, gliding arc discharge and dielectric barrier discharge (DBD). Among these, DBD is preferred due to its simple electrode configuration and its ability to produce stable plasma discharge (Tang et al., 2018). Due to larger surface area, the reactive species produced by the DBD discharge are greater than that of glow discharges produced by plasma torches (Leduc et al., 2010). Homogenous discharge can be produced in DBD discharge system by using gases like helium or argon in the feed gas (Bruggeman & Leys, 2009; Kogelschatz, 2003). In DBD discharge system, the discharge is ignited between the high voltage and ground electrodes covered with the dielectric barrier material. The dielectric layer prevents the direct contact between the electrodes

during discharge, thus preventing electrode damage (Kogelschatz, 2003). In this study DBD discharge was used to produce plasma. In most of the food applications, non-continuous batch type systems are used to activate liquid substrates like water, fruit juices, milk etc. However, to harness the complete potential of this technology at the industrial scale, a continuous production system and its efficiency in producing a highly reactive PAW shall be studied. Different continuous NTP liquid treatment systems have been reported in studies related to the degradation of pollutants and dyes from water (Zeghioud et al., 2020).

3.2 Design considerations

In this work, a falling film continuous flow co-planar, symmetrical DBD reactor was initially conceptualized and tested. However, due to non-uniformity in the water flow and difficulties in having a dielectric barrier over the inner electrode without a gap, a symmetrical parallel plate planar DBD configuration was used to generate a filamentary discharge in the gas gap between the two electrodes.

The following design considerations were made in the development of the DBD discharge PAW generation system.

1. Dielectric barrier discharge plasma generation system which can work under atmospheric pressure and at voltages less than 10 kV.
2. Continuous flow of water in the reactor with at least 100 ml of water per batch capacity.
3. Maximum coverage of the discharge by the liquid to improve the transfer of reactive species from NTP.
4. Flexible system to facilitate the changes in gas flow rate, water flow rate and capable of running for 60 min without interruption.
5. Safe access to the treated liquid during operation.

3.3 Preliminary Configuration

3.3.1 Reactor design

According to the design considerations, a preliminary design of a planar DBD reactor was developed and the design of the reactor, schematic diagram and the experimental setup are given in Figures 3.1, 3.2, and 3.3 respectively. The system was made of acrylic, and copper foil was used as the electrodes with 2 mm thick quartz glass plates (permittivity $\epsilon_r = 4.9$) that were used as the

dielectric barrier to avoid the arc or streamer discharges between the electrodes. The surface areas of the high voltage electrode and ground electrode are $6 \times 10^{-3} \text{ m}^2$ and $15 \times 10^{-3} \text{ m}^2$ respectively. Two cylinders were used as the water reservoirs at the beginning and end of the reactor. The electrodes were pasted over the glass plates and a 4 mm gap was maintained between the plates by inserting an acrylic spacer between the plates. The high voltage and ground supplies from the high voltage generator were glued on to the electrodes using electrically conductive adhesive. Two acrylic cylinders of 50 mm diameter were used as the gas and water inlet and outlet reservoirs and were attached to the dielectric barrier plates. The provisions for gas and water supply to and from the reservoir were given on the upper and lower parts of the cylinders respectively. The water was pumped using a peristaltic pump with a flow rate of 125 ml/min. The whole setup was mounted on a clamp holder with prongs at an angle of 20-30°. Premixed Ar (98%) O₂ (2%) gas mixture was supplied into the system at different flow rates according to the chosen experimental conditions.

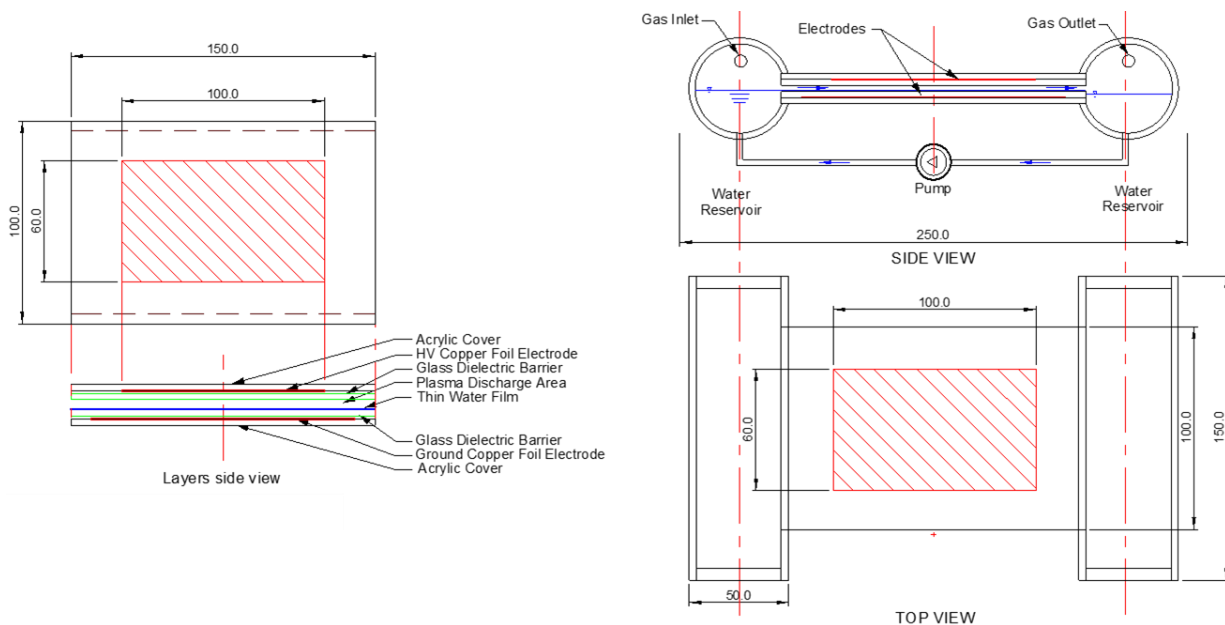


Figure 3.1 Design of dielectric barrier discharge PAW generator

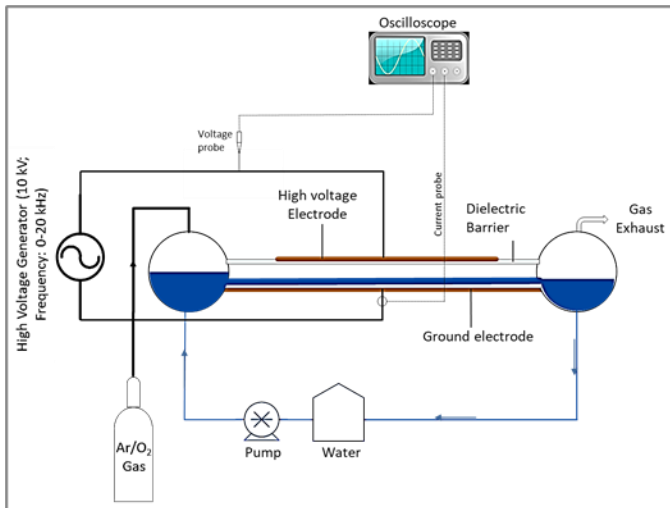


Figure 3.2a: Schematic representation of experimental setup

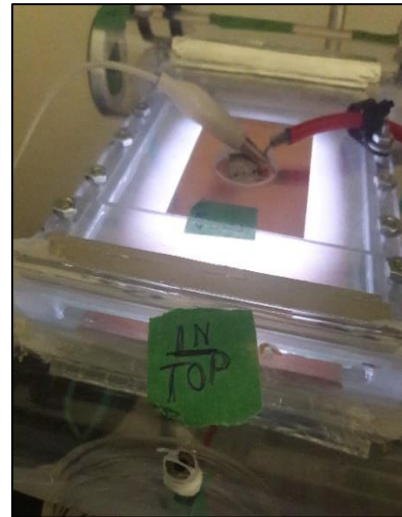


Figure 3.2b: Picture of Dielectric Barrier Discharge

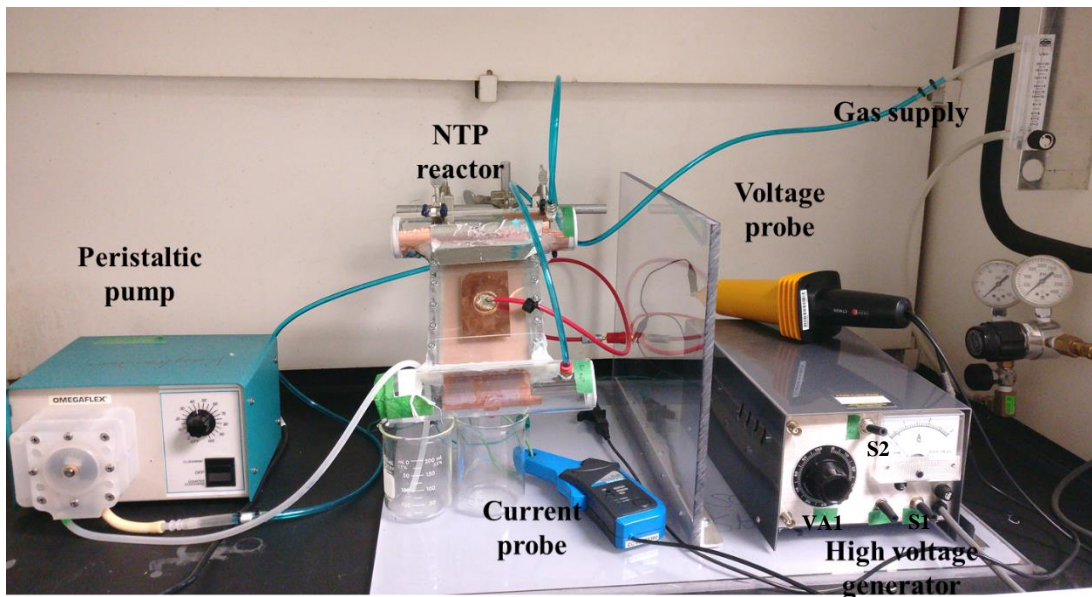


Figure 3.3: Experimental set-up of preliminary continuous flow DBD PAW generation system

3.3.2 Electrical system

For the power supply, a high voltage generator (PVM 500, Information Unlimited, Amherst, USA) which can produce 10 kV (peak-to-peak) voltage at 0-20 kHz frequency was used. A high voltage probe (Cal Tec CT4026, 1000X, 150 MHz) and a current probe (CC650,10X) were used to measure the voltage and current in the reactor during discharge. The complete system was placed inside a fume hood and proper safety precautions were followed while working with the high voltage generator. The voltage-current waveforms were monitored using a two-channel digital oscilloscope (Agilent Infinium 54833D MSO).

For the planar configuration the capacitance of the dielectric barrier (C_d), gas gap (C_g) and the dielectric barrier cell (C_{cell}) were calculated using equations 3.1 to 3.3 ((Flores-Fuentes et al., 2009; Pipa et al., 2012).

$$C_d = \frac{\epsilon_0 k_1 A}{d} \quad \text{--- --- --- --- ---} \quad (3.1)$$

$$C_g = \frac{\epsilon_0 k_2 A}{d} \quad \text{--- --- --- --- ---} \quad (3.2)$$

$$C_{cell} = \frac{C_d C_g}{C_d + C_g} \quad \text{--- --- --- --- ---} \quad (3.3)$$

Where, ϵ_0 - permittivity of vacuum ($8.854 \times 10^{-12} \text{ Fm}^{-1}$)

k_1 – dielectric constant of dielectric material

k_2 – dielectric constant of working gas

d – thickness of dielectric barrier (m)

g – thickness of discharge gap (m)

A – electrode area (m^2)

3.3.3 PAW preparation

For PAW preparation, 150 ml of distilled water was circulated into the system using a peristaltic pump. The feed gas flow rate was adjusted by a flowmeter attached on the supply line. Before switching on the electrical system, the reactor was run with gas and water to wet the glass surface and to saturate the discharge gap with feed gas. To start the system, the high-voltage power supply and the oscilloscope were switched on. On the power supply unit (Fig. 3.3), the S1/frequency switch was turned on and kept at the maximum to achieve the maximum frequency of 20 kHz. The

voltage control (VA1) was then turned to 90 and then the S2 switch was kept at HI to double the voltage in the system. The voltage control knob was then adjusted to keep the supply voltage at 10 kV (peak-peak) which was read from the oscilloscope. At around 1 kV applied voltage weak discharges were observed between the electrodes.

3.4 Methods

3.4.1 Evaluation of PAW physicochemical properties

The chemical composition of PAW depends on the production method and process conditions (Thirumdas et al., 2018). It is possible to alter the PAW characteristics by changing the operating conditions. It is evident from the literature review, that the most important factors affecting the chemical properties of DBD PAW are the discharge gap, voltage, treatment time, pH of water, gas composition and gas flow rate. For pH adjustment, nitric acid was used to lower the pH of water and sodium hydroxide was used to increase the pH. To analyze the combined effects of some of these factors on PAW properties, and to optimize the process conditions, Response Surface Methodology (RSM) with face-centered central composite design (CCD) ($\alpha=1$) was used for the study. Due to the physical limitations in the system design, the discharge gap and voltage were kept constant in this study. The factors used for the optimization of PAW were treatment time, gas flow rate and pH, which were chosen based on previous published reports (Baek et al., 2016; Hosseinpour et al., 2019; Zhou et al., 2018). The liquid flow rate was kept constant as 125 ml/min and the treatment time was varied. The factors and their levels are given in Table 3.1. The dependent variables used for the preliminary optimization of PAW process conditions were pH, oxidation reduction potential (ORP), electrical conductivity and hydrogen peroxide. Five center points were used in the design and second order polynomial model (equation 3.4) was used to fit the data of each response variable.

$$Y = \beta_0 + \beta_1 X_1 + \beta_2 X_2 + \beta_3 X_3 + \beta_{12} X_1 X_2 + \beta_{13} X_1 X_3 + \beta_{23} X_2 X_3 + \beta_{11} X_1^2 + \beta_{22} X_2^2 + \beta_{33} X_3^2 \quad (3.4)$$

Where, β_0 is constant (intercept), $\beta_1, \beta_2, \beta_3, \beta_{12}, \beta_{23}, \beta_{11}, \beta_{22}$ and β_{33} are regression coefficients and X_1, X_2, X_3 are independent factors. The significance of each factor in the model was analyzed using analysis of variance (ANOVA) for each response.

Table 3.1 Experimental design for process optimization of preliminary setup

Factors	Levels			Response Variables
	-1	0	1	
pH (x_1)	4	6	8	•Hydrogen peroxide (H_2O_2) concentration (μM)
Time (min) (x_2)	10	20	30	
Gas Flow Rate (slm) (x_3)	6	9	12	•pH, ORP(mV) and EC (μS)

3.4.2 NTP gas analysis using FTIR

The reactive species generated by the NTP in gas phase was determined using FTIR (Nicolet iS5, Thermo Scientific) according to the method described in Sivachandiran and Khacef (2017) with some modifications. Accordingly, the discharge gas was collected from the system and using the 10 cm gas cell and the spectra were collected with 30 scans per spectrum. The background spectrum was collected under air with 16 scans per spectrum.

3.4.3 UV Absorption spectroscopy measurement of PAW reactive species

Presence of reactive species in PAW has been determined by optical absorbance measurement in the UV region (190-450 nm) using a UV-VIS spectrophotometer according to the method described in (Dascalu et al., 2019). Deionized water was used as a reference and the absorption spectra of PAW was read from 190-450 nm. The whole absorption spectrum was used as a measure of concentration of reactive species in PAW.

3.4.4 Determination of pH, ORP and electrical conductivity

pH, ORP and electrical conductivity were analyzed immediately after PAW generation. pH and ORP were measured using Reed (SD-230-KIT2) ORP/pH meter, while the temperature and electrical conductivity were measured using a Hanna EC meter (HI98129). The measuring range and accuracy of the Reed meter is 0.00 to 14.00 (± 0.02) for pH and 0-1999 mV $\pm (0.5\%)$ for ORP. The measuring range and accuracy of the Hanna EC meter is 0 to 3999 $\mu S/cm \pm 2\%$ for EC and 0.0 to 60.0°C $\pm 0.5^\circ C$ for temperature.

3.4.5 Determination of hydrogen peroxide

A titanium oxysulfate spectrometric method was used for the hydrogen peroxide assay in PAW based on the methods given by Eisenberg (1943) and Satterfield and Bonnell (1955) with slight

modifications. Briefly, immediately after PAW generation, 1 ml of sodium azide (60 mM) was added to 10 ml of PAW to avoid the degradation of peroxides by the nitrates and nitrites. Then 5 ml of titanium sulfate reagent was added to the sample. If the sample contains peroxides, it will produce a yellow color. This color development was measured using a UV-Vis spectrophotometer at 407 nm. All measurements were performed in triplicates. The amount of hydrogen peroxide in the PAW samples was read from a produced standard curve.

3.5 Characterization of preliminary PAW reactor

3.5.1 Electrical characteristics

The capacitance of the dielectric barrier, gas gap and the dielectric barrier cell was calculated as 49.8 pF, 23.4 pF and 15.91 pF respectively. The discharge characteristics of the plasma was studied based on the applied voltage and the corresponding discharge current values. The gas gap voltage was calculated using equation (3). At atmospheric pressure, the breakdown voltages with gas plasma and gas plasma with water circulation were recorded. It could be seen from the voltage-current waveform (Figure 3.4) showing sinusoidal wave following a high voltage (kV) and low current (mA) in the range of 15-20 kHz frequency attributing to glow-filamentary discharges. The first spike in the current (Figure 3.4a) happened during the first half-cycle of the applied voltage giving the breakdown voltage of Ar/O₂ as ~0.9kV at the given gas gap of 3 mm. The current waveform without individual spike indicates the glow micro discharges in the plasma region (Zhao et al., 2018). The two spikes in the gas discharge indicate a pseudo glow discharge (Figure 3.4a) and the uniform current waveform with water indicates the homogenous glow discharge in water (Figure 3.4b) (Gadkari & Gu, 2017). This was attributed to the increase in the moisture level in the discharge gap due to the vapor pressure of water, which increased the breakdown voltage (~3kV).

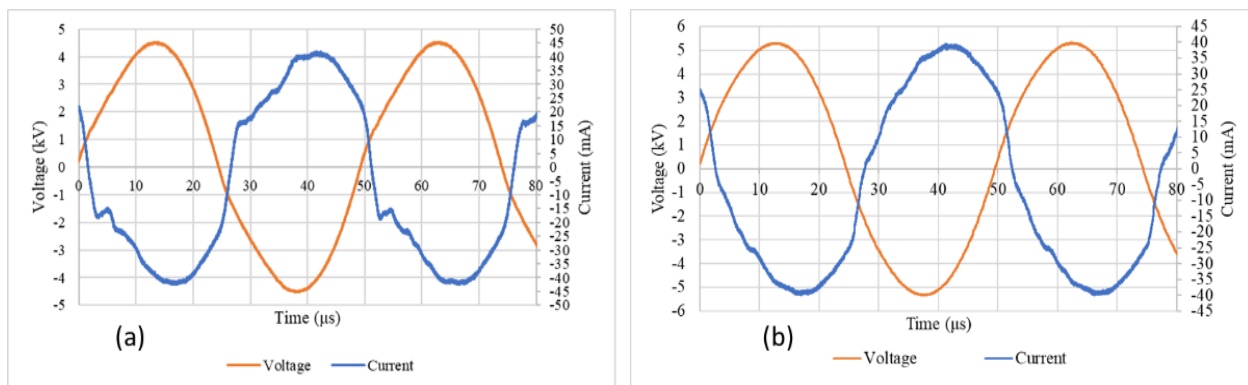


Figure 3.4. Voltage current characteristics measures at 9 slm gas flow rate, for
 (a) gas phase plasma (b) PAW

3.5.2 NTP gas phase analysis

The gas from the exhaust of the system was analysed using FTIR, to identify the reactive species produced in the gas phase during ionization. The gas was collected during 20 min NTP treatment at 9 slm gas flow rate. There was at least 10 min time difference between the gas collection and the gas analysis. Atmospheric air environment was used to capture the background spectrum. Figure 3.5 shows the FTIR spectrum of exhaust gas obtained for different water pH. The important stable species identified were nitrous oxide (N_2O), ozone (O_3) and radicals like OH. Strong nitrogen species were found with water treatment at pH 8 due to the addition of sodium nitrate to increase the pH. However, less nitrogen species was found with pH 4 despite using nitric acid to reduce the pH of water.

3.5.3 UV absorption spectra of PAW

To identify the diffused reactive species in water, UV absorption spectra of the PAW was recorded for different treatment times and different gas flow rates. The water flow rate was used as 100 ml/min and, the gas flow rate 6 slm gas flow rate was used for Figure 3.6(a). The spectra was deconvoluted to a sum of individual Gaussian absorption peaks (Dascalu et al., 2019) using the Spectrograph software (trial version). There was a time gap of 10 min between the treatment and UV-vis measurements. It could be seen from Figure 3.6 that after the 390 nm wavelength, the spectra were almost identical. The stable reactive species like H_2O_2 , NO_2 and NO_3 have the absorption spectral range of 200- 340 nm (Jun-Seok et al., 2018). Further, due to the time delay between the treatment and measurement, the short-lived species like hydroxyl radicals, peroxy nitrates are expected to have been extinguished. The absorption peaks from 190-390 nm

indicated the presence of reactive oxygen and nitrogen species (RONS) and O₂ while peaks at 250-265 nm show the presence of ozone (Jun-Seok et al., 2018). It is evident from the figure that the treatment time linearly increased the concentration of RONS in PAW.

There was a slight shift in the peak of the 30 min treatment indicating the increase in dissolved ozone concentration in PAW. In the case of gas flow rate, the broader area under 9 slm gas flow rate shows the increase in the diffusion of gas species into the liquid phase. The reduction in contact time between the reactive species and water at 12 slm gas flow rate could have resulted in a reduced diffusion of species, thus giving a lower absorption spectrum area. The results are in accordance with Dascalu et al. (2019), who stated that, diffusion of reactive species from gas phase to liquid phase is a relatively slow process and a longer residence time of gas species with liquid is required to increase the concentration of reactive species in water.

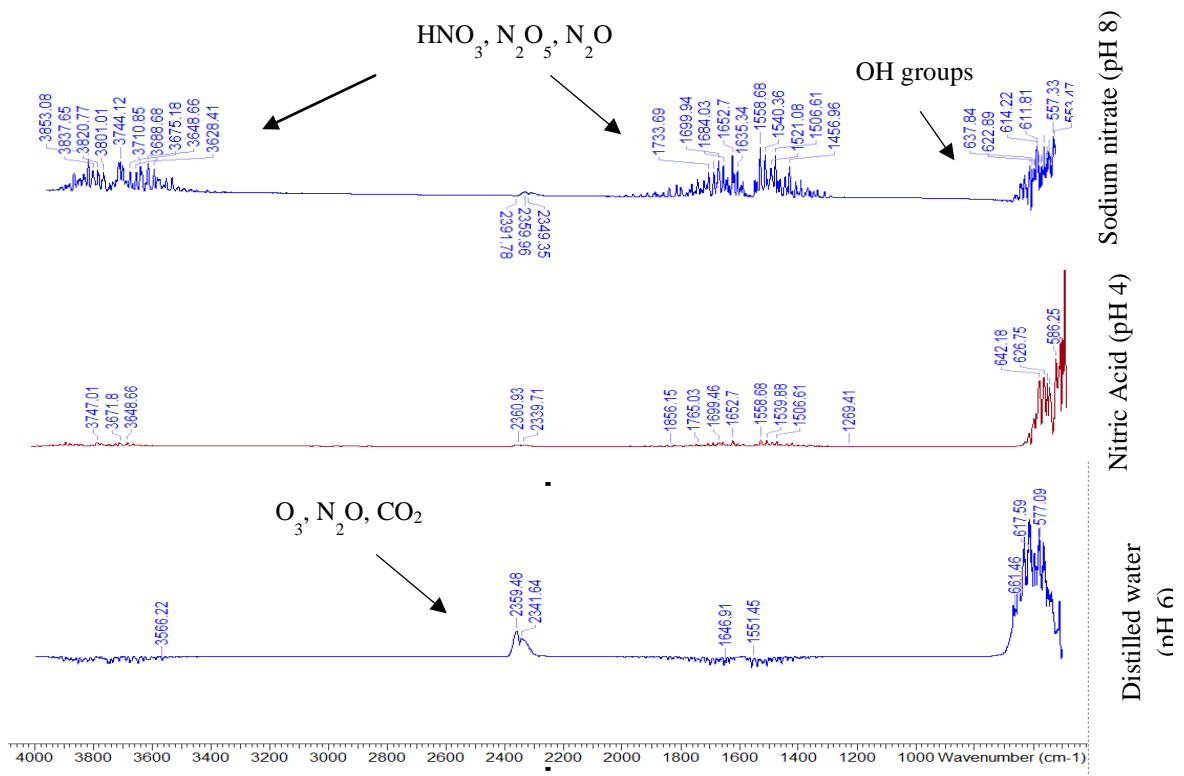


Figure 3.5. NTP gas species – FTIR spectrum (After 20 min treatment at 9slm gas

$$PAW\ pH = 5.68 + 1.2x_1 - 0.004x_2 + 0.01x_3 - 0.12x_1 + 0.06x_1x_3 + 0.09x_2x_3 - 0.29x_1^2 + 0.9x_2^2 + 0.1x_3^2 \quad \text{--- (3.6)}$$

$$Electrical\ conductivity\ \left(\frac{\mu S}{cm}\right) = 7.21 - 1532x_1 - 1.7x_2 - 1.21x_3 + 2x_1x_2 + 1.25x_1x_3 - 1.5x_2x_3 + 18.7x_1^2 - 0.9x_2^2 + 0.6x_3^2 \quad \text{--- (3.7)}$$

$$ORP\ (mV) = 78.18 - 71.34x_1 - 0.78x_2 - 5.57x_3 + 7.11x_1x_2 - 2.63x_1x_3 - 6.18x_2x_3 + 19.92x_1^2 - 3.26x_2^2 - 2.96x_3^2 \quad \text{--- (3.8)}$$

Table 3.2 Coded factors and the corresponding experimental results of response variables

Run	X1 (pH)	X2 (time)	X3 (gas flow rate)	PAW pH	ORP (mV)	EC (μS/cm)	H ₂ O ₂ (μM)
1	-1	-1	-1	4.3	166.6	45	587.30
2	-1	-1	1	4.13	175.5	45	268.79
3	-1	0	0	4.22	172.2	41	858.03
4	-1	1	-1	4.34	164.5	41	815.57
5	-1	1	1	4.69	143.6	32	1213.71
6	0	-1	0	6.11	59.0	5	720.01
7	0	0	-1	5.87	74.1	9	884.58
8	0	0	0	5.91	71.4	4.5	1229.63
9	0	0	0	5.3	84.6	12	1532.22
10	0	0	0	5.86	73.3	6	1011.98
11	0	0	0	5.3	104.0	9	1086.30
12	0	0	0	5.3	83.33	7.8	1215.03
13	0	0	1	6.05	63.5	5	1086.30
14	0	1	0	5.8	78.0	6	1452.59
15	1	-1	-1	6.68	22.06	10	290.02
16	1	-1	1	6.9	15.36	12	327.18
17	1	0	0	6.93	11.17	9	889.89
18	1	1	-1	6.42	43.36	11	1675.55
19	1	1	1	6.83	16.95	10	1272.10

It can be seen from equations 5-8, that the hydrogen peroxide concentration in PAW is affected by time with a linear effect. pH and gas flow rate did not have any linear effect on H₂O₂ concentration, however there was a significant interaction effect of pH and treatment time. The PAW pH (after treatment) was not affected by any linear or interactive effects except for the initial pH. This could be due to the influence of addition of nitric acid and sodium nitrate which were added to alter the pH of water.

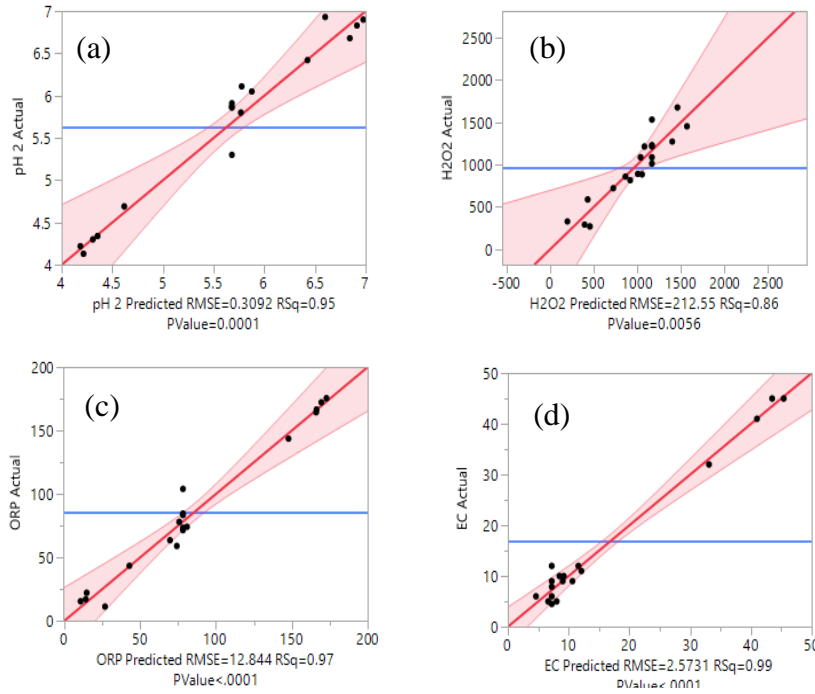
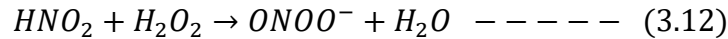
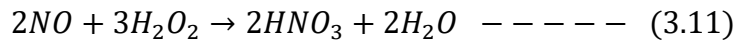
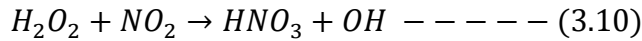
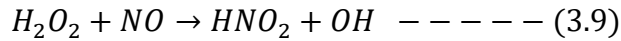


Figure 3.7. Predicted Vs experimental values of PAW (a) pH (b) H₂O₂ (c) ORP (d) Electrical Conductivity (EC)

The nitrites present in the liquid disintegrate the hydrogen peroxide and consume hydroxyl radical in water thus preventing the formation of hydrogen peroxide in water (Tian et al., 2015). Since the addition of HNO₃ and NaNO₃, to alter the pH, induced the production of nitrates and nitrites in PAW, the effect of pH on hydrogen peroxide at different pH levels was diminished. Gas flow rate had a significant linear and interactive effect on the electrical conductivity of PAW. ORP of PAW had a linear effect on water pH and significant interaction effect on time and gas flow rate. The predicted values and experimental values of the responses are compared in Figure 3.7. It is evident from the coefficient of determination (R²) that the predictability of the regression models is statistically significant (p<0.05%) with non-significant lack of fit.

The response profiles of PAW variables and the desirability curves are given in Figure 3.8. The interaction of time and pH showed a maximum effect on PAW hydrogen peroxide concentration (Figure 3.8a). It is also evident that the maximum hydrogen peroxide content was obtained when the pH was around 7. This indicated that addition of nitrogen compounds to alter the pH induced the production of reactive nitrogen species in PAW. These reactive species reduced the production of hydrogen peroxide by consuming the hydroxyl radicals and denaturing the hydrogen peroxide into water through the reactions in equations (3.9–3.12) (Jung et al., 2015a).



Similar trend was found with gas flowrate and pH interaction effect on H₂O₂ concentration. Increase in gas flow rate above 9 slm led to the reduction in the hydrogen peroxide concentration. However, previous results showed (Van Boxem et al., 2017) an increase in hydrogen peroxide concentration with an increase in the gas flow rate in the range of 1-3 slm. Van Boxem et al. (2017) claimed that the formation of hydrogen peroxide in water depends on (a) direct diffusion of H₂O₂ from the gas phase to the liquid phase, and (b) recombination of two OH radicals to form H₂O₂ in water. Since the gas flow rates are very high compared to the one used in the above study, the formation of OH radicals would be greater; however, it might not have reached the liquid to form hydrogen peroxide. Further the presence of nitrogen at pH 4 and pH 8 is also speculated to be the cause of reduction in H₂O₂ concentration.

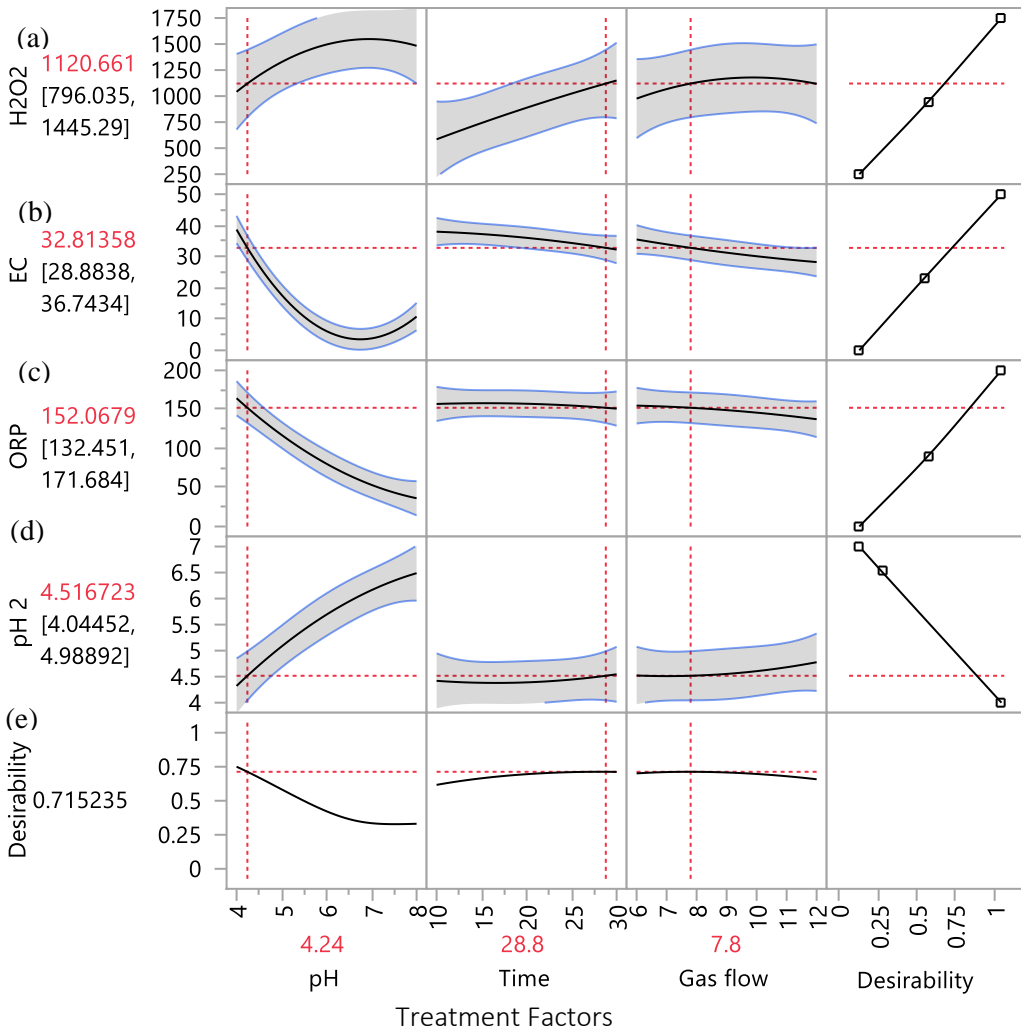


Figure 3.8 Response profiles of treatment factors on PAW (a) Hydrogen peroxide concentration (μM), (b) electrical conductivity ($\mu\text{S}/\text{cm}$), (c) ORP (mV) and (d) post-treatment pH (e) desirability function

The increase in the pH of PAW was observed with an increase in the gas flow rate and the optimum gas flow rate from the model was estimated as 9 slm (Fig. 3.8). In all cases, treatment time has a significant influence on all response variables. The optimum values of the process parameters for each of the dependent variables were determined using desirability function (Fig. 3.8). The optimum points of H_2O_2 , EC, ORP and PAW pH (pH 2) were estimated as 1120.7 μM , 32.8 $\mu\text{S}/\text{cm}$, 152.1 mV and 4.5 respectively for 28.8 min treatment time, 4.24 water pH and 7.8 slm gas flow rate with the corresponding desirability value of 0.72. However, it was found that the addition of nitrogen compounds to water, for adjusting pH, had significant effect on the PAW chemical

properties. To get further insight, additional investigation will be conducted using other physical process conditions such as water flow rate, voltage, etc., for optimizing PAW production.

3.6 Remodeling the Preliminary System

After running the trial experiments in the preliminary system, the following observations were made.

1. The system was able to produce nonthermal plasma in 3 kV range with Ar/O₂ gas mixture with the high voltage generator
2. The electrode sizes were broad enough to produce a wide discharge area
3. Due to the rigid connection of top and bottom plates, the ground side dielectric barrier glass plate was breaking when the system was run for more than 10 min.
4. Formation of rivulet flow channels was caused by the wider plate and low velocity of water
5. Less coverage of discharge section by water was due to the rivulet flow condition
6. Adding chemicals such as nitric acid and sodium hydroxide, to adjust the pH of water before treatment, increased the complexity in understanding the effect of processes variables and reactive species formation in PAW.

3.6.1 Design of an improved PAW reactor

To overcome the issues such as breakage of glass plate and formation of rivulet flow, a modified reactor was designed (Figure 3.9) without any rigid fixtures. For this modified system, a rectangular glass section with 3 mm internal spacing was used with gas and water inlets attached on the top. To avoid a thick rivulet flow with low wetted area, the width of the plate was reduced from 80 mm to 50 mm and the length of the plate was increased from 150 mm to 300 mm. Further the inlet of water to the system was moved to the top, for producing a complete wetted area throughout the electrode length. Also, instead of a peristaltic pump, a submersible aquarium pump was used to have constant flow of water in the reactor. The experimental setup of the new PAW generation system is shown in Figure 3.10.

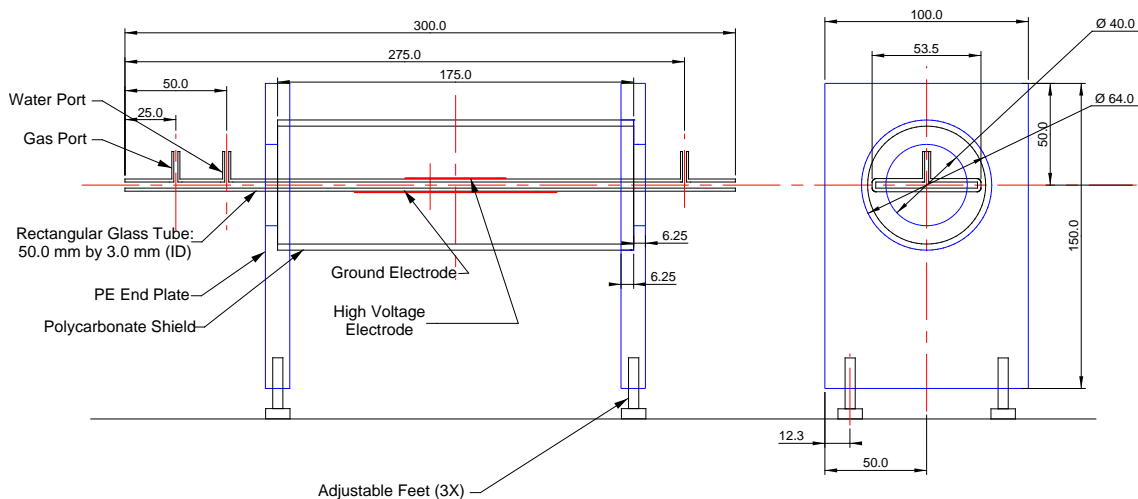


Figure 3.9 Design of remodeled DBD-PAW system (All dimensions are in mm)

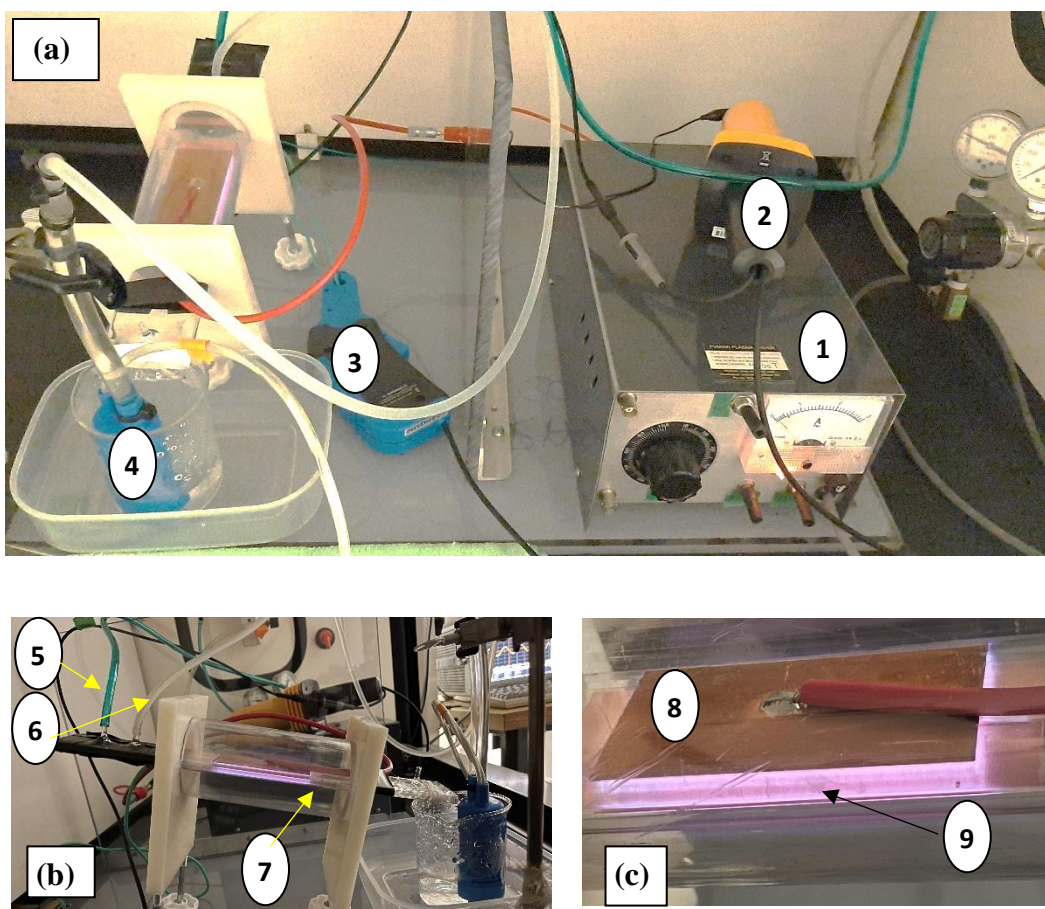


Figure 3.10 Remodeled PAW generation system (a) experimental set up (b) reactor section and (c) discharge inside the glass section; (1) High voltage generator, 2. Voltage probe, 3. Current probe, 4. Pump, 5. Gas inlet, 6. Water inlet, 7. Reactor glass section, 8. High voltage electrode, 9. DBD discharge.

3.7 Summary

Based on the literature review and its design simplicity, a dielectric barrier discharge concept was chosen to produce nonthermal plasma in this study. Accordingly, a preliminary PAW reactor was designed, developed, and tested, and argon/oxygen gas mixture was used to produce the nonthermal plasma in the discharge gap. From the PAW optimization studies it was found that adding chemicals to adjust the pH of the liquid altered the formation of hydrogen peroxide in PAW. Further, from the observations made during the preliminary studies, the discharge was not covered efficiently by water during treatment. Therefore, modifications were made in the reactor to improve the system's performance. Characterization of PAW produced in the remodeled system is discussed in detail in Chapter IV.

CONNECTING TEXT

As described in Chapter III, the dielectric barrier discharge was produced with Argon/Oxygen gas mixture at 3 kV voltage. To overcome the breakage of DBD glass and to have uniform flow of water over the plates, the preliminary reactor was redesigned. In chapter IV, the characteristics of the new PAW generation system are evaluated. The voltage-current characteristics of the discharge at different gas flow rates was examined along with the gas species analysis using FTIR spectrum. Then the effect of PAW activation time and post-activation time on PAW properties in terms of hydrogen peroxide concentration, ozone concentration, pH and *Escherichia coli* inactivation were analyzed. Further, the process parameters were optimized based on H₂O₂ and O₃ concentrations using Box-Behnken design.

CHAPTER IV

EVALUATION OF PLASMA ACTIVATED WATER CHARACTERISTICS, ANTIMICROBIAL PROPERTY, TIME STABILITY AND PROCESS OPTIMIZATION

4.1 Abstract

Plasma activated water (PAW) is an emerging technology for the disinfection of foods and it is also widely evaluated for its applications in medicine. The long-lived reactive oxygen species such as hydrogen peroxide and ozone are mainly responsible for the disinfecting properties of Ar/O₂ produced PAW. In this study, PAW characteristics were evaluated with respect to the process conditions and the post-treatment time to understand the effect of process conditions and the time stability of PAW. PAW was generated using a continuous flow dielectric barrier discharge Ar/O₂ atmospheric pressure plasma system at different PAW treatment times. PAW properties were evaluated based on the concentration of hydrogen peroxide, ozone, pH, and the disinfection of *Escherichia coli*. From the time stability analysis, it was found that the hydrogen peroxide was more stable than ozone in PAW when stored at room temperature for 2 days. The *E. coli* inactivation was mainly attributed to the ozone concentration than H₂O₂ or pH. The Box-Behnken design was adopted to optimize the operating conditions viz., water flow rate, plasma treatment time and gas flow rate. The optimum condition was found to be 104 ml/min water flow rate, 20 min plasma treatment time and 4 slm gas flow rate.

4.2. Introduction

In recent years, the consumption of fresh fruits and vegetables and ready-to-eat fresh-cut products, has increased due to their contribution to a healthy lifestyle and convenience. On the other side, 51.7% of the foodborne disease outbreaks are related to leafy vegetables and 27.8% are related to soft fruits (Machado-Moreira et al., 2019). This could be due to the post-processing contamination, ineffective washing and disinfection process and development of resistance in pathogenic microorganisms against the active components in the commonly used chemical disinfectants (Callejón et al., 2015). This indicates the limitations in the existing fresh food disinfection methods. Further, the conventional chemical disinfectants such as chlorine and quaternary ammonium salts leave residues on the food material which may pose health risks to the consumers.

Atmospheric pressure nonthermal plasma (NTP) is an emerging field in food processing which is being extensively researched for its suitability in food surface disinfection and functionalization. In addition to atmospheric pressure NTP, plasma functionalized water also known as Plasma Activated Water (PAW) is being investigated in larger extent for the disinfection of fresh and ready-to-eat fresh-cut produce (Schnabel et al., 2021; Thirumdas et al., 2018). Apart from food disinfection, PAW is also reported to be successful in degrading pesticide residues from food materials, applications in biomedicine (Kaushik et al., 2018; Zhou et al., 2020), seed germination, plant growth regulation, and pest and disease control in agriculture (Sajib et al., 2020). As the reactive species in PAW are transient and decompose in the water during storage, it has been considered as a green disinfectant (Zhou et al., 2018).

Plasma activated water is generated by treating water with nonthermal plasma either directly in contact with water or indirectly. Through this process, reactive species from the gas plasma are transferred to water through various physicochemical processes like penetration, diffusion and reactions between reactive species and water molecules (Bruggeman et al., 2016). The concentration of reactive species in PAW highly depends on the PAW production method and process conditions (Tian et al., 2015). When plasma is created directly inside water or water is placed in the discharge gap of the plasma system, the reaction efficiency is very high. However, in-water reaction kinetics are very complex, and not yet completely understood (Bruggeman et al., 2016; Oehmigen et al., 2011a). Further, treatment of living cells in medical and food applications is possible; however, this method is not preferred due to drastic cell damage (Stoffels et al., 2008). In indirect plasma applications, gas-phase plasma is generated at plasma-liquid interface, where reactive species are transferred into the liquid by diffusion. This facilitates better understanding and control over the transfer of reactive species from gas phase plasma to liquid phase (Bruggeman et al., 2016).

Among the reactive species, hydrogen peroxide and ozone are the two major reactive oxygen species responsible for the disinfection characteristics of PAW produced by Argon/oxygen NTP (Matthew et al., 2011; Pavlovich et al., 2013). Post-treatment stability of these reactive species is also important to determine the storability and the residual effect of these species on food material (Niquet et al., 2018). The process parameters like the discharge type feed gas composition, exposure time, gas flow rate, discharge gap and power densities influence the reactive species

concentration and the disinfection characteristics of PAW (Surowsky et al., 2015), (Royintarat et al., 2019). Ercan et al. (2013) conducted an accelerated storage study of plasma activated liquids (PAL) and reported that plasma activated N-actyle-cysteine in phosphate buffered saline solution retained its antimicrobial property for up to two years at room temperature. They speculated that the antimicrobial property was not just by the reactive species produced during the plasma treatment of the PAL but generation of additional species after plasma treatment. In another study, Niquet et al. (2018) compared the antimicrobial properties of PAW generated by two different plasma systems, namely microwave and dielectric barrier discharge. They reported that in both cases the antimicrobial activity of PAW was lost within days and the antimicrobial property was dependent on the discharge type, gas composition, electrode configuration, etc. They also reported that the antimicrobial property of PAW cannot be generalized, and system specific characterization of PAW is required.

The objective of this work to evaluate the effect of NTP activation time on the disinfection properties and physicochemical properties of PAW. Further, the effect of post-treatment time on these properties was also evaluated. To understand the influence of the system and process parameters on the PAW characteristics, an optimization study was conducted in a continuous flow DBD PAW system.

4.3. Materials and Methods

4.3.1 PAW generation system

In this study, an asymmetrical parallel plate planar configuration DBD atmospheric pressure NTP system was developed (Figure 4.1). Copper foil was used as the electrode and 2 mm thick quartz glass plates (permittivity $\epsilon_r = 4.9$), were used as the dielectric barrier to avoid arc or streamer discharges between the electrodes. The area of high voltage electrode and ground electrode was $4 \times 10^{-3} \text{ m}^2$ and $8 \times 10^{-3} \text{ m}^2$ respectively. The electrodes were pasted over a rectangular glass section $300 \times 50 \text{ mm}$ with 3 mm internal gap. Premixed Ar (98%) O₂ (2%) gas mixture was supplied into the system at different flow rates according to the chosen experimental conditions. Water was circulated in the glass section using a propeller pump and a flow controller was used to adjust the water flow rate. For power supply, a high voltage generator (PVM 500) which can produce up to 10 kV (peak-to-peak) voltage and 0-20 kHz frequency was used. A high voltage probe (Cal Tec

CT4026, 1000X, 150MHz) and a current probe (Hantek CC650, 10X) were used to measure the voltage and current in the reactor during discharge. The voltage-current waveforms are monitored using a two-channel digital oscilloscope (Agilent Infinium 54833D MSO).

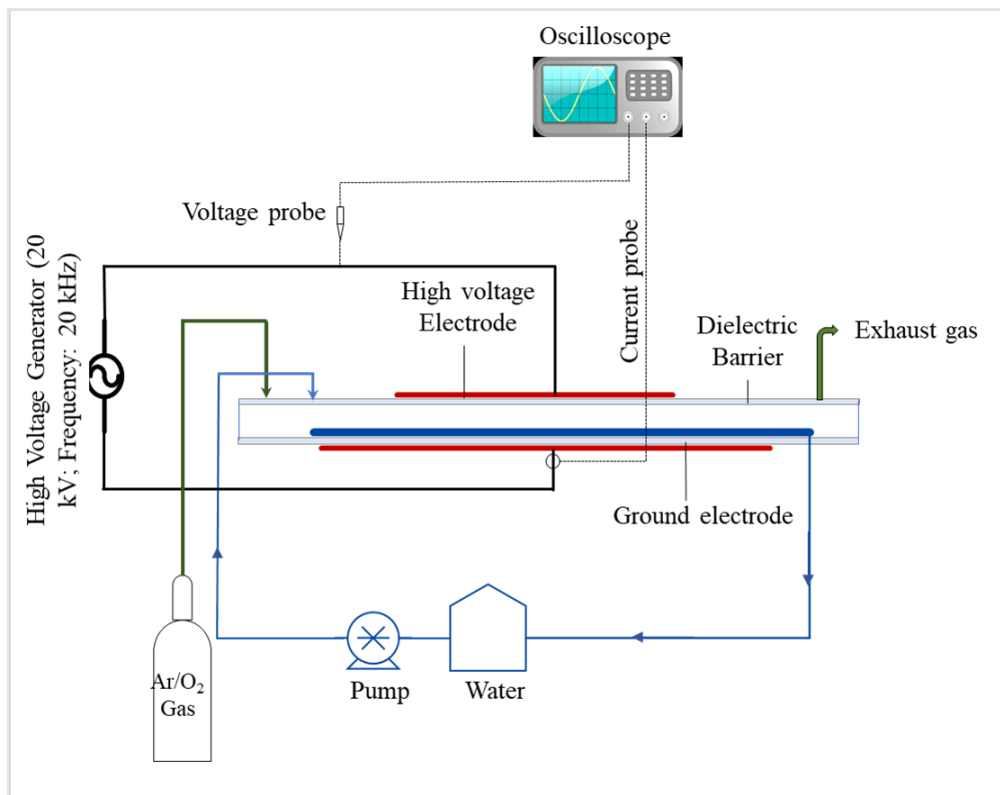


Figure 4.1 Schematic diagram of the remodeled PAW generation system

4.3.2 Nonthermal plasma (NTP) gas analysis using FTIR

The reactive species generated by the NTP in gas phases were determined for three plasma treatment times (10 min, 20 min and 30 min) using FTIR (Nicolet iS5, Thermofisher, MA, USA). The 10 cm gas cell was used to feed the gas and the spectra were collected with 40 scans per spectrum in the range of 4000-400 cm^{-1} and the resolution of 4 cm^{-1} (Sivachandiran & Khacef, 2017). Omnic™ Spectra Software was used for the spectral data visualization and analysis.

4.3.3 PAW time stability

To assess the effect of post-treatment time on the characteristics of PAW, deionized water was treated with NTP for 10 min, 20 and 30 min at 100 ml/min water flowrate and 4 slm gas flow rate. Then the treated water was stored at room temperature in a closed container. The characteristics

of PAW during the post-treatment storage time was evaluated at 0 min, 10 min, 20 min, 30 min, 1 h, 2 h, 1 day and 2 days.

4.3.4 Hydrogen peroxide concentration, pH and ORP

The titanium oxysulphate colorimetric method as described by Eisenberg (1943) was used to quantify the hydrogen peroxide concentration in PAW with slight modifications according to Lukes et al. (2014). Briefly, titanium oxysulphate reagent was prepared by dissolving 25 g of titanium oxysulphate in 1L of 2 M H₂SO₄. 10 ml of sample was added to 1 ml 60 mM sodium azide to stop the degradation of hydrogen peroxide by nitrates and then 5 ml of the titanium oxysulphate was added. The development of yellow color was measured using the UV-Vis spectrophotometer at 407 nm. The standard curve was prepared using varying hydrogen peroxide standard solutions and the concentrations of hydrogen peroxide in the PAW samples were read from the standard curve ($y = 0.0526x + 0.442$; $R^2 = 0.9994$).

The pH and ORP of PAW samples were analyzed immediately after PAW generation using an Accumet AB250 pH meter.

4.3.5 Ozone analysis

The ozone concentrations in the PAW samples were analyzed using the Indigo method (Bader & Hoigné, 1982; Guo et al., 2021c; Pavlovich et al., 2013). Indigo I and Indigo II reagents were prepared from the indigo stock solution. To avoid the loss of ozone in air, the indigo reagent was immediately (<30 s) to the PAW without mixing or bubbling of air inside the PAW. As the range of ozone in the PAW sample under different process conditions were not known, both the reagent methods were used for each treatment and according to the differences in the absorbance, the appropriate data was chosen for further calculation. The indigo reagent was added to the PAW samples immediately after generation and the concentration of ozone was measured based on the reduction in the indigo dye color read at 600±5nm and using the following equation (Eqn. 4.1).

$$\text{Ozone concentration (mg/l)} = \frac{\Delta A \cdot 100}{f \cdot b \cdot V} \text{ --- (4.1)}$$

Where, ΔA = Difference in absorbance between sample and blank

b = Pathlength of the cuvette in cm

V = Volume of the sample added in ml

f = indigo sensitivity coefficient (0.42)

4.3.6 Microbiological analysis

To evaluate the antimicrobial property of PAW, *Escherichia coli* K12 strain (ATCC 15597; C-3000) was used. PAW was generated at three plasma treatment times of 10 min, 20 min and 30 min, with 4 slm gas flow rate and 104 ml/min water flow rate. The effect of post-treatment time on the antimicrobial property of PAW was evaluated after 0, 0.5, 1, 2, 24, and 48 h of PAW production. For control, sterile water was used in place of PAW. The lyophilized *Escherichia coli* K12 strain was cultured in EC broth (Oxoid, England) and streaked on EC agar plates and kept refrigerated until further use. For the experiments, a loop full of bacterial cells were inoculated into 100 mL of freshly prepared nutrient broth and incubated for 12 h at room temperature. Then the cell concentration was adjusted by dilution based on the OD values at 600 nm and the growth curve of the strain. In this study, 1 ml of approximately 10^8 cells/ml concentration of bacterial culture was exposed to 9 ml PAW samples for 30 min. After exposure, the samples were serially diluted up to 10^6 dilution and 0.1 ml of the sample was plated on EC agar plates and incubated. After 24 h incubation, the colonies were counted, and the mean was calculated. The antimicrobial property of PAW was assessed through the log CFU/ml of *E.coli* population in the treatments.

4.3.7 Experimental design for optimization

Box Behnken design (BBD) is widely considered as an efficient design for optimization experiments with a minimum number of experimental units (Montgomery, 2017). In this study, to optimize the PAW production conditions, a Box-Behnken design was used with three factors (water flow rate, time, and gas flow rate) and four responses (H_2O_2 concentration, ozone concentration, pH and ORP). The BBD has three levels coded as -1, 0, +1, corresponding to the low, middle, and high range of the factors, respectively (Table 4.1). The experimental design had fifteen runs with three replicates at the center point.

In the design, the water flow rate (WFR) ranged between 100-200 ml/min, the time ranged between 5-20 min and the gas flow rate (GFR) ranged between 4-8 slm. Design Expert 11 (Stat-Ease, Inc.) was used for the construction and analysis of the optimization experiment. The second order polynomial model as shown in equation (4.2) was used to predict the responses.

$$Y = \beta_0 + \beta_1 X_1 + \beta_2 X_2 + \beta_3 X_3 + \beta_{12} X_1 X_2 + \beta_{13} X_1 X_3 + \beta_{23} X_2 X_3 + \beta_{11} X_1^2 + \beta_{22} X_2^2 + \beta_{33} X_3^2 \quad (4.2)$$

Where, Y is the response (Hydrogen peroxide, Ozone concentration, pH and ORP), β_0 is the constant (intercept), $\beta_1, \beta_2, \beta_3, \beta_{12}, \beta_{23}, \beta_{11}, \beta_{22}$ and β_{33} are the regression coefficients of the parameters for linear, interaction and squared effects and X_1, X_2, X_3 are the tested parameters (WFR, time and GFR respectively). The significance of each factor in the model was analyzed using analysis of variance (ANOVA) for each response.

4.3.8 Statistical Analysis

For time stability analysis all the experiments were conducted at least three times and the mean values with standard deviation were shown. The statistical significance of the results was analyzed through one-way ANOVA and Fisher's least significant difference (LSD) ($p < 0.05$) and the means are compared by Tukey's multiple range test using JMP[®] software (version 15. SAS Institute Inc., Cary, NC).

Table 4.1 Box-Behnken experimental design with coded factors and the experimental and predicted values of the response variables.

Run	WFR	Time	GFR	H ₂ O ₂ (mM)		O ₃ (mg/l)		pH		ORP (mV)	
Order	(ml/min)	(min)	(slm)	Actual	Predicted	Actual	Predicted	Actual	Predicted	Actual	Predicted
				Value	Value	Value	Value	Value	Value	Value	Value
1	100 (-1)	20 (1)	6 (0)	0.951	0.994	0.192	0.187	5.62	5.62	68.5	68.96
2	150 (0)	12.5 (0)	6 (0)	0.925	0.948	0.043	0.048	5.82	5.84	62.3	62.43
3	100 (-1)	12.5 (0)	8 (1)	0.701	0.689	0.187	0.188	5.86	5.87	58.6	58.53
4	200 (1)	5 (-1)	6 (0)	0.441	0.399	0.068	0.073	6.33	6.33	30.4	29.94
5	150 (0)	5 (-1)	4 (-1)	0.542	0.574	0.052	0.047	6.03	6.05	50.6	50.99
6	150 (0)	12.5 (0)	6 (0)	0.954	0.948	0.051	0.048	5.81	5.84	63.7	62.43
7	200 (1)	12.5 (0)	4 (-1)	0.653	0.664	0.091	0.090	6.22	6.21	39.4	39.48
8	200 (1)	20 (1)	6 (0)	0.796	0.811	0.097	0.102	6.07	6.08	42.9	43.94
9	150 (0)	5 (-1)	8 (1)	0.466	0.493	0.101	0.105	6.05	6.05	50.6	51.71
10	200 (1)	12.5 (0)	8 (1)	0.572	0.588	0.133	0.124	6.27	6.27	30.8	30.15
11	100 (-1)	5 (-1)	6 (0)	0.544	0.529	0.097	0.092	5.97	5.96	53.7	52.66
12	150 (0)	12.5 (0)	6 (0)	0.964	0.948	0.049	0.048	5.89	5.84	61.3	62.43
13	100 (-1)	12.5 (0)	4 (-1)	0.893	0.876	0.121	0.130	5.78	5.78	58.2	58.85
14	150 (0)	20 (1)	4 (-1)	1.090	1.060	0.125	0.121	5.67	5.67	72.8	71.69
15	150 (0)	20 (1)	8 (1)	0.913	0.882	0.149	0.154	5.85	5.84	61.7	61.31

4.4. RESULTS AND DISCUSSION

4.4.1 Voltage-Current Characteristics

The discharge characteristics of the system was assessed through the applied voltage $V(t)$ and total current $I(t)$ oscillograms (Figure 4.2). the NTP discharge can be diagnosed based on V-I characteristics of the system. The observed peak-to-peak voltage was 11.06 kV associated with the 20 kHz frequency, 3 mm gap discharge of Ar/O₂ gas plasma at atmospheric pressure. When the breakdown voltage is reached, the discharge is propagated on the surface of the high-voltage electrode and drifts towards the ground electrode. To better understand the discharge characteristics, the $V-I$ waveform was recorded at different gas flow rates of 4 slm, 6 slm and 10 slm. As it can be seen in Fig. 4.2, the number of peaks per voltage cycle decreases with the increase in the Ar/O₂ gas flow rate. Further, the maximum amplitude of the discharge current peak increases with an increase in the gas flow rate. At 4 slm gas flow rate, the DBD was typically operating under filamentary mode with numerous micro discharges separated from each other. The peak value of total current at this gas flow rate was measured as 38.3 mA. However, when the gas flow rate was increased from 4 slm to 6 and 10 slm, distinct, fewer discharges are observed representing a homogenous discharge with higher peak values of total current (62 mA and 124 mA respectively). Increase in gas pressure at higher gas flow rate increased the collision of electrons. Further, as argon gas has low breakdown voltage for ionization, argon metastable atoms increase the ionization thus increasing the conductivity of plasma. Further, at higher gas flow rates the residence time of the gas in the dielectric barrier cell is reduced. At lower gas flow rates, due to pre-ionization of gas molecules, the breakdown voltage increases and reduces the emission diameter, while the opposite effect of less pre-ionization and wider emission diameter was observed at higher flow rates (Abdel-Fattah, 2019).

4.4.2 FTIR analysis of gas phase species

Many reactive species are produced during the plasma discharge in Ar/O₂ gas. In the gas phase, depending on the discharge time, gas flowrate and input energy, argon, oxygen and water molecules form radicals and excited species through dissociation by electrons and radiation in the discharge. From Figure 4.3, it is observed that the spectra contain three pairs of bands. Bands located at 2100-2000 cm⁻¹ and 1050-1030 cm⁻¹ correspond to the 1st overtone and fundamental absorptions of ozone. The bands at 3200-3600 cm⁻¹ correspond to the O-H stretching vibration

caused by the presence of water molecules in the exhaust gas (Al-Abduly & Christensen, 2015; Pavlovich et al., 2013). Increase in the treatment time increases humidity at longer treatment times increase the absorption peaks of water.

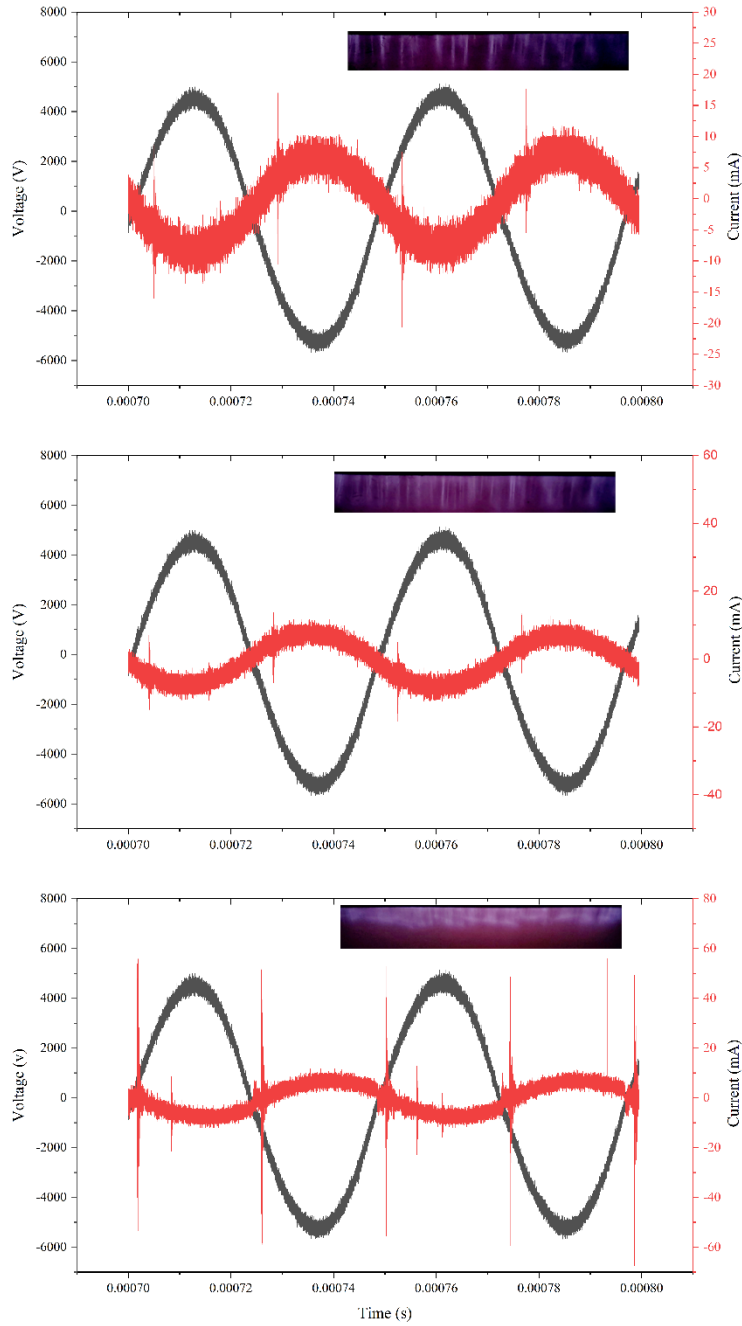


Figure 4.2 V-I characteristics of Ar/O₂ NTP

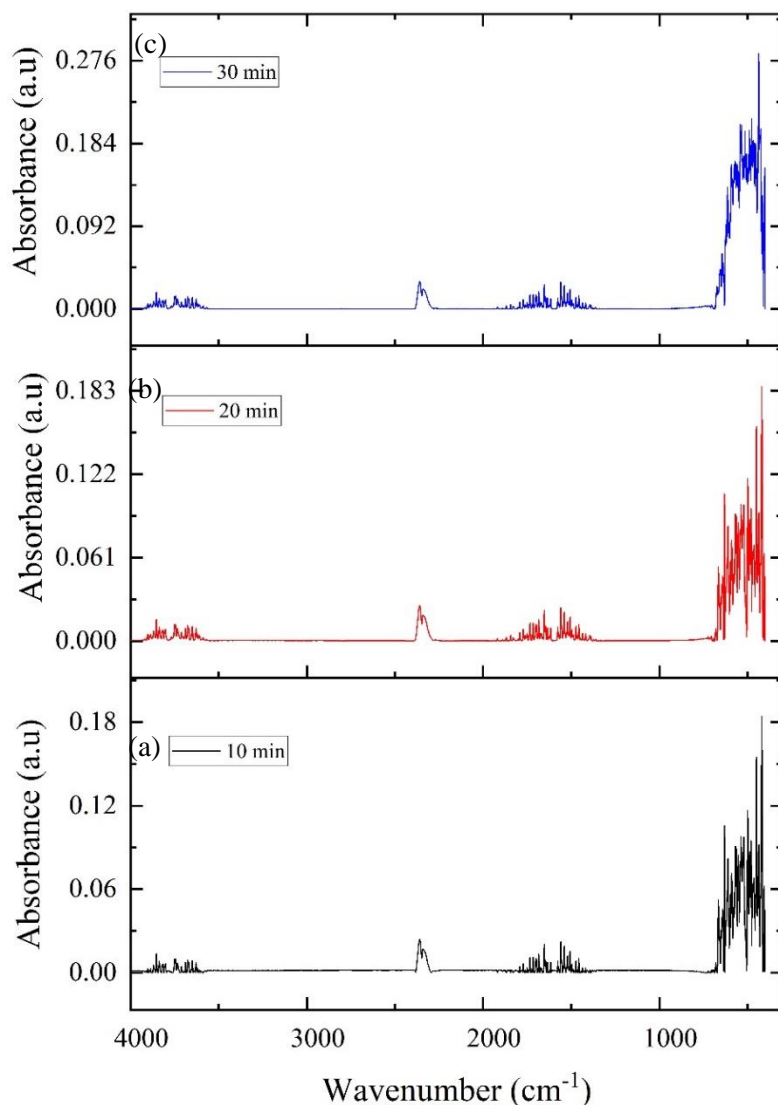
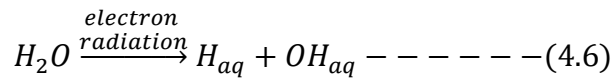
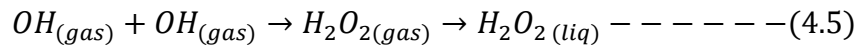
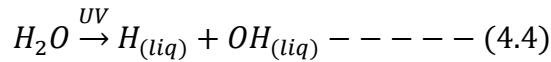
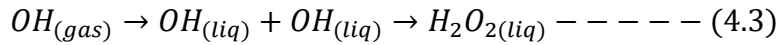


Figure 4.3 Ar/O₂ NTP gas phase FTIR spectrum acquired at (a)10 min, (b) 20 min and (c) 30 min

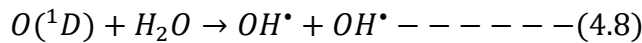
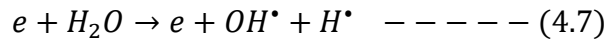
4.4.3. Effect of NTP treatment time and post-treatment time on PAW characteristics

The selectivity of reactive species in PAW depends on the carrier gas composition, NTP system operating conditions, treatment time, etc. In this study Ar/O₂ gas was used to produce the dielectric barrier discharge. As there is no nitrogen present in the feed gas, mixing of atmospheric nitrogen during the PAW treatment was considered negligible and only reactive oxygen species are studied for the characterization of PAW. Effect of plasma treatment time and the post-treatment time on the hydrogen peroxide concentration, ozone concentration and the pH of the PAW is given in

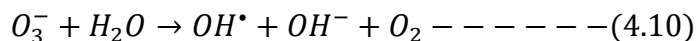
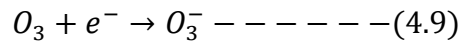
Figure 4.4. Hydrogen peroxide concentration increased significantly with the treatment time from 0.65 mM at 10 min treatment to 2.09 mM after 30 min treatment ($p < 0.05$) (Figure 4.4a). H_2O_2 is produced in the water through the breakdown and re-integration of hydroxyl radicals from the gas phase while entering into the liquid phase and by disintegration of water molecules by UV and electron radiation produced from the plasma (equations 4.3-4.6) (Zhou et al., 2020). Hence the contact time of the hydroxyl radicals and the plasma radiation with water molecules is an important factor affecting the concentration of H_2O_2 in PAW. The singlet oxygen and the super oxide anions are also responsible to produce perhydroxyl radicals (HO_2^*) and hydroxyl ions in water (Liu et al., 2016; Wu et al., 2012).



Water vapor in the discharge gap also has a significant influence on the reactive species. Water vapor in the discharge gap increases with an increase in the treatment time. These water molecules interact with the gas phase plasma through the reactions 4.7-4.8 and produce highly reactive hydroxyl radicals (Machala et al., 2018) which act as a precursor for the production of H_2O_2 .



Similarly, ozone concentration increased from 0.17 mg/l to 0.19 mg/l after 20 min treatment. There was a reduction in the ozone concentration after 30 min treatment and there was no significant difference in the ozone concentration of PAW10 and PAW30 treatments (Fig. 4b). Ozone in the discharge reacts with the electrons and produces ozonoids (Eqn. 4.9-4.10) (Chen & Wang, 2021). Increase in humidity at discharge gap during longer treatment times lead to the conversion of ozonoids to hydroxyl radicals instead of ozone.



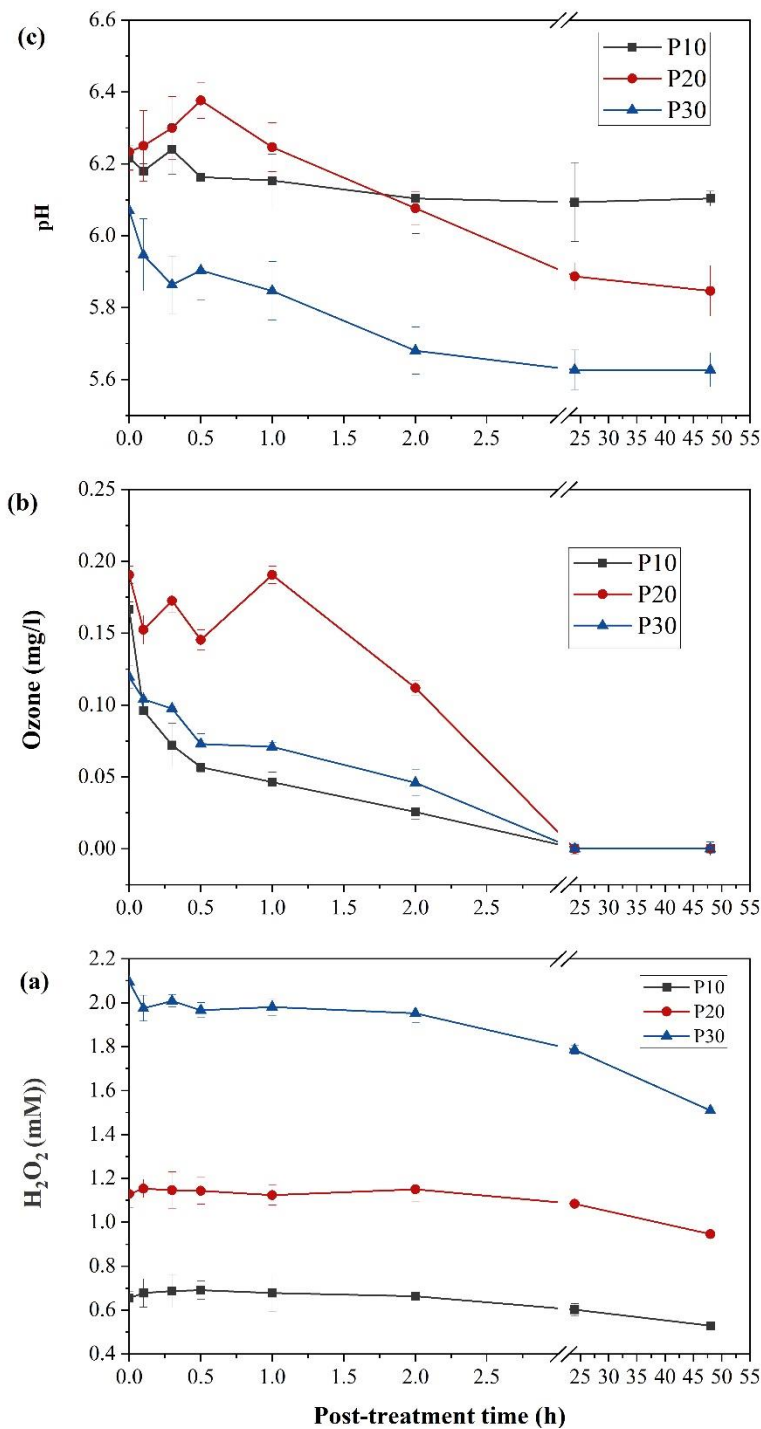
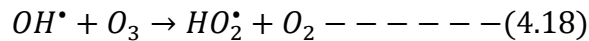
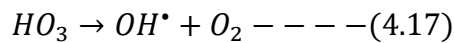
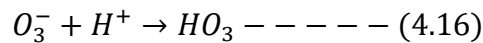
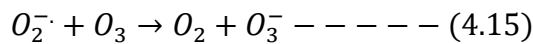
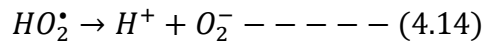
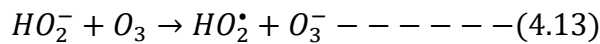
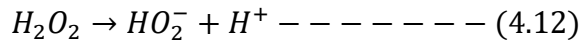
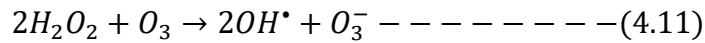


Figure 4.4 Properties of PAW produced at 10 min (PAW 10), 20 min (PAW 20) and 30 min (PAW 30); (a) hydrogen peroxide concentration (mM); (b) ozone concentration mg/l; (c) pH

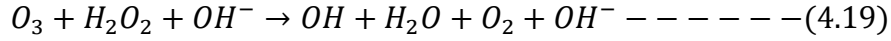
H₂O₂ also reacts with ozone directly, producing more hydroxyl radicals and ozonoids. In the liquid phase H₂O₂ produced in the water then partially dissociates into hydroperoxide ion (HO₂⁻). This hydroperoxide ion decomposes the dissolved ozone in PAW and creates the chain reactions involving hydroxyl radicals (Eqn. 4.11 - 4.18) (Plimpton et al., 2013). Interaction of these hydroxyl radicals with ozone further increases the hydroperoxide ions and thus accelerates the degradation of ozone. According to Staehelin and Hoigne (1982), this degradation process is enhanced by pH <6 and is linear with the hydrogen peroxide concentration. This could be the reason for the reduction in ozone concentration from 0.19 mg/l to 0.12 mg/l between PAW 20 and PAW 30 treatment.



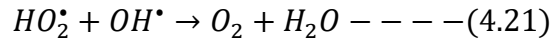
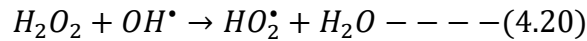
In the time stability analysis, a gradual decrease in the hydrogen peroxide concentration was found in all treatments. No significant reduction in the H₂O₂ concentration was found during the first 2 hours of storage. After 2 days of storage, 0.53 mM, 0.95 mM and 1.51 mM H₂O₂ was detected in PAW 10, PAW 20 and PAW 30 min treatments, respectively (Fig. 4.4a). In the case of ozone, drastic reduction of its concentration was observed, and its concentration was reduced to an undetectable level after 1 day of storage in all treatments (Fig. 4.4b). Reduction in the pH was observed during storage in PAW 30 and it is unclear which reaction was specifically involved in this process.

As the treatment time increased from 10 min to 20 and 30 min, the pH of the water was reduced (Fig. 4.4c). When the pH of water is between 5-6, the reaction between ozone and hydrogen

peroxide is accelerated and produces more hydroxyl radicals through the peroxone process (Eqn. 4.19) (Shen et al., 2019a). This reduces the concentration of both ozone and hydrogen peroxide in PAW 20 min and PAW 30 min treatments throughout the storage period.



Further reduction in the hydrogen peroxide concentration during storage could be due to the degradation of hydrogen peroxide by scavenging hydroxyl radicals (Eqn. 4.20-4.21). After one day of storage the dissolved ozone concentration in all treatments was reduced to undetectable levels. The reduction rate was also found to be increasing with the increase in the hydrogen peroxide concentration through the reactions (Eqns. 4.13-4.21).



4.4.4. Effect of NTP treatment time and post-treatment time of PAW on *E. coli* inactivation

The antimicrobial property of PAW is contributed by the reactive species produced during NTP treatment. In this study, effect of treatment time and the time stability of PAW on its antimicrobial property was evaluated using *E. coli*. In control, the average *E. coli* population of 7.10 ± 0.87 log CFU/ml was recorded. Significant reduction in the *E. coli* population was observed in all PAW treatments. 5.27 log reduction in the microbial population was detected in PAW 30 treatment, whereas 2.75 log and 1.37 log reduction in the *E. coli* population was recorded in PAW 20 and PAW 10 treatments, respectively (Figure 4.5). During storage, drastic reduction in the inactivation percentage was observed in PAW 10 and almost negligible reduction in the microbial population was observed in PAW 10 treatment after 2 days storage. However, in PAW 20 and 30 treatments were able to attain 0.5 log reduction in the *E. coli* population after 24 h. In Figure 4.6, a correlation matrix was constructed among the treatment factors and response variables to establish the relationship between treatment time, post-treatment time and the reactive species concentration on *E. coli* inactivation percentage. It is evident that the plasma treatment time, ozone concentration, H₂O₂ concentration had a positive correlation (>0.5) on *E. coli* inactivation percentage while the post-treatment time had a negative correlation (-0.7). It is also evident that the pH of the solution

did not influence the *E. coli* inactivation (correlation coefficient =0.1). Reduction in the *E. coli* inactivation percentage after 24 hours of storage in PAW 20 and PAW 30 treatments could be attributed to the reduction in ozone concentration during PAW storage. Pavlovich et al. (2013) studied the effect of indirect DBD discharge in water on inactivation of *E. coli* cells. They suggested that the antimicrobial property was in correlation with the ozone concentration rather than the low pH or H₂O₂ concentration.

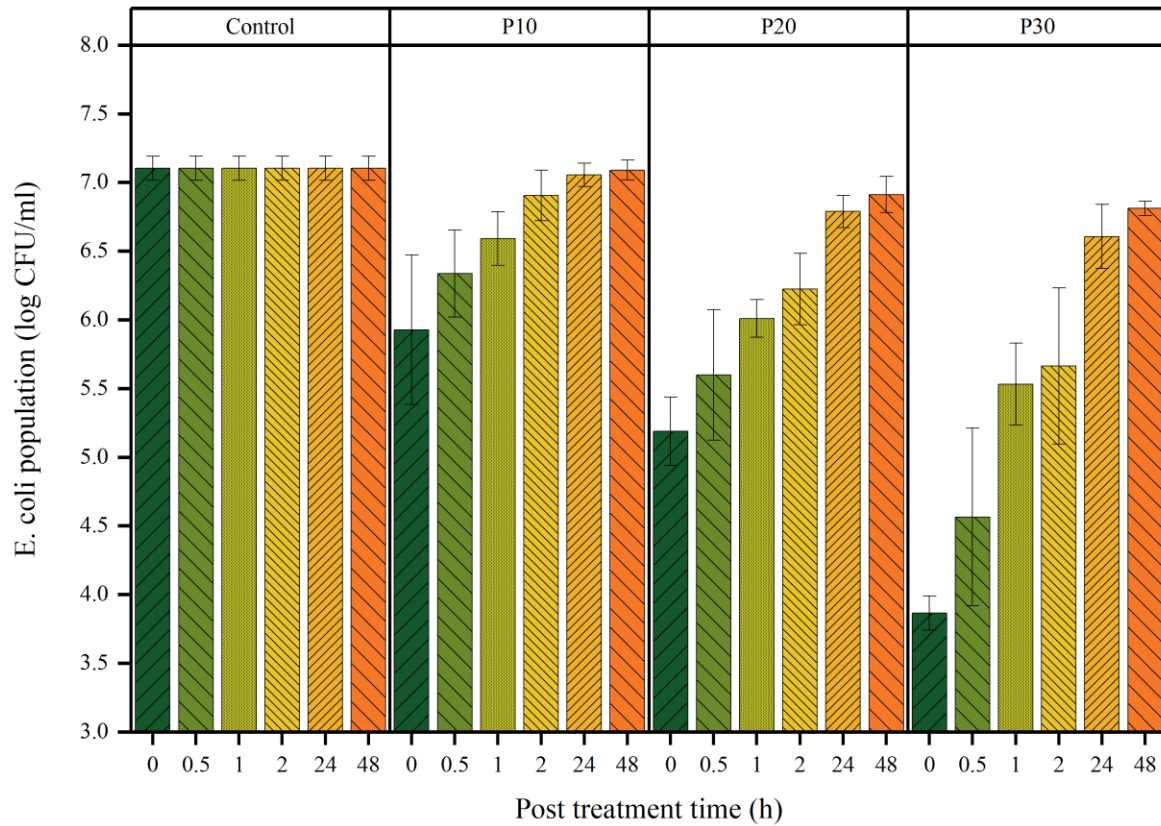


Figure 4.5. Effect of treatment time and post-treatment time on *E. coli* population

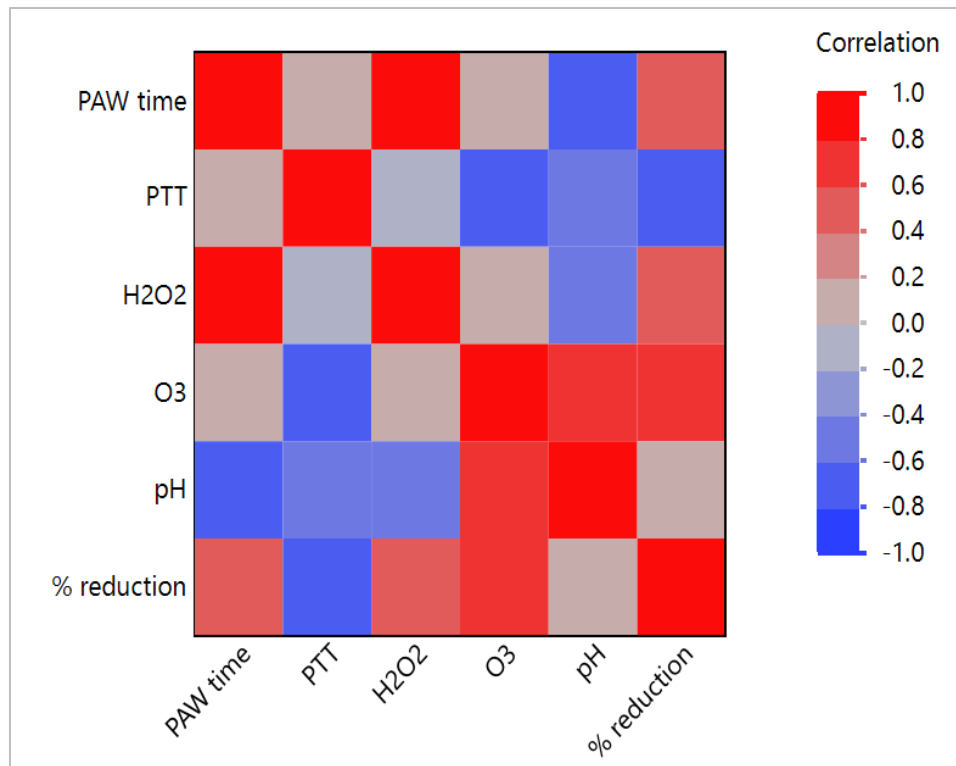


Figure 4.6 Correlation heat map on the relationship between the *E. coli* inactivation percentage with PAW process conditions and properties

When water is exposed to nonthermal plasma containing oxygen, various reactive oxygen species such as hydroxyl radical, atomic oxygen, superoxide anion radical, ozone, etc., are transported into the liquid phase through different physicochemical pathways. The major long lived reactive oxygen species such as hydrogen peroxide and ozone are produced in the PAW along with other short lived species such as hydroxyl radicals, perhydroxyl radicals, and atomic oxygen (Shen et al., 2019a). These reactive species which are highly oxidative in nature reduce the membrane potential of the microbial cells and damage the intracellular contents by oxidation (Ikawa et al., 2010). Increase in the treatment time increases the concentration of ROS such as hydrogen peroxide, ozone and hydroxyl radicals in PAW leading to an increase in bactericidal properties with PAW treatment time. Cell wall damage and transportation of extracellular reactive oxygen species into the cell leads to the accumulation of oxidative species inside the bacterial cell and subsequent cell death (Shen et al., 2019a).

It is found that the ozone was degraded in the presence of hydrogen peroxide (Eqns. 4.12-4.19) producing more hydroxyl radicals. In turn, this increases the overall reactivity of PAW, since the reactivity of the hydroxyl radical is much higher than that of O_3 despite having shorter lifetime (<2 ns) (Wu et al., 2017; Zhou et al., 2020). The prolonged microbial inactivity after treatment is mainly due to the long-lived reactive species, hydrogen peroxide, and ozone to certain extent and not the hydroxyl radicals. It is also evident that the post-discharge reactions continue for at least 2 hours as there was no significant reduction in the antimicrobial property that was observed particularly in PAW 20 and PAW 30 treatments (Figure 4.5). Immediate application of PAW generated by Ar/ O_2 plasma therefore becomes crucial to achieve higher disinfection efficiency.

4.4.5 Response surface optimization of PAW treatment conditions

4.4.5.1 *Fitting the model*

To assess the effects of system process parameters on the properties of PAW, the independent variables of water flow rate (X1), time (X2) and gas flow rate (X3) were optimized to maximize the concentrations of H_2O_2 , ozone and ORP while minimizing the pH using a response surface methodology. The Box-Behnken experimental design and the corresponding response values are given in Table 4.1. The experimental values of the response variables were fitted against a quadratic polynomial equation using Design Experts software. The statistical significance of the model fitting was analyzed by F-test and only the significant terms at 95% confidence level are included in the reduced equation for each response. The reduced polynomial models describing the relationship between the three variables and the responses are given in Equations 4.23-4.26. The regression coefficients for each response are presented in Table 4.2.

Table 4.2 Fitted second-order polynomial model with ANOVA details

Quadratic models	df of pure error	R ²	Lack of fit	F value	P value
H2O2 concentration (μM) = 0.948 $- 0.078x_1 + 0.219x_2$ $- 0.0657x_3 - 0.156x_1^2$ $- 0.108x_2^2 - 0.086x_3^2$ -- --- (4.22)	2	0.985	0.128	37.55	0.0005
Ozone (mg/l) $= 0.047 - 0.026x_1$ $+ 0.031x_2 + 0.023x_3$ $- 0.017x_1x_2 + 0.046x_1^2$ $+ 0.019x_2^2 + 0.039x_3^2$ -- --- (4.23)	2	0.987	0.131	45.24	0.0003
PAW pH = 5.84 + 0.208x₁ - 0.146x₂ $+ 0.041x_3 + 0.04x_2x_3$ $+ 0.145x_1^2 + 0.048x_3^2$ ----- (4.24)	2	0.992	0.89	69.98	0.0001
PAW ORP = 62.43 - 11.94x₁ + 7.57x₂ $- 2.41x_3 - 2.25x_1x_2$ $- 2.77x_2x_3 - 12.87x_1^2$ $- 2.82x_3^2$ ----- (4.25)	2	0.996	0.437	141.48	<0.0001

(x₁-water flow rate; x₂- time and x₃ - gas flow rate)

4.4.5.2 Effect on hydrogen peroxide

The ANOVA table (Table 4.2) for hydrogen peroxide shows the significant F value of 37.55 with the associated P value of 0.0005. Further the coefficient of determination (R²) which indicates the goodness of fit of the model was estimated at 0.985 and the model lack of fit was estimated to be non-significant (p<0.05). These parameters suggested that the developed model could adequately represent the real relationship among the variables on hydrogen peroxide concentration in PAW. Maximum concentration of 1.09 mM H₂O₂ was found in 20 min treatment with 150 ml/min water flow rate and 4 slm gas flow rate. All individual factors, namely water flow rate, time and gas flow rate and their interactions (quadratic terms) were found to have a significant (p<0.05) effect on the PAW hydrogen peroxide concentration. The three-dimensional response surface plots for the variables influencing the hydrogen peroxide concentration are presented in Figure 4.7. It could be seen from the surface plots, that the treatment time had a positive effect on the hydrogen

peroxide concentration while water flow rate and gas flow rate had a negative effect. When the water flow rate is increased the water film thickness increases inside the system. This reduces the discharge gap and increases the humidity inside the discharge gap. Due to this higher moisture, the breakdown voltage is increased leading to the electrolysis of water. This causes the simultaneous degradation of H_2O_2 into water and oxygen (Lu et al., 2017). In the case of gas flow rate, increasing the gas flow rate reduces its residence time inside the system, which leads to the reduction in the intensity of reactive species in the gas phase (Baek et al., 2016). Further transformation of the discharge from a filamentary mode to the homogenous mode, at higher gas flow rates, as discussed in the section 4.4.1, could have also reduced the reactive species concentration in the discharge itself.

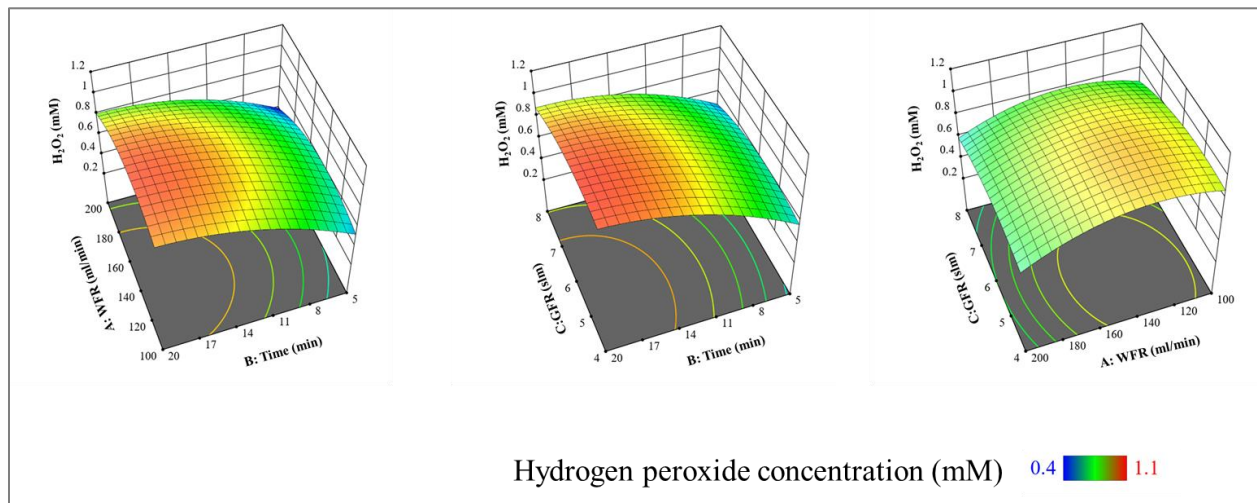
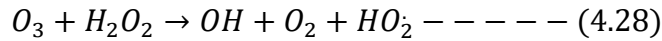
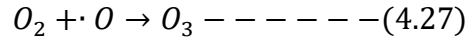
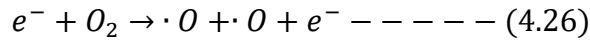


Figure 4.7 Response surface plots on PAW hydrogen peroxide concentration

4.4.5.3 Effect on ozone concentration

The main and interaction effects of ozone concentration in PAW were determined using ANOVA. The F-value of 45.24 and p-value of 0.003 indicated that the model was significant. For ozone concentration, all the main effects and quadratic interaction effects were found to be significant at 95% confidence level. Further, the cross-product interaction between the water flow rate and treatment time was significant with a p-value of 0.0134. After discarding the non-significant model terms, the reduced model (Table 4.2) was considered significant in explaining the variability in the ozone concentration in PAW. The surface-plots of each variable are presented in Figure 4.8. It was evident that the treatment time and gas flow rate had a positive effect on the ozone concentration

while the water flow rate had a negative effect. Further the cross-product of water flow rate (X_1) and the treatment time (X_2) also had a negative effect on the ozone concentration. Ozone in PAW is produced by mass transfer of ozone from the gas phase (Qi et al., 2018) and by reaction of molecular oxygen with electrons or by the deprotonation of the hydroperoxyl radical, superoxide anions and hydroxyl radicals (Equations 4.26-4.29) (Gorbanev et al., 2016; Jiang et al., 2016) .



Mixing of the liquid increases the mass transfer of ozone from the gas phase to the liquid phase (Pavlovich et al., 2013). The surface to volume ratio also plays an important role in the transfer of reactive species from the gas phase to the liquid phase at higher water flow rates. Having a thin film of water in the DBD discharge increases the solvation of O_3 and hydrogen peroxide.

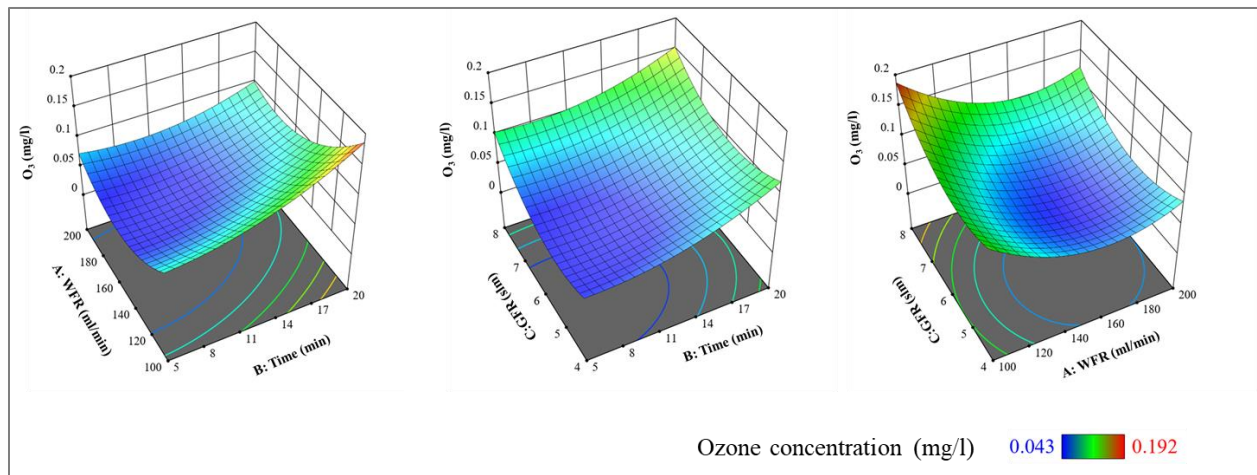


Figure 4.8 Response surface plots on PAW ozone concentration

The continuous flow of water reduces the depletion of ozone by de-solvation and degradation by gas phase superoxide anions (Soheila et al., 2020). However, the lower contact time between the water and the gas phase ozone could be the reason behind the negative impact of water flow rate on ozone concentration in PAW. Further, an increase in the humidity levels inside the treatment chamber could also be the reason for the reduction in the PAW ozone concentration at higher flow

rates (Burlica et al., 2006). The ozone concentration of PAW also increased with the increase in gas flow rate which could be due to the increased availability of O₂ from the feed gas. Increasing the concentration of O₂ helps in the conversion of O atoms into O₃ through the reaction given in equation (4.27), within few micrometers inside the liquid (Jiang et al., 2016) .

4.4.5.4 Effect of pH and ORP

The F value of pH and ORP models were 69.98 and 141.48 respectively, indicating that the models are significant for both the responses at 95% confidence level. Water flow rate and gas flow rate had a positive effect on pH while time had a negative effect (Figure 4.9). The opposite trend was found for ORP (Figure 4.10). Reduction in the pH and increase in the ORP is mainly attributed to the production of hydronium ion (H₃O⁺) by plasma reactive species interaction with water molecules. The reduction in the pH of liquid while using non-nitrogen containing feed gas was caused by the electron and ion bombardment reaction pathways (Equations 4.30-4.31) (Burlica et al., 2006). The recent results suggest that by increasing the water flow rate and gas flow rate, the production of hydronium ions is minimized due to the lower contact times between the plasma species and water molecules.

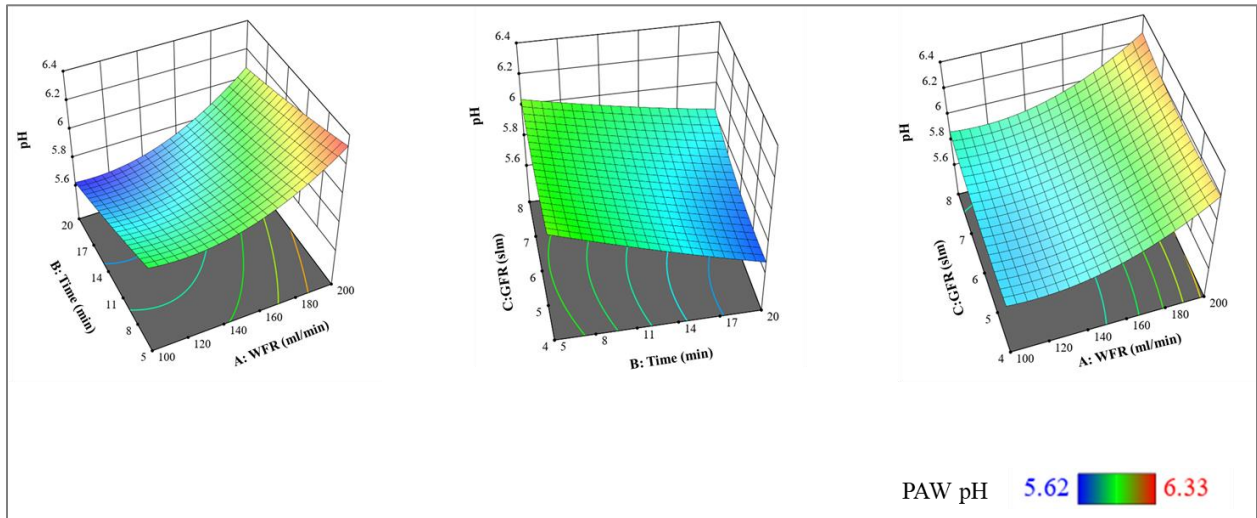
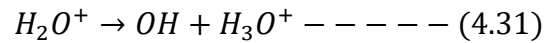
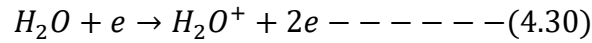


Figure 4.9 Response surface plots of the pH of PAW

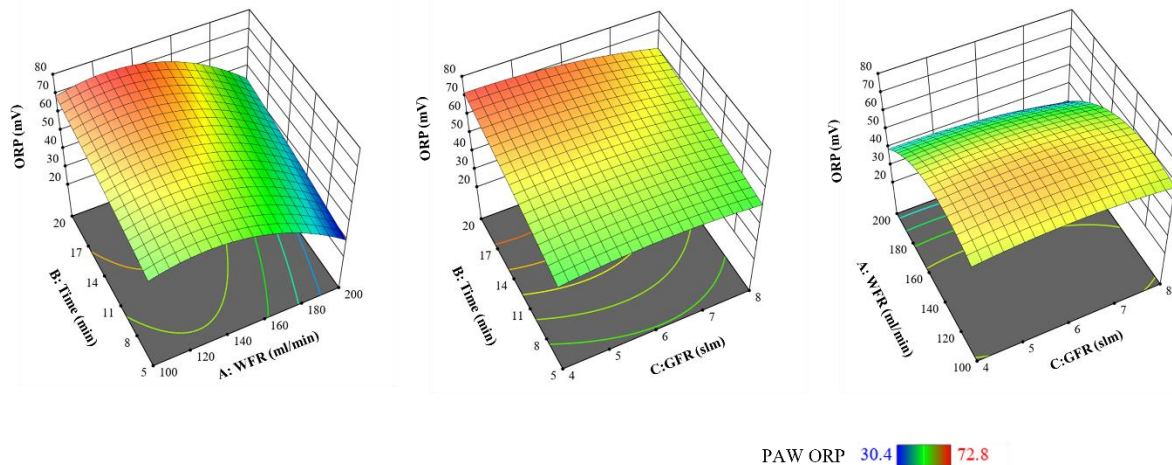


Figure 4.10 Response surface plots on PAW ORP

4.4.5.5 Optimum condition

The aim of this optimization experiment was to increase the hydrogen peroxide and ozone concentrations in PAW while reducing the pH and increasing the ORP. The optimum conditions were obtained using the multiple-response method from the statistical software with a desirability value of 0.962. The obtained optimum condition was 104.6 ml/min water flow rate, 20 min treatment time and 4 slm gas flow rate. Under these optimum conditions the predicted value of hydrogen peroxide was 1.043 mM, ozone concentration was 0.192 (mg/l), pH value was 5.58 and the ORP was 70.4 mV.

4.5. CONCLUSION

Nonthermal plasma-liquid interactions are complex and understanding the effect of process variables on the PAW characteristics is crucial for the adequate scale-up of the technology. In this study, novel information on PAW characteristics and the factors influencing its microbial inactivation efficiency was presented. It was found that hydrogen peroxide and dissolved ozone in PAW was mainly responsible for the inactivation of *E. coli* cells. PAW was able to reduce 5.27

log reduction in the *E.coli* population was observed with 30 min PAW activation and the its disinfection property reduced to significantly with 48 h storage. Further, the effects of continuous flow PAW generation system process parameters on the characteristics of PAW were analyzed through the response surface method. It was found that the water flow rate and gas flow rate have a negative impact on the hydrogen peroxide concentration. The treatment time was found to have a significant positive correlation with the hydrogen peroxide concentration, ozone concentration, pH and the ORP of PAW. The optimum condition was derived by fitting a second-order polynomial model and the conditions of 104.6 ml/min water flow rate, 20 min treatment time and 4 slm gas flow rate were found as the optimum values. The results of this study help in understanding the time stability of PAW and its antimicrobial property and the interaction between the basic process conditions in a continuous flow PAW generation system.

CONNECTING TEXT

It is evident from chapter IV that PAW generated from the continuous flow system is capable of disinfecting *E. coli* cells. The optimization studies showed that the plasma activation time of water has a major influence on the reactive species concentration in PAW. Therefore, in the subsequent studies, the PAW activation time alone was taken as a variable. The optimum point gas flowrate (4 slm) and water flow rates (100 ml/min) were used in the forthcoming studies.

From chapter II it is evident that only a limited number of studies are available that have evaluated the effect of nonthermal plasma reactive species on food components and there are no studies available on this aspect with PAW. PAW reactive species such as hydrogen peroxide and ozone are relatively more stable in the liquid phase than in the gas phase plasma. Therefore, it is important to assess the effect of these reactive species on food components to ensure that PAW does not cause any adverse changes in the food quality. To investigate this, in the following Chapter V, whey protein isolate (WPI) was used as a model food system for proteins. WPI at different concentrations was treated with PAW activated for 10 min to 45 min. The physicochemical, structural, and functional changes in the treated WPI was then assessed. Based on the obtained results, the possible reaction mechanism of the PAW reactive species with proteins is also discussed in detail.

CHAPTER V

ASSESSMENT OF CHANGES IN WHEY PROTEIN ISOLATE AFTER PLASMA ACTIVATED WATER TREATMENT

5.1 Abstract

This study was aimed at evaluating the changes in whey protein isolate induced by plasma activated water (PAW) as a function of plasma activation time of water and the concentration of protein. Effects of PAW reactive species on physicochemical, functional, and structural properties of WPI were investigated. The results showed mild oxidation of WPI evidenced from the decrease in the sulfhydryl group content and increase in the surface hydrophobicity. Increase in b^* value and whitening index of the WPI sample with an increase in the PAW activation time was observed in all concentrations. Increase in the soluble protein content was observed with 45 min PAW treatment. Foaming capacity and foam stability of the PAW treated samples increased significantly following PAW treatment. SDS-PAGE analysis revealed that there was no insoluble aggregation formed by the reactive oxygen species in WPI. TGA analysis and FTIR spectrum of the treated WPI samples showed that there were no new functional groups formed by the PAW treatment. Increase in β -sheet, random coil percentage and reduction in α -helix percentage was observed in 5 mg/ml concentration. The results suggest that the reactive oxygen species in the PAW lead to a mild oxidation of the WPI and this reaction is influenced by the post-discharge reaction chemistry in PAW.

5.1 Introduction

Proteins are important nutrients in the human diet and can be used as an important food ingredient for the enhancement of functional properties in foods. The functional properties and the interfacial characteristics with other components like carbohydrates and lipids depend on the amino acid composition and its structural formations. Several methods are used to modify the protein functional properties such as heat, pH (Chen et al., 2017), ultrasound (Amiri et al., 2018), high pressure processing and enzyme hydrolysis (Wu et al., 2020). Advanced oxidation methods are also being studied for the selective modification of the functional properties of proteins. Segat et

al. (2014) evaluated the effect of ozone to modify the properties of a whey protein isolate while Feng et al. (2022); Sutariya and Patel (2017) used hydrogen peroxide to modify whey proteins. Changes in the functional properties of egg white proteins by radical-cross linking method, using hydrogen peroxide and ascorbic acid, was reported by Alavi et al. (2019).

Nonthermal plasma is an advanced nonthermal food processing technology that has increasing applications in food processing from disinfection of food materials to altering the functional properties of the foods. Nonthermal plasma or cold plasma is produced by partial ionization of a gas while maintaining the temperature of the gas at atmospheric pressure and temperature. During this ionization process, various reactive gas species are produced in the gas along with free radicals, ions, electrons, and UV radiation (Thirumdas et al., 2015). These reactive species are utilized for various applications in foods and their reactivity with pathogens, enzymes, and food components, depending on the chemistry of the chosen plasma process. Nonthermal plasma has been extensively studied for its disinfection capacity with various food pathogenic organisms (Liao et al., 2017), inactivation of enzymes (Han et al., 2019) and also to modify the functional properties of numerous food ingredients (Sharma, 2020; Sruthi et al., 2022). Structural changes in pea protein isolate have been reported after cold plasma treatment (Bußler et al., 2015). Structural unfolding of peanut protein isolate and improvement in its functional properties such as emulsifying capacity, solubility and water holding capacity were reported after cold plasma treatment (Ji et al., 2019). Further, these conformational changes caused by the cold plasma, have also been investigated for the elimination or reduction of the allergenicity from food proteins (Tolouie et al., 2018). Furthermore, the direct application of NTP still presents many challenges like, difficult controlled application of plasma, undesirable quality changes in food, non-uniform exposure of rough food surface leading to the inefficient processing, and complicated system design making it difficult to treat large size food materials (Herianto et al., 2021; Thirumdas et al., 2015). Highly oxidative reactive species and the free radicals from the direct nonthermal plasma treatment can cause protein oxidation and denaturation of the protein structure in food materials (Coutinho et al., 2018). Further, the degree of variability in the plasma chemistry is very high, even with the slightest modification in the operating conditions. The use of plasma-activated water could be the solution to mitigate the drawbacks of nonthermal plasma in food disinfection and its use in other food applications.

Plasma activated water is produced by treating water with nonthermal plasma, thereby transferring the reactive species from the nonthermal plasma to the water through various physico-chemical processes. Reactive oxygen and nitrogen species react with water molecules and with themselves and form relatively stable reactive species in water such as hydrogen peroxide, ozone, nitrites and peroxyxynitrite species. Their presence in the water helps in the quantification of these reactive components and to control their dosage (Guo et al., 2021b). In a recent study, oxidation of chicken myofibrillar proteins, protein aggregation and exposure of sulfhydryl containing amino acids were reported after PAW treatment (Qian et al., 2021). They claimed that the oxidation of proteins was beneficial in terms of enhancing the water holding capacity of protein gels. However, in other studies, no adverse effects on the quality of proteinaceous foods such as shrimp, beef and tofu were reported (Frías et al., 2020; Liao et al., 2018b; Liao et al., 2020). Still, there are many of the fundamental understandings of the interaction between the food biomolecules and the plasma reactive species that are still to be explored. Presence of lipids, sugars, enzymes, and antioxidants in the food material increases the complexity of interactions between the PAW reactive species and the proteins (Hellwig, 2019; Zhao et al., 2020).

The objective of this study was to investigate the effect of PAW oxidative species on proteins. For this, whey protein isolate was chosen as a model protein. PAW was produced from a dielectric barrier discharge nonthermal plasma system at atmospheric pressure using Argon/Oxygen as the working gases. The effect of PAW on the physicochemical and structural changes in whey protein were then evaluated with respect to the plasma activation time of the water.

5.2 Materials and Methods

5.2.1 Materials

Commercially available whey protein isolate (97% purity) (Canadian Protein™, Ontario, Canada) was used for this study. 5,5'-Dithiobis (2-nitrobenzoic acid) (DTNB) was obtained from Sigma chemicals (St. Louis, MO, USA). Coomassie Brilliant Blue (G-250) (CBBG), Pierce™ BCA protein assay kit was obtained from Thermo Fisher Scientific, Canada. All other reagents and chemicals used were of analytical grade.

5.2.2 Experimental setup for PAW production and sample preparation

In this study, a parallel plate dielectric barrier discharge system was used to produce nonthermal atmospheric pressure plasma (Fig. 5.1). Premixed argon and oxygen gases in the ratio of 98% and 2% were used as the carrier gas and the discharge gap between the dielectric plates was 3 mm. Deionized water was circulated in-between the dielectric plates using a pump at the flow rate of 100 ml/min. The dielectric plates were made of 2 mm thick quartz glass with the permittivity of 4.9. A high voltage generator (PVM 500), which can produce up to 30 kV (peak-to-peak) voltage and 0-70 kHz frequency, was used to generate the nonthermal plasma in the discharge gap. Water was treated with the nonthermal plasma for 10 min (P10), 20 min (P20), 30 min (P30) and 45 min (P45) to obtain the plasma activated water. Then 10 ml of PAW was immediately added to WPI, pre-weighed in centrifuge tubes, such that the final concentration of WPI in the PAW solution was 5 mg/ml, 10 mg/ml, and 50 mg/ml. For control, the WPI samples were mixed with 10 ml of deionized water. Samples of PAW treated, and control samples were vortexed for 2 min and stored at 4°C (for maximum of 24 h) until used for the analysis of sulfhydryl group content, foaming properties, turbidity, and total soluble protein content. The remaining solutions were freeze dried (Labconco Corporation, Kansas City, USA) and used for all other physicochemical and structural properties analyses.

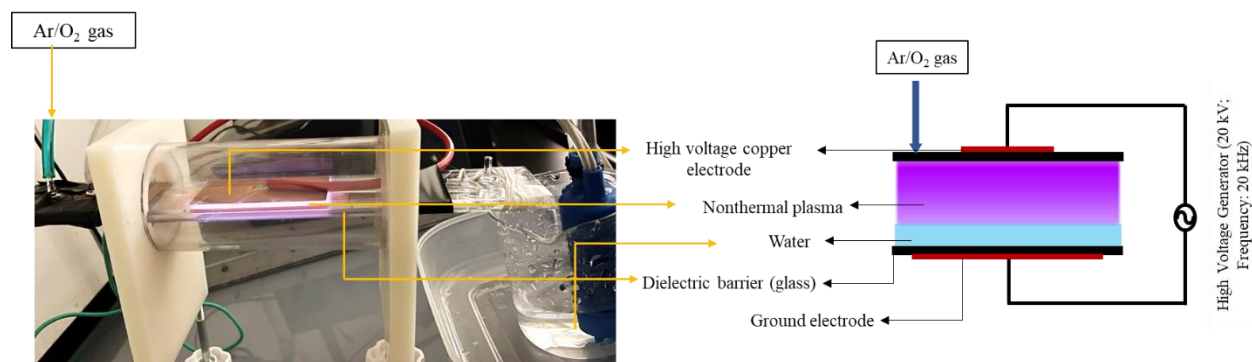


Figure 5.1. Schematic diagram of plasma activated water system

5.2.3 PAW properties measurement

5.2.3.1 Hydrogen peroxide and ozone concentrations

Hydrogen peroxide concentration in the PAW was measured using the titanium oxysulphate colorimetric method as described by Eisenberg (1943) with slight modifications according to

(Lukes et al., 2014). Briefly, 10 ml of sample was added to 1 ml 60 mM sodium azide to stop the degradation of hydrogen peroxide by nitrates followed by the addition of 5 ml of the titanium oxysulphate reagent (25 g of titanium oxysulphate in 1L of 2 M H₂SO₄). The development of yellow color was measured using the UV-Vis spectrophotometer at 407 nm and the concentrations of hydrogen peroxide in the PAW samples were read from the standard curve.

The ozone concentrations in the PAW samples were analyzed using the Indigo method (Bader & Hoigné, 1982; Burlica et al., 2006). 1 ml of indigo II reagent was added to 9 ml of PAW immediately after generation and the concentration of ozone was measured based on the reduction in indigo dye color read at 600±5nm and using the following formula (Equation 5.1).

$$\text{Ozone concentration (mg/l)} = \frac{\Delta A \cdot 100}{f \cdot b \cdot V} \text{ --- (5.1)}$$

Where, ΔA = Difference in absorbance between sample and blank

b = Pathlength of the cuvette in cm

V = Volume of the sample added in ml

f = indigo sensitivity coefficient (0.42)

5.2.3.2 pH and temperature

The pH of PAW samples was analyzed immediately after PAW generation using an Accumet AB250 pH meter. Temperature of the PAW water was measured using a digital thermometer.

5.2.4 Turbidity measurement

Turbidity of PAW treated WPI solution and controls was determined by measuring the absorbance at 600 nm at room temperature with 1 cm path length cuvette using UV-Vis spectrometer (Segat et al., 2014).

5.2.5 Color measurement

Color of control and PAW treated WPI freeze dried samples were measured in CIE (L*, a*, b*) color scale using a colorimeter (Konica Minolta, Japan). For each sample four measurements were taken, and the mean values were reported. Changes in the color value was evaluated in terms of b* value. Then the total color difference (ΔE) and whiteness index (WI) were calculated using the following equations 5.2 and 5.3 (Gökkaya Erdem et al., 2019).

$$\Delta E = \sqrt{(L_{control}^* - L_{sample}^*)^2 + (a_{control}^* - a_{sample}^*)^2 + (b_{control}^* - b_{sample}^*)^2} \text{ --- (5.2)}$$

$$WI = 100 - [(100 - L^*)^2 + (a^{*2} + b^{*2})]^{1/2} \text{ --- (5.3)}$$

5.2.6 Determination of total soluble protein content

The PAW treated and untreated WPI solutions were diluted to 1mg/ml concentration using 0.1 M phosphate buffered saline (pH 7.0). The solutions were incubated for 30 min at 25°C and then centrifuged at 4000 × g at 4°C for 10 min (Dong et al., 2021). The supernatant was then used for the determination of total soluble proteins using Pierce™ BCA protein assay kit (Thermo Fisher Scientific, Canada) according to the manufacturer's protocol for microplate method.

5.2.7 Determination of sulfhydryl group (SH) content

The exposed and total sulfhydryl group content in the PAW treated samples were analyzed using (Ellman, 1959) method with modifications according to (Beveridge et al., 1974). Briefly, for exposed SH group, 0.5 ml of WPI solution was added to 0.5 ml of 0.1M phosphate buffer (pH 8.0) containing 0.01 ml of Ellman's reagent [4 mg of 5,5'- dithiobis-2-nitrobenzoic acid (DTNB) in 1 mL of Tris–glycine buffer (0.086 mol L⁻¹ Tris, 0.09 mol L⁻¹ glycine, 4 mmol L⁻¹ EDTA, pH 8.0)]. The mixture was incubated for 20 min at 25°C, then the absorption was read at 412 nm. For total SH group, 0.1 ml of protein solution was added to 0.9 ml of phosphate buffer containing 0.01 ml of Ellman's reagent and 8 M of urea. After incubating the mixture for 15 min at 40°C, the absorbance was measured at 412 nm. The micromole of sulfhydryl group content per gram of protein was calculated from Equation 5.4.

$$\mu M \text{ SH/g} = (73.53 \times A_{412 \text{ nm}} \times D)/C \text{ --- (5.4)}$$

Where, the factor 73.53 is derived from the molar absorptivity constant, $A_{412 \text{ nm}}$ is the absorbance at 412 nm, D is the dilution factor and C is the concentration of WPI solution (mg/ml).

5.2.8 Determination of surface hydrophobicity

The surface hydrophobicity of PAW treated freeze dried WPI samples was measured by Coomassie Brilliant Blue (G-250) (CBBG) dye binding in accordance with Cao et al. (2016).

Briefly, 5 mg/ml solutions of WPI were made from freeze dried PAW treated WPI sample in 20 mM phosphate buffer (pH 6.0) which was mixed with 300 μ l of 0.1 mg/ml CBBG solution. For the control 1.2 ml phosphate buffer was added with 300 μ l of CBBG solution. Samples and the control were vortexed at 2000 rpm for 3 min and then centrifuged at 2000 \times g for 10 min. The supernatant was separated and centrifuged again at the same condition. The absorbance of the supernatant was then read at 585 nm. The basic and aromatic amino acid residues of proteins bind and form a complex in the anionic form of the CBBG stain which was then evaluated at 585 nm.

The amount of CBBG bound was calculated using equation 5.5 where, A=absorbance at 585 nm:

$$CBBG \text{ bound } (\mu g) = 30 \mu g \times \frac{(A_{control} - A_{sample})}{A_{control}} \text{ --- (5.5)}$$

5.2.9 Determination of foaming properties

In a graduated tube, 10 ml of PAW treated WPI solutions were homogenized at 15000 rpm for 2 min (Fischer Scientific 850 homogenizer). For the control, untreated WPI was mixed with deionized water according to the concentrations of the samples. Foaming capacity and the foam stability of the samples were calculated according to the following equations 5.6 and 5.7.

$$Foaming \text{ capacity } (\%) = \frac{(VF_0 - VL)}{VL} \times 100 \text{ --- (5.6)}$$

$$Foam \text{ stability } (\%) = \frac{VF_{30}}{VF_0} \times 100 \text{ --- (5.7)}$$

Where, VL, VF_0 , VF_{30} are volume of non-whipped WPI solution, volume of foam immediately after whipping and volume of foam after standing at room temperature for 30 min respectively.

5.2.10 Thermogravimetric analysis (TGA)

The thermal stability of the PAW treated, and freeze-dried samples were measured using a TGA Q50 (TA Instruments, DE, USA). For that purpose, 5-10 g of WPI powder was placed in a platinum pan and the experiment was conducted between 25°C to 600°C at 10°C/min under nitrogen atmosphere (Azevedo et al., 2017).

5.2.11 Fourier transform infrared (FTIR) spectroscopy

The FTIR spectral analysis of freeze-dried and PAW treated WPI samples was conducted using the Nicolet iS5 attenuated total reflectance (ATR)-FTIR spectrometer. Samples were placed onto the diamond crystal and were tightly clamped for the IR analysis. The spectra were collected as 40 scans at 4 cm^{-1} resolution and an empty diamond crystal in air was used for collecting the background spectrum (Vanga et al., 2016). The spectra were analyzed using OMNIC software (version 8, Thermo Nicolet Instrument Corp., Madison, WI, USA) and the second derivatives were calculated using OriginPro (Version 9, OriginLab Corporation, Northampton, MA, USA).

5.2.12 Sodium dodecyl sulfate polyacrylamide gel electrophoresis (SDS-PAGE) analysis

The PAW treated and freeze dried WPI samples were analyzed for changes in polypeptide patterns using SDS-PAGE assay under reducing condition (Laemmli, 1970). All the reagents and buffers for this experiment were obtained from BIO-RAD Bio-rad, California, USA. 0.5% of WPI solutions were mixed with the Laemmli sample buffer in 1:1 (v/v) ratio with 2% β -mercaptoethanol. Then the mixture was heated to 95°C for 5 min and cooled to room temperature. The running buffer (1x) was diluted with water from the 10x Tris/Glycine/SDS running buffer containing 25 mM Tris, 192 mM glycine and 0.1% SDS, pH 8.3. Precast gel (4–20% Mini-PROTEAN® TGX Stain-Free™ Protein Gels) was loaded with 10 μl of molecular weight marker of 10-250 kDa (Precision Plus Protein™ Dual Color Standards, BIO-RAD, USA) was loaded on to the gel along with 10 μl of samples in each lane. The gel was run using a vertical electrophoresis system (Fisherbrand™ FB-VE10-1). After electrophoresis, the gel was stained with 0.02% Coomassie Brilliant Blue R-250 (Sigma-Aldrich Chemical, St. Louis, MO, USA) in 50% v/v methanol and 7.5% v/v acetic acid for 30 min. The gel image was captured after overnight de-staining in 50% methanol and 7.5% acetic acid solution.

5.2.13 Statistical analysis

Experimental data were analyzed by two-way analysis of variance and are shown as mean \pm SD of at least three replicates. The significant differences ($p < 0.05$) between the treatments were evaluated using Tukey's HSD test using JMP Pro (Version 15, SAS Institute Inc, NC, USA). The TGA, SDS-PAGE and FTIR results were analyzed descriptively.

5.3. Results

5.3.1 PAW properties

The plasma activated water was evaluated for its hydrogen peroxide content, ozone content, pH and temperature after 10, 20, 30 and 45 min of plasma treatment. In control, 0(PAW) represents the deionized water without WPI. In P10, P20, P30 and P45, 0(PAW) represents the property of PAW at the respective activation time. The properties of PAW after different plasma treatment time are summarized in Figure 5.2, where Control indicates the untreated deionized water. The hydrogen peroxide concentration was increasing linearly with treatment time with maximum concentration of 2.32 mM after 45 min plasma treatment. In the case of ozone concentration, the 20 min treatment had the maximum concentration of 2.07 mg/l. There was a reduction in the ozone concentration after 20 min treatment, which is due to the conversion of ozone into hydrogen peroxide with the increase in the hydroxyl radical concentration (Chen & Wang, 2021). Significant increase in the temperature of water was observed during plasma treatment and an increase of 8.7°C ($p>0.05$) was observed after 45 min treatment when compared with the untreated water temperature.

5.3.2 Turbidimetric analysis & color analysis of WPI

Turbidimetric analysis was conducted to determine aggregation of proteins due to covalent and non-covalent protein-protein association following PAW treatment (Table 5.1). As it could be seen, no significant ($p>0.05$) change in the turbidity of samples after PAW treatment was observed from the control with concentrations of 5 mg/ml and 10 mg/ml. There was a slight increase in the turbidity of PAW30 and PAW45 treated samples at 50 mg/ml concentration. This indicates mild oxidation of proteins by the PAW reactive species at higher protein concentration which enhances the non-covalent protein-protein association (Feng et al., 2015). Availability of more reactive sites in protein at higher concentrations resulted in the increased aggregation of proteins and turbidity (Aicardo et al., 2018). The oxidative reactive species present in the PAW, particularly hydrogen peroxide and ozone can cause the formation of disulfide bonds from the free thiols causing the covalent aggregation of proteins. Formation of dityrosine from the oxidation of tyrosine could also lead to the covalent aggregation (Zhou et al., 2016b).

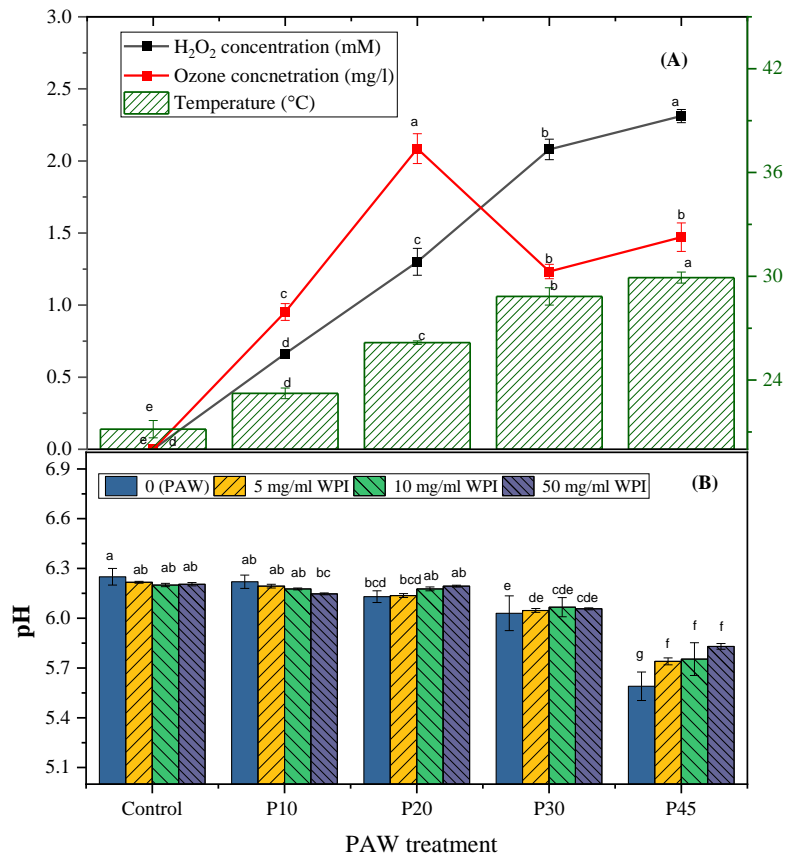


Figure 5.2 Plasma activated water properties: (A) changes in hydrogen peroxide concentration, ozone concentration and temperature (B) Changes in pH of PAW. (Values that are not connected by same letter are significantly different at $p < 0.05$)

Color changes in PAW treated samples and the control samples after drying are given in Table 5.1. Increases in the b^* value and the whiteness index (WI) were observed with increase in PAW time, while there was a reduction in ΔE value at 5 mg/ml and 10 mg/ml protein concentrations. No significant change in the ΔE value and WI was observed in 50 mg/ml protein samples after PAW treatment. Increase in the whiteness of the samples could be due to discoloration of WPI by hydrogen peroxide in PAW (Croissant et al., 2009). Increase in the b^* value of cold plasma treated WPI solution by cold plasma was also reported by Segat et al. (2015). They reported that this increase is due to the reaction between plasma reactive species and the aromatic rings of amino acid residues of whey proteins when the WPI solution was directly exposed to the cold plasma. Similar findings were reported by Xu et al. (2021b) in BSA after high voltage cold plasma

treatment, due to the reduction in the pH of the BSA solution particularly caused by the reactive nitrogen species in the plasma. The present finding suggests that such vigorous reactions do not take place when the WPI is treated with the PAW produced by this experiment due to the absence of reactive nitrogen species in the PAW and the negligible changes in the pH of PAW with different plasma treatment times. pH of the PAW was reported along with the changes in the pH of WPI solution after adding the PAW (Fig. 5.2). No significant change ($P>0.05$) in pH of PAW was observed till 30 min of plasma treatment and the pH was reduced to 6.03 and 5.6 from 6.26 after 30 min and 45 min treatments respectively. No significant change in the WPI solutions were observed after the addition of PAW, except in P45 treatment, in which there was a slight increase in the pH of the samples observed with respect to the concentration of WPI.

Table 5.1: Effect of PAW treatment on color, turbidity, and soluble protein content of WPI

PAW treatment	b* value	ΔE	Whiteness index	Turbidity	Soluble protein content (mg/ml)
5 mg/ml concentration					
Control	7.67±0.1d	0.17±0.03g	77.51±0.16gh	0.105±0.01f	0.907±0 e
P10	6.01±0.03fg	2.05±0.57ef	77.1±1.01hi	0.096±0 f	0.929±0.01 b
P20	6.33±0.06f	2.36±0.17def	79.78±0.19d	0.107±0.01f	0.917±0.01d
P30	5.68±0.02gh	2.85±0.19de	80.06±0.26cd	0.105±0f	0.902±0 e
P45	5.26±0.03h	4.4±0.09abc	81.76±0.11b	0.105±0.01f	0.926±0.01 bc
10 mg/ml concentration					
Control	9.62±0.06b	0.17±0.07g	79.47±0.19de	0.177±0e	0.906±0 e
P10	10.35±0.08a	5.05±0.22a	74.66±0.21l	0.18±0e	0.921±0 bcd
P20	7.21±0.25de	4.65±1.12ab	84.09±1.15a	0.178±0e	0.917±0.01d
P30	6.93±0.05e	2.73±0.11def	80.92±0.32bc	0.185±0e	0.893±0 f
P45	7.1±0.13e	2.61±0.12def	80.77±0.62c	0.19±0d	0.927±0 bc
50 mg/ml concentration					
Control	9.63±0.07b	0.21±0.07g	78.72±0.24ef	0.765±0b	0.906±0 e
P10	9.23±0.47b	3.26±0.16cde	75.99±0.38jk	0.753±0c	0.908±0.01 e
P20	9.5±0.19b	2.45±0.88def	76.58±0.89ij	0.757±0bc	0.925±0.01bcd
P30	10.78±0.07	3.42±0.14bcd	75.34±0.14kl	0.783±0a	0.914±0 cd
P45	8.73±0.1c	1.51±0.38f	78.02±0.38fg	0.788±0a	0.949±0.01 a

Values that are not connected by same letter are significantly different at $p<0.05$

5.3.3 Total soluble protein content

The total soluble protein content provides information on the solubility of the protein samples. The results on the soluble protein content of PAW treated and untreated samples are given in Table 5.1. It was observed that the soluble protein content increased in all protein concentrations after PAW treatment, except in P30 treatment. Similar increase in the solubility of peanut protein isolate after 3 min cold plasma treatment were reported by Ji et al. (2018). However, maximum reduction in the soluble protein content of 0.89 mg/ml was observed in P30 treatment of 10 mg/ml WPI sample. Exposure of the active sites on the surface of the proteins to the water molecules caused by the reactive species in PAW, thereby increased the interaction with the water molecules, which could explain the increase in the soluble protein content of the samples (Dong et al., 2017).

5.3.4 Sulfhydryl (SH) group content

Effect of PAW reactive species on aromatic and sulfur-containing amino acid side chains which are sensitive to oxidation was studied through -SH group content. Changes in the sulfhydryl content of the protein is also an indicator of functional and structural modifications (Li et al., 2020). The total and exposed -SH content of PAW treated WPI at different concentration levels are given in Table 5.2. Gradual reduction in both exposed and total -SH content was observed in all concentrations after PAW treatment indicating unfolding of proteins and exposure of the cysteinyl -SH groups upon PAW treatment. In 5 mg/ml WPI concentration, 43% and 46% reductions respectively, in exposed and total -SH content, were observed. In the case of 50 mg/ml concentration only, 22% and 34% reductions in the exposed and total -SH contents were observed. Slight increase in the -SH group content was observed from P30 to P45 treatments. The results demonstrate that the free sulfhydryl groups are oxidized by the reactive species in PAW into sulfinic/sulfonic acids leading to the reduction in the free -SH group content (Xu et al., 2021b). Similar decrease in the -SH group content was reported in peanut protein isolate after 3 min of cold plasma treatment (Ji et al., 2018). The non-significant increase in -SH group content between P30 and P45 could be due to either the disruption of disulfide bonds by reactive species (Ji et al., 2018) or attainment of equilibrium between the reactive species and -SH groups (Segat et al., 2015).

Table 5.2 Effect of PAW on SH group content of WPI

PAW	5mg/ml		10 mg/ml		50 mg/ml	
	Exposed SH ($\mu\text{M/g}$ protein)	Total SH($\mu\text{M/g}$ protein)	Exposed SH ($\mu\text{M/g}$ protein)	Total SH($\mu\text{M/g}$ protein)	Exposed SH ($\mu\text{M/g}$ protein)	Total SH($\mu\text{M/g}$ protein)
Control	2.17 \pm 0.06a	4.35 \pm 0.12a	3.52 \pm 0.09a	6.35 \pm 0.3a	4.34 \pm 0.22a	8.67 \pm 0.64a
P10	2.12 \pm 0.1a	3.9 \pm 0.23b	3.11 \pm 0.1b	4.61 \pm 0.22b	3.99 \pm 0.07ab	7.07 \pm 0.06b
P20	1.69 \pm 0.1b	2.95 \pm 0.13c	2.75 \pm 0.12c	4.04 \pm 0.14bc	3.75 \pm 0.15bc	6.59 \pm 0.16bc
P30	1.36 \pm 0.05c	2.06 \pm 0.04d	2.49 \pm 0.1cd	3.71 \pm 0.25c	3.18 \pm 0.17d	6.12 \pm 0.09c
P45	1.24 \pm 0.11c	2.32 \pm 0.13d	2.22 \pm 0.1d	3.82 \pm 0.32c	3.37 \pm 0.1cd	5.75 \pm 0.31c

Values that are not connected by same letter are significantly different at $p < 0.05$

5.3.5 Foaming properties

In order to investigate the changes in the surface hydrophobicity from the PAW treatment on the foaming properties of WPI, the foaming capacity and foam stability of the PAW treated WPI solutions were studied. Figure 5.3(A) shows the foaming properties of WPI at different concentrations as a function of PAW treatment times. As reported in Fig. 5.3(A), the foaming properties of the PAW treated samples improved significantly ($p < 0.05$) with PAW treatment time at all concentrations. The foaming capacity and foam stability increased by 33% and 16.7% respectively from the control with PAW 45 treatment at 5% concentration. However, there was a decrease in these properties at 10 mg/ml concentration when compared to 5 mg/ml concentration, with 25% and 11.1% increase in the foaming capacity and foam stability respectively after PAW 45 treatment. Highest foaming capacity of 225% was observed in 50 mg/ml WPI with PAW 45 treatment. As observed in surface hydrophobicity, exposure of hydrophobic groups and unfolding of the protein structure enabled the formation of a better air-water interface and the ability to form a more stable foam (Segat et al., 2015). Similar findings on increase in the foaming properties of whey protein and soy protein was reported by Segat et al. (2015) and Sharafodin and Soltanizadeh (2022) after cold plasma treatment.

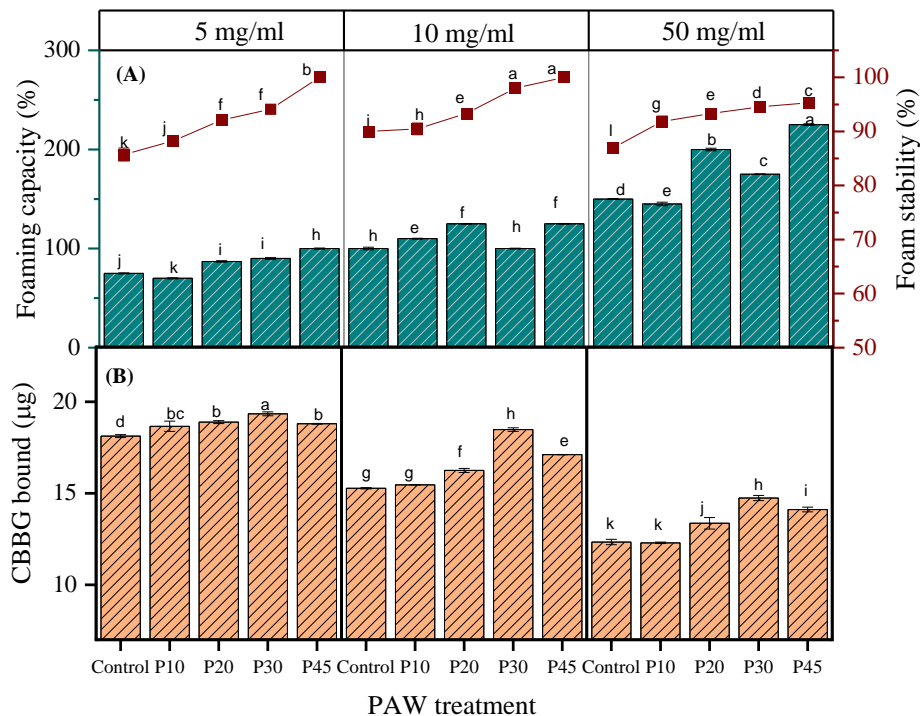


Figure 5.3 Effect of PAW treatment on foaming properties (A) and surface hydrophobicity (B) of WPI

5.3.6 Surface hydrophobicity

The surface hydrophobicity of the samples was determined using the dye binding method and the results are presented in Figure 5.3(B). The anionic CBBG dye binds with the aromatic and basic amino acid residues of protein by hydrophobic interactions and van der Waals forces (Cao et al., 2016). It is evident from the figure that the dye binding was increased with an increase in the PAW production time. Protein concentration was also found to have an influence on the hydrophobicity of the samples. When compared with the control, 14.34%, 12.05% and 3.75% increases in the hydrophobicity of protein samples were observed with PAW 45 treatment in 50 mg/ml, 10 mg/ml and 5mg/ml concentrations respectively. Maximum exposure of hydrophobic groups in CBBG bound values of 19.34 µg, 18.48 µg, 14.74 µg respectively ($p > 0.05$) were observed in PAW30 treatment in WPI concentrations (5 mg/ml, 10 mg/ml and 50 mg/ml). Exposure of amino acid residues from the interior of the protein structure and molecular unfolding could have increased the CBBG binding (Segat et al., 2015). The reactive species present in the PAW could have caused the surface amino acid chain modification, cross linking and unfolding of molecular proteins (Ji et

al., 2018; Segat et al., 2014). A slight reduction in the hydrophobicity was observed with PAW 45 treatment compared with PAW 30. Feng et al. (2015) reported a reduction in the hydrophobicity of oxidized WPI samples and they proposed that aggregation of protein by oxidation could partially shield the effects of unfolding by oxidation (Li et al., 2012). This can be the cause of reduction in the hydrophobicity of WPI samples at PAW 45.

5.3.7 TGA analysis

TGA analysis was conducted to assess the changes in the thermal stability of WPI after PAW treatment. The thermogravimetry (TG) and derivative thermogravimetry (DTG) curves of PAW treated WPI at different concentrations are given in the Fig.5.4 (a) (c) (e) and Fig.5.4 (b) (d) (f) respectively. It is evident from the figure that the protein undergoes a two-stage degradation in the analyzers temperature range of 30°C to 600°C. Degradation from 30°C to 200°C corresponds to the moisture loss from the samples and the second stage from 200-600°C is attributed to the chemical decomposition of the WPI samples (Azevedo et al., 2015). The thermal degradation parameters of PAW treated and untreated WPI samples at different concentrations are given in Table 5.3. No drastic change in the initial degradation (T_i), maximum degradation (DTG_{max}) and final degradation (T_f) temperatures of the PAW treated samples were observed except for P20 treatment. Reduction in these values for P20 treatment indicates the decrease in the thermal stability of the WPI. Reductions in the mass loss percentage and maximum degradation temperature were observed in P20. From the PAW properties, it is evident that the ozone concentration of PAW increased significantly at P20. Therefore, the reduction in the thermal stability values in P20 indicates the oxidation of protein by ozone rather than hydrogen peroxide (Sutariya & Patel, 2017). Increases in the thermal stability parameters were observed with respect to the concentration of the WPI in untreated samples. Cold plasma treatment decreased the thermal stability of pea protein isolate (Ji et al., 2019) and zein protein (Dong et al., 2017) due to the surface etching and loosening of peptide bonds of the protein by direct exposure.

Table 5.3. Thermogravimetric characteristics of PAW treated WPI

PAW treatment	Initial degradation temperature T_i (°C)	Final degradation temperature T_f (°C)	DTG _{max} (°C)	Weight loss (%) (T_i - T_f)	Residual at 600°C (%)
5 mg/ml					
Control	261.37	338.89	298.07	52.2	26.06
P10	261.05	344.84	299.45	58.4	26.28
P20	249.7	328.72	297.64	50.2	27.22
P30	262.81	332.56	298.92	54.3	27.15
P45	253.07	345.64	300.70	56.0	28.07
10 mg/ml					
Control	258.34	339.58	298.34	52.1	28.97
P10	271.59	337.82	302.41	60.5	26.86
P20	252.87	328.88	296.73	55.8	27.34
P30	258.34	342.13	299.89	57.5	27.59
P45	256.59	348.09	302.79	66.3	21.89
50 mg/ml					
Control	263.77	343.09	303.26	56.5	29.06
P10	267.28	356.33	299.43	61.2	24.21
P20	253.07	324.58	293.98	43.8	22.61
P30	261.77	337.82	300.27	55.6	26.09
P45	258.34	333.36	299.03	54.3	26.55

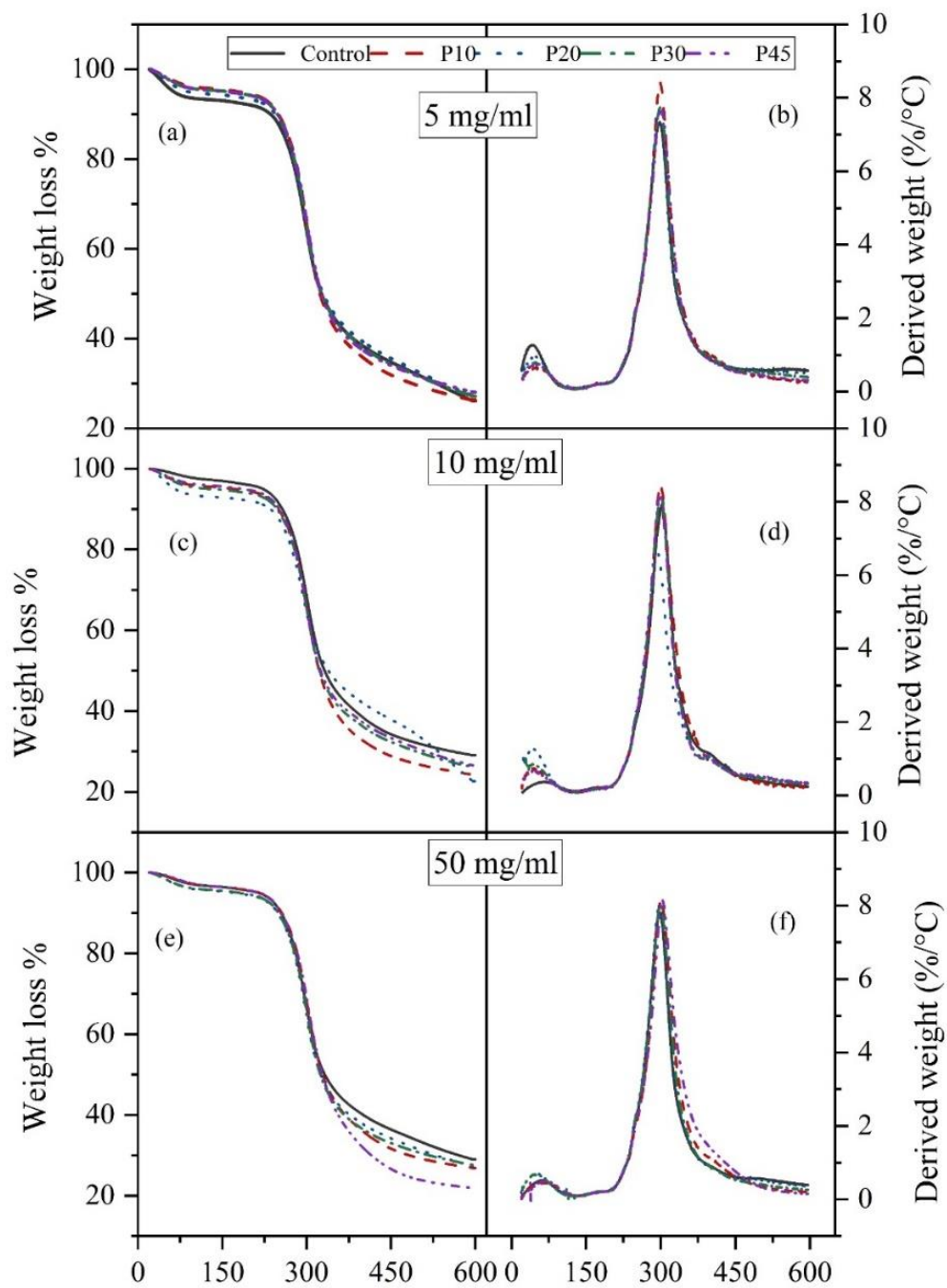


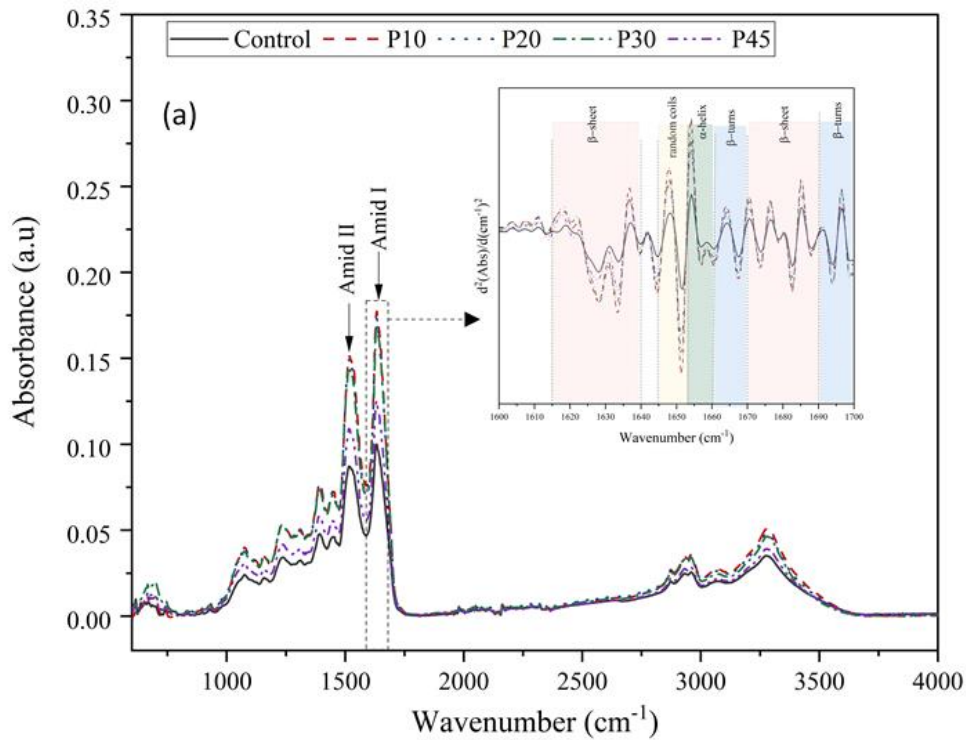
Figure 5.4. Thermogravimetric profiles of PAW treated WPI samples: Profiles (a) (c) (e) are Weight loss % vs temperature ($^{\circ}\text{C}$) and profiles (b) (d) (f) are Derived weight ($\%/\text{^{\circ}\text{C}}$) vs temperature ($^{\circ}\text{C}$)

5.3.8 FTIR spectroscopy

PAW treated whey protein isolate was evaluated through Fourier transform infrared (FTIR) spectroscopy analysis to obtain information on its secondary structural properties. The nine infrared absorption bands attributed to proteins and peptides namely Amide I-VII band ranged from 200 cm^{-1} to 1700 cm^{-1} and Amide A and B ranged from 3100 cm^{-1} to 3300 cm^{-1} . The Amide I bands are attributed to the C=O stretching (80%) with minor C—N stretching, Amide II are from N—H bending (60%) and C—N stretching (40%) and Amide III bands are contributed by the C—N stretch (40%) and N—H bend (30%). The FTIR spectrogram of the control and PAW treated WPI freeze dried samples are given in Fig 5.5(a-c). The figure presents clear peaks in N-H stretching (3281 cm^{-1}), C=O stretching (1634 cm^{-1}), C—N stretching (1511 cm^{-1}) and N-H bending (1395 cm^{-1}) regions. Further, all the infrared spectrum of the PAW treated samples displayed similar spectrum to that of the control, indicating that the functional groups of the WPI samples were not altered by the PAW treatment. Increase in the peak intensity in P10 samples was observed in all WPI concentrations. In the case of 5 mg/ml treatment, peak intensity increased with the increase in PAW time. Nevertheless, in the 50 mg/ml concentration, decrease in the peak intensity was observed in P30 and P45 treatments. The changes in peak intensity may be because of unfolding and cross-linking of the proteins in relation to the reactive species concentration in PAW (Jiang et al., 2020).

Amide I (1600–1700 cm^{-1}) band is widely used in the analysis of protein secondary structure components namely α -helix (1650-1660 cm^{-1}), β -sheet (1618-1640 cm^{-1} & 1670-1690 cm^{-1}), β -turn (1660-1670 cm^{-1} & 1690-1700 cm^{-1}), and random coils (1645 -1652 cm^{-1})(Carbonaro & Nucara, 2010; Meng et al., 2021; Xu et al., 2021b). The secondary derivative band narrowing/peak sharpening method was used to identify a hidden peak in the Amide I region (1600-1700 cm^{-1}). The spectra were processed by Origin Pro 2021 software (OriginLab Corporation, Northampton, USA). The percentage of secondary structure components are calculated from the band area of the second derivative spectrum (Zhang et al., 2020) and the results are given in Table 5.4. It is evident from the figure that the conformational changes in the secondary structure were influenced by the concentration of WPI solutions. In 5 mg/ml concentration, increase in β -sheet percentage from the 46.56% found in the control to 48.52% observed with P30 treatment is indicating the cross-linking of whey proteins (Ng et al., 2021). Whereas in 10 mg/ml concentration there was a reduction in

the β -sheet percentage from 46.73% for the control to 44.58% with P30 treatment. Maximum increase in the β -sheet percentage was observed in P45 treatment of 50mg/ml treatment concentration. Herein, the maximum reduction in the random coil percentage was also observed (1.21%). In α -helix content, reduction in its percentage was observed in all concentrations after PAW treatment except in P45 in 5 mg/ml concentration where there was a 0.63% increase in α -helix which was recorded. Increase in the β -sheet percentage of whey proteins after oxidation was observed by Feng et al. (2022). Correspondingly, reduction in β -turns was mostly observed in all treatments except in PAW30 treatment of 10 mg/ml concentration. Apparently, there was a partial folding and unfolding of the protein secondary structure caused by PAW treatment. Similar increase in β -sheet and random coils contents with a 4.1 % reduction in α -helix content for peanut protein isolate was reported by Ji et al. (2018) within 4 min of cold plasma treatment.



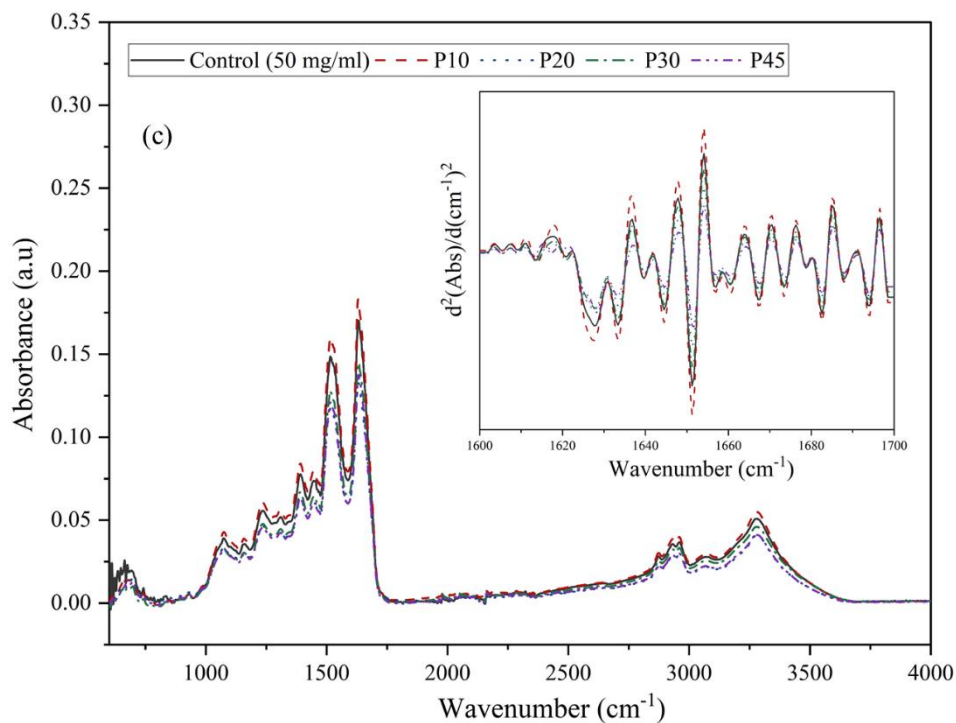
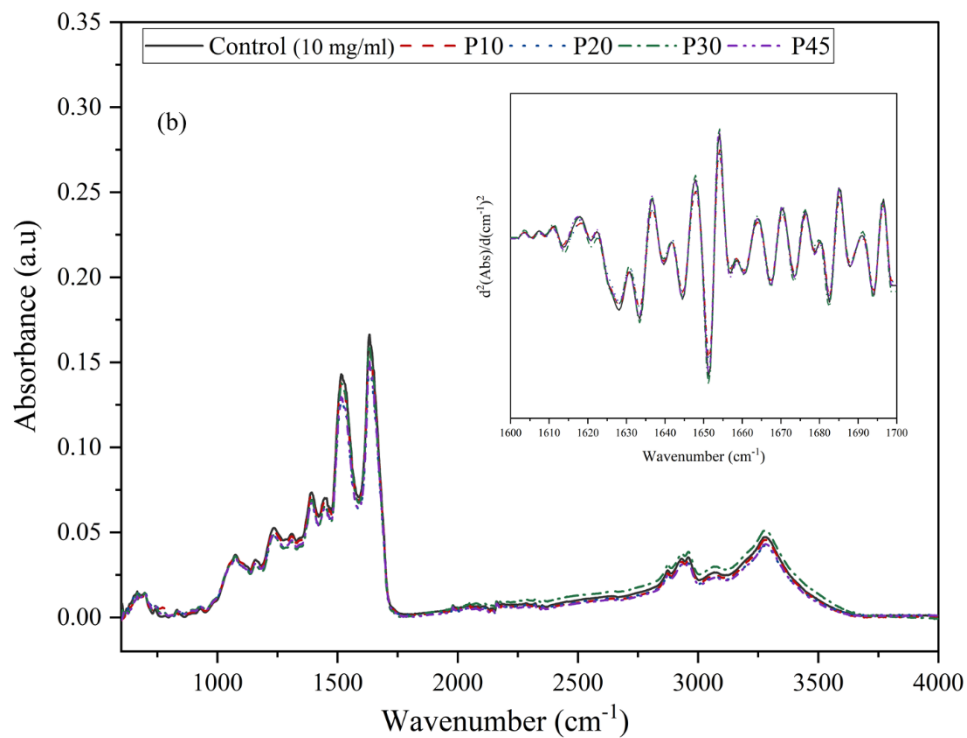


Figure 5.5 FTIR Spectrum of PAW treated WPI samples : (a) 5 mg/ml (b) 10 mg/ml (c) 50 mg/ml

Table 5.4 Secondary structural components of PAW treated WPI

PAW treatment	β -sheet (%)	Random coils (%)	α -helix (%)	β turn (%)
5 mg/ml				
Control	46.23±0.36fg	8.08±0.1ef	21.65±0.08b	17.66±0.47b
P10	47.62±0.1cd	9.13±0.07bc	21.75±0.07b	15.56±0.03ef
P20	47.97±0.15bc	9.25±0.08b	21.68±0.05b	15.62±0.23ef
P30	48.56±0.1b	9.12±0.08bc	20.64±0.07de	15.48±0.11ef
P45	46.98±0.1def	8.69±0.03cd	22.28±0.09a	14.96±0.08g
10 mg/ml				
Control	46.73±0.08ef	8.16±0.12def	21.05±0.12c	16.57±0.13d
P10	47.16±0.13de	7.99±0.13f	20.78±0.11cde	16.43±0.14d
P20	46.96±0.03def	8.05±0.11ef	20.6±0.37e	17.18±0.1bc
P30	44.58±0.1h	8.1±0.12ef	20.96±0.11cde	19.06±0.09a
P45	45.88±0.08g	7.96±0.02f	21.57±0.08b	17.51±0.17b
50 mg/ml				
Control	46.67±0.07ef	8.04±0.06ef	21.07±0.13c	16.57±0.16d
P10	47.17±0.09de	8.56±0.09de	21.85±0.12b	15.18±0.11fg
P20	47.55±0.07cd	7.14±0.07g	21±0.12cde	16.67±0.06cd
P30	46.52±0.06efg	9.96±0.12a	21.02±0.15cd	16.54±0.13d
P45	50.6±0.37a	6.83±0.09g	19.06±0.11f	14.89±0.11e

Values that are not connected by same letter are significantly different at p<0.05

5.3.9 SDS-PAGE analysis

The electrophoretic profile of PAW treated, and control samples is shown in Fig. 5.6. The gel was run under reducing condition using β -mercaptoethanol as a reducing agent. The bands at 11 kDa, 17 kDa, 35 kDa and 66 kDa are characteristics of α -lactalbumin, β -lactoglobulin(monomer), β -lactoglobulin (dimer) and bovine serum albumin (BSA) respectively (Qi & Onwulata, 2011). The patterns reveal that there were no new bands formed in the WPI samples after PAW treatment indicating that no new functional groups are formed, and the results are consistent with the findings from FTIR spectral analysis. A slight decrease in the β -lactoglobulin(monomer) band intensity of

P45 treatment in 10 mg/ml is due to the formation of β -lactoglobulin aggregates and decrease in the solubility of protein (Ng et al., 2021). However, all other bands showed no change in their intensity, indicating that there was no protein aggregation caused by the PAW reactive species.

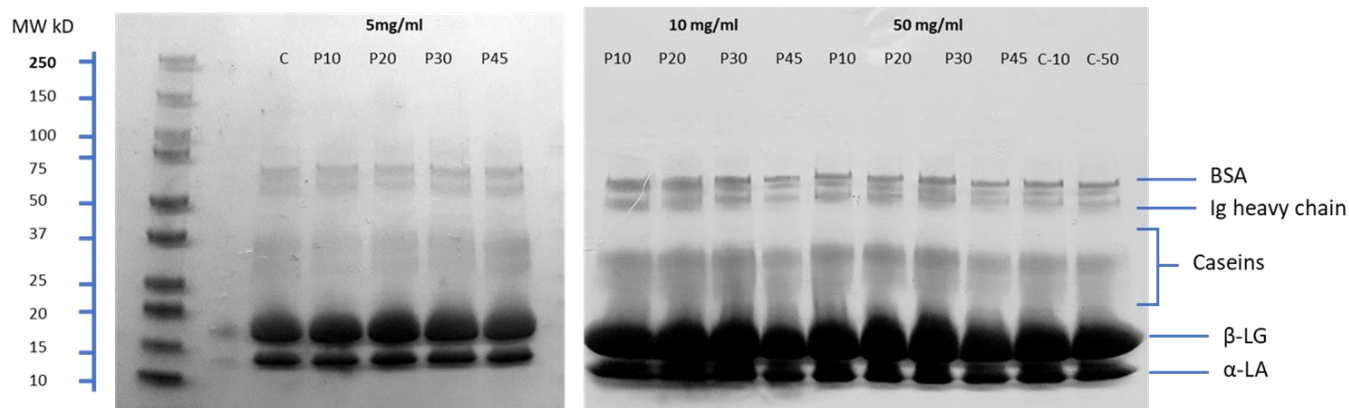


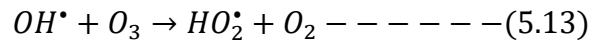
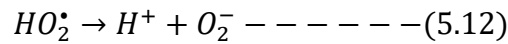
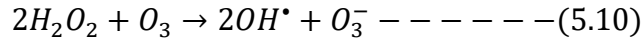
Figure 5.6 SDS-PAGE band profile of PAW treated WPI

5.4. Discussion

Plasma activated water is being considered as a versatile alternative to the use of direct plasma applications in food to overcome the undesirable changes in food quality caused by the plasma reactive species. Plasma activated water does contain the reactive species produced in the nonthermal plasma and while its chemistry continues to change by various post-discharge reactions inside the liquid phase making it a complex chemical system (Thirumdas et al., 2018). On the other hand, proteins are very sensitive to the oxidative species present in the PAW, and it is expected to undergo functional and conformational changes after PAW treatment due to oxidative stresses. From the results it is evident that the reduction in SH group content and increase in the surface hydrophobicity of the PAW treated WPI samples was due to the partial unfolding of the protein caused by oxidation of the amino acid side chains. However, the TGA, SDS-page and FTIR results indicate that no changes in functional groups and disulphide induced aggregations of proteins were not promoted by the ROS in PAW.

Hydrogen peroxide and ozone are the primary long-lived reactive oxygen species in argon-oxygen nonthermal plasma activated water. The results indicate that the concentration of hydrogen peroxide increases with time whereas the concentration of ozone has a non-linear relationship with the plasma activation time. This is due to the post-discharge reactions between hydrogen peroxide and ozone through the peroxone process. Further, the hydrogen peroxides also continue to react

with each other the hydroxyl radicals, HO_2^\bullet radicals and water molecules through varied chemical reactions (Equations 5.8 to 5.14) below (Brisset & Pawlat, 2016; Shen et al., 2019a; Zhou et al., 2020).



These hydroxyl radicals and HO_2^\bullet radicals, break the structurally important C-N bonds by hydrogen abstraction in the peptide chains of the proteins (Xu et al., 2018). Hydrogen abstraction from the protein back bone (C-H) leads to cleavage and hydrogen abstraction from the amino acid side chains of the protein leads to protein hydroxylation. Further, as the carbonyl oxygen has the ability to form multiple hydrogen bonds simultaneously, the NH and C=O form a kinetic trap for hydrogen abstraction by the free radicals (OH^\bullet and HO_2^\bullet)(Scheiner & Kar, 2010). The HO_2^\bullet radicals, from the dissociation of hydrogen peroxide, are also involved in the breakage of C-O bonds and double bond formation causing changes in the structure of proteins (Jiang et al., 2020). These radicals along with ozone also cause cleavage in C-N bonds by formation of resonance-stabilized radicals or by producing primary alkyl radicals via interactions with amino acids (Yusupov et al., 2013a).

Hydrogen peroxide concentration also plays an important role in preventing or promoting the denaturation of protein. Aggregation of β -lactoglobulin oligomers in the whey protein by the formation of intermolecular disulfide, involving sulfhydryl–disulfide interchange, is considered one of the major mechanisms of protein aggregation. Modification of sulfur containing amino acids in β -lactoglobulin to a non-reversible form of sulfonic acid at higher H_2O_2 concentrations inhibits the intermolecular disulfide formation thus preventing the formation of protein aggregates

resulting in better thermal stability of the proteins (Sutariya & Patel, 2017). This explains the variations in the functional and physicochemical properties of PAW treated WPI samples according to the concentration of hydrogen peroxide and ozone. Apart from this, these reactive species interact with the protein molecules and produce amino acid-derived peroxy radicals which propagate inter- and intra- molecular oxidation at higher concentrations (Aicardo et al., 2018). Further, the amino acid composition also influences the interaction of these ROS with the proteins. Sulfur containing and aromatic amino acids such as cysteine, methionine, phenylalanine, tyrosine and tryptophan are highly susceptible to oxidation by the reactive oxygen species of Ar/O₂ plasma specifically hydroxyl radicals and ozone. The aliphatic amino acids undergo modifications by the hydroxyl radicals (Wenske et al., 2021). The results also indicate that an increase in ozone concentration in P20 caused changes in the thermal stability of the sample. Still its impact on other physicochemical or functional properties of WPI were found non-significant. The shorter lifetime of ozone in the presence of hydrogen peroxide, due to the peroxone process (Equation 5.10), could reduce the impact of ozone on protein.

5.5. Conclusion

The present study demonstrates that the functional and structural properties of WPI are affected by the reactive oxygen species in PAW. Hydrogen peroxide and its post discharge reactions with ozone and water molecules result in the mild oxidation of proteins. The foaming property of WPI increased with both WPI concentrations and PAW treatment times while there were no such improvements observed in the solubility of proteins. Further, the oxidation induced changes in the surface hydrophobicity, solubility and sulfhydryl content of proteins did not form insoluble aggregates or disulfide bonds in WPI. It is also evident that the protein concentration also played an important role in countering the oxidation by PAW. As nonthermal plasma and PAW chemistry are still under research for commercialization, the findings of this study are important in understanding the mechanisms of reactivity between the reactive oxygen species in PAW and proteins. Future investigation on the effects of both reactive oxygen and nitrogen species on proteins and the protein-induced radical formation upon PAW treatment will help in understanding the synergistic reaction behavior, stability, and toxicity of plasma species.

CONNECTING TEXT

The effect of PAW on the protein was investigated in the previous chapter. From the results it is evident that PAW is not causing any changes in the functional groups of the protein. However, milder oxidation of the protein samples was observed. With this background, the disinfection properties of PAW on fresh foods was tested in the next chapter. From the previous chapters it is apparent that PAW has the potential to be used as a disinfectant. Nonthermal plasma has the disadvantage of inefficient disinfection on irregularly shaped food materials. Although PAW has a better coverage over the surface of food materials, it is important to investigate if there is a change in the disinfection properties of PAW with different textures of food materials. To explore this area, two leafy vegetables, kale and spinach were disinfected with PAW and the disinfection efficiency and the changes in the quality parameters were evaluated in Chapter VI. The kale and spinach samples were pre-inoculated with *E. coli* cells and the disinfection efficiency of PAW activated for different times from 10 min to 60 min was evaluated.

CHAPTER VI

EFFECT OF PLASMA ACTIVATED WATER ON *ESCHERICHIA COLI* DISINFECTION AND QUALITY OF KALE AND SPINACH

6.1 Abstract

Plasma activated water (PAW) is one of the promising technologies for fresh food disinfection. In this study, PAW was generated by activating water under nonthermal plasma for 10, 20, 30, 45 and 60 min. The effectiveness of *Escherichia coli* inactivation by PAW treatment on kale and spinach samples was assessed. The differences between kale and spinach samples in terms of the product quality and nutritional characteristics upon PAW treatment was also investigated. Further, changes in leaf structure and surface morphology upon PAW treatment were also evaluated through FTIR cuticle analysis and SEM imaging of leaf surfaces. Results showed that, around 6 log CFU/g reduction in *E. coli* population was observed in PAW-45 min treatment. However, PAW treatment significantly reduced the total chlorophyll content in both kale and spinach. Overall reduction in the total phenolic content, flavonoid content and ascorbic acid content were observed according to the PAW activation time. Further, kale and spinach behaved differently in terms of antioxidant activity and membrane electrolytic leakage values upon PAW treatment. Clear changes in the cuticular layer and the surface morphological characteristics of the leaf samples were observed after PAW which could be the reason for the significant differences between kale and spinach sample characteristics in response to PAW treatments.

6.2. Introduction

Present global demand for healthy, fresh, and convenient foods are being addressed by the fresh-cut food and ready-to-eat sectors. This industry is also constantly evolving and innovating new technologies to enhance product safety and quality attributes to meet the consumer demands. Still, fresh and fresh-cut, ready-to-use fruits and vegetables are being the major cause of food borne outbreaks around the world (Machado et al., 2019). Most of these food safety concerns are linked to the cross-contamination during cultivation, post-harvest handling and packaging of these fresh-

cut products and the increasing resistance of microorganisms to conventional sanitizers (Machado et al., 2019). Chlorine and other chemical sanitizers presently used for fresh food disinfection are usually found to be effective against major food pathogens. However, the residual effect of the chemical sanitizers and their by-products pose a serious risk to humans and environmental health (Coroneo et al., 2017). Therefore, there is a need for an effective disinfection method in fresh food industry which can protect the food material from spoilage microorganisms while preserving its nutritional quality.

Atmospheric nonthermal plasma (NTP) is a novel nonthermal processing technology which has been reported to have great disinfection efficiency for many food pathogens. NTP is produced by the partial ionization of gas, producing gas reactive species, UV radiation, free radicals, charged ions, and electrons. The composition of the reactive species in NTP depends on the working gas and the system's operating conditions. Reactive oxygen and nitrogen species such as hydrogen peroxide, ozone, hydroxyl radicals, superoxide ions, nitrate and nitrite are involved in the decontamination mechanism of food pathogens. NTP has been demonstrated efficient in disinfection of fresh fruits and vegetables (Baier et al., 2014), fruit juices (Ozen & Singh, 2020), dairy products (Rathod et al., 2021) and meat products (Misra et al., 2017). Apart from inactivation of food pathogens, it is also reported to have applications in altering food functional properties (Thirumdas et al., 2017a) and removal of pesticide residues (Gavahian & Khaneghah, 2020). Despite this huge potential, NTP does have some major drawbacks such as inefficient disinfection of irregularly shaped products, site specific, surface application (Noriega et al., 2011) and uncontrolled exposure to many reactive species can cause undesirable changes in food quality (Xiang et al., 2020). Plasma activated water could be a possible alternative to NTP, where we can harvest the benefits of reactive species while having a dose dependent, complete disinfection of food materials.

Plasma activated water is produced by exposing the water to nonthermal plasma either directly or indirectly, thereby favoring the diffusion and transfer of reactive species from NTP to the water. These reactive species react with each other and with water molecules, producing long-lived reactive species in water through various post-discharge reactions (Lukes et al., 2014). Thus, combining PAW in fresh food washing process can be a possible solution for the existing chemicals-based washing methods in fresh-cut produce. Reduction in the population of *Listeria innocua* and *Pseudomonas fluorescens* inoculated on lettuce leaves after cold plasma functionalized water

washing was reported by (Patange et al., 2019). They have also reported a successful disinfection of the wash water by cold plasma treatment. Effective inactivation of food pathogens without compromising the quality was reported in celery and radicchio (Berardinelli et al., 2016), mung-bean sprouts (Xiang et al., 2019b), fresh-cut apples (Liu et al., 2020), grapes (Guo et al., 2017), rocket leaves (Laurita et al., 2021) and lettuce (Patange et al., 2019). In most of these studies it was concluded that the reactive species in the PAW create oxidative stress in the microbial cells thus causing their inactivation. However, these reactive species could also react with the food matrix and accelerate changes and possible degradation of the bioactive components in the food materials. Apart from the process conditions, the possible changes induced by reactive species also depend on the type of bioactive components present in the food (Chen et al., 2019a; Grzegorzewski et al., 2011). Most of these studies also emphasized the need for further research on the interactions between the reactive species and the food matrix and their toxicity levels in order to scale-up this technology.

Hence in this present work was carried out with an objective to evaluate the disinfection property of PAW on, two leafy vegetables, kale, and baby spinach. As these two leafy greens are rich in antioxidants and differ in their surface morphology, effect of PAW on surface morphology and its influence on other quality parameters and surface morphology was also discussed.

6.3. Materials and Methods

6.3.1 Materials

Fresh, organically grown kale (*Brassica oleracea* var. sabellica) and spinach (*Spinacia oleracea* var. bloomsdale) were purchased from the local market in Pointe-Claire, Quebec, Canada, and stored at 4°C until its further use, for a maximum of 24 hours. Leaves of same maturity were selected for the experiments. Gallic acid ($\geq 98\%$), Quercetin (95%), L-Ascorbic acid (99%), 2,2-diphenyl-1-picrylhydrazyl (DPPH), Folin-Ciocalteu's phenol reagent, 2,4,6-Tripyridyl-Striazine (TPTZ), sodium nitrite, sodium hydroxide, ferric chloride, oxalic acid, hydrogen peroxide (30%), titanium oxysulphate, were obtained from Sigma-Aldrich, Canada. 2,6-dichlorophenol indophenol (DCIP), Trolox[®] (97%), acetic acid, indigo stock solution, HPLC grade methanol, ethanol and acetone were procured from Fisher Scientific, Canada.

6.3.2 Nonthermal plasma system and PAW generation

An atmospheric pressure dielectric barrier discharge nonthermal plasma system was used for the generation of PAW (Figure 6.1). Briefly, the nonthermal plasma (NTP) system consists of two copper electrodes placed over a glass section and connected to a high voltage generator (PVM 500, Information Unlimited, USA). The glass section also acted as a dielectric barrier and the internal spacing in the section was 3 mm. An argon and oxygen gas mixture (98%: 2%) was used as a working gas and the plasma was generated at 10 kV (peak-peak) voltage and 20 kHz frequency. Distilled water was circulated inside the glass section to expose the water to plasma in the discharge gap at 100 ml/min flowrate to produce PAW. PAW was activated with NTP for 10 min (P10), 20 min (P20), 30 min (P30), 45 min (P45) and 60 min (P60).

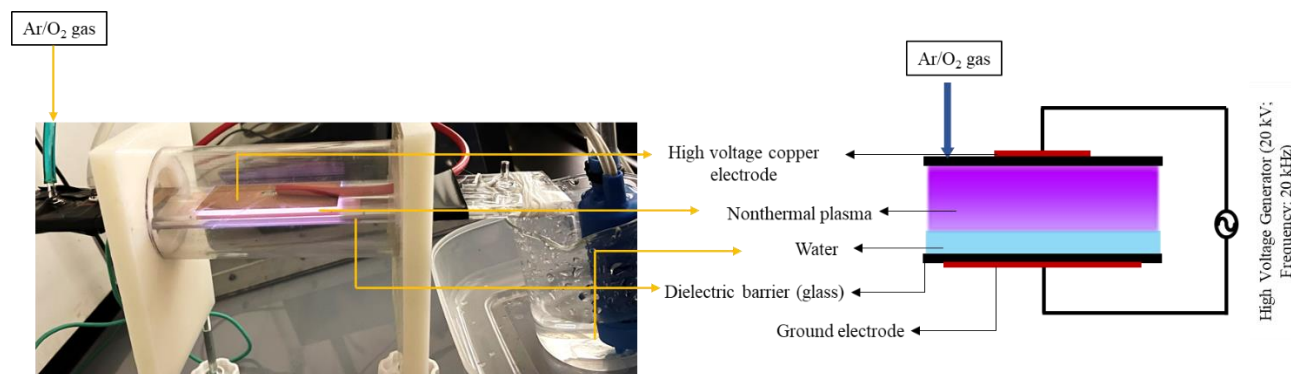


Figure 6.1 Schematic diagram of the PAW generation system

6.3.3 PAW properties

Hydrogen peroxide concentrations in PAW samples were analyzed by titanium oxysulphate colorimetric method as described in Eisenberg (1943). Briefly, 10 ml of PAW was added to 5 ml of titanium oxysulphate reagent prepared by dissolving 25 g of titanium oxysulphate in 1L of 2M H_2SO_4 . Development of yellow color was measured using a UV-Vis spectrophotometer at 407 nm and the concentrations of hydrogen peroxide in the PAW samples were read from the standard curve.

Ozone concentrations in the PAW samples were analyzed using the Indigo method (Bader & Hoigné, 1982; Burlica et al., 2006). The indigo reagent II prepared from the stock solution was added to the PAW samples immediately after generation and the concentration of ozone was measured based on the reduction in the indigo dye color read at 600 ± 5 nm and using equation 6.1.

$$\text{Ozone concentration (mg/l)} = \frac{\Delta A. 100}{f. b. V} \text{ --- (6.1)}$$

Where, ΔA = Difference in absorbance between sample and blank

b = Pathlength of the cuvette in cm

V = Volume of the sample added in ml

f = indigo sensitivity coefficient (0.42)

The pH and temperature of PAW samples were measured immediately after PAW generation using a digital pH meter (Accumet AB250, Fisher Scientific, USA) and digital thermometer respectively.

6.3.4 PAW treatment of kale and spinach leaves

Immediately after production, the PAW was used for kale and spinach washing treatments. Both kale and spinach were cut into 2 cm × 2 cm pieces from the same part of the leaves and washed with PAW. For the treatment, approximately 5 g of the cut leaf samples were immersed in 200 ml of PAW in a sterile beaker and agitated for 10 min. For the control, the samples were treated with distilled water at the same sample to water ratio for 10 min. After treatment, the samples were blot dried and stored in Ziploc® bags at 4°C for 24 hr for further analysis.

6.3.5 *Escherichia coli* disinfection procedure

For disinfection studies, overnight culture of *Escherichia coli* K12 strain (ATCC 15597; C-3000) in EC broth (Oxoid, Canada) (approximately 10⁷ cells /ml) was incubated over the leaf samples. For this step, the leaf samples were cut into 2 cm × 2 cm pieces and the surface was sterilized with alcohol. Then the samples were inoculated with 0.1 ml of *E. coli* culture on the abaxial side and incubated at 4°C overnight to facilitate cell attachment to the leaf surface.

The overnight inoculated leaves (1g) were then immersed in PAW (40 ml) produced at different activation times for 10 min with continuous agitation. For control, the leaves were agitated in distilled water. After the treatment, the leaf samples were homogenized in 10 ml of sterile water and serially diluted. From 10⁻³ and 10⁻⁴ dilutions, 0.1 ml of aliquot was spread over the nutrient agar plate and incubated at room temperature for 24 hours with three replications in each dilution. The number of cells in each dilution was then counted and presented as log CFU/g of sample.

6.3.6 Color, pH and TSS measurement

Color values of the leaves in CIE (L^* , a^* , b^*) color scale was measured using a chroma meter (CR-300 Chroma, Minolta, Japan). At least five color values were recorded from each sample at different locations on the abaxial (?) side of the leaf. The L^* value is a measure of the lightness, the a^* value of the greenness-redness and the b^* value of the blueness-yellowness. Total color difference, ΔE^* , was calculated using Hunter-Scofield's equation (Equation 6.2)

$$\Delta E = \sqrt{(L^*_{control} - L^*_{sample})^2 + (a^*_{control} - a^*_{sample})^2 + (b^*_{control} - b^*_{sample})^2} \text{ --- (6.2)}$$

To determine pH, 2 g of the sample was homogenized with 10 ml of deionized water to measure the pH value of the samples using a digital pH meter. Homogenate of 1g of sample was used to determine the TSS of the samples using a Reichert™ digital refractometer.

6.3.7 Total chlorophyll and carotenoid contents

Total chlorophyll and carotenoid contents in kale and spinach samples were analyzed according to the method given by Wellburn (1994) with a slight modification. Briefly, 1g of sample was homogenized with 10 ml of 80% (v/v) acetone and the mixture was centrifuged at 4000×g for 10 min at 4°C. After centrifugation, the supernatant was separated, and the residue was re-extracted twice with 10 ml acetone under the same condition. Supernatants from all the extracts were combined and filtered through a syringe filter and the absorbance was measured at 470 nm, 645 nm and 663 nm using a UV-Vis spectrometer. The chlorophyll and carotenoid contents were calculated from the absorbance values using the following expressions (Equations 6.3-6.6) given by Wibowo et al. (2019) and Ramazzina et al. (2015).

$$\text{Chlorophyll } a \text{ (mg/g)} = \frac{12.7 \text{ Abs}_{663} - 2.69 \text{ Abs}_{645} \times \text{ml acetone}}{\text{mg}} \text{ --- (6.3)}$$

$$\text{Chlorophyll } b \text{ (mg/g)} = \frac{21.5 \text{ Abs}_{645} - 5.1 \text{ Abs}_{663} \times \text{ml acetone}}{\text{mg}} \text{ --- (6.4)}$$

$$\text{Total chlorophyll} = \text{chlorophyll } a + \text{Chlorophyll } b \text{ --- (6.5)}$$

$$\text{Total carotenoid content} = (1000\text{Abs}_{470} - 2.270 \text{ Chl } a - 81.4 \text{ Chl } b)/227 - - - (6.6)$$

6.3.8 Determination of ascorbic acid (AA) content

The ascorbic acid (AA) content in kale and spinach samples was quantified by measuring the discoloration of 2,6-dichlorophenol indophenol (DCIP). Briefly, 5 g of the leaf sample was mixed with 15 ml of 4% oxalic acid. The supernatant obtained after centrifugation was titrated against DCIP until the appearance of stable pink color for 15 s (AOAC, 1990). Then the ascorbic acid content in the sample was determined from the standard curve prepared using analytical grade L-ascorbic acid. Ascorbic acid content in samples is expressed as mg/g fresh weight of sample.

6.3.9 Antioxidant properties

6.3.9.1 Methanolic extract preparation

For all antioxidant property experiments, methanolic extracts of the PAW treated and control samples were used. Accordingly, 1 g of leaf sample was homogenized with 10 ml of 80% methanol and centrifuged at $4000 \times g$ for 20 min at 4°C. The supernatant was collected, and the solids were re-extracted under the same conditions. The collected supernatant was used for the analysis of phenolic content, flavonoid content and antioxidant activity of the PAW treated kale and spinach samples.

6.3.9.2 Total phenolic content

Total phenolic content in the leaf samples were determined using the Folin–Ciocalteu method (Singleton & Rossi, 1965) with a slight modification. Accordingly, 0.5 ml methanolic extract of the sample was mixed with 2.5 ml of distilled water and 0.5 ml of Folin–Ciocalteu reagent. The mixture was allowed to react for 5 min and 4 ml of 7.5% sodium carbonate solution was added and the mixture was incubated for 90 min in the dark at room temperature. After incubation, absorbance was measured at 765 nm and the total phenolic content in the sample was obtained from the gallic acid standard curve and expressed as mg gallic acid equivalent (GAE) per gram of fresh weight sample.

6.3.9.3 Total flavonoid content

Total flavonoid contents in the leaf extracts were determined by aluminum chloride colorimetric assay as described by Chang et al. (2002) with some modifications. The assay involved mixing 1 ml of methanolic extract of the samples with 4 ml of distilled water and 0.3 ml of 5% sodium nitrite. After standing for 5 min, 0.3 ml of 10% aluminum chloride was added to the sample and

left to react for 5 min. Then 2 ml of 1M sodium hydroxide and 2.4 ml of distilled water were added to the sample. Then the absorbance was read at 510 nm and compared with a Quercetin standard curve that was prepared to quantify the total flavonoid content in the samples.

6.3.9.4 Total antioxidant capacity

Total antioxidant capacity was analyzed by using DPPH (2,2-diphenyl-1-picryl-hydrazyl-hydrate free radical method) and FRAP (Ferric Reducing Antioxidant Power) assays. The DPPH radical scavenging activity of the samples was determined using the method described by (Blois, 1958). For this analysis, 0.5 ml of sample extract was added to 1 ml of distilled water and 1 ml of freshly prepared 0.1mM 2,2-diphenyl 1-1-picrylhydrazyl (DPPH). The mixture was incubated for 20 min in the dark and the absorbance was measured at 517 nm. The free radicals scavenged by DPPH radicals was expressed as percentage inhibition and calculated using equation 6.7.

$$\text{Inhibition (\%)} = (Abs_{control @ 517 nm} - Abs_{sample @ 517 nm}) / Abs_{control @ 517 nm} \times 100 \quad (6.7)$$

The ferric-reducing antioxidant power (FRAP) assay of the samples was conducted according to the procedure given by Benzie and Strain (1996). Briefly, FRAP reagent was freshly prepared by mixing 300 mM acetate buffer (pH 3.6), 20 mM ferric chloride solution and 10 mM of 2,4,6-tripyridyl-s-triazine (TPTZ) solution in 40 mM HCL in the volume ratio of 10:1:1 respectively. The FRAP solution was maintained at 37°C in a water bath. Trolox was used as a standard and distilled water was used for the blank. For the assay, 2.85 ml of freshly prepared FRAP reagent was mixed with 150µl of standard Trolox solution or sample extract or blank. The mixture was then placed in the dark for 30 min and then the absorbance was measured at 593 nm. The antioxidant capacity of the samples was expressed as FRAP value in micromoles of Trolox equivalents per gram of sample (mmol TE/g).

6.3.10 Electrolytic leakage

Electrolytic leakage in the leaf samples was determined using the method described by Xu et al. (2021b) with some modifications. The leaf samples were cut into 1 cm discs and 10 of these discs were put in a 50 ml falcon tube with 25 ml of distilled water. The tubes were kept at 25°C for 30 min and the initial conductivity value (C_1) was measured using a digital conductivity meter (Hanna HI98129, Canada). Then the tubes were placed in a water bath at 100°C for 10 min, cooled to room

temperature and the conductivity of the samples were again measured (C_2). The electrolytic leakage was calculated using Equation 6.8 and expressed as a percentage.

$$\text{Electrolytic leakage (\%)} = \frac{C_1}{C_2} \times 100 \text{ --- (6.8)}$$

6.3.11 FTIR cuticle analysis

Changes in the cuticles of kale and spinach leaves were evaluated using FTIR spectroscopy according to a protocol described by Shah et al. (2019). Accordingly, the abaxial side of the leaves were kept over the diamond crystal sample platform of a Nicolet iS5® ATR-FTIR (Thermo Nicolet Instrument Corp., Madison, WI, USA). Then the IR spectrum of the samples were collected with 40 scans/sample and 4 cm^{-1} resolutions. The spectra of each sample were recorded at three different locations on the leaf and the average of these three spectra was used for further descriptive analysis after processing the spectral data using the OMNIC software (version 8, Thermo Nicolet Instrument Corp., Madison, WI, USA) for baseline.

6.3.12 SEM imaging of leaf surfaces

The images of the leaf samples were captured using a Scanning Electron Microscope (TM3000, Hitachi High-Technologies Corporation., Tokyo, Japan). A small piece from the tip portion of the PAW treated leaf samples were placed over the carbon tape of the aluminum sample stub. The abaxial side of the leaf was captured at 1000 \times magnification at 5 kV accelerating voltage.

6.3.13 Statistical analysis

Completely randomized design was used in this study. All analyses were conducted in triplicates and the results are presented as mean \pm standard deviation. The data was analysed by one-way ANOVA and the significant difference in the treatment means at 5% level are compared by Tukey's multiple range test using JMP Pro (Version 15, SAS Institute Inc, NC, USA). Results of FTIR and SEM imaging were analyzed descriptively.

6.4. Results and Discussion

6.4.1 PAW properties

The effect of the plasma activation times on the PAW properties is presented in Figure 6.2. It is evident from the figure that the hydrogen peroxide concentration and ozone concentration in the PAW increased significantly ($p < 0.05$) with increase in the plasma activation time. Maximum concentrations of 3.01 ± 0.27 mM and 2.38 mg/l of hydrogen peroxide and ozone respectively were recorded after 60 min of plasma activation. Similarly, significant reduction in the pH value of PAW was recorded after 30 min activation and a maximum reduction in the pH of 4.66 was recorded after 60 min plasma activation. Increase in the temperature of PAW to 31.3°C from 21.5°C was observed after 60 min plasma activation. In the present study, Ar/O₂ mixture was used for the generation of plasma, hence only the reactive oxygen species were expected in the plasma activated water. Hydrogen peroxide in PAW is produced by water dissociation and recombination of hydroxyl radicals from the gas phase plasma. Further, at higher hydrogen peroxide concentrations, ozone also reacts with the hydrogen peroxide through the peroxone process and produces more hydroxyl radicals and perhydroxyl radical (HOO) (Shen et al., 2019a). This reaction could be the reason for the reduction in ozone concentration after P20 treatment. Further, production of these post-discharge short-lived radicals along with the long-lived species such as hydrogen peroxide and ozone aids in the disinfection efficiency of PAW (Plimpton et al., 2013).

6.4.2 Impact of PAW treatment on *E. coli* disinfection

The disinfection property of PAW against *E. coli*, inoculated on kale and spinach leaves are presented in Figure 6.3. *E. coli* population in the control after washing with deionized water was 6.01 ± 0.39 log cfu/g and 5.89 ± 0.26 log cfu/g in kale and spinach leaves respectively. The *E. coli* population started decreasing with the application of PAW treatments. However, until the P20 treatment, no significant difference ($p > 0.05$) in the *E. coli* population was observed in both kale and spinach samples. In P30 treatment, 3.48 log cfu/g reduction was observed in kale whereas in the case of spinach, complete inactivation of the *E. coli* population was observed when compared to that of the control. Rodriguez et al. (2020) reported 0.45 log reduction in the *E. coli* K12 population with 11.5 min plasma activation of water and 1 h incubation with PAW. Complete reduction in the *E. coli* population was observed in kale with P45 treatment. In P45 and P60 PAW

treatments 100% reduction in the *E. coli* population was observed in both kale and spinach. As it can be seen from Figure 6.3 the *E. coli* inactivation was in correlation with the hydrogen peroxide concentration. There was a spike in ozone concentration in P20 treatment, however, there was no significant reduction in *E. coli* population that was observed with P20 treatment. Further, the changes in pH or temperature were not high enough to cause the microbial disinfection on their own (Ma et al., 2016). According to Ma et al. (2015), pH aids in the inactivation of microbial cells by enabling the penetration of reactive species from PAW into the cells. The results obtained here agree with this, where significant reduction in the pH and the *E. coli* population were observed from the P30 treatments.

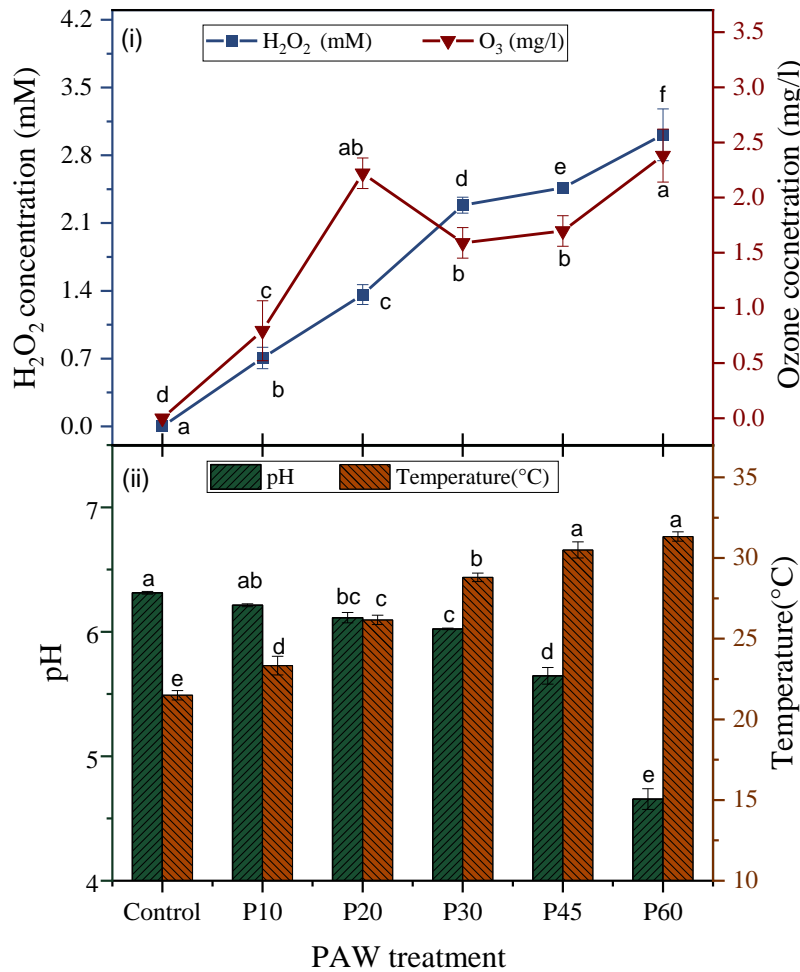


Figure 6.2 Properties of PAW with respect to plasma activation time (i) hydrogen peroxide and ozone concentrations (ii) pH and temperature

Along with PAW activation time, other factors that could influence the microbial inactivation efficiency of PAW are the synergistic effect of long-lived reactive species and their post discharge reaction chemistry (Matthew et al., 2011). Furthermore, differences in the *E. coli* inactivation following PAW treatments were observed between kale and spinach. 3.8 log reduction in *E. coli* population was observed in kale with P30 treatment whereas 5.3 log reduction in microbial population was observed in spinach with the same treatment. The surface roughness and curves on the kale leaves could have reduced the disinfection efficiency of washing (Wang et al., 2009). It is evident from the SEM images (section 3.8.) of the surface roughness of the kale leaves was higher than that of spinach. Similar reduction in the disinfection efficiency of *E. coli* O157:H7 due to leaf surface roughness was reported by Phaephiphat et al. (2018).

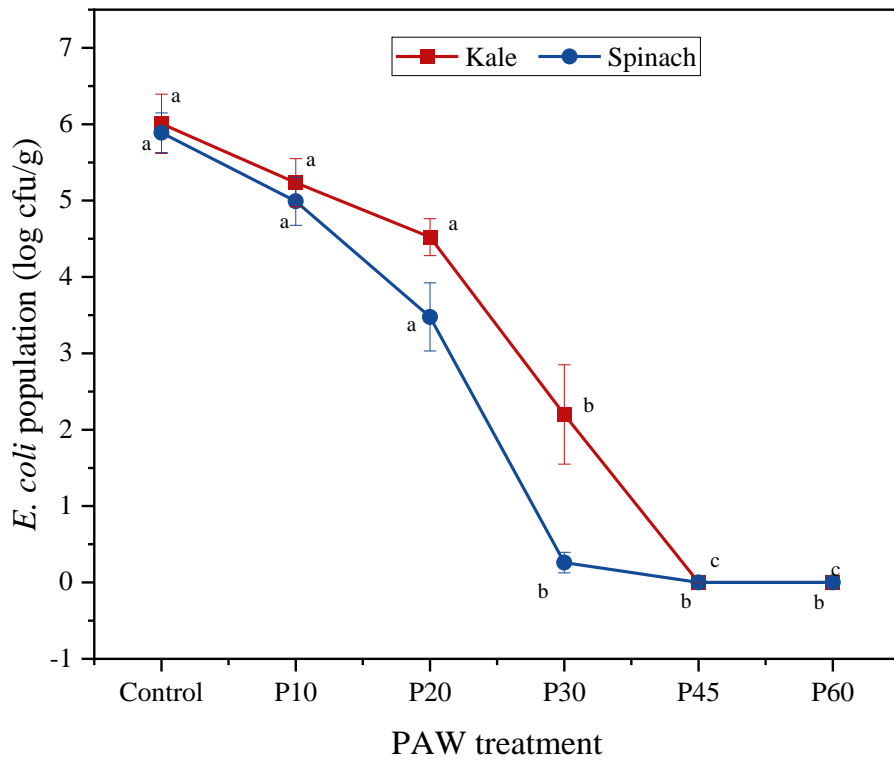


Figure 6.3 Effect of PAW treatment, at different activation times, on *E. coli* population

6.4.3 Color analysis

Changes in the color values of kale and spinach after PAW treatment are presented in Table 6.1. As shown in Table 6.1, no significant ($P > 0.05$) difference in the brightness values of both kale and spinach was observed following PAW treatment. However, significant increases ($P < 0.05$) in the a^* values of kale samples were observed in P20 and P30 treatments indicating darkening of the samples. Increase in the a^* values of the spinach samples were also observed in P30 and P45 treatments. Similar increase in the a^* values of leafy vegetables was reported by Berardinelli et al. (2016) following 30 min and 60 min of plasma treatment in water medium, and by Grzegorzewski et al. (2011) in lettuce leaves after plasma treatment.

Perceivable color differences are analytically classified using ΔE values as very distinct ($\Delta E > 3$), distinct ($1.5 < \Delta E < 3$) and less distinct ($\Delta E < 1.5$) (Ma et al., 2015). Accordingly, in all PAW treated samples, there was a distinct perceivable color difference when compared to that of the control, except for the P60 treatment of spinach. In spinach, the ΔE value of P60 treatment was less than 1.5 indicating there was no difference between the control and P60 treated samples. The L^* , a^* and b^* values of the P60 treated spinach samples also had no significant change when compared to that of the control.

The soluble solid content of kale and spinach samples after PAW treatment are given in Table 6.1. In the P10, P20 and P30 treatments of kale, the TSS increased significantly whereas in the case of spinach there was a significant reduction in the TSS values of P10 and P20 treatments as it was observed. Increase in the spinach TSS was observed in P30, P45 and P60 treatments. Increase in the TSS of PAW treated Chinese bay berries and button mushrooms during storage was reported by Ma et al. (2016) and Zhao et al. (2021) respectively. The increase in TSS could be due to the reduction in the metabolic activity of the leaves after PAW treatment due to the oxidative stress induced by the PAW reactive species (Ma et al., 2016). Differences in the response of kale and spinach samples in color and TSS values following PAW treatment clearly shows that there is a difference in the effect of PAW on different plants and plant types (Park et al., 2013).

Table 6.1 Changes in the color values and soluble solid content of kale and spinach after PAW treatment

PAW Treatment	L*	a*	b*	Δ E	TSS (°brix)
Kale					
Control	38.89a	-10.82b	10.25bc		7.77c
P10	37.13a	-10.36b	9.22c	2.40b	10.81a
P20	35.43a	-7.57a	6.02d	6.36a	9.04b
P30	38.66a	-12.31c	13.10a	3.88b	9.33b
P45	39.32a	-10.48b	9.58bc	1.89b	7.50c
P60	38.97a	-10.75b	10.28b	1.96b	7.26c
Spinach					
Control	35.22a	-8.05a	9.80a		11.03c
P10	36.00a	-7.64a	7.97b	2.07a	10.42d
P20	35.05a	-8.48a	7.93b	2.14a	9.01e
P30	35.54a	-9.77b	10.72a	2.19a	13.1b
P45	36.27a	-9.55b	9.94a	1.92ab	13.2b
P60	35.11a	-8.44a	10.45a	0.81b	14.6a

6.4.4 Chlorophyll and carotenoid contents

Effects of PAW treatment on chlorophyll and carotenoids contents of kale and spinach samples are illustrated in Figure 6.4. Chlorophyll (Chl) is an important pigment in green leafy vegetables which is highly sensitive to oxidative stress and its degradation indicates the senescence of the leaves (Waghmare & Annapure, 2017). The results showed that the Chl a, b and total Chl contents decreased with the increase in the PAW activation time. In kale, the Chl a content of the control sample was 323.6 ± 0.52 mg/g and it was reduced to 214.5 ± 0.09 mg/g in P60 treatment and a similar trend was found in Chl b and total chlorophyll contents. In spinach, Chl a content was reduced from 99.3 ± 0.15 mg/g in the control sample to 85.5 ± 0.05 after P60 treatment. However, the maximum reduction in Chl a content of spinach was recorded in P20 treatment (74.8 ± 0.11 mg/g) and concomitant reduction in Chl b and total Chl was observed in P20 treatment for spinach leaves. The results indicate that PAW induces the degradation of chlorophylls in both kale and spinach and this effect was more intense in kale than in spinach.

On the other hand, there was an increase (29%) in the total carotenoid content of kale observed upon PAW treatment with the maximum of 1647.29 ± 49.02 mg/g which was observed in P30 treatment. Whereas in spinach 12.2% reduction in total carotenoid content was recorded in P20 treatment while a 7.9% increase was observed in P30 treatment when compared to the control samples. These findings are corroborated with the color values where darkening of the leaves was observed particularly in P20 and P30 treatments. Activation of senescence enzymes such as peroxidase, chlorophyllase and chlorophyll oxidases by the ROS in PAW could have resulted in the degradation of chlorophylls and accumulation of carotenoids as a defense mechanism (Yilmaz & Gökmen, 2016). According to Yamauchi (2015) and Smirnoff (2008) under oxidative stress, chlorophylls were degraded and the carotenoids were *de novo* synthesized to protect the cells from damage. This phenomenon could have caused the increase in the total carotenoid content in the PAW treated kale samples.

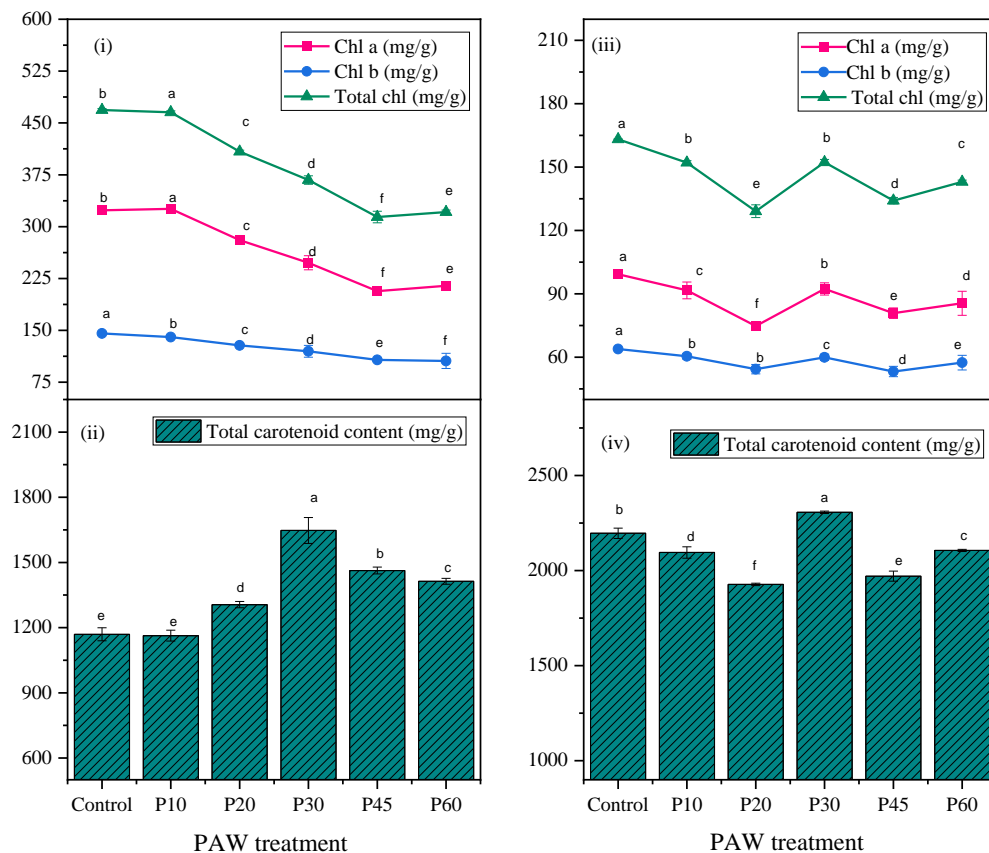


Figure 6.4 Effect of paw treatment on (i) kale chlorophyll content (mg/g); (ii) kale carotenoid content (mg/g); (iii) spinach chlorophyll content (mg/g); (iv) spinach carotenoid content (mg/g)

6.4.5 Antioxidant properties and antioxidant activity of kale and spinach samples after PAW treatment

6.4.5.1 Ascorbic acid, TPC and TFC contents

Kale and spinach are great sources of antioxidants such as ascorbic acid, flavonoids, and polyphenols. Both kale and spinach are being consumed for their high antioxidant properties and related health benefits. Results of ascorbic acid content, TPC, TFC and antioxidant activity are summarized in Table 6.2. Ascorbic acid is one of the major antioxidants present in both kale and spinach. The ascorbic acid content of the PAW treated samples increased significantly by 43.7% in the P45 treatment when compared to that of the control sample. While in spinach, a maximum increase in the ascorbic acid content of 63.4% was observed in P30 treatment and a significant reduction ($p < 0.05$) was observed at higher PAW activation times.

Reduction in total phenolic content of kale and spinach samples was observed following PAW treatments (Table 6.2). However, there was a non-linear relationship between the reduction in total phenolics content and PAW activation time in both cases. In kale, a maximum of 10 % reduction was observed with the P20 treatment. In the case of spinach, a 27.8 % reduction in the TPC content was observed with the P20 treatment. Slight reduction in the TPC content of rocket leaves after 5 min PAW washing treatment was reported (Laurita et al., 2021). However, above P20, the TPC content started increasing with increase in the PAW activation time to the maximum of 0.6% with P60 treatment in spinach. The increase in the phenolic compounds at higher PAW activation times (P30, P45 and P60) could ascribe to the accumulation of phenolic compounds as a defense mechanism to the excessive oxidative stress by the ROS in PAW. Similarly, TFC of kale samples were reduced after PAW treatment and maximum reduction of 45.8% was observed with the P20 treatment when compared to the control. In the case of spinach, no significant difference ($P > 0.05$) in TFC content in the PAW treated samples was observed except P20. Reduction in the TFC content was observed in both kale and spinach after P20 treatment. Similar findings on TPC and TFC were reported by Laurita et al. (2015) in PAW treated rocket (arugula) leaves. Reduction in the TPC after PAW treatment was reported by Liu et al. (2020) in fresh-cut apples washing. They speculated the role of enzymatic oxidation of the endogenous phenols for the reduction in the phenolic content after PAW treatment. Further, the type of phenolic compounds present in the food sample also influences the response to reactive oxygen species in NTP or PAW. (Li et al., 2019) reported the increase in gallic acid, protocatechuic acid and p-coumaric acid and reduction

in p-hydroxybenzoic acid and caffeic acid in fresh-cut pitaya fruit following plasma treatment. Similarly, Grzegorzewski et al. (2011) reported reduction in the quantities of protocatechuic acid, chlorogenic acid and caffeic acid, while reporting 44% increase in the diosmetin level and no change in the luteolin levels by the reactive species in NTP in Lambs lettuce. They claimed that the degradation of flavonoids is higher than that of phenolic acids and the degradation of the compounds depends on their molecular structure. Mono- and polyphenols are more easily oxidized by the reactive species in the plasma into volatile compounds leading to the lower levels of phenolic compounds following a plasma treatment. The ROS present in the plasma leads to the erosion of epidermal tissue layers on the leaves which exposes the flavonoids to the ROS causing their degradation (Grzegorzewski, 2011). Further, activation of phenylalanine ammonia lyase (PAL) by ROS as a stress response and subsequent synthesis of phenolic compounds can contribute to the increase in the TPC and TFC contents (Sarangapani et al., 2017b). However, they reported that with longer treatment times, the TPC content of blueberries started decreasing due to oxidative degradation of phenolic compounds. In contrary, the present findings show that TPC and TFC contents increased with longer PAW activation times. Damage of cell membrane can lead to the exposure of bioactive compounds and enhanced extractability of bioactive compounds thus potentially increasing the TFC and TPC contents. Alothman et al. (2010) also speculated that the cell wall modifications caused by ozone treatments freed some of the conjugated phenolic compounds in the cell wall of pineapple and banana leading to the increase in TPC and TFC contents. Hence, the changes induced by the ROS in PAW on the TPC and TFC contents is not only dose dependent but is also highly dependent on the bioactive components present in the food material.

6.4.5.2 Antioxidant activity

DPPH and FRAP assays were used to evaluate the changes in the antioxidant properties of the PAW treated leaf samples and the results are presented in Table 6.2. As it is evident from the results, DPPH inhibition % was more pronounced in kale than in spinach whereas FRAP activity was more in spinach than in kale. Concomitant to TPC and TFC contents, the antioxidant activity of kale and spinach samples increased with increasing PAW activation times. DPPH inhibition percentage increased to 9.8% in P10 when compared to the control and significantly reduced with further increase in PAW activation times. In spinach the DPPH inhibition was increased with PAW treatment time with a 17.65% increase with P20 when compared to control. Significant increase

in the FRAP activity of kale samples were observed except in P20 where the FRAP activity was reduced to 1.63 ± 0.04 mM TE/g. Like DPPH activity, decrease in the FRAP activity was observed up to 15.74% in P20 while a 9% increase in the FRAP value was observed in the P45 treatment. Increase in the TPC and TFC after PAW treatment could have resulted in increasing the antioxidant activity of PAW treated leaf samples. This is corroborated by the decrease in the antioxidant activity with P20 treatment where there was a significant reduction in the TPC observed in both kale and spinach. Chen et al. (2019a) also reported an increase in the DPPH and ABTS activity in PAW treated fresh-cut pear samples, while a decrease in the DPPH inhibition percentage of fresh-cut apples was reported by Liu et al. (2020) after PAW treatment. These findings emphasize the complex interaction mechanism between food bioactive compounds and the reactive species in PAW.

Table 6.2 AA, TPC, TFC contents, DPPH inhibition and FRAP of kale and spinach following PAW treatments

Treatment	Ascorbic acid content (mg/ml)	TPC (mg/g)	TFC (mg/g)	DPPH inhibition (%)	FRAP (mM TE/g FW)
Kale					
Control	85.35±1.61 d	6.97±0.05 a	0.31±0.02 b	71.66±0.85 f	1.85±0.02 b
P10	113.31±2.65 b	6.46±0.15 c	0.29±0.02 cd	81.39±0.3 a	1.97±0.02 a
P20	108.69±12.65 c	6.27±0.04 d	0.19±0.03 e	78.86±0.05 b	1.63±0.04 c
P30	107.28±2.52 c	6.72±0.10 b	0.33±0.03 a	75.17±0.16 d	1.98±0.03 a
P45	122.69±1.82 a	6.38±0.23 cd	0.28±0.04 d	72.91±0.21 e	1.93±0.04 ab
P60	104.77±1.33 c	6.35±0.01 cd	0.29±0.08 c	76.64±0.4 c	1.98±0.03 a
Spinach					
Control	23.56±0.06 e	9.28±0.01 b	0.24±0.05 a	49.41±0.12 f	4.38±0.11 c
P10	19.57±0.07 f	7.25±0.13 e	0.15±0.01 bc	56.57±0.17 d	3.94±0.06 d
P20	27.15±0.04 d	6.69±0.04 f	0.13±0.06 c	67.06±0.51 a	3.69±0.11 f
P30	38.86±0.03 a	8.09±0.22 d	0.18±0.03 abc	54.80±0.45 e	3.75±0.04 e
P45	30.83±0.04 b	8.56±0.11 c	0.2±0.03 abc	62.75±0.15 c	4.82±0.04 a
P60	28.43±0.03 c	9.34±0.16 a	0.22±0.04 ab	64.61±0.18 b	4.5±0.01 b

6.4.6 Electrolytic leakage

Cell membrane electrolyte leakage assessment measures membrane integrity and physical or chemical damages in the plant tissue (Allende et al., 2004). Thus, this parameter indicates the senescence and quality of the leaves following PAW treatment. Changes in the membrane electrolytic leakage of kale and spinach samples after PAW treatment are illustrated in Figure 6.5. In kale, reduction in the electrolytic leakage was observed in P10 and P20 treatments while a significant increase ($P < 0.05$) in the electrolyte leakage was recorded with P30, P45 and P60 with maximum of 5.05% leakage observed in P30. This indicates the membrane stability for the PAW treated kale samples which increased until P20 treatment. After that the increase in the reactive species concentration could have damaged the cell membrane and the cuticle layer of the kale leaves resulting in the higher electrolyte leakage. Rivero Pena (2020) also reported an increase in the electrolyte leakage in alfalfa sprouts, broccoli sprouts, and clover sprouts after PAW treatment. It was reported that the increase in the electrolyte leakage was more pronounced in broccoli sprouts than in alfalfa and clover sprouts. Further, the cell wall polysaccharides are readily cleaved by the OH radicals from hydrogen peroxide resulting in cell wall softening (Barceló & Laura, 2009). This explains the increase in the membrane electrolytic leakage in kale with increasing PAW activation times.

Overall, the electrolytic leakage in spinach was higher than that of kale in all treatments including the control. It was reported by Lu et al. (2015) that the epicuticular wax contents of spinach leaves were in the range of 5-10 $\mu\text{g}/\text{cm}^2$ whereas in kale it was in the range of 78-82 $\mu\text{g}/\text{cm}^2$. This difference in the cuticular layer could have resulted in the higher electrolytic leakage of spinach leaves when compared to that of kale. Interestingly, significant reduction ($p < 0.05$) in the electrolytic leakage of spinach samples was observed after PAW treatment with a maximum reduction of 6.05% in the P30 treatment. The results demonstrate that spinach leaves are more resistant to the oxidative stresses induced by PAW ROS than kale leaves. Similar reduction in the membrane leakage of button mushrooms after PAW treatment was reported by Zhao et al. (2021). It is evident from the present results that the PAW interaction with the leaves vary as a function of the type of cuticle and the cell wall composition of the leaves. Hence to further analyze these effects, cuticle analysis of the leaf samples was conducted using ATR-FTIR.

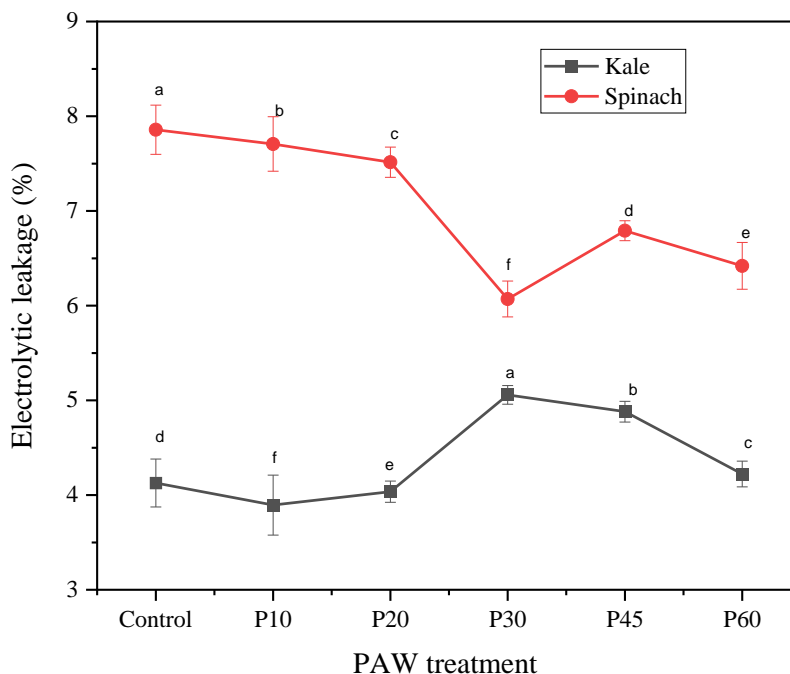


Figure 6.5 Electrolytic leakage (%) in kale and spinach after PAW treatment.

6.4.7 FTIR cuticle analysis

To assess the changes in the functional groups and characteristics of the cuticles after PAW treatment, the leaf samples were analyzed through ATR-FTIR spectroscopy. Cuticles are present in the most external, continuous membrane over the epidermal cells of the plant tissues. It is one of the most important plant barriers and it helps in protecting the plant cells from moisture loss, pests, pathogens, and UV radiation. The cuticle matrix is composed of cutin polymer, polysaccharides, soluble waxes and phenolic compounds (Heredia-Guerrero et al., 2014). This composition, however, is different among plants, plant parts and it is also altered by the environmental factors (Yeats & Rose, 2013).

The ATR-FTIR spectra of PAW treated kale and spinach leaf samples are presented in Figure 6.6 and the functional groups assigned to the major vibrational bands are given in Table 6.3. The FTIR spectrum of PAW treated kale leaf samples showed a significant change in absorption of most of the functional group bands. The strong, sharp (C-H) bands at wavenumbers 2914 cm^{-1} and 2847 cm^{-1} correspond to the asymmetric and symmetric CH_2 stretching bands due to the aliphatic absorption of cutin and waxes (Grzegorzewski, 2011). Clear reduction in these absorption bands were observed after PAW treatment indicating the denaturation of the cuticular waxes by the PAW

treatments. Further, the observable increase in the OH vibrational band between 3000-3500 cm^{-1} accounts for the changes in water absorption and crystallization characteristics of the leaf surface following PAW treatment. This shows that the hydrophobicity of the kale leaf samples was reduced due to the changes in the cuticles thus increasing the absorption of OH bands. Furthermore, in the fingerprint region from 1500 to 400 cm^{-1} , the decrease in the (C-H) absorption bands at 1473 cm^{-1} , 1461 cm^{-1} and 719 cm^{-1} confirms the degradation of cutin and waxes by the reactive oxygen species from PAW. Grzegorzewski (2011) also reported similar degradation of cuticular layer in kale upon NTP treatment. Interestingly, the (C=C) stretching bands (1632 cm^{-1}) corresponding to the phenolic compounds, OH bending (1244 cm^{-1}) and glycosidic bands (1017, 1104 cm^{-1}) attributed to the polysaccharides increased after PAW treatment. This could be due to the exposure of phenolic compounds and polysaccharides by cutin polymer cleavage by the ROS in PAW.

In contrast to kale, an increase in the CH_2 stretching bands was observed in PAW treated spinach samples. While comparing the spinach IR spectra with kale, it was observed that the intensity of the asymmetric and symmetric methylene stretching bands at 2916 cm^{-1} and 2848 cm^{-1} were less intense and broader. This shows that the cuticular layers of spinach leaves are thinner than that of kale. Further, the response of the cuticle layer to PAW ROS also increased the absorption bands of cutin and reduced the absorption bands of water. According to Barceló and Laura (2009), in dicots, the non-reducing arabinose and galactose terminals of pectic polysaccharides in the cell wall are feruloylated by the ester-bonding with ferulic acid. These feruloyl residues form covalent bonds with each other by oxidative coupling in the presence of hydrogen peroxide and peroxidase enzyme. This cross-linking leads to the cell wall stiffening in plants. This could be a reason for the increase in the cutin and wax absorption bands and reduction in the OH stretching bands in spinach. Fich et al. (2016) speculated that the formation of cutin monomers and the association of cutin monomers to waxes is a membrane repair mechanism in plant cells under oxidative stress. Further, as opposed to kale, no drastic increase in the absorption bands of phenolic compounds was observed in spinach, emphasizing the intact nature of the cuticle layer in spinach leaves. These finds are in correlation with the electrolytic leakage values where the electrolytic leakage of spinach was reduced after PAW treatment.

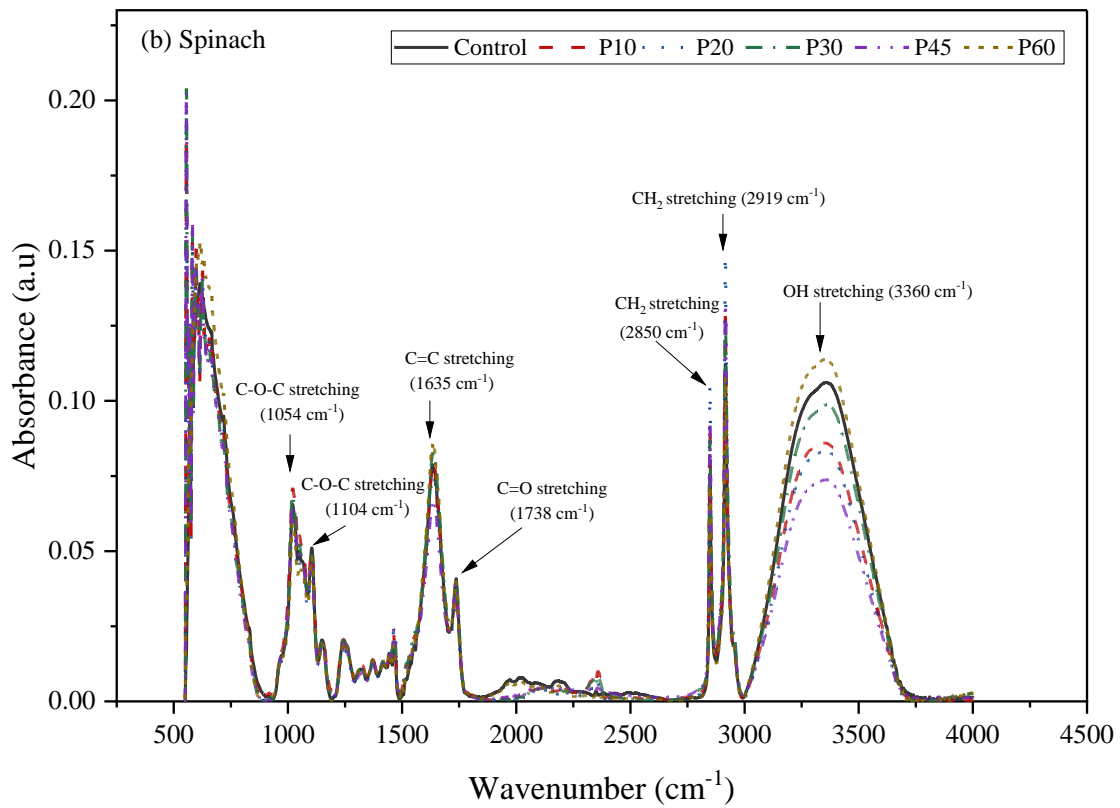
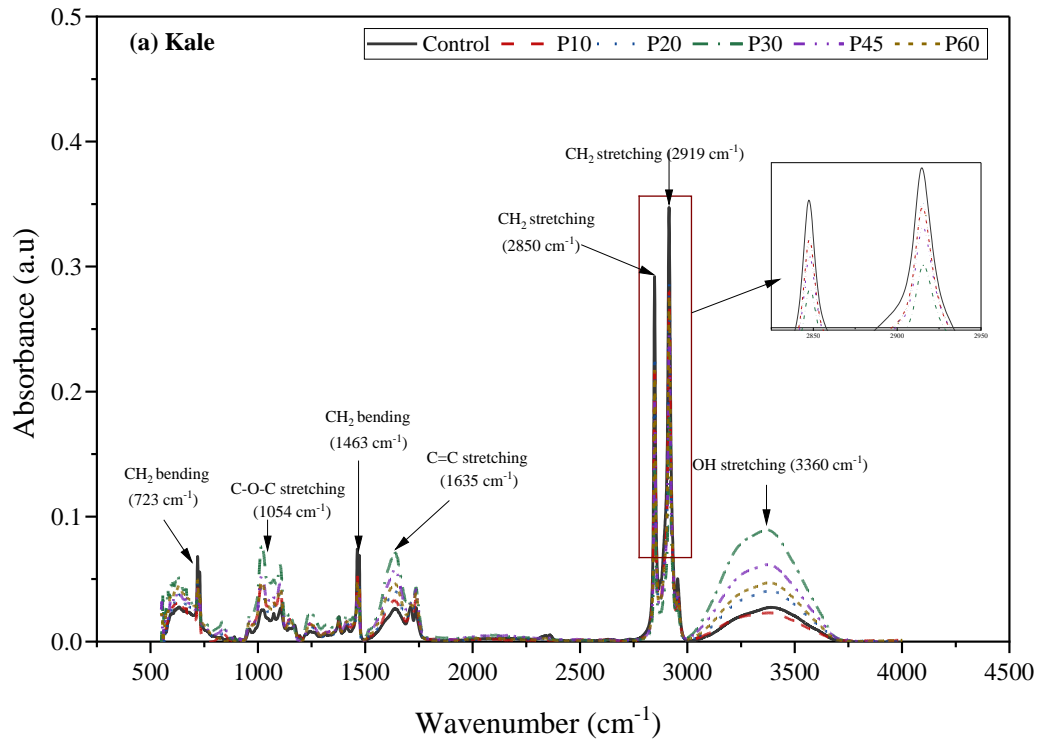


Figure 6.6 ATR-FTIR spectrum of kale (a) and spinach (b)

Table 6.3 Assignments of main absorption bands and their corresponding cell wall component

ATR-FTIR absorption band (cm⁻¹)	Functional group	Cuticle component	Reference
3390	OH stretching	Cutin, polysaccharides	(Grzegorzewski, 2011; Hama et al., 2019; Heredia-Guerrero et al., 2014)
2919	CH ₂ stretching (asymmetric)	Cutin, waxes	(Grzegorzewski, 2011; Harris et al., 2021; Heredia-Guerrero et al., 2014)
2850	CH ₂ stretching (symmetric)	Cutin, waxes	(Bermudez-Garcia et al., 2019; Grzegorzewski, 2011; Heredia-Guerrero et al., 2014)
1738	C=O stretching	Cutin	(Bermudez-Garcia et al., 2019; Hama et al., 2019; Harris et al., 2021)
1641	C-O-C stretching	Cutin	(Bermudez-Garcia et al., 2019)
1635	(C=C) stretching phenolic acid	Phenolic compounds	(Heredia-Guerrero et al., 2014)
1463	CH ₂ bending	Cutin, waxes	(Bermudez-Garcia et al., 2019)
1244	OH bending	Cutin, polysaccharides	(Grzegorzewski, 2011; Heredia-Guerrero et al., 2014)
1104	C-O-C stretching (ester)	Cutin	(Bermudez-Garcia et al., 2019; Hama et al., 2019)
1054	C-O-C stretching (glycosidic bond)	polysaccharides	(Harris et al., 2021; Heredia-Guerrero et al., 2014)
724, 719	CH ₂ bending	Cutin, waxes	(Grzegorzewski, 2011; Heredia-Guerrero et al., 2014)

6.4.8 SEM imaging of PAW treated kale and spinach leaf surfaces

To confirm the findings from ATR-FTIR and electrolytic leakage, leaf morphology was observed by SEM (Figures 6.7 & 6.8). In kale, an increase in the surface smoothness and reduction in the cuticular waxes was observed with increasing PAW activation time. Comparatively, spinach had less surface roughness in the cuticles. Further, in both kale and spinach the number of open stomata was reduced with the increase in the PAW activation time. In spinach, damages in the stomatal cell walls were observed from treatments P20 onwards. Prominent shriveling of the leaf surface was also observed in spinach in P30 and P60 treatments. Grzegorzewski et al. (2011) observed a rougher, stressed, and dry surface of lamb's lettuce after nonthermal plasma treatment. The closure of stomata in leaves could be attributed to the stress response of the plant cells to the ROS from the PAW treatment. Increase in the stomatal closure with hydrogen peroxide concentration and its contact time was reported in pea epidermal cells by Desikan et al. (2004). They claimed that hydrogen peroxide at concentrations less than 10 mM caused a reversible stomatal closure without compromising the cell viability. Ozone in the PAW also contributes to the closure of the stomata. The oxidative stress caused by ozone and its degradation products elevates the Ca^{2+} ions in the cytoplasm of guard cells making the stomata close (Glowacz & Rees, 2016). Further, ROS such as H_2O_2 , O_3 and hydroxyl radicals can initiate lipid peroxidation in the cell membrane which reduces the membrane stability of the leaves and allows the accumulation of ROS inside the plant cell causing damages to the intracellular components (Akishev et al., 2002).

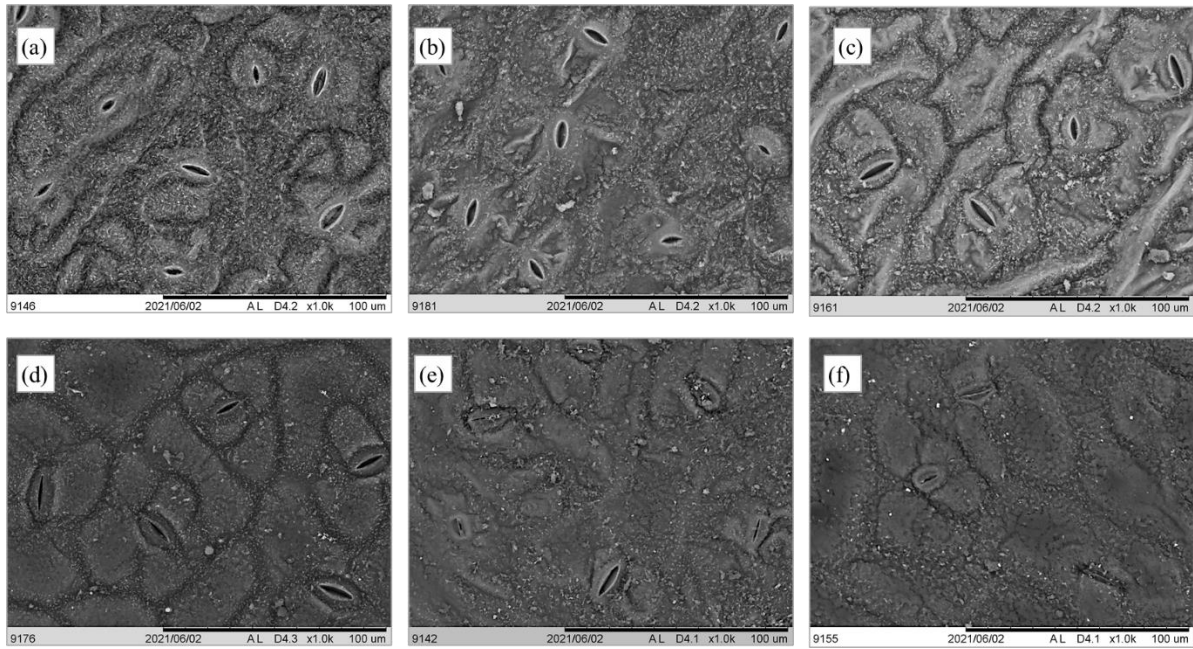


Figure 6.7 SEM surface images of fresh and PAW treated kale leaves (a) control (b) P10 (c) P20 (d) P30 (e) P45 and (f) P60

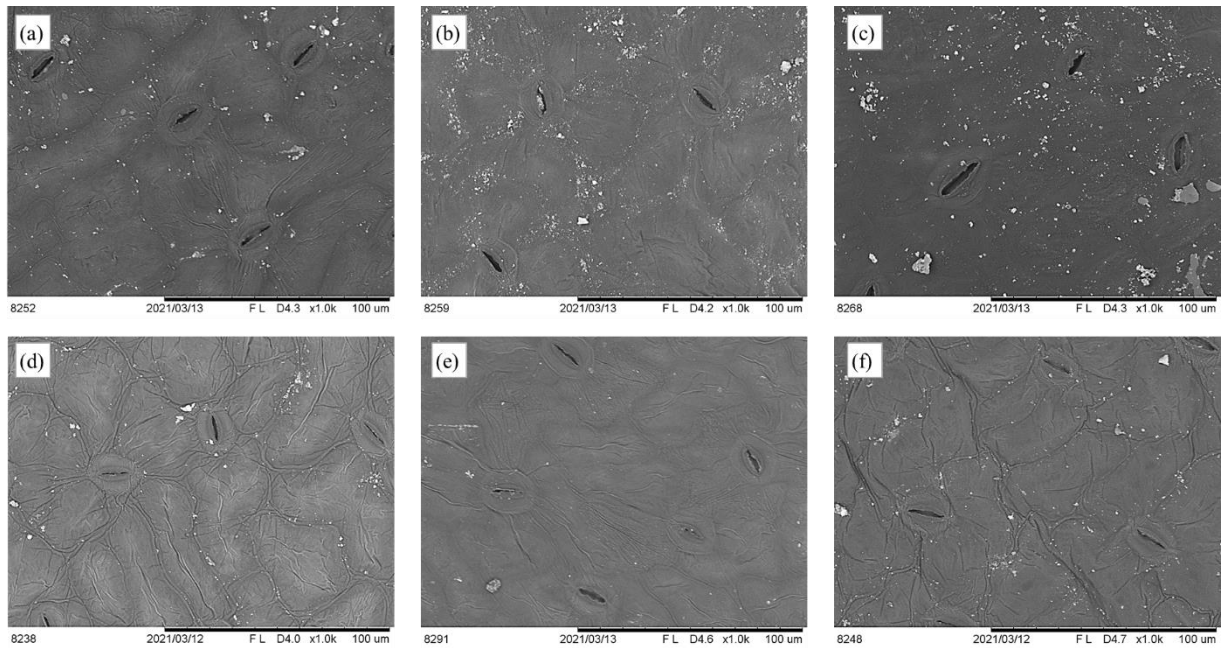


Figure 6.8 SEM surface images of fresh and PAW treated spinach leaves (a) control (b) P10 (c) P20 (d) P30 (e) P45 and (f) P60

6.5. Conclusion

The results from this study showed that PAW is effective at disinfecting against *Escherichia coli* on leafy vegetables and its disinfection efficiency increases with the increase in concentration of reactive oxygen species in PAW. However, significant changes in the chlorophyll and carotenoid contents and antioxidant properties of kale and spinach leaves were observed at higher PAW activation times. Further, kale and spinach had difference in responses to the reactive oxygen species present in the PAW due to the changes in the cuticular layer of these leaves. This study emphasizes that the interaction of fresh food to PAW varies with its structure and composition. Future studies on the interaction of PAW reactive species on specific bioactive components of foods and food matrices should be investigated in detail to optimize the process condition according to the food material.

CONNECTING TEXT

Many fresh-cut fruits and vegetables are susceptible to enzymatic browning. The commonly used thermal processing and chemical based technologies for enzyme inactivation result in the loss of nutritional components and quality deterioration. Nonthermal plasma is reported to be effective in enzyme inactivation and only a limited number of studies are available reporting on the evaluation of the effect of PAW washing on the prevention of enzymatic browning in fresh-cut fruits and vegetables. Conversely, from chapter V it was observed that PAW causes mild oxidation of proteins, and this may cause an increase in the oxidation sensitive enzyme activity in fresh-cut fruits and vegetables. Therefore, in Chapter VII, the effect of PAW on polyphenol oxidase and peroxidase enzymes in fresh-cut apples was studied. Detailed investigation on the physicochemical quality, respiration, enzyme activity and microbial quality during 12 days of refrigerated storage is also reported.

CHAPTER VII

INFLUENCE OF PLASMA ACTIVATED WATER ON ENZYME ACTIVITY AND STORAGE QUALITY OF FRESH-CUT APPLES

7.1 Abstract

Plasma activated water (PAW) is a new approach to disinfecting surfaces including fresh-cut foods while maintaining their quality attributes. The aim of this study was to evaluate the effect of PAW on enzyme activity, microbial and physicochemical quality of fresh-cut apples. PAW was produced at different production activation times of 10 min, 20 min, 30 min, 45 min and 60 min and the fresh-cut apple slices were washed with PAW for 5 min and stored at 4°C for 12 days. Results showed that PAW treatments reduced the polyphenol oxidase activity immediately after treatment and the lowest activity was recorded in PAW-20 min (5.10 ± 0.16 U/g FW) after 12 days. Conversely, peroxidase activity of the samples increased immediately after PAW treatment and the samples treated with PAW activated for 30 min had the lowest peroxidase activity at the end of 12 days of storage. No significant changes in the total phenolic content and FRAP antioxidant activity of the fresh-cut apple samples were reported after PAW treatments. The results from firmness, membrane permeability, respiration rate and microstructural imaging showed that at higher PAW activation times (45 min and 60 min), PAW had adverse effects on the quality of fresh-cut apples. On the other hand, significant reductions in the total aerobic bacteria and total yeast and molds were observed in all PAW treatments except PAW activated for 10 min. The results suggests that plasma activated water could maintain the quality of the fresh-cut apples during storage for plasma activation times of 20 min and 30 min for up to 12 days of storage.

7.2. Introduction

Fresh-cut fruits and vegetables are minimally processed foods which are washed, peeled, and cut into a usable form and packaged to offer fresh, convenient and ready-to-use healthy products. The demand for these ready to eat fresh-cut products has increased in recent times due to an increase in consumer awareness on healthy eating habits. However, because of the damages caused by the minimal processing operations, these fresh-cut products deteriorate faster than the fresh foods

(Belgacem et al., 2020). Further, the cut and exposed tissues of fresh-cut foods make them vulnerable to microbial contamination, enzymatic degradation, softening and decay (Dar et al., 2020). According to a 2019 CDC report, 5 out of 18 food borne outbreaks in Canada were from fresh-cut and minimally processed fruits and vegetables (CDC). Apart from conventional chlorine-based disinfection methods which pose a risk of toxicity to human health, various novel nonthermal processing methods such as electrolyzed water, pulsed light, ozone and nonthermal plasma are being assessed for the preservation of fresh-cut foods (Dar et al., 2020).

Non-thermal plasma (NTP) is a novel nonthermal processing method being extensively researched for the microbial disinfection and quality enhancement of food products. NTP is produced by partial ionization of gas, and by doing so, reactive species are formed in the plasma at atmospheric pressure and temperature (Pankaj & Keener, 2017). These reactive species, along with the other plasma components such as charged particles, electrical field and UV radiation are the effective bactericidal agents responsible for the inactivation of microorganisms (Pan et al., 2013). However due to its nature as a surface application, this method is not suitable for the complete disinfection of irregularly shaped food materials (Noriega et al., 2011; Xiang et al., 2020). PAW is produced by direct or indirect exposure of water to nonthermal plasma. Upon plasma exposure, the reactive species from the NTP are transferred to the water through diffusion and many other plasma-water chemical processes (Zhou et al., 2020). The concentrations of reactive species in the PAW can be controlled by plasma activation time, feed gas composition, applied voltage, water flow rate and the method of application (Lu et al., 2017). Further the use of PAW can avoid some of the damages caused by the direct exposure to NTP components and its potential storability enables the possibility of using it as an alternative to the conventional chemical sanitizers used in wash waters (Cong et al., 2022; Herianto et al., 2021).

Many recent studies have demonstrated the bactericidal activity of PAW against various food pathogenic bacteria in fresh-cut products (Zhao et al., 2020). Increase in the shelf life of mung bean sprouts (Xiang et al., 2019b), mushrooms (Xu et al., 2016), fresh-cut kiwi (Zhao et al., 2019) and fresh-cut pears (Chen et al., 2019a) has been reported following PAW treatments. The bactericidal effect of PAW is mainly contributed by the reactive oxygen species (ROS) developed in PAW such as hydrogen peroxide, ozone and hydroxyl radicals (Matthew et al., 2011). These ROS react with bacterial cells and damage the cell membrane by oxidization. However, this

oxidative stress could also have a negative impact on the food material particularly with foods with high antioxidant properties and foods which are susceptible to enzymatic browning. Subtle increase in the superoxide dismutase activity in button mushroom following PAW treatments has been reported by (Xu et al., 2016). Contradictorily, a reduction in the peroxidase activity in PAW treated kimchi cabbage was reported by (Choi et al., 2019).

Therefore, the objective of this study is to assess the effect of plasma activated water on the enzyme activity and quality of fresh-cut apples during storage. For this purpose, PAW was produced at different activation times ranging from 10 min to 60 min. The physicochemical properties, respiration rate, microbial quality and enzyme activity of the PAW treated fresh-cut apples were monitored and evaluated during 12 days of refrigerated storage.

7.3. Materials and Methods

7.3.1 Materials

Apples (*Musa domestica* cv. 'Red delicious') were procured from a local grocery store in L'Île-Perrot, Quebec Canada and kept in a refrigerator at 4°C until treatment. Apples were selected for similar weight, maturity, outer skin color and size.

Gallic acid ($\geq 98\%$), catechol (99%), 2,2-diphenyl-1-picrylhydrazyl (DPPH), Folin-Ciocalteu's phenol reagent, 2,4,6-Tripyridyl-Striazine (TPTZ), guaiacol, polyvinylpolypyrrolidone (PVPP), trichloroacetic acid (TCA), 2,4-dinitrophenylhydrazine (DNPH), malondialdehyde tetrabutylammonium salt (TBA), 1,1,3,3-tetraethoxypropane (TEP), sodium nitrite, sodium hydroxide, ferric chloride, hydrogen peroxide (30%), were obtained from Sigma-Aldrich, Canada. Trolox[®] (97%), Triton X-100, potato dextrose agar, plate count agar, HPLC grade methanol, ethanol and acetone were procured from Fisher Scientific, Canada.

7.3.2 Plasma device and PAW treatment

Nonthermal dielectric barrier discharge plasma at atmospheric pressure was used for PAW generation. As shown in Figure 7.1, the plasma system consists of two copper electrodes placed over a rectangular glass section. The glass section acts as the dielectric barrier and carries water during plasma activation. The internal spacing in the glass section was kept as 3 mm. The copper electrodes are connected to a high voltage source (PVM 500, Information Unlimited, USA) with

10 kV (peak-peak) voltage and 20 kHz frequency. Premixed argon and oxygen gas mixture in 98%:2% proportion was used to produce NTP within the discharge gap. The gas flow rate was maintained at 4 slm and the water flow rate was 100 ml/min. Distilled water was used for PAW production and 150 ml water was activated for 10 min (P10), 20 min (P20), 30 min (P30), 45 min (P45) and 60 min (P60). Immediately after activation, hydrogen peroxide, ozone concentration, pH and temperature of the PAW were determined, and the values are given in Table 7.1.

The apples were washed and air dried before peeling and cutting into 2 cm³ cubes with a sterile sharp stainless-steel knife before PAW treatment. For the treatment, 10 g of fresh-cut apple cubes were immersed for 5 min in 150 ml of PAW, activated at different times. For the control sample, apple cubes were placed in 150 ml distilled water for 5 min. After treatment, the samples were blot dried and packed in Ziploc® bags and stored for 12 days at 4±1°C and 90% relative humidity. For each treatment six replicates were made.

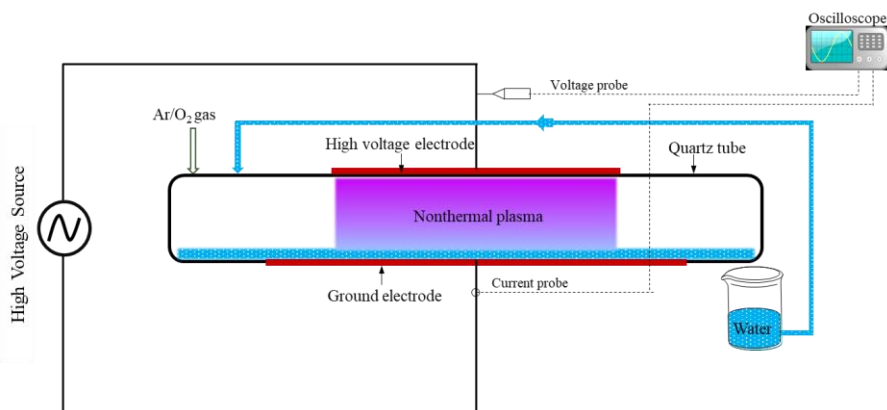


Figure 7.1 Schematic diagram of plasma activated water system.

Table 7.1 Properties of PAW at different activation times.

PAW activation time (min)	H ₂ O ₂ (mM)	O ₃ (mg/l)	pH	Temperature (°C)
Control (0 min)	-	-	6.31±0.01	21.33±0.29
10 (P10)	0.71±0	0.71±0.24	6.21±0.01	23.33±0.58
20 (P20)	1.36±0	2.22±0.14	6.11±0.04	26.17±0.29
30 (P30)	2.24±0.01	1.59±0.14	6.02±0.01	28.8±0.26
45 (P45)	2.46±0.01	1.66±0.41	5.65±0.07	30.5±0.5
60 (P60)	3.01±0.01	2.38±0.24	4.66±0.08	31.33±0.29

7.3.3 Weight loss and soluble solid content

Weight loss and soluble solids content (SSC) was measured from three replicates of each treatment combinations during the span of the storage period. Weight loss and SSC of the samples were measured on day 1, day 3, day 6, day 9 and day 12. Weight of the samples was taken during the storage period using a balance with a precision of ± 0.0001 g and the weight loss percentage was calculated from its difference from the initial weight of the sample. SSC of the samples were measured using a refractometer (Reichert™ digital refractometer) at 20°C. The apple samples were squeezed to release the juice and a drop of it was placed on the refractometer prism to measure the SSC in °Brix.

7.3.4 Color measurement

Color values of the PAW treated fresh-cut apple samples in CIE (L^* , a^* , b^*) color scale were measured using a chromameter (CR-300 Chroma, Minolta, Japan). At least five color values were recorded for each sample at different locations on the samples. The L^* value is a measure of the lightness, the a^* value of the greenness-redness and the b^* value of the blueness-yellowness. Total color difference, ΔE^* , was calculated using Hunter-Scofield's equation (Equation 7.1).

$$\Delta E = \sqrt{(L_{fresh}^* - L_{sample}^*)^2 + (a_{fresh}^* - a_{sample}^*)^2 + (b_{fresh}^* - b_{sample}^*)^2} \text{ --- (7.1)}$$

The browning index (BI) was calculated using the following expressions (Equations 7.2-7.3) from the L^* , a^* and b^* color values (Chen et al., 2016)

$$BI = \frac{100(x - 0.31)}{0.172} \text{ --- (7.2)}$$

where

$$x = \frac{a^* + 1.75L^*}{5.645L^* + a^* - 3.012b^*} \text{ --- (7.3)}$$

For ΔE^* and browning index, L^* , a^* , b^* values of a freshly cut apple without washing were used for the calculation.

7.3.5 Membrane permeability

The membrane permeabilities of the fresh-cut apple samples were analyzed from the electrical conductivity values as described by Xu et al. (2021a). Accordingly, the apple samples were cut into 1 cm discs and 10 of these discs were put in a 50 ml falcon tube with 20 ml of distilled water. The tubes were kept at 25°C for 30 min and the initial conductivity value (C_1) was measured using a digital conductivity meter (Hanna HI98129, Canada). Then the tubes were placed in a water bath at 100°C for 10 min, cooled to room temperature and the conductivities of the samples were again measured (C_2). The membrane permeability of the samples was calculated using the following expression (equation 7.4) as a percentage.

$$\text{Membrane permeability (\%)} = \frac{C_1}{C_2} \times 100 \text{ --- (7.4)}$$

7.3.6 Respiration rate measurement

Respiration rates of the samples during storage were measured according to the method described by Meng et al. (2014). Fresh-cut apple samples were taken at 3 days interval. In a 150 ml airtight container, 10 g of sample was placed and hermitically sealed with a resealable septum on top of the lid to allow the drawing of gas samples. The jars were placed at 4°C for 12 h, after which 0.1 ml gas sample from the head space was drawn using a syringe and injected into the gas chromatograph (Hewlett Packard HP 5890A, USA) for gas composition analysis. The gas chromatograph was operated with the thermal conductivity detector (TCD) set at 125°C for the measurement of the gas composition. Other chromatograph settings used for the analysis were as follows: Alltech CTR1 column (1.83 m × 0.006 m), injector temperature 125°C, detector temperature of 125°C, column temperature of 50°C and helium as the carrier gas. The measurement of respiration rate per treatment was made in triplicate. The data was used to calculate the mg of O₂ consumed (RRO₂) and mg of CO₂ produced (RRCO₂) h⁻¹ kg⁻¹ of sample using the following expressions (Equations 7.5 and 7.6) (Tappi et al., 2014).

$$RRO_2 = \frac{mmO_2 \times V_{head} \times \left(\frac{20.8 - \%O_{2,head}}{100} \right) \times 101.325}{t \times m \times R \times 283} \text{ --- (7.5)}$$

$$RRCO_2 = \frac{mmCO_2 \times V_{head} \times \left(\frac{\%CO_{2,head}}{100} \right) \times 101.325}{t \times m \times R \times 283} \text{ --- (7.6)}$$

Where m_{O_2} and m_{CO_2} refer to the gas molar mass in (g/mol) of O_2 and CO_2 respectively; V_{head} refers to the headspace volume of the container (dm^3); % $O_{2,head}$ and % $CO_{2,head}$ represent the gas percentages measured in the headspace; t is number of hours the sample was incubated for the analysis (h); m is mass of sample (kg) and R is the universal gas constant ($8.314472 dm^3 kPa K^{-1} mol^{-1}$).

7.3.7 Firmness

Firmness of the fresh-cut apple slices during storage was measured using the Instron 4502 universal testing machine (Instron, Norwood, USA). Firmness of the samples was measured in terms of force required (in N) to puncture through 5 mm in the sample with a speed of 0.6 mm/s. For this test, 50 N load cell and a 4 mm diameter cylindrical probe were used. Five replications for each sample were used for the firmness testing.

7.3.8 Antioxidant properties

7.3.8.1 Total phenolic content

Total phenolic content (TPC) in the apple samples was determined by the Folin-Ciocalteu method (Singleton & Rossi, 1965) with a slight modification. For the analysis, 5 g of fresh-cut apple sample was homogenized with 20 ml of methanol and the mixture was centrifuged at $3000 \times g$ ($4^\circ C$) for 20 min. After that, 1 ml of the supernatant was mixed with 5 ml distilled water and 1 ml of Folin-Ciocalteu reagent and allowed to react for 5 min. Then 4 ml of 7.5% sodium carbonate solution was added to the mixture and incubated in the dark for 90 min and the absorbance was measured at 765 nm. The total phenolic content in the samples was calculated from the gallic acid standard curve and the results were expressed as mg of gallic acid equivalent (GAE)/g of sample.

7.3.8.2 DPPH radical scavenging activity

Antioxidant activity of fresh-cut apple samples was analyzed by DPPH (2,2-diphenyl-1-picrylhydrazyl-hydrate) radical scavenging and FRAP (Ferric Reducing Antioxidant Power) assays. The DPPH radical scavenging activity of the samples was measured using the method described by (Blois, 1958) with some modifications. Briefly, 0.5 ml methanolic extract prepared for the TPC analysis were mixed with 3.5 ml of freshly prepared 0.1mM DPPH solution in methanol. The mixture was incubated for 20 min in the dark and the absorbance was measured at 517 nm. The

free radicals scavenged by DPPH radicals was expressed as percentage inhibition and calculated using the following equation (Equation 7.7). Methanol was used as the blank.

DPPH Inhibition (%)

$$= (Abs_{blank @ 517 \text{ nm}} - Abs_{Sample @ 517 \text{ nm}}) / Abs_{blank @ 517 \text{ nm}} \times 100 \quad (7.7)$$

7.3.8.3 Ferric-reducing antioxidant power (FRAP) assay

The ferric-reducing antioxidant power (FRAP) assay of the samples was conducted according to the procedure given by Benzie and Strain (1996) with slight changes. Briefly, FRAP reagent was freshly prepared by mixing 300 mM acetate buffer (pH 3.6), 20 mM ferric chloride solution and 10 mM of 2,4,6-tripyridyl-s-triazine (TPTZ) solution in 40 mM HCl in the volume ratio of 10:1:1 respectively. For the assay, 2.85 ml of freshly prepared FRAP reagent was mixed with 150 µl of standard Trolox solution or sample extract or blank. The mixture was then placed in the dark for 30 min and then the absorbance was measured at 593 nm. The antioxidant capacity of the samples was expressed as FRAP value in micromoles of Trolox equivalents per gram of sample (mmol TE/g).

7.3.9 Enzyme activity assay

Enzyme extraction, polyphenol oxidase (PPO) and peroxidase (POD) enzyme activities of the samples were assayed according to the methods described by Shinwari and Rao (2021) and Amiour and Hambaba (2016) with some modifications. For crude enzyme extraction, 1g sample was homogenized with 10 ml of ice cold 0.1M sodium phosphate buffer with 3% polyvinylpolypyrrolidone (PVPP), 0.1% Triton X100 and 1 M sodium chloride at pH 7. The homogenate was filtered through a cotton cloth and centrifuged at $3000 \times g$ for 20 min at 4°C. The supernatant was used for the assay of PPO and POD activities. PPO activity in the apple samples was determined by measuring the oxidation of catechol substrate at 420 nm. Accordingly, the reaction mixture was prepared with 40 mM catechol (1.5 ml) and 0.1 M sodium phosphate buffer at pH 6.5 (2.3 ml) and placed in a 25°C water bath for 5 min. To this mixture, 0.2 ml of crude enzyme extract was added. Immediately after adding the enzyme extract, changes in the optical density of the reaction mixture were read at 420 nm at 30 s interval for 5 min or until a constant value was reached. The PPO activity was expressed as U g⁻¹ fresh weight of sample where U is the change in the OD value per minute at 420 nm.

The POD activity was assayed using hydrogen peroxide as the oxidant. Briefly, the substrate solution was prepared with 20 mM guaiacol (0.32 ml) and 1.5% v/v hydrogen peroxide (0.16 ml) in 2.42 ml 0.1 M phosphate buffer at pH 7.0. To this mixture, 0.1 ml crude enzyme extract was added and the change in absorbance was read at 490 nm for 5 min at 30 s interval or until a constant absorption value was attained. Buffer was used in place of enzyme extract for the blank sample. The POD activity was expressed as U g⁻¹ fresh weight of sample where U is the change in the OD value per minute at 490 nm.

7.3.10 Malondialdehyde (MDA) content

Malondialdehyde (MDA) content in the samples was determined by modified 2,4-dinitrophenylhydrazine (DNPH) derivatization method as described by Mendes et al. (2009) with slight changes. The MDA in the samples was derivatized by DNPH and converted into pyrazole and hydrazone derivatives. These MDA derivatives were measured by HPLC separation and absorption at 310 nm using Agilent 1100 series HPLC system. For MDA analysis, apple samples were taken from Day 0, Day 6, and Day 12 of storage. A standard curve was prepared using 1,1,3,3-tetraethoxypropane (TEP) diluted in 7.5% TCA solution as the MDA standard over concentrations ranging from 1 µM, 2 µM, 5 µM, 8 µM and 10 µM. 2g of sample was homogenized with 7.5% TCA solution with 0.1% EDTA and 0.1% propyl gallate. The homogenate was filtered through Whatman #1 filter paper and centrifuged for 10 min at 6000 rpm. The sample supernatant or standard or blank solution was filtered through 0.2 µm PTFE syringe filter and 200 µl was taken in an HPLC vial and 20 µl of 5mM DNPH (in 2 M HCL) was added and mixed thoroughly. The MDA-DNPH complex was separated using a Supelco C18 column (5µm, 250 mm × 4.6 mm) with mobile phase consisting of water, acetonitrile, and glacial acetic acid in the ratio of 55:45:0.2 (v/v) and pumped at 1.0 ml/min. The sample run time was fixed at 18 min with the MDA-DNPH retention time of 12.2 min. The MDA absorption was detected at 310 nm using the UV/Vis detector and the results are expressed as µM of MDA per kilogram of sample.

7.3.11 Microbiological analysis

The microbial quality of the fresh-cut apple samples was evaluated during the 12 days storage period to examine the growth of bacteria, yeast, and mold. Fresh-cut apple sample of 1 g was homogenized with 20 ml of 0.1% peptone water. For total aerobic count of bacteria, 1 ml of the homogenate was serially diluted up to 10⁻³ and 10⁻⁴ dilution in sterile water under aseptic

conditions. From each dilution, 0.1 ml of the sample was uniformly spread over the plate count agar media (bacteria) plates with three plates for each dilution for total aerobic count. The plates were incubated at 37°C for 48 h for the enumeration of total aerobic count. For yeast and mold count, potato dextrose agar plates were used, and the plates were incubated at 30°C for 3-5 days. At the end of the incubation period, the colonies were enumerated, and the results were expressed as log₁₀ CFU/g.

7.3.12 Scanning electron microscopy

The exposed surface of the fresh-cut apple sample to PAW treatment was analyzed through the scanning electron microscope (SEM) to assess the structural changes in the material. A thin slice (2-3 mm) of exposed surface from the sample was sliced using a sharp blade. The sliced part was then immediately placed in 100% methanol for 2 min for fixation and dehydration (Pathan et al., 2010; Talbot & White, 2013). After 2 min, the apple sample slices were air-dried for 30 min. Following this, the samples were mounted on aluminum stubs with carbon sticky tape and the exposed surface was viewed under SEM (TM3000, Hitachi High-Technologies Corporation., Tokyo, Japan) at 5kV.

7.3.13 Statistical Analysis

A completely randomized experimental design was performed with three replicates in each treatment. One-way analysis of variance (ANOVA) was used to analyze the experimental data using JMP Pro (Version 15, SAS Institute Inc, NC, USA). Data were shown as mean± standard deviation, the significant difference among the treatment means were compared using Tukey's multiple range test at 5% significance level. Results of SEM imaging were analyzed descriptively.

7.4. Results and Discussion

7.4.1 Weight loss, and soluble solids content

The weight loss percentage during storage indicates the loss of water content in the sample due to respiration and desiccation. Weight loss in fresh-cut apple samples increased during the storage and all PAW treatments had less weight loss percentage till day 3 (Figure 7.2(i)).

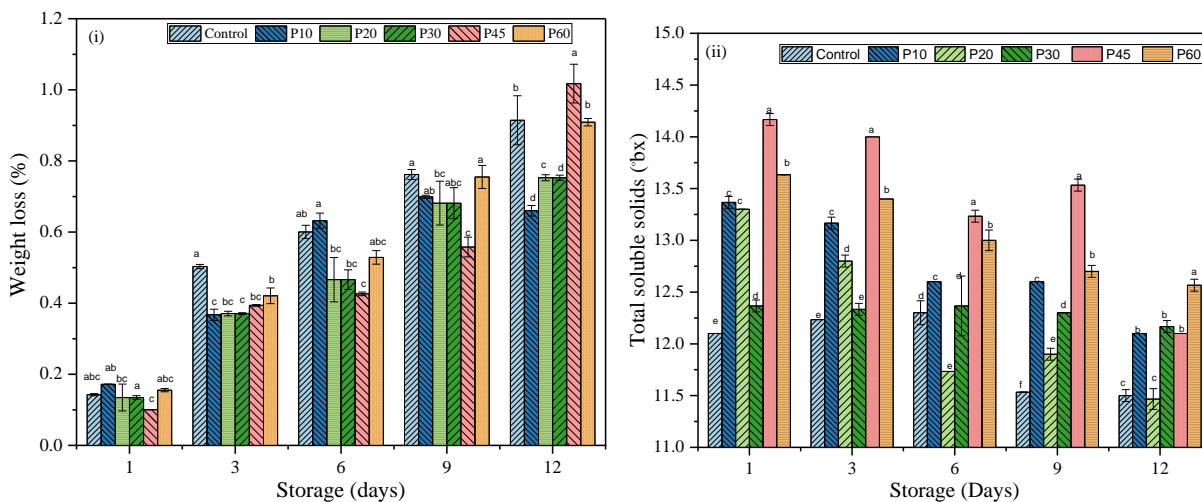


Figure 7.2 Effect of PAW treatment on (i) weight loss % and (ii) soluble solid content (°Bx) of fresh-cut apples during storage. (Means connected with the same letter are not significant at $P < 0.05$)

At the end of 12 days storage, P45 had the maximum weight loss of 1.02 ± 0.055 % while the minimum weight loss of 0.65 ± 0.05 % was recorded in P20 treatment. Reduction in the weight loss of PAW treated samples during storage has been reported in fresh-cut pear (Chen et al., 2019a), fresh-cut apples (Liu et al., 2020) and in goji berries (Cong et al., 2022). The SSC of PAW treated fresh-cut apple samples was observed from day 1 of storage and the SSC started to decrease in all treatments and control throughout the storage period (Figure 7.2(ii)). Consumption of sugars and acid during storage by the respiratory metabolism has been shown to reduce the SSC of samples during storage (Ma et al., 2016). Reduction in the metabolic activity caused by the PAW reactive species has led to the minimum reduction in the SSC of PAW treated samples when compared with control samples as reported by Zhao et al. (2021).

7.4.2 Color

The fresh-cut product color is strongly related to the consumer acceptability, and it is also an indicator of enzymatic browning in fresh-cut apples. The changes in fresh-cut apple color were studied after PAW treatment and over the course of 12 days of storage. The color parameters L^* (lightness), perceivable color difference ΔE value and the browning index percentage are presented in Table 7.2. The L^* value depends on the reflectivity of the sample and lower L^* value indicates the darkening of the samples (Xu et al., 2016). The L^* values in all samples started declining

during the storage period and there were no significant ($P > 0.05$) changes in L^* value of the PAW treated apple samples that were observed immediately following treatment. Among the PAW treatments, P60 had the maximum lightness reduction with a L^* value of 75.49 ± 2.11 at the end of 12 days storage. Perceivable color differences are analytically classified using ΔE values as very distinct ($\Delta E > 3$), distinct ($1.5 < \Delta E < 3$) and less distinct ($\Delta E < 1.5$) (Ma et al., 2015). No significant changes in ΔE value between control and PAW treated samples was observed during the first 3 days of storage. However the ΔE value of all samples were more than 3, indicating that there was a distinct change in the perceivable color, for all PAW treated and control samples when compared to the fresh apples. Illera et al. (2019) also reported a significant change in the cloudy apple juice color after nonthermal plasma treatment. The browning index of all samples were increasing during the storage period. Significant increase in BI values for the P45 and P60 treatments was observed on day 0. The browning may have been affected by an increase in temperature since there was about 10°C increase in the temperature for the samples treated with PAW activated for 45 min and 60 min (Table 7.1). Indeed, when the apples slices were immediately dipped inside the P45 and P60 PAW, along with the highly oxidative ROS, the temperature (around 31°C) could have accelerated the enzymatic browning of the apple surface. Due to this initial spike in the BI for the P45 and P60 treatments, they subsequently had higher BI and until the end of the storage period. However, the rate of increase in the BI was lower than that for the control samples. Similar to L^* value, P30 and P20 had the minimum BI at the end of storage period. This reduction could be due to the inactivation of polyphenol oxidase enzymes and reduction in the microbial load during storage. Apart from that, the free oxygen radicals in PAW could also act as a bleaching agent and increase the whiteness of the samples (Xu et al., 2016). Xu et al. (2016) and Liu et al. (2020) also reported a reduction in the browning index of PAW treated mushroom and fresh-cut apple samples respectively.

Table 7.2 Changes in the color parameters of PAW treated fresh-cut apple samples during storage.

Color factor	Treatment	Day 0	Day 3	Day 6	Day 9	Day 12
L*	Control	82.61±1.51 a	82.87±1.09 a	79.59±3.03 ab	76.05±4.55 b	74.58±1.44 c
	P10	82.95±1.75 a	82.5±1.66 a	81.82±0.67 a	77.88±4 ab	79.95±1.85 b
	P20	81.32±1.2 a	81.47±1.86 ab	80.76±1.08 a	79.76±1.3 ab	81.06±1.06 ab
	P30	82.03±0.76 a	83.58±1.03 a	82.43±0.79 a	82.43±1.84 a	83.27±0.48 a
	P45	83.13±1.14 a	81.74±1.46 ab	81.84±0.54 a	80.7±1.54 a	75.41±2.76 c
	P60	81.71±1.23 a	79.26±3.59 b	78.56±3.22 b	76.88±3.73 b	75.49±2.11 c
ΔE	Control	4.05±0.4 ab	4.21±0.76 ab	6.89±0.58 a	7.37±0.89 ab	11.47±0.64 a
	P10	3.37±0.37 b	3.7±0.66 b	4.63±0.83 b	7.06±0.96 bc	8.45±0.34 c
	P20	4.13±0.64 ab	4.34±0.53 ab	3.84±0.82 b	5.76±0.85 d	5.53±0.28 d
	P30	4.31±0.54 a	3.91±0.32 b	4.47±0.91 b	5.52±0.49 d	5.64±0.46 d
	P45	4.23±0.75 ab	3.54±1.26 b	4.12±0.6 b	6.28±0.55 cd	9.21±0.51 b
	P60	4.88±0.75 a	5.09±0.55 a	6.7±0.55 a	8.2±1.2 a	9.73±0.87 b
Browning index	Control	30.37±1.46 c	33.43±2.57 abc	35.29±3.01 ab	39.63±2.64 a	42.59±2.47 a
	P10	30.12±1.08 c	35.6±2.68 ab	35.17±2.68 ab	38.81±1.52 a	39.06±3.63 ab
	P20	32.55±1.44 b	31.88±2.77 bc	33.74±1.98 b	34.36±2.59 b	35.22±2.73 b
	P30	31.96±0.63 c	30.61±2.19 c	31.9±1.59 b	32.37±1.42 b	28.18±2.95 c
	P45	34.41±1.39 a	36.51±3.26 a	35.35±2.5 ab	34.9±3.98 b	38.88±3.85 ab
	P60	35.51±1.54 a	36.98±1.71 a	38.14±3.34 a	39.66±0.61 a	41.47±2.35 a

(Means connected with the same letter are not significantly different at p<0.05)

7.4.3 Membrane permeability and MDA content

Membrane permeability indicates the stability of cell membrane and its intactness. Higher value of this parameter suggests higher cell membrane damage which will lead to faster senescence of the fresh food material. As presented in Figure 7.3, the membrane permeabilities in the PAW treated samples were significantly (p<0.05) higher than the control samples throughout the storage period. The P45 and P60 had the highest leakage percentage of 90.7±0.25 % and 86.38±1.13% respectively by day 12. Among the PAW treatments, P30 had the lowest membrane permeability

percentage of $83.87 \pm 0.86\%$ at the end of the tested storage period. The increase in the membrane permeability of the PAW treated samples indicated the oxidation induced damage of the cell membrane of fresh-cut apple samples by PAW ROS.

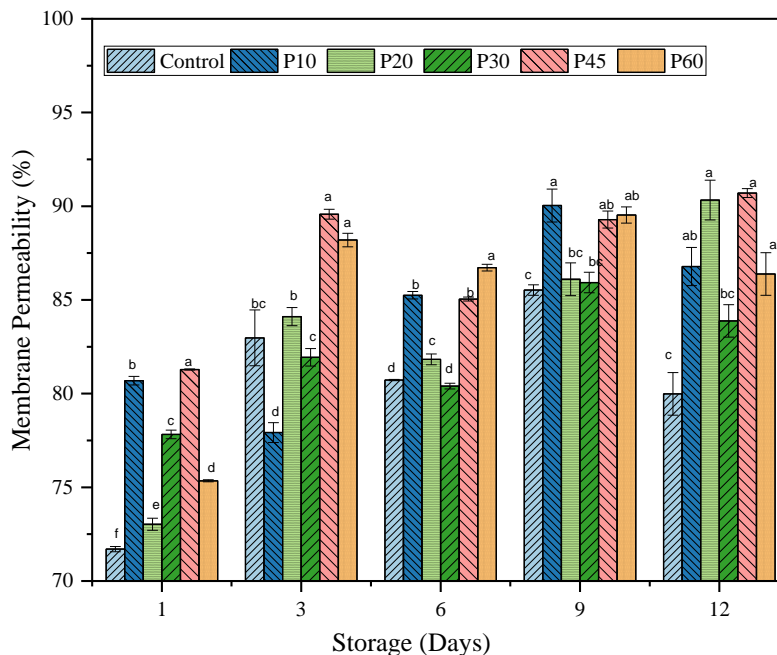


Figure 7.3 Changes in the membrane permeability of fresh-cut apple samples upon PAW treatment ((Means connected with the same letter are not significant at $p < 0.05$)).

Table 7.3 MDA content of PAW treated fresh-cut apple samples during storage.

PAW treatment	MDA content (μM of MDA/kg).		
	Day 0	Day 6	Day 12
Control	0.02 c	4.01 b	4.51 ab
P10	2.04 b	3.42 c	4.56 ab
P20	2.39 ab	3.34 c	4.64 a
P30	2.29 ab	3.43 c	3.91 b
P45	2.79 a	4.33 a	4.38 ab
P60	2.62 ab	4.60 a	4.86 a

((Means connected with the same letter are not significant at $p < 0.05$))

As PAW is rich in ROS, it can induce oxidative damages to the plant tissue. To further analyze this effect, MDA contents of the samples were determined. MDA is the main product of cell membrane lipid oxidation and its content can give information on cell membrane damage upon PAW treatment (Shen et al., 2019b). MDA contents in PAW treated samples during storage are presented in Table 7.3. Accordingly, the MDA content of the samples increased during storage irrespective of the treatment condition. In all PAW treated samples, MDA content increased significantly immediately following the PAW treatment, indicating the oxidation of cell membrane lipids. Maximum increase was observed in P45, in which a 138.5% increase in MDA content was recorded when compared with the control. However, the rate of increase in MDA content drastically increased during the storage period in the control samples when compared with the PAW treated samples. At the end of the 12 days storage period, no significant difference ($p>0.05$) was observed in the MDA contents of both the control and PAW treated samples, except for P30, wherein the minimum MDA content of 3.91 μM of MDA/ kg of sample was recorded. Thus, P30 treatment was found to be effective in reducing lipid peroxidation in cell membranes and the formation of MDA. These findings corroborated well with the membrane leakage results of the samples. Increase in the MDA content of PAW treated mushroom samples was reported by Xu et al. (2016). However, they claimed that oxidative stress induced by the ROS in PAW was alleviated by the antioxidants present in the mushrooms.

7.4.4 Respiration rate

The physiological stresses in the fresh-cut products, due to the exposure of the cut surface to the atmosphere, increase the respiration rate of the plant product. When the respiration rate is increased, the plant cells utilize the energy reserves and thus reduce the quality and shelf life of the products (Yousuf et al., 2020). In this study, the respiration of fresh-cut apple samples during storage was determined through the measurement of O_2 and CO_2 concentrations. In all samples, the rate of CO_2 production was higher than the rate of O_2 consumption throughout the storage period (Figure 7.4). PAW treated samples exhibited greater CO_2 and O_2 concentrations on day one, following the PAW treatment, than the control. Maximum of 37.3% increase in CO_2 production was recorded in P30 while 43.62% increase in O_2 consumption was recorded in P60 on day 1. On day 3, the concentrations of CO_2 and O_2 were reduced in all treatments including the control samples and then started increasing during the storage period. Similar drop in the

respiration rate of fresh-cut pear samples, during storage following in-package cold plasma treatment, was reported by Zhang et al. (2021). At the end of day 12, there was a 31.2% and a 34.51% increase in the CO₂ production and O₂ consumption of the control samples. In PAW treated samples, P60 and P45 had the maximum CO₂ concentration on day 12. Minimum CO₂ production and O₂ consumption were observed in P20 and P30 samples at the end of the storage period.

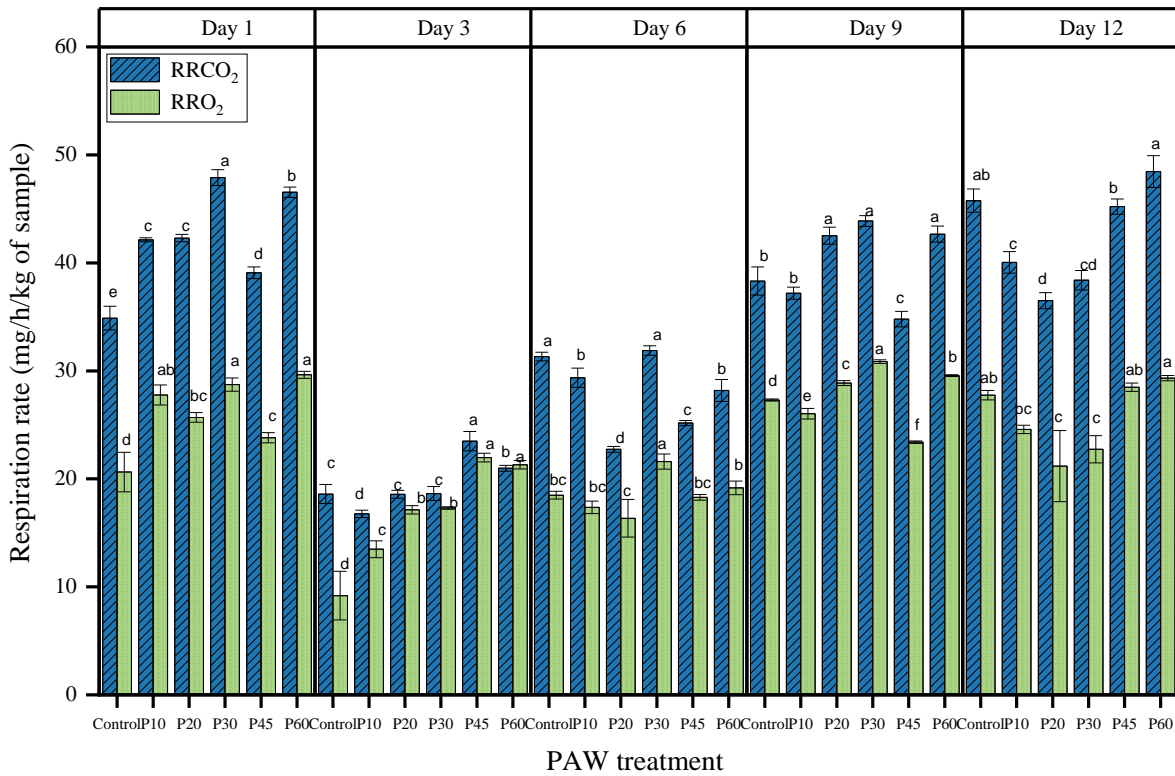


Figure 7.4 Respiration rate of PAW treated fresh-cut apple samples during 12 days of refrigerated storage in mg/h/kg of sample. (Means connected with the same letter are not significant at $p < 0.05$)

It is evident from the results that the changes in respiration rates did not correspond directly with the PAW activation times. At higher PAW activation times, particularly with P45 and P60, the respiration rate of the apple samples was increasing during storage. Further, with PAW activation times up to 30 min (P30), the reactive species in the PAW helped in reducing the respiration rate of the samples. Xu et al. (2016) also reported fluctuations in the respiration rate of button

mushrooms with respect to the PAW activation times. Changes in the cell respiratory pathways resulting from the reactive species in cold plasma are speculated to be the reason for the changes in the respiration rates of fresh-cut pears and apples (Tappi et al., 2014; Zhang et al., 2021). However, at P45 and P60, the high concentration of reactive species in PAW such as hydrogen peroxide, ozone, and the low pH values (Table 7.1) would have accelerated the oxidative stress responses in the cells thus increasing the respiration rate of the samples.

7.4.5 Firmness

Firmness is one of the important factors influencing the product acceptability of fresh-cut food products. Changes in the textural properties of fresh-cut products are mainly influenced by cell wall structure and degradation of the cell wall components (Liu et al., 2021). The firmness of the control sample was reduced by 7.91% at the end of the 12 days of storage while the PAW treatments P10 and P60 also had a similar firmness reduction percentage ($\approx 6\%$) (Figure 7.5). Increase in the electrolyte leakage of the samples and increase in the enzyme activity at higher PAW activation times could have led to the softening of the tissues in the samples. Conversely, P30 treatment had significantly ($p < 0.05$) higher firmness value of 13.45 ± 0.83 N than the control (10.47 ± 1.18 N) on day 12. There was a slight increase in the firmness values in other PAW treatments observed, however the differences were not significant ($p > 0.05$). PAW treatments increased the firmness of Chinese bay berries (Ma et al., 2016) and fresh-cut pears (Chen et al., 2019a). Guo et al. (2021a) speculated that the inactivation of enzymes or degradation of genes involved in the metabolic activity of plant cells by PAW ROS could be attributed to the increase in the firmness after PAW treatment. In a recent study by Liu et al. (2021) which evaluated the changes in the textural properties of fresh-cut apples by aqueous ozone treatment, reported that the firmness of the apple samples was increased by aqueous ozone treatment which was mainly due to the regulation of the hemicellulose degradation and inactivation of β -galactosidase, α -arabinofuranosidase enzymes and their expression during storage.

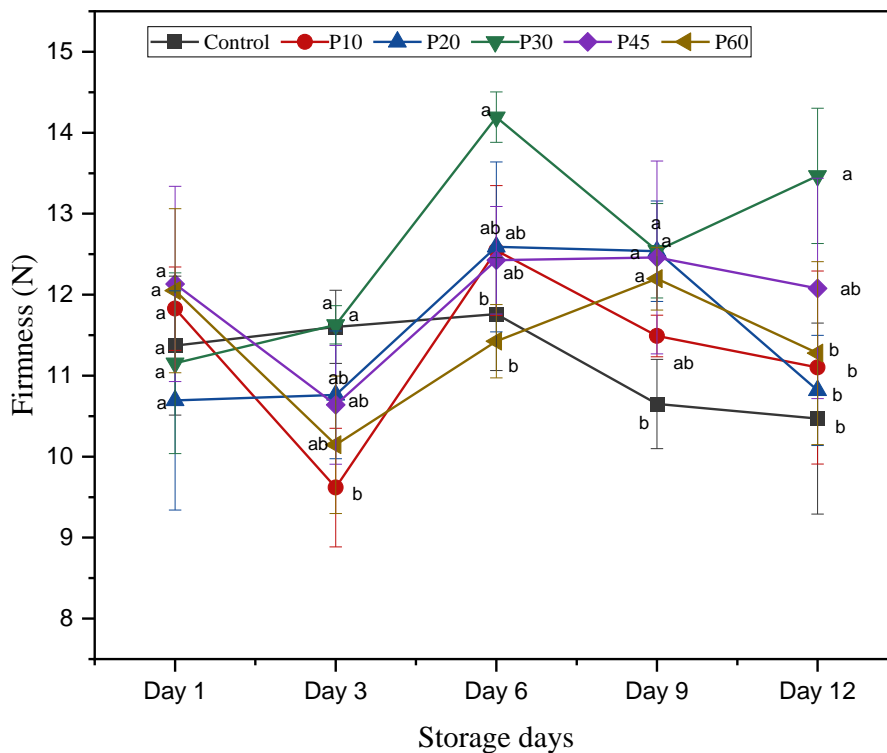


Figure 7.5 Firmness (N) of the fresh-cut apple samples after PAW treatment and 12 days of storage. (Means connected with the same letter are not significant at $p < 0.05$)

7.4.6 Antioxidant properties

7.4.6.1 Total phenolics content

The total phenolic contents of the apple samples, expressed as mg of gallic acid equivalent per g of fresh weight, are presented in Figure 7.6. Phenolic contents in apple samples decreased throughout the 12 days of storage in all treatments and in the control samples. On day one, no significant changes ($p > 0.05$) in the TPC of PAW treated samples and control samples was observed except in P10 samples. In P10, a 32% increase in the TPC content was observed on day 1. After 6 days, the TPC content of the control samples was reduced drastically (by 35%). In PAW treated samples, 88.10%, 56.40% and 55.48% higher TPC contents were recorded in P10, P20 and P30 treatments respectively when compared to that of the control samples on day 12. Among the PAW treated samples, P45 and P60 had significant reductions ($p < 0.05$) in the TPC content when compared to the other PAW treatments. Similar increase in the phenolic content of fresh-cut apples following PAW treatments was reported by Liu et al. (2020). The increase in TPC could be attributed to the activation of defense mechanisms in the plant cells in response to the ROS in

PAW, which could have led to the synthesis of phenolic compounds in the cells to scavenge the ROS (Liu et al., 2020). Activation of phenylalanine ammonia lyase (PAL) enzyme responsible for the synthesis of phenolic compounds can also be attributed to the increase in the TPC of fresh-cut apple samples following PAW treatment (Sarangapani et al., 2017b). Another hypothesis could be an increase in the extractability of phenolic compounds from the cells due to the increase in membrane permeability (as presented in section 7.4.3) of the samples after PAW treatment. In addition, with a further increase in the PAW activation time, the ROS concentration in PAW increased. Consequently, the higher ROS concentration degrades the phenolic compounds in fresh-cut apples resulting in the reduction in the concentration of TPC at higher activation times (P45 and P60)(Chen et al., 2019a).

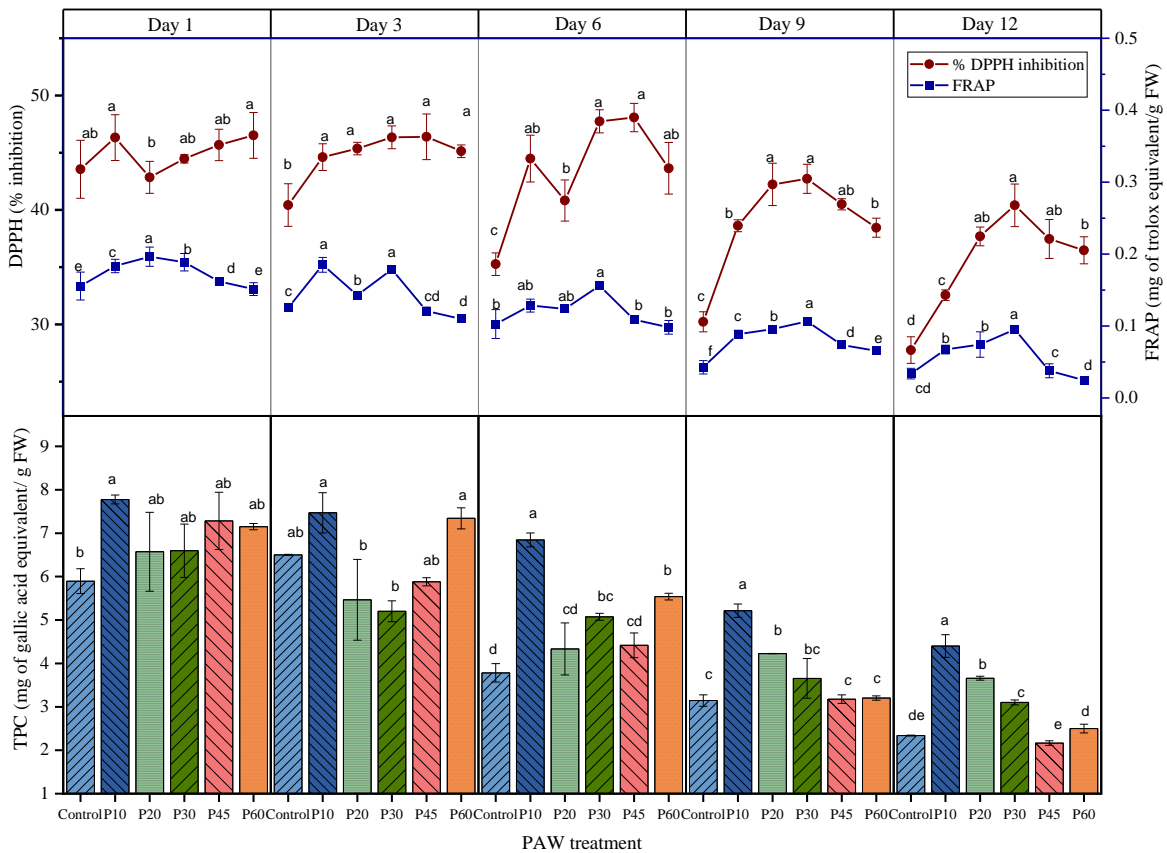


Figure 7.6 Changes in the antioxidant properties of the PAW treated fresh-cut apples for 12 days of storage (Means connected with the same letter are not significant at $p < 0.05$)

7.4.6.2 Antioxidant activity

The DPPH inhibition percentages of PAW treated apple samples were higher than for the control samples throughout the tested storage period. Like for the TPC content, the DPPH inhibition percentage was greater in P10, P20 and P30 treatments than in P45 and P60 treatments. Maximum inhibition percentage of 48.07% was observed in P45 after 6 days of storage. Drastic increase in the antioxidant activity of PAW treated samples compared to the control was observed from day 6 onwards. At the end of 12 days of storage, the control samples had 15.80% reduction in the DPPH inhibition percentage whereas, the minimum reduction of 4.06% and 5.15% were observed in P45 and P30 treatments respectively, when compared with day 1 values. In the case of FRAP activity, reduction in its activity was observed during storage in all treatments including the control samples. However, maximum increase of 25.6% in the FRAP activity was observed in P20 when compared with the control samples on day 1. The increase in the antioxidant activity of the PAW treated fresh-cut apple samples emphasizes the ROS induced oxidative stress in the PAW treated samples. Increase in the total phenolic content could have also resulted in an increase in antioxidant activity of the PAW treated fresh-cut apples (Ramazzina et al., 2015).

7.4.7 PPO and POD enzyme activity

Changes in the activities of PPO and POD during the storage period for the PAW treated and control samples are shown in Figures 7.7(i) and 7.7(ii) respectively. As shown in Figure 7.7(i), immediately following PAW treatment, the PPO activity of the apple samples reduced when compared to the control samples. The P20 treatment showed maximum reduction of 32.3% immediately after PAW washing. Similar reduction in the PPO activity after cold plasma treatment in banana was reported by Gu et al. (2021). Exposing the cut surfaces of the apple samples to PAW reactive species could have caused the degradation of PPO enzymes by denaturation of the enzyme proteins present at the surface level (Han et al., 2019). This could have caused the reduction in the enzyme activity immediately after PAW treatment. During the storage period, the PPO content was increasing in all treatments till day 6 and decreased afterwards. Among the treatments, P20 and P30 had the slowest increasing rate during the first 6 days of storage and the lowest enzyme activity was observed in P20 (5.10 ± 0.16 U/g FW) after 12 days of storage under refrigerated conditions.

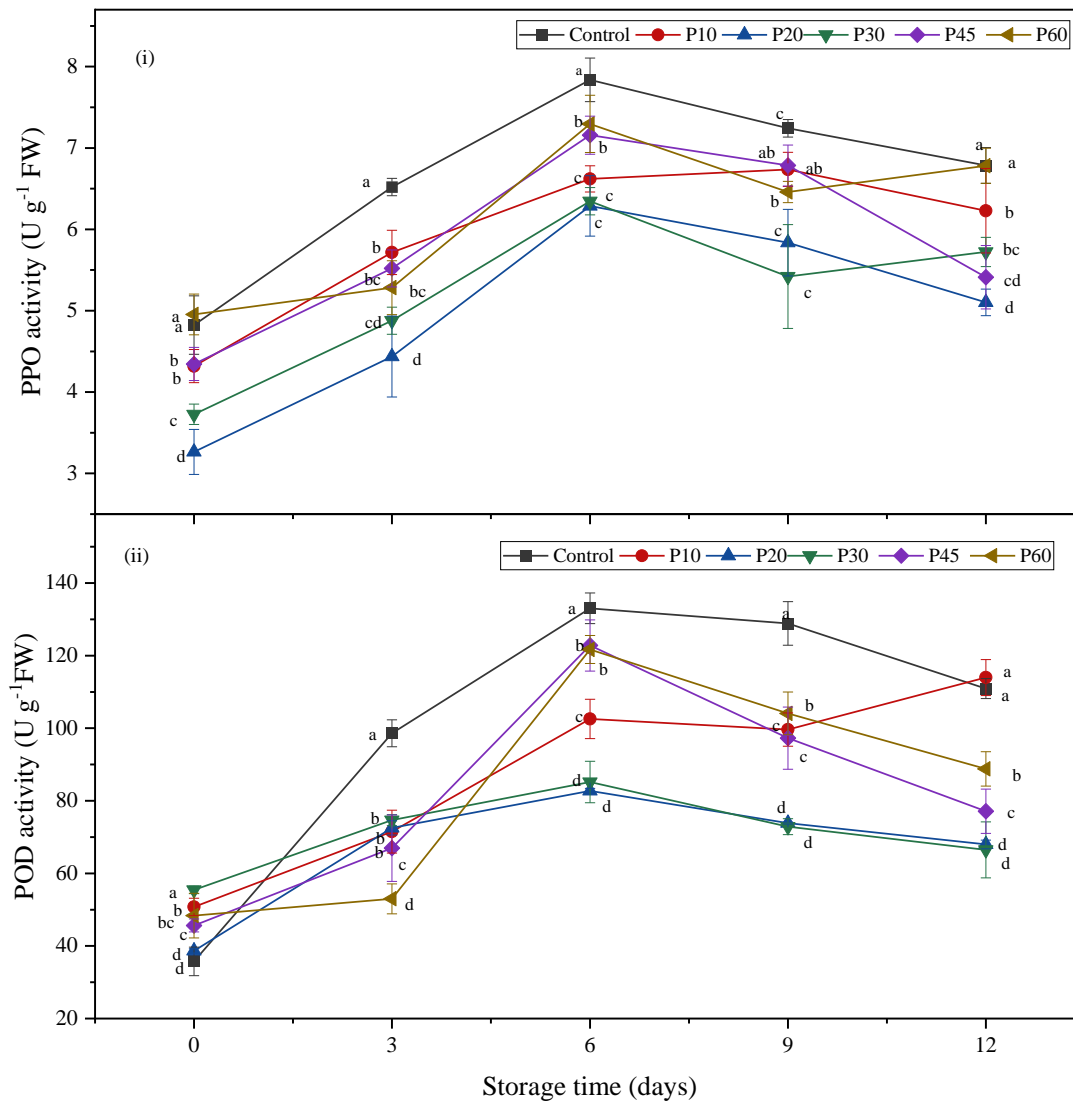


Figure 7.7 Effect of PAW treatment on fresh-cut apple (i) PPO enzyme activity (ii) POD enzyme activity (Means connected with the same letter are not significant at $p < 0.05$)

Like PPO, POD activity also increased during the initial storage period and then started declining (Figure 7.7(ii)). However, immediately after PAW treatment, as opposed to PPO activity, significant increase ($p < 0.05$) in the POD activity was observed in all PAW treated samples when compared to that of the control samples. P30 treatment had the maximum increase in the enzyme activity of 55.43 ± 1.02 U/g FW. Differences in the structure between PPO and POD enzymes could have influenced their response to the oxidative stresses from PAW (Gu et al., 2021). Similar

increase in the POD activity after PAW treatment was reported by Zhao et al. (2019) in fresh-cut kiwi fruit. They attributed this effect to the regulatory mechanisms in the plant cells to alleviate the lipid peroxidation by ROS. Nevertheless, the rate of increase in the POD activity of P30 and P20 samples were much lower than other PAW treatments and the control samples throughout the storage period. Consequently, P30 and P20 had the lowest enzyme activity on day 12 with 66.46 ± 7.71 U/g FW and 67.98 ± 1.19 U/g FW respectively.

Cold plasma has been reported as an effective method for the inactivation of exogenous enzymes such as PPO and POD in food systems (Han et al., 2019). However, effects of PAW reactive species on these enzymes are not yet studied in detail. From the present results it is evident that PAW is effective in reducing the PPO and POD enzyme activity in apple samples, however, this inactivation kinetics was not proportional to the PAW activation times. It is evident that at higher PAW activation time, such as P60, the PPO activity was equal to that of the control at the end of 12 days storage period. Though there was a significant reduction in the enzyme activity of POD which was observed on day 12 in P60 treatment when compared with the control, the values were higher than for P20, P30 and P45 treatments. Changes in the inactivation efficiency of PPO and POD activities with oxygen concentration in the feed gas was reported by Surowsky et al. (2013) in model enzyme solutions. They also reported POD to be less effective than PPO under Ar/O₂ cold plasma treatment. The ROS in plasma and PAW react with the side chain amino acids in proteins such as cysteine and tyrosine causing loss of enzyme activity (Pankaj et al., 2013). Yet not all amino acids were equally susceptible to degradation under oxidative stress (Takai et al., 2014) and the degradation kinetics of the POD with cold plasma treatment time were better explained by Weibull and logistic models than with a first-order kinetic model (Pankaj et al., 2013). This could be the reason for the variations between the PPO and POD enzyme inactivation in this present study. Further mechanistic studies on these enzymes upon exposure to the PAW reactive species are needed to affirm these hypotheses.

7.4.8 Microbial quality

The wounded surface of the fresh-cut products acts as an ideal condition for the growth of microorganisms. The total counts of aerobic bacteria (TAC) and yeasts and molds (TYMC) in PAW treated and control samples during 12 days of refrigerated storage are given in Figure 7.8(i & ii).

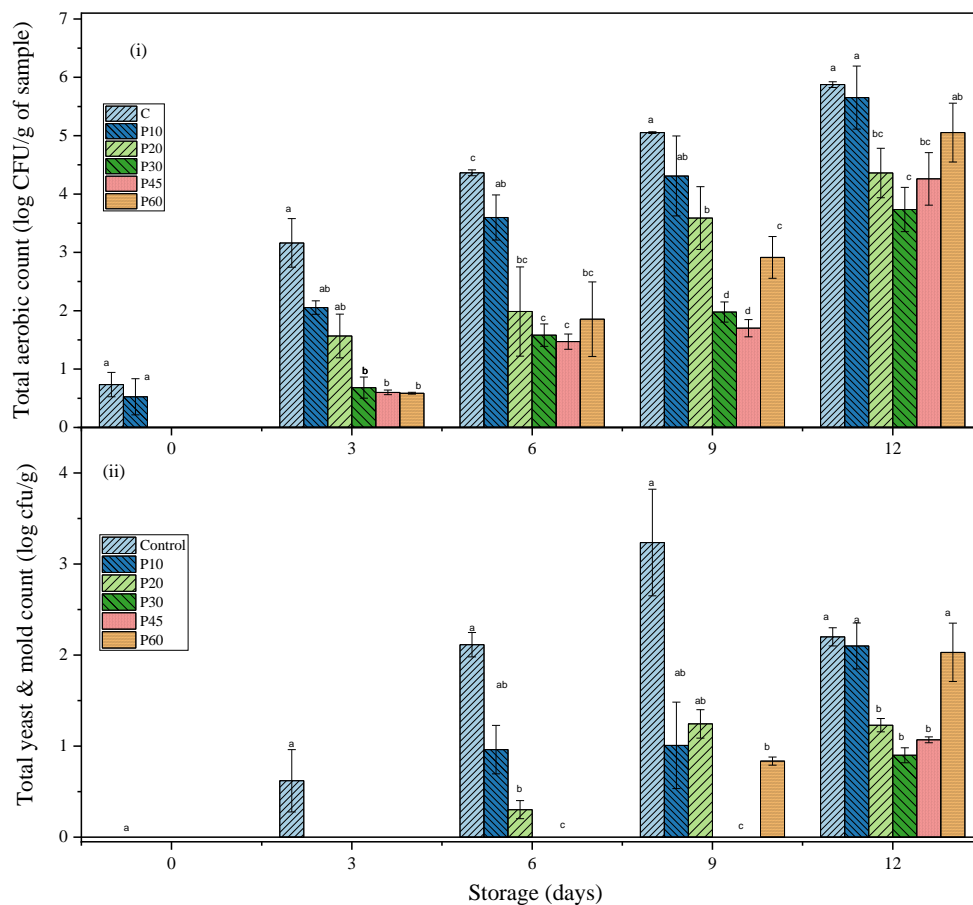


Figure 7. 8 Microbial quality of PAW treated fresh-cut apples during storage (i) Total aerobic count (log CFU/g) (ii) Total yeast and molds count (log CFU/g) (Means connected with the same letter are not significant at $p < 0.05$)

Regardless of the treatment, less than 1 log cfu/g of aerobic bacterial count was detected at the beginning of the storage period. The bacterial count started increasing gradually in all treatments from day 2 onwards, however there was a delay in the PAW treated samples when compared to the control samples except with P10 treatment (Figure 7.8(i)). From the beginning of the storage period, P10 exhibited no significant difference ($p > 0.05$) in the aerobic bacterial population when compared to the control. This could be due to the low concentration of ROS in PAW with 10 min activation time which was not sufficient to inactivate the bacterial population. Until day 9, all PAW treatments, except P10, had significantly ($p < 0.05$) lower numbers of bacterial population than the

control samples. Nevertheless, on day 12, P30 recorded the lowest aerobic bacterial count (3.73 ± 0.62 log cfu/g) followed by P20 and P45. In P60, the bacterial population increased (5.05 ± 0.5 log cfu/g) to a non-significant level when compared with the control ($p > 0.05$). Similar reduction in the aerobic bacterial population during storage was reported by Chen et al. (2019a) in PAW treated fresh-cut pears.

The total yeast and mold count (TYMC) of the PAW treated samples exhibited similar trend to that of total aerobic count results (Figure 7.8(ii)). The TYMC gradually increased in the control samples during the storage period, while, except for P10 and P60, all PAW treated samples had significantly ($p < 0.05$) lower TYM counts. Among the treatments, P30 recorded the lowest TYMC of 0.92 ± 0.08 log cfu/g at the end of the 12 days of storage. The results suggests that PAW30 is effective in ensuring the microbial safety of fresh-cut apple samples during 12 days of refrigerated storage. Xu et al. (2016) reported that the inactivation efficiency of PAW increases with the PAW activation time. In the present study though this trend was followed for P20 and P30, while higher microbial populations were reported in P45 and P60 when compared with P30. This could be attributed to the damages in cell membranes due to high ROS induced oxidative stress at higher PAW activation times. Thus, optimized activation of PAW and product specific application is necessary to ensure the microbial safety of fresh cut apples.

7.4.9 SEM image analysis

Following PAW treatment, the treated and control apple sample cubes were observed under SEM to monitor changes in apple parenchyma cell structure. As shown in Figure 7.9, there was a noticeable change in the parenchyma cell structure observed in all PAW treated samples. Though there were no visible changes in the fresh apple samples immediately after treatment, these changes were prominent under SEM. In control samples (Figure 7.9a) the cells were more uniform, and the cell walls were intact. After PAW treatment, clear deformation, shrinkage, and collapse of the cell walls was observed and this effect was apparent in P45 (Figure 7.9e) and P60 (Figure 7.9f) treatments. These findings are supported by the increase in electrolytic leakage and reduction in the firmness of P45 and P60 treatments. Surface sculpturing in cell walls of kumquat skin was reported after PAW treatment and the severity of the damage to cell wall was dependent on the PAW activation time (Guo et al., 2021a). Damages to the cell wall and cellular damage in microorganisms by the ROS in PAW are widely reported (Zhao et al., 2020). Though the effect of

PAW ROS is not as severe in eukaryotic cells, the wounded cells in fresh-cut apple samples could allow the penetration of highly oxidative ROS such as hydrogen peroxide, ozone, and hydroxyl radicals. This could lead to the oxidation of lipids and polysaccharide bonds in the cell membrane causing the loss of cell turgor and shrinkage of cells (Guo et al., 2021a; Liu et al., 2021).

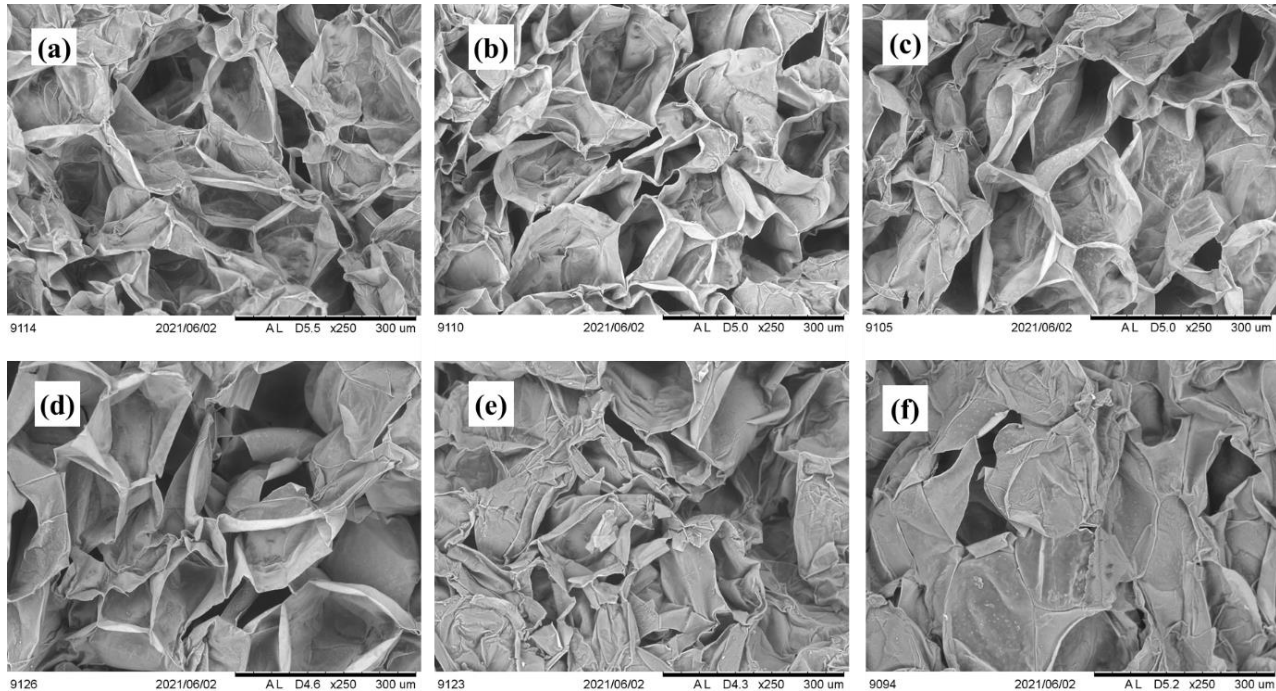


Figure 7.9 SEM microstructure images of PAW treated apple samples (a) control, (b) P10, (c) P20, (d) P30, (e) P45, and (f) P60.

7.5 Conclusion

This study investigated the effects of different PAW activation times on the enzymatic, microbial, and physicochemical quality of fresh-cut apples during refrigerated storage for 12 days. The results indicated that PAW is effective in maintaining the microbial quality of the fresh-cut apples and the effect was dependent on the PAW activation time. In the case of enzyme inactivation, the inactivation efficiency was dependent on the PAW activation time as well as the type of enzyme. The physicochemical properties such as color, weight loss and TSS of the samples were maintained throughout the storage period in P20 and P30 treatments. Reduction in the textural properties and

the membrane permeability of the samples treated with P45 and P60 indicate that the PAW activation time does not have a proportional effect on the quality of the fresh-cut apples. The varying effect of PAW activation time on the enzyme activity and the quality parameter of fresh-cut apple emphasizes the complex interaction of ROS with food metabolic and bioactive compounds. The SEM imaging also revealed the structural changes in the fruit tissue at higher ROS concentration. Future research on product specific optimization of PAW reactive species and their effect on different types of enzymes and metabolic activity of the fresh foods can facilitate the better understanding of PAW reactive species and their effects on food matrices.

CHAPTER VIII

CONCLUSIONS AND RECOMMENDATIONS

8.1 General summary and conclusion

Plasma activated water (PAW) is an emerging technology and the present work was intended to provide a deeper understanding on the complex interactions of PAW reactive species with food materials. The reactive species in PAW have the potential to disinfect a wide range of food pathogenic microorganisms. Conversely, the highly oxidative species in PAW pose some uncertainty in using this technology for foods susceptible to oxidative damages. So far, only limited research was undertaken on evaluating both the positive and negative aspects of PAW on food material. It is essential to understand the effect of these oxidative reactive species in PAW on food material to harness the full potential of this technology and for their successful application in food processing.

The major objective of this work was to evaluate the suitability of plasma activated water for fresh food disinfection and to understand its effect on food quality. In chapter II, various methods available for the generation of PAW and the chemistry of reactive species in gas and liquid phases was comprehensively studied and it was identified that dielectric barrier discharge was the commonly used and the simplest method of producing nonthermal plasma and most of the systems used were batch generating systems with less than 100 ml PAW capacity. Further, from the status of nonthermal plasma and PAW applications in food, it was revealed that the effect of PAW reactive species on food components was not explored in detail.

The first step towards achieving this aim was to design and develop a continuous flow PAW generation system. In this study, a dielectric barrier discharge, continuous flow PAW system was developed. In chapter III, a simple, preliminary setup was conceptualized and developed; it was demonstrated that the dielectric barrier discharge was produced with argon/oxygen gas mixture at voltage levels of 3 kV and lower. The continuous flow system worked well in generating reactive oxygen species with mainly hydrogen peroxide in PAW. The flow conditions revealed that with broader reactors, the discharge was not completely covered with the flowing water, thus reducing the efficiency of the system. Further, altering the pH of water using nitric acid and sodium hydroxide before treatment influenced the reactive species formation in PAW. With the knowledge

gained from the preliminary set-up, a new reactor was designed, fabricated, and used in the subsequent chapters.

In chapter IV, the remodeled reactor was evaluated based on the produced PAW's chemical and disinfection properties. Further the time stability of the PAW stored at room temperature was also analyzed. The discharge was transformed from filamentary discharge to homogenous glow discharge with an increase in the gas flow rate from 4 slm to 10 slm. The FTIR spectrum of the gas phase revealed the presence of ozone and O-H stretching bands. From the time stability analysis of PAW, it was revealed that the PAW activation time increased the hydrogen peroxide and ozone concentration. The stability of hydrogen peroxide was higher than ozone during room temperature storage of PAW. The *E. coli* disinfection efficiency of PAW was also increased with PAW activation time and the PAW produced by 20 min and 30 min NTP activation retained their disinfection property against *E. coli* for almost 2 h. The process variables were then optimized using response surface methodology. The optimum operating conditions of 104.6 ml/min water flow rate, 20 min treatment time, and 4 slm gas flow rate were found for the maximum hydrogen peroxide and ozone concentrations, ORP, and minimum pH of produced PAW.

Before proceeding with the study of treating fresh foods with PAW, it was important to know the interaction of PAW reactive species with food components. Hence to evaluate the effect of PAW on proteins, whey protein isolate (WPI) at different concentrations was used and the changes in the WPI physicochemical and functional properties were evaluated in chapter IV. Mild oxidation of WPI was observed after PAW treatment. PAW treatment increased the foam stability and foam capacity of the WPI samples and no significant changes in the thermal stability of the samples were observed. Further, no insoluble disulfide bonds or aggregates were formed in WPI after PAW treatment. The FTIR spectral analysis and the SDS-page analysis of the WPI revealed that PAW treatment did not induce the formation of new functional groups in the samples.

In chapter V, the effectiveness of *E. coli* inactivation by PAW treatment on kale and spinach samples was assessed and the differences between kale and spinach samples in terms of the product quality and nutritional characteristics upon PAW treatment were also investigated. PAW treatment significantly reduced the *E. coli* population on both kale and spinach leaves. The disinfection efficiency was lower in kale when compared to spinach due to the differences in the surface roughness of the leaves. PAW treatment caused a significant reduction in the chlorophyll content

and total phenolics content of both kale and spinach leaves. The surface morphological analysis of kale and spinach leaves through FTIR and SEM imaging revealed that PAW treatment reduced the cuticular wax content in kale leaves and stomatal closure was observed in both kale and spinach leaves due to the oxidative stress induced due to the PAW treatment.

Finally, in chapter VI, the effect of PAW washing treatment on enzyme activity, microbial and physicochemical quality of fresh-cut apples during 12 days of storage were studied. PAW treatment increased the peroxidase activity and reduced the polyphenol oxidase activity immediately after washing. The physicochemical properties such as color, weight loss and TSS of the samples were maintained throughout the storage period in P20 and P30 treatments. Reduction in the textural properties and the membrane permeability of the samples treated with P45 and P60 indicate that the PAW activation time does not have a proportional effect on the quality of the fresh-cut apples. At higher PAW activation times, structural changes in the fresh-cut apple tissues were observed. PAW activated for 30 and 45 min could maintain the microbial quality of fresh-cut apples up to 9 days under refrigerated storage conditions.

In summary, plasma activated water can be produced using a relatively simple reactor with continuous flow developed and presented in this thesis. The successful use of PAW for fresh food disinfection and its time stability and storability were demonstrated in this study. Further, a deeper understanding of the PAW reactive species interaction with proteins and the fresh food nutritional components was illustrated. It is evident from this study that this technology can be exploited for the commercial disinfection of fresh foods in the future.

8.2 Contribution to knowledge

The findings from this thesis have led to significant novel contributions in the field of nonthermal plasma applications in food. The following are the important contributions to knowledge:

1. *Novel continuous flow PAW generation system*: A simple, continuous flow PAW generating system was developed and successfully demonstrated its robustness through the time-intensive experiments presented in this work.

2. *Optimization of PAW production parameters and time stability*: For the first time, a continuous flow PAW generating system was optimized for its process parameters. The results from the time stability analysis established the ideal process conditions to store PAW up to 2 hours at room temperature without losing its disinfection properties.

3. *Insight on PAW interaction with protein*: Through a detailed study, it was demonstrated that PAW did not cause oxidative damages in protein and it improved the foaming properties of protein.

4. *Insight on PAW interaction with leafy vegetables*: The study revealed that PAW is effective in disinfecting the *E. coli* populations on different textured leaves. For the first time, changes in the morphological characteristics of the spinach and kale leaves upon PAW treatment were established.

5. *Improving the shelf life of fresh-cut product*: this study shows that PAW treatment to be useful in maintaining the microbial and physicochemical quality of fresh-cut apples up to 9 days under refrigerated storage.

6. *Insight on complexities in PAW treatment*: From the results obtained, PAW reactivity with food samples varies with the process conditions and the product's physical, chemical and morphological characteristics.

8.3 Recommendations for future work

Nonthermal plasma and plasma activated water applications in food are an emerging field of study. From the insights gained from this thesis work, the following recommendations could lead to further understanding of the PAW reactive species and their interactions with food materials.

1. Scale-up studies on the present PAW generating system are recommended for further evaluation of its applicability on the industrial scale.
2. The time stability analysis of PAW can be further expanded to different storage conditions.
3. Simulation and modelling studies on the formation of varied reactive species in PAW in a continuous flow system could be exploited for better understanding of the mechanisms and chemistry of plasma-water interactions.

4. Further investigation on the residual toxicity of PAW reactive species in food materials and their penetration inside the porous food materials is required.
5. Apart from using PAW as a disinfectant, the current system can be explored to produce other disinfectants like peracetic acid.
6. From the kale and spinach PAW treatment studies, it was observed that PAW treatment removed the cuticular layer on the leaves. Further, in fresh-cut apples PAW treatment caused tissue damage at higher activation times. This aspect can be explored as pretreatment for the extraction of bioactive compounds from the biomaterials.
7. Kinetic studies on the microbial disinfection with respect to the reactive species concentration and treatment time.

BIBLIOGRAPHY

- Abdel-Fattah, E. (2019). Atmospheric pressure helium plasma jet and its applications to methylene blue degradation. *Journal of Electrostatics*, *101*, 103360.
- Abou-Ghazala, A., Katsuki, S., Schoenbach, K. H., Dobbs, F., & Moreira, K. (2002). Bacterial decontamination of water by means of pulsed-corona discharges. *Ieee Transactions on Plasma Science*, *30*(4), 1449-1453.
- Ahn, H. J., Kim, K. I., Kim, G., Moon, E., Yang, S. S., & Lee, J.-S. (2011). Atmospheric-pressure plasma jet induces apoptosis involving mitochondria via generation of free radicals. *Plos One*, *6*(11), e28154.
- Aicardo, A., Mastrogiovanni, M., Cassina, A., & Radi, R. J. F. r. r. (2018). Propagation of free-radical reactions in concentrated protein solutions. *Free Radical Research* *52*(2), 159-170.
- Ajo, P., Kornev, I., & Preis, S. (2017). Pulsed Corona Discharge Induced Hydroxyl Radical Transfer Through the Gas-Liquid Interface. *Scientific Reports*, *7*(1), 16152.
- Akishev, Y., Grushin, M., Napartovich, A., & Trushkin, N. (2002). Novel AC and DC non-thermal plasma sources for cold surface treatment of polymer films and fabrics at atmospheric pressure [Article]. *Plasmas and Polymers*, *7*(3), 261-289. <https://doi.org/10.1023/a:1019990508769>
- Al-Abduly, A., & Christensen, P. (2015). An in situ and downstream study of non-thermal plasma chemistry in an air fed dielectric barrier discharge (DBD). *Plasma Sources Science & Technology*, *24*(6), 065006.
- Alavi, F., Emam-Djomeh, Z., Momen, S., Mohammadian, M., Salami, M., & Moosavi-Movahedi, A. A. (2019). Effect of free radical-induced aggregation on physicochemical and interface-related functionality of egg white protein. *Food Hydrocolloids*, *87*, 734-746.
- Allende, A., Luo, Y., McEvoy, J. L., Artés, F., & Wang, C. Y. (2004). Microbial and quality changes in minimally processed baby spinach leaves stored under super atmospheric oxygen and modified atmosphere conditions. *Postharvest Biology and Technology*, *33*(1), 51-59.
- Almeida, F. D. L., Cavalcante, R. S., Cullen, P. J., Frias, J. M., Bourke, P., Fernandes, F. A. N., & Rodrigues, S. (2015). Effects of atmospheric cold plasma and ozone on prebiotic orange juice. *Innovative Food Science & Emerging Technologies*, *32*, 127-135.
- Alothman, M., Kaur, B., Fazilah, A., Bhat, R., & Karim, A. A. (2010). Ozone-induced changes of antioxidant capacity of fresh-cut tropical fruits. *Innovative Food Science & Emerging Technologies*, *11*(4), 666-671. <https://doi.org/10.1016/j.ifset.2010.08.008>
- Alves Filho, E. G., Almeida, F. D. L., Cavalcante, R. S., de Brito, E. S., Cullen, P. J., Frias, J. M., . . . Rodrigues, S. (2016). 1H NMR spectroscopy and chemometrics evaluation of non-thermal processing of orange juice. *Food Chemistry*, *204*(Supplement C), 102-107.
- Amiour, S. D., & Hambaba, L. (2016). Effect of pH, temperature and some chemicals on polyphenoloxidase and peroxidase activities in harvested Deglet Nour and Ghars dates. *Postharvest Biology and Technology*, *111*, 77-82.
- Amiri, A., Sharifian, P., & Soltanizadeh, N. (2018). Application of ultrasound treatment for improving the physicochemical, functional and rheological properties of myofibrillar proteins. *Int J Biol Macromol*, *111*, 139-147. <https://doi.org/10.1016/j.ijbiomac.2017.12.167>
- Anderson, C. E. (2016). *Interactions of Non-Thermal Air Plasmas with Aqueous Solutions* UC Berkeley.
- AOAC. (1990). Association of official analytical chemists. Official methods of analysis. In: AOAC Arlington, VA.

- Aoki, H., Kitano, K., & Hamaguchi, S. (2008). Plasma generation inside externally supplied Ar bubbles in water. *Plasma Sources Science and Technology*, 17(2), 025006.
- Attri, P., Kim, Y. H., Park, D. H., Park, J. H., Hong, Y. J., Uhm, H. S., . . . Choi, E. H. (2015). Generation mechanism of hydroxyl radical species and its lifetime prediction during the plasma-initiated ultraviolet (UV) photolysis. *Scientific Reports*, 5, 9332. <https://doi.org/10.1038/srep09332>
- Azevedo, V. M., Borges, S. V., Marconcini, J. M., Yoshida, M. I., Neto, A. R. S., Pereira, T. C., & Pereira, C. F. G. (2017). Effect of replacement of corn starch by whey protein isolate in biodegradable film blends obtained by extrusion. *Carbohydrate Polymers*, 157, 971-980. <https://doi.org/10.1016/j.carbpol.2016.10.046>
- Azevedo, V. M., Dias, M. V., Borges, S. V., Costa, A. L. R., Silva, E. K., Medeiros, É. A. A., & Soares, N. d. F. F. (2015). Development of whey protein isolate bio-nanocomposites: Effect of montmorillonite and citric acid on structural, thermal, morphological and mechanical properties. *Food Hydrocolloids*, 48, 179-188. <https://doi.org/10.1016/j.foodhyd.2015.02.014>
- Bader, A., & Hoigné. (1982). Determination of ozone in water by the indigo method: a submitted standard method. *Ozone: Science & Engineering*, 4(4), 169-176, DOI: 10.1080/01919518208550955
- Baek, E. J., Joh, H. M., Kim, S. J., & Chung, T. (2016a). Effects of the electrical parameters and gas flow rate on the generation of reactive species in liquids exposed to atmospheric pressure plasma jets. *Physics of Plasmas*, 23(7), 073515.
- Baier, M., Görgen, M., Ehlbeck, J., Knorr, D., Herppich, W. B., & Schlüter, O. (2014). Non-thermal atmospheric pressure plasma: screening for gentle process conditions and antibacterial efficiency on perishable fresh produce. *Innovative Food Science Emerging Technologies*, 22, 147-157.
- Banaschik, R., Lukes, P., Jablonowski, H., Hammer, M. U., Weltmann, K.-D., & Kolb, J. F. (2015). Potential of pulsed corona discharges generated in water for the degradation of persistent pharmaceutical residues. *Water Research*, 84, 127-135.
- Barceló, A. R., & Laura, V. G. R. (2009). Reactive oxygen species in plant cell walls. In L. A. Rio & A. Puppo (Eds.), *Reactive Oxygen Species in Plant Signaling* (pp. 73-93). Springer Berlin Heidelberg. <https://doi.org/10.1007/978-3-642-00390-5-5>
- Baroch, P., Saito, N., & Takai, O. (2008). Special type of plasma dielectric barrier discharge reactor for direct ozonization of water and degradation of organic pollution. *Journal of Physics D: Applied Physics*, 41(8), 085207.
- Belgacem, I., Schena, L., Teixidó, N., Romeo, F. V., Ballistreri, G., & Abadias, M. (2020). Effectiveness of a pomegranate peel extract (PGE) in reducing *Listeria monocytogenes* in vitro and on fresh-cut pear, apple and melon. *European Food Research and Technology*, 246(9), 1765-1772. <https://doi.org/10.1007/s00217-020-03529-5>
- Benstaali, B., Boubert, P., Cheron, B., Addou, A., & Brisset, J. (2002). Density and rotational temperature measurements of the OH and NO radicals produced by a gliding arc in humid air. *Plasma Chemistry and Plasma Processing*, 22(4), 553-571.
- Benzie, I. F., & Strain, J. (1996). The ferric reducing ability of plasma (FRAP) as a measure of "antioxidant power": the FRAP assay. *J Analytical biochemistry*, 239(1), 70-76.
- Berardinelli, A., Pasquali, F., Cevoli, C., Trevisani, M., Ragni, L., Mancusi, R., & Manfreda, G. (2016). Sanitisation of fresh-cut celery and radicchio by gas plasma treatments in water medium. *Postharvest Biology and Technology*, 111, 297-304.
- Bermudez-Garcia, E., Pena-Montes, C., Martins, I., Pais, J., Pereira, C. S., Sanchez, S., & Farres, A. (2019). Regulation of the cutinases expressed by *Aspergillus nidulans* and evaluation of their role

- in cutin degradation. *Appl Microbiol Biotechnol*, 103(9), 3863-3874. <https://doi.org/10.1007/s00253-019-09712-3>
- Beveridge, T., Toma, S., & Nakai, S. (1974). Determination of SH-and SS-groups in some food proteins using Ellman's reagent. *Journal of Food Science*, 39(1), 49-51.
- Bhunia, A. K. (2018). *Foodborne microbial pathogens: mechanisms and pathogenesis*. Springer.
- Bie, P., Pu, H., Zhang, B., Su, J., Chen, L., & Li, X. (2016). Structural characteristics and rheological properties of plasma-treated starch. *Innovative Food Science & Emerging Technologies*, 34(Supplement C), 196-204. <https://doi.org/10.1016/j.ifset.2015.11.019>
- Blois, M. S. (1958). Antioxidant determinations by the use of a stable free radical. *Nature*, 181(4617), 1199-1200.
- Boudam, M., Moisan, M., Saoudi, B., Popovici, C., Gherardi, N., & Massines, F. (2006). Bacterial spore inactivation by atmospheric-pressure plasmas in the presence or absence of UV photons as obtained with the same gas mixture. *Journal of Physics D: Applied Physics*, 39(16), 3494.
- Bourke, P., Ziuzina, D., Boehm, D., Cullen, P. J., & Keener, K. (2018). The potential of cold plasma for safe and sustainable food production. *Trends in Biotechnology*. 36(6), 615-626 <https://doi.org/10.1016/j.tibtech.2017.11.001>
- Bradford, K. J., Dahal, P., Van Asbrouck, J., Kunusoth, K., Bello, P., Thompson, J., & Wu, F. (2018). The dry chain: Reducing postharvest losses and improving food safety in humid climates. *Trends in Food Science & Technology*, 71, 84-93.
- Brisset, J.-L., Benstaali, B., Moussa, D., Fanmoe, J., & Njoyim-Tamungang, E. (2011). Acidity control of plasma-chemical oxidation: applications to dye removal, urban waste abatement and microbial inactivation. *Plasma Sources Science and Technology*, 20(3), 034021.
- Brisset, J.-L., & Pawlat, J. (2016). Chemical effects of air plasma species on aqueous solutes in direct and delayed exposure modes: discharge, post-discharge and plasma activated water. *Plasma Chemistry and Plasma Processing*, 36(2), 355-381.
- Bruggeman, P., Kushner, M. J., Locke, B. R., Gardeniers, J. G., Graham, W., Graves, D. B., . . . Ceriani, E. (2016). Plasma-liquid interactions: a review and roadmap. *Plasma Sources Science and Technology*, 25(5), 053002.
- Bruggeman, P., & Leys, C. (2009). Non-thermal plasmas in and in contact with liquids. *Journal of Physics D: Applied Physics*, 42(5), 053001.
- Burlica, R., Grim, R., Shih, K. Y., Balkwill, D., & Locke, B. (2010). Bacteria inactivation using low power pulsed gliding arc discharges with water spray. *Plasma Processes and Polymers*, 7(8), 640-649.
- Burlica, R., Kirkpatrick, M. J., Finney, W. C., Clark, R. J., & Locke, B. R. (2004). Organic dye removal from aqueous solution by glidarc discharges. *Journal of Electrostatics*, 62(4), 309-321.
- Burlica, R., Kirkpatrick, M. J., & Locke, B. R. (2006). Formation of reactive species in gliding arc discharges with liquid water. *Journal of Electrostatics*, 64(1), 35-43. <https://doi.org/10.1016/j.elstat.2004.12.007>
- Bursać Kovačević, D., Gajdoš Kljusurić, J., Putnik, P., Vukušić, T., Herceg, Z., & Dragović-Uzelac, V. (2016a). Stability of polyphenols in chokeberry juice treated with gas phase plasma. *Food Chemistry*, 212, 323-331. <https://doi.org/10.1016/j.foodchem.2016.05.192>
- Bursać Kovačević, D., Putnik, P., Dragović-Uzelac, V., Pedišić, S., Režek Jambrak, A., & Herceg, Z. (2016b). Effects of cold atmospheric gas phase plasma on anthocyanins and color in pomegranate juice. *Food Chemistry*, 190, 317-323. <https://doi.org/10.1016/j.foodchem.2015.05.099>

- Bußler, S., Steins, V., Ehlbeck, J., & Schlüter, O. (2015). Impact of thermal treatment versus cold atmospheric plasma processing on the techno-functional protein properties from *Pisum sativum* 'Salamanca'. *Journal of Food Engineering*, 167(Part B), 166-174. <https://doi.org/10.1016/j.jfoodeng.2015.05.036>
- Callejón, R. M., Rodríguez-Naranjo, M. I., Ubeda, C., Hornedo-Ortega, R., Garcia-Parrilla, M. C., & Troncoso, A. M. (2015). Reported foodborne outbreaks due to fresh produce in the united states and european union: trends and causes. *Foodborne Pathogens and Disease*, 12(1), 32-38. <https://doi.org/10.1089/fpd.2014.1821>
- Campo, M. G., & Grigera, J. R. (2005). Classical molecular-dynamics simulation of the hydroxyl radical in water. *The Journal of chemical physics*, 123(8), 084507.
- Cao, Y., Zhao, J., & Xiong, Y. L. (2016). Coomassie Brilliant Blue-binding: a simple and effective method for the determination of water-insoluble protein surface hydrophobicity. *Analytical Methods*, 8(4), 790-795.
- Carbonaro, M., & Nucara, A. (2010). Secondary structure of food proteins by Fourier transform spectroscopy in the mid-infrared region. *Amino Acids*, 38(3), 679-690. <https://doi.org/10.1007/s00726-009-0274-3>
- Carstens, C. K., Salazar, J. K., & Darkoh, C. (2019). Multistate Outbreaks of Foodborne Illness in the United States Associated With Fresh Produce From 2010 to 2017. *10(2667)*. <https://doi.org/10.3389/fmicb.2019.02667>
- CDC. <https://www.cdc.gov/listeria/outbreaks/caramel-apples-12-14/index.html>
- Chang, C.-C., Yang, M.-H., Wen, H.-M., & Chern, J.-C. (2002). Estimation of total flavonoid content in propolis by two complementary colorimetric methods. *Journal of food drug analysis*, 10(3).
- Chen, C., Hu, W., He, Y., Jiang, A., & Zhang, R. (2016). Effect of citric acid combined with UV-C on the quality of fresh-cut apples. *Postharvest Biology Technology*, 111, 126-131.
- Chen, C., Liu, C., Jiang, A., Guan, Q., Sun, X., Liu, S., . . . Hu, W. (2019a). The effects of cold plasma-activated water treatment on the microbial growth and antioxidant properties of fresh-cut pears. *Food and Bioprocess Technology*, 12(11), 1842-1851. <https://doi.org/10.1007/s11947-019-02331-w>
- Chen, C., Liu, D. X., Liu, Z. C., Yang, A. J., Chen, H. L., Shama, G., & Kong, M. G. (2014a). A model of plasma-biofilm and plasma-tissue interactions at ambient pressure. *Plasma Chemistry and Plasma Processing*, 34(3), 403-441. <https://doi.org/10.1007/s11090-014-9545-1>
- Chen, C. W., Lee, H.-M., & Chang, M. B. (2008). Inactivation of aquatic microorganisms by low-frequency AC discharges. *Ieee Transactions on Plasma Science*, 36(1), 215-219.
- Chen, D., Chen, P., Cheng, Y., Peng, P., Liu, J., Ma, Y., . . . Ruan, R. (2019b). Deoxynivalenol decontamination in raw and germinating barley treated by plasma-activated water and intense pulsed light. *Food and Bioprocess Technology*, 12(2), 246-254. <https://doi.org/10.1007/s11947-018-2206-2>
- Chen, H., Cao, S., Fang, X., Mu, H., Yang, H., Wang, X., . . . Gao, H. (2015). Changes in fruit firmness, cell wall composition and cell wall degrading enzymes in postharvest blueberries during storage. *Scientia Horticulturae*, 188(Supplement C), 44-48. <https://doi.org/10.1016/j.scienta.2015.03.018>
- Chen, H., & Wang, J. (2021). Degradation and mineralization of ofloxacin by ozonation and peroxone (O₃/H₂O₂) process. *Chemosphere*, 269, 128775.
- Chen, J., Tao, X.-Y., Sun, A.-D., Wang, Y., Liao, X.-J., Li, L.-N., & Zhang, S. (2014b). Influence of pulsed electric field and thermal treatments on the quality of blueberry juice. *International Journal of Food Properties*, 17(7), 1419-1427. <https://doi.org/10.1080/10942912.2012.713429>

- Chen, N., Zhao, M., Niepceron, F., Nicolai, T., & Chassenieux, C. (2017). The effect of the pH on thermal aggregation and gelation of soy proteins. *Food Hydrocolloids*, *66*, 27-36.
- Choi, E. J., Park, H. W., Kim, S. B., Ryu, S., Lim, J., Hong, E. J., . . . Chun, H. H. (2019). Sequential application of plasma-activated water and mild heating improves microbiological quality of ready-to-use shredded salted kimchi cabbage (*Brassica pekinensis* L.). *Food Control*, *98*, 501-509. <https://doi.org/10.1016/j.foodcont.2018.12.007>
- Cong, K.-P., Li, T.-T., Wu, C.-E., Zeng, K.-F., Zhang, J.-H., Fan, G.-J., . . . Suo, A.-D. (2022). Effects of plasma-activated water on overall quality of fresh goji berries during storage. *Scientia Horticulturae*, *293*, 110650. <https://doi.org/10.1016/j.scienta.2021.110650>
- Conrads, H., & Schmidt, M. (2000). Plasma generation and plasma sources. *Plasma sources science and technology*, *9*(4), 441.
- Cooper, M., Fridman, G., Fridman, A., & Joshi, S. G. (2010). Biological responses of *Bacillus stratosphericus* to floating electrode-dielectric barrier discharge plasma treatment. *Journal of Applied Microbiology*, *109*(6), 2039-2048. doi:10.1111/j.1365-2672.2010.04834.x
- Coroneo, V., Carraro, V., Marras, B., Marrucci, A., Succa, S., Meloni, B., . . . Schintu, M. (2017). Presence of trihalomethanes in ready-to-eat vegetables disinfected with chlorine. *Food Addit Contam Part A Chem Anal Control Expo Risk Assess*, *34*(12), 2111-2117. <https://doi.org/10.1080/19440049.2017.1382723>
- Coutinho, N. M., Silveira, M. R., Rocha, R. S., Moraes, J., Ferreira, M. V. S., Pimentel, T. C., . . . Cruz, A. G. (2018). Cold plasma processing of milk and dairy products. *Trends in Food Science & Technology*, *74*, 56-68. <https://doi.org/10.1016/j.tifs.2018.02.008>
- Croissant, A. E., Kang, E. J., Campbell, R. E., Bastian, E., & Drake, M. A. (2009). The effect of bleaching agent on the flavor of liquid whey and whey protein concentrate. *Journal of dairy science*, *92*(12), 5917-5927. <https://doi.org/10.3168/jds.2009-2535>
- Cullen, P. J., Lalor, J., Scally, L., Boehm, D., Milosavljević, V., Bourke, P., & Keener, K. (2018). Translation of plasma technology from the lab to the food industry. *Plasma Processes and Polymers*, *15*(2).
- Dar, A. H., Bashir, O., Khan, S., Wahid, A., & Makroo, H. A. (2020). 4 - Fresh-cut products: Processing operations and equipments. In M. W. Siddiqui (Ed.), *Fresh-Cut Fruits and Vegetables* (pp. 77-97). Academic Press. <https://doi.org/10.1016/B978-0-12-816184-5.00004-5>
- Dascalu, A., Besleaga, A., Shimizu, K., & Sirghi, L. (2019). Activation of water by surface DBD micro plasma in atmospheric air. In G. Laukaitis, *Recent Advances in Technology Research and Education* Cham.
- Desikan, R., Cheung, M.-K., Clarke, A., Golding, S., Sagi, M., Fluhr, R., . . . Neill, S. (2004). Hydrogen peroxide is a common signal for darkness- and ABA-induced stomatal closure in *Pisum sativum* *Functional Plant Biology*, *31*(9), 913-920, <https://doi.org/10.1071/FP04035>
- Dobrynin, D., Fridman, G., Friedman, G., & Fridman, A. (2009). Physical and biological mechanisms of direct plasma interaction with living tissue. *New Journal of Physics*, *11*(11), 115020.
- Dong, S., Gao, A., Xu, H., & Chen, Y. (2017). Effects of dielectric barrier discharges (DBD) cold plasma treatment on physicochemical and structural properties of zein powders. *Food Bioprocess Technology*, *10*(3), 434-444.
- Dong, X., Wang, J., & Raghavan, V. (2021). Impact of microwave processing on the secondary structure, in-vitro protein digestibility and allergenicity of shrimp (*Litopenaeus vannamei*) proteins. *Food Chem*, *337*, 127811. <https://doi.org/10.1016/j.foodchem.2020.127811>

- Du, C. M., Sun, Y., & Zhuang, X. (2008). The effects of gas composition on active species and byproducts formation in gas–water gliding arc discharge. *Plasma Chemistry and Plasma Processing*, 28(4), 523-533.
- Ehlbeck, J., Schnabel, U., Polak, M., Winter, J., Von Woedtke, T., Brandenburg, R., . . . Weltmann, K. (2010). Low temperature atmospheric pressure plasma sources for microbial decontamination. *Journal of Physics D: Applied Physics*, 44(1), 013002.
- Eisenberg, G. (1943). Colorimetric determination of hydrogen peroxide. *Industrial & Engineering Chemistry Analytical Edition*, 15(5), 327-328.
- Ekezie, F.-G., Sun, D.-W., & Cheng, J.-H. (2017). A review on recent advances in cold plasma technology for the food industry: Current applications and future trends. *Trends in Food Science & Technology*, 69(Part A), 46-58. <https://doi.org/10.1016/j.tifs.2017.08.007>
- Elez Garofulić, I., Režek Jambrak, A., Milošević, S., Dragović-Uzelac, V., Zorić, Z., & Herceg, Z. (2015). The effect of gas phase plasma treatment on the anthocyanin and phenolic acid content of sour cherry Marasca (*Prunus cerasus* var. Marasca) juice. *LWT - Food Science and Technology*, 62(1, Part 2), 894-900. <https://doi.org/10.1016/j.lwt.2014.08.036>
- Ellman, G. L. (1959). Tissue sulfhydryl groups. *Archives of biochemistry and biophysics*, 82(1), 70-77.
- Ercan, U. K., Wang, H., Ji, H., Fridman, G., Brooks, A. D., & Joshi, S. G. (2013). Nonequilibrium plasma-activated antimicrobial solutions are broad-spectrum and retain their efficacies for extended period of time. *Plasma Processes and Polymers*, 10(6), 544-555.
- FDA. (2008). *Guidance for Industry: Guide to Minimize Microbial Food Safety Hazards of Fresh-cut Fruits and Vegetables*.
- Feng, X., Li, C., Ullah, N., Cao, J., Lan, Y., Ge, W., . . . Chen, L. (2015). Susceptibility of whey protein isolate to oxidation and changes in physicochemical, structural, and digestibility characteristics. *Journal of dairy science*, 98(11), 7602-7613.
- Feng, Y., Wang, J., Hu, H., & Yang, C. (2022). Effect of oxidative modification by reactive oxygen species (ROS) on the aggregation of whey protein concentrate (WPC). *Food Hydrocolloids*, 123, 107189. <https://doi.org/10.1016/j.foodhyd.2021.107189>
- Fich, E. A., Segerson, N. A., & Rose, J. K. (2016). The Plant Polyester Cutin: Biosynthesis, Structure, and Biological Roles. *Annu Rev Plant Biol*, 67, 207-233. <https://doi.org/10.1146/annurev-arplant-043015-111929>
- Flores-Fuentes, A., Pena-Eguiluz, R., Lopez-Callejas, R., Mercado-Cabrera, A., Valencia-Alvarado, R., Barocio-Delgado, S., & Piedad-Beneitez, A. d. l. (2009). Electrical model of an atmospheric pressure dielectric barrier discharge cell. *Ieee Transactions on Plasma Science*, 37(1), 128-134. <https://doi.org/10.1109/TPS.2008.2006844>
- Frías, E., Iglesias, Y., Alvarez-Ordóñez, A., Prieto, M., González-Raurich, M., & López, M. (2020). Evaluation of cold atmospheric pressure plasma (CAPP) and plasma-activated water (PAW) as alternative non-thermal decontamination technologies for tofu: Impact on microbiological, sensorial and functional quality attributes. *Food Research International*, 129, 108859.
- Gadkari, S., & Gu, S. (2017). Numerical investigation of co-axial DBD: Influence of relative permittivity of the dielectric barrier, applied voltage amplitude, and frequency. *Physics of Plasmas*, 24(5), 053517. <https://doi.org/10.1063/1.4982657>
- Gavahian, M., & Khaneghah, A. M. (2020). Cold plasma as a tool for the elimination of food contaminants: Recent advances and future trends. *Critical reviews in food science nutrition*, 60(9), 1581-1592.

- Glowacz, M., & Rees, D. (2016). The practicality of using ozone with fruit and vegetables. *Journal of the Science of Food and Agriculture*, 96(14), 4637-4643. <https://doi.org/10.1002/jsfa.7763>
- Gökkaya Erdem, B., Dıblan, S., & Kaya, S. (2019). Development and structural assessment of whey protein isolate/sunflower seed oil biocomposite film. *Food and Bioproducts Processing*, 118, 270-280. <https://doi.org/10.1016/j.fbp.2019.09.015>
- Gombas, D., Luo, Y., Brennan, J., Shergill, G., Petran, R., Walsh, R., . . . Deng, K. (2017). Guidelines to validate control of cross-contamination during washing of fresh-cut leafy vegetables. *Journal of Food Protection*, 80(2), 312-330. <https://doi.org/10.4315/0362-028x.Jfp-16-258>
- Gorbanev, Y., O'Connell, D., & Chechik, V. (2016). Non-thermal plasma in contact with water: the origin of species. *Chemistry—A European Journal*, 22(10), 3496-3505.
- Grzegorzewski, F. (2011). Influence of non-thermal plasma species on the structure and functionality of isolated and plant-based 1, 4-benzopyrone derivatives and phenolic acids. Technische Universität Berlin.
- Grzegorzewski, F., Ehlbeck, J., Schlüter, O., Kroh, L. W., & Rohn, S. (2011). Treating lamb's lettuce with a cold plasma—Influence of atmospheric pressure Ar plasma immanent species on the phenolic profile of *Valerianella locusta*. *LWT-Food Science and Technology*, 44(10), 2285-2289.
- Gu, Y., Shi, W., Liu, R., Xing, Y., Yu, X., & Jiang, H. (2021). Cold plasma enzyme inactivation on dielectric properties and freshness quality in bananas. *Innovative Food Science & Emerging Technologies*, 69, 102649. <https://doi.org/10.1016/j.ifset.2021.102649>
- Guo, J., Huang, K., Wang, X., Lyu, C., Yang, N., Li, Y., & Wang, J. (2017). Inactivation of yeast on grapes by plasma-activated water and its effects on quality attributes. *Journal of food protection*, 80(2), 225-230. <https://doi.org/10.4315/0362-028x.Jfp-16-116>
- Guo, J., Qin, D., Li, W., Wu, F., Li, L., & Liu, X. (2021a). Inactivation of *Penicillium italicum* on kumquat via plasma-activated water and its effects on quality attributes. *Int J Food Microbiol*, 343, 109090. <https://doi.org/10.1016/j.ijfoodmicro.2021.109090>
- Guo, L., Xu, R., Gou, L., Liu, Z., Zhao, Y., Liu, D., . . . Kong, M. G. (2018). Mechanism of virus inactivation by cold atmospheric-pressure plasma and plasma-activated water. *Applied and Environmental Microbiology*, AEM. 00726-00718.
- Guo, L., Yao, Z., Yang, L., Zhang, H., Qi, Y., Gou, L., . . . Kong, M. G. (2021b). Plasma-activated water: An alternative disinfectant for S protein inactivation to prevent SARS-CoV-2 infection. *Chem Eng J*, 421, 127742. <https://doi.org/10.1016/j.cej.2020.127742>
- Guo, Y., Zhan, J., Yu, G., & Wang, Y. (2021c). Evaluation of the concentration and contribution of superoxide radical for micropollutant abatement during ozonation. *Water Research*, 194, 116927. <https://doi.org/10.1016/j.watres.2021.116927>
- Gupta, S., & Bluhm, H. (2007). Pulsed underwater corona discharges as a source of strong oxidants: •OH and H₂O₂. *Water science and technology*, 55(12), 7-12.
- Gurol, C., Ekinici, F. Y., Aslan, N., & Korachi, M. (2012). Low temperature plasma for decontamination of *E. coli* in milk. *International Journal of Food Microbiology*, 157(1), 1-5. <https://doi.org/10.1016/j.ijfoodmicro.2012.02.016>
- Hama, T., Seki, K., Ishibashi, A., Miyazaki, A., Kouchi, A., Watanabe, N., . . . Hasegawa, T. (2019). Probing the molecular structure and orientation of the leaf surface of brassica oleracea l. by polarization modulation-infrared reflection-absorption spectroscopy. *Plant Cell Physiol*, 60(7), 1567-1580. <https://doi.org/10.1093/pcp/pcz063>

- Hamdan, A., Liu, J.-L., & Cha, M. S. (2018). Microwave plasma jet in water: characterization and feasibility to wastewater treatment. *Plasma Chemistry and Plasma Processing*, 38(5), 1003-1020. <https://doi.org/10.1007/s11090-018-9918-y>
- Han, Y., Cheng, J.-H., & Sun, D.-W. (2019). Activities and conformation changes of food enzymes induced by cold plasma: A review. *Critical Reviews in Food Science and Nutrition*, 59(5), 794-811. <https://doi.org/10.1080/10408398.2018.1555131>
- Harris, A. F., Lacombe, J., Liyanage, S., Han, M. Y., Wallace, E., Karsunky, S., . . . Zenhausem, F. (2021). Supercritical carbon dioxide decellularization of plant material to generate 3D biocompatible scaffolds. *Scientific Reports*, 11(1), 3643. <https://doi.org/10.1038/s41598-021-83250-9>
- Hellwig, M. (2019). The chemistry of protein oxidation in food. *Angew Chem Int Ed Engl*, 58(47), 16742-16763. <https://doi.org/10.1002/anie.201814144>
- Herceg, Z., Kovačević, D. B., Kljusurić, J. G., Jambrak, A. R., Zorić, Z., & Dragović-Uzelac, V. (2016). Gas phase plasma impact on phenolic compounds in pomegranate juice. *Food Chemistry*, 190(Supplement C), 665-672. <https://doi.org/10.1016/j.foodchem.2015.05.135>
- Heredia-Guerrero, J. A., Benítez, J. J., Domínguez, E., Bayer, I. S., Cingolani, R., Athanassiou, A., & Heredia, A. (2014). Infrared and Raman spectroscopic features of plant cuticles: a review. *Frontiers in plant science*, 5(305). <https://doi.org/10.3389/fpls.2014.00305>
- Herianto, S., Hou, C.-Y., Lin, C.-M., & Chen, H.-L. (2021a). Nonthermal plasma-activated water: A comprehensive review of this new tool for enhanced food safety and quality. *Comprehensive Reviews in Food Science and Food Safety*, 20(1), 583-626. <https://doi.org/10.1111/1541-4337.12667>
- Hosseinpour, M., Zendehtnam, A., Hamidi Sangdehi, S. M., & Ghomi Marzdashti, H. (2019). Effects of different gas flow rates and non-perpendicular incidence angles of argon cold atmospheric-pressure plasma jet on silver thin film treatment. *Journal of Theoretical and Applied Physics*, 13(4), 329-349. <https://doi.org/10.1007/s40094-019-00351-7>
- Ikawa, S., Kitano, K., & Hamaguchi, S. (2010). Effects of pH on bacterial inactivation in aqueous solutions due to low-temperature atmospheric pressure plasma application. *Plasma Processes and Polymers*, 7(1), 33-42.
- Illera, A., Chaple, S., Sanz, M., Ng, S., Lu, P., Jones, J., . . . Bourke, P. J. F. c. X. (2019). Effect of cold plasma on polyphenol oxidase inactivation in cloudy apple juice and on the quality parameters of the juice during storage. *Food Chemistry: X*, 3, 100049.
- Jampala, S. N., Manolache, S., Gunasekaran, S., & Denes, F. S. (2005). Plasma-enhanced modification of xanthan gum and its effect on rheological properties. *Journal of agricultural and food chemistry*, 53(9), 3618-3625.
- Ji, H., Dong, S., Han, F., Li, Y., Chen, G., Li, L., & Chen, Y. (2018). Effects of dielectric barrier discharge (DBD) cold plasma treatment on physicochemical and functional properties of peanut protein. *Food and Bioprocess Technology*, 11(2), 344-354. <https://doi.org/10.1007/s11947-017-2015-z>
- Ji, H., Han, F., Peng, S., Yu, J., Li, L., Liu, Y., . . . Chen, Y. (2019). Behavioral solubilization of peanut protein isolate by atmospheric pressure cold plasma (ACP) treatment. *Food and Bioprocess Technology*, 12(12), 2018-2027. <https://doi.org/10.1007/s11947-019-02357-0>
- Jiang, J., Tan, Z., Shan, C., Pan, J., Pan, G., Liu, Y., . . . Wang, X. (2016). A new study on the penetration of reactive species in their mass transfer processes in water by increasing the electron energy in plasmas. *Physics of Plasmas*, 23(10), 103503.

- Jiang, N., Yang, J., He, F., & Cao, Z. (2011). Interplay of discharge and gas flow in atmospheric pressure plasma jets. *Journal of Applied Physics*, *109*(9), 093305.
- Jiang, Y.-H., Cheng, J.-H., & Sun, D.-W. (2020). Effects of plasma chemistry on the interfacial performance of protein and polysaccharide in emulsion. *Trends in Food Science & Technology*, *98*, 129-139. <https://doi.org/10.1016/j.tifs.2020.02.009>
- Joshi, I., Salvi, D., Schaffner, D. W., & Karwe, M. V. (2018). Characterization of microbial inactivation using plasma-activated water and plasma-activated acidified buffer. *Journal of Food Protection*, *81*(9), 1472-1480. <https://doi.org/10.4315/0362-028x.Jfp-17-487>
- Joshi, S. G., Cooper, M., Yost, A., Paff, M., Ercan, U. K., Fridman, G., . . . Brooks, A. D. (2011). Non-thermal dielectric-barrier discharge (DBD) Plasma-induced inactivation involves oxidative-DNA damage and membrane lipid peroxidation in *Escherichia coli*. *Antimicrobial agents and chemotherapy*. *55*(3), 1053–1062. <https://doi.org/10.1128/AAC.01002-10>
- Julák, J., Hujacová, A., Scholtz, V., Khun, J., & Holada, K. (2018a). Contribution to the chemistry of plasma-activated water. *Plasma Physics Reports*, *44*(1), 125-136.
- Julák, J., Soušková, H., Scholtz, V., Kvasničková, E., Savická, D., & Kříha, V. (2018b). Comparison of fungicidal properties of non-thermal plasma produced by corona discharge and dielectric barrier discharge. *Folia Microbiologica*, *63*(1), 63-68. <https://doi.org/10.1007/s12223-017-0535-6>
- Jun-Seok, O., Endre, J. S., Kotaro, O., Robert, D. S., Masafumi, I., Hiroshi, F., & Akimitsu, H. (2018). UV–vis spectroscopy study of plasma-activated water: Dependence of the chemical composition on plasma exposure time and treatment distance. *Japanese Journal of Applied Physics*, *57*(1), 102-109.
- Jung, S., Kim, H. J., Park, S., In Yong, H., Choe, J. H., Jeon, H.-J., . . . Jo, C. (2015a). The use of atmospheric pressure plasma-treated water as a source of nitrite for emulsion-type sausage. *Meat Science*, *108*, 132-137. <https://doi.org/10.1016/j.meatsci.2015.06.009>
- Jung, S., Kim, H. J., Park, S., Yong, H. I., Choe, J. H., Jeon, H.-J., . . . Jo, C. (2015b). Color developing capacity of plasma-treated water as a source of nitrite for meat curing. *Korean journal for food science of animal resources*, *35*(5), 703.
- Kamgang-Youbi, G., Herry, J., Meylheuc, T., Brisset, J., Bellon-Fontaine, M., Doubla, A., & Naitali, M. (2009). Microbial inactivation using plasma-activated water obtained by gliding electric discharges 48(13). *Letters in Applied Microbiology*, *49*(2), 292-292.
- Kaushik, N. K., Ghimire, B., Li, Y., Adhikari, M., Veerana, M., Kaushik, N., . . . Masur, K. (2018). Biological and medical applications of plasma-activated media, water and solutions. *Biological chemistry*, *400*(1), 39-62.
- Kim, H.-J., Sung, N.-Y., Yong, H. I., Kim, H., Lim, Y., Ko, K. H., . . . Jo, C. (2016). Mutagenicity and immune toxicity of emulsion-type sausage cured with plasma-treated water. *Korean journal for food science of animal resources*, *36*(4), 494-498. <https://doi.org/10.5851/kosfa.2016.36.4.494>
- Kim, H.-J., Yong, H. I., Park, S., Kim, K., Choe, W., & Jo, C. (2015). Microbial safety and quality attributes of milk following treatment with atmospheric pressure encapsulated dielectric barrier discharge plasma. *Food Control*, *47*, 451-456. <https://doi.org/10.1016/j.foodcont.2014.07.053>
- Kogelschatz, U. (2003). Dielectric-Barrier Discharges: Their history, discharge physics, and industrial applications . *Plasma Chemistry and Plasma Processing*, *23*(1), 1-46. <https://doi.org/10.1023/a:1022470901385>
- Korachi, M., & Aslan, N. (2011). The effect of atmospheric pressure plasma corona discharge on pH, lipid content and DNA of bacterial cells. *Plasma Science and Technology*, *13*(1), 99.

- Krohmann, U., Ehlbeck, J., Neumann, T., Schnabel, U., Andrasch, M., Lehmann, W., & Weltmann, K.-D. (2018). Plasma-generated gas sterilization method and device. In: Google Patents.
- Laemmli, U. K. (1970). Cleavage of structural proteins during the assembly of the head of bacteriophage T4. *Nature*, 227(5259), 680-685. <https://doi.org/10.1038/227680a0>
- Laroussi, M. (2002). Nonthermal decontamination of biological media by atmospheric-pressure plasmas: review, analysis, and prospects. *Ieee Transactions on Plasma Science*, 30(4), 1409-1415. <https://doi.org/10.1109/TPS.2002.804220>
- Laurita, R., Barbieri, D., Gherardi, M., Colombo, V., & Lukes, P. (2015). Chemical analysis of reactive species and antimicrobial activity of water treated by nanosecond pulsed DBD air plasma. *Clinical Plasma Medicine*, 3(2), 53-61. <https://doi.org/10.1016/j.cpme.2015.10.001>
- Laurita, R., Gozzi, G., Tappi, S., Capelli, F., Bisag, A., Laghi, G., . . . Vittori, S. (2021). Effect of plasma activated water (PAW) on rocket leaves decontamination and nutritional value. *Innovative Food Science Emerging Technologies*, 73, 102805.
- Leduc, M., Guay, D., Coulombe, S., & Leask, R. L. (2010). Effects of Non-thermal Plasmas on DNA and Mammalian Cells. *Plasma Processes and Polymers*, 7(11), 899-909. doi:10.1002/ppap.201000032
- Lee, W.-N., Huang, C.-H., & Zhu, G. (2018). Analysis of 40 conventional and emerging disinfection by-products in fresh-cut produce wash water by modified EPA methods. *Food Chemistry*, 256, 319-326. <https://doi.org/10.1016/j.foodchem.2018.02.134>
- Li, C., Xiong, Y. L., & Chen, J. (2012). Oxidation-induced unfolding facilitates Myosin cross-linking in myofibrillar protein by microbial transglutaminase. *J Agric Food Chem*, 60(32), 8020-8027. <https://doi.org/10.1021/jf302150h>
- Li, C., Yang, F., Huang, Y., Huang, C., Zhang, K., & Yan, L. (2020). Comparison of hydrodynamic and ultrasonic cavitation effects on soy protein isolate functionality. *Journal of Food Engineering*, 265, 109697.
- Li, X., Li, M., Ji, N., Jin, P., Zhang, J., Zheng, Y., . . . Li, F. (2019). Cold plasma treatment induces phenolic accumulation and enhances antioxidant activity in fresh-cut pitaya (*Hylocereus undatus*) fruit. *LWT*, 115, 108447. <https://doi.org/10.1016/j.lwt.2019.108447>
- Liao, L. B., Chen, W. M., & Xiao, X. M. (2007). The generation and inactivation mechanism of oxidation–reduction potential of electrolyzed oxidizing water. *Journal of Food Engineering*, 78(4), 1326-1332. <https://doi.org/10.1016/j.jfoodeng.2006.01.004>
- Liao, X., Li, J., Muhammad, A. I., Suo, Y., Chen, S., Ye, X., . . . Ding, T. (2018a). Application of a dielectric barrier discharge atmospheric cold plasma (DBD-ACP) for *Escherichia coli* inactivation in apple juice. *Journal of Food Science*, 83(2), 401-408.
- Liao, X., Liu, D., Xiang, Q., Ahn, J., Chen, S., Ye, X., & Ding, T. (2017). Inactivation mechanisms of non-thermal plasma on microbes: A review. *Food Control*, 75, 83-91. <https://doi.org/10.1016/j.foodcont.2016.12.021>
- Liao, X., Su, Y., Liu, D., Chen, S., Hu, Y., Ye, X., . . . Ding, T. (2018b). Application of atmospheric cold plasma-activated water (PAW) ice for preservation of shrimps (*Metapenaeus ensis*). *Food Control*, 94, 307-314. <https://doi.org/10.1016/j.foodcont.2018.07.026>
- Liao, X., Xiang, Q., Cullen, P. J., Su, Y., Chen, S., Ye, X., . . . Ding, T. (2020). Plasma-activated water (PAW) and slightly acidic electrolyzed water (SAEW) as beef thawing media for enhancing microbiological safety. *LWT*, 117, 108649.
- Liu, C., Chen, C., Jiang, A., Sun, X., Guan, Q., & Hu, W. (2020). Effects of plasma-activated water on microbial growth and storage quality of fresh-cut apple. *Innovative Food Science & Emerging Technologies*, 59, 102256. <https://doi.org/10.1016/j.ifset.2019.102256>

- Liu, C., Chen, C., Zhang, Y., Jiang, A., & Hu, W. (2021). Aqueous ozone treatment inhibited degradation of cellwall polysaccharides in fresh-cut apple during cold storage. *Innovative Food Science & Emerging Technologies*, 67, 102550. <https://doi.org/10.1016/j.ifset.2020.102550>
- Liu, D., Liu, Z., Chen, C., Yang, A., Li, D., Rong, M., . . . Kong, M. (2016). Aqueous reactive species induced by a surface air discharge: Heterogeneous mass transfer and liquid chemistry pathways. *Scientific Reports*, 6, 23737.
- Liu, F., Sun, P., Bai, N., Tian, Y., Zhou, H., Wei, S., . . . Fang, J. (2010). Inactivation of bacteria in an aqueous environment by a direct-current, cold-atmospheric-pressure air plasma microjet. *Plasma Processes and Polymers*, 7(3-4), 231-236. <https://doi.org/doi:10.1002/ppap.200900070>
- Locke, B., Sato, M., Sunka, P., Hoffmann, M., & Chang, J.-S. (2006). Electrohydraulic discharge and nonthermal plasma for water treatment. *Industrial & engineering chemistry research*, 45(3), 882-905.
- Lu, L., Ku, K. M., Palma-Salgado, S. P., Storm, A. P., Feng, H., Juvik, J. A., & Nguyen, T. H. (2015). Influence of epicuticular physicochemical properties on porcine rotavirus adsorption to 24 leafy green vegetables and tomatoes. *Plos One*, 10(7), e0132841. <https://doi.org/10.1371/journal.pone.0132841>
- Lu, P., Boehm, D., Bourke, P., & Cullen, P. J. (2017). Achieving reactive species specificity within plasma-activated water through selective generation using air spark and glow discharges. *Plasma Processes and Polymers*, 14(8), 1600207. <https://doi.org/https://doi.org/10.1002/ppap.201600207>
- Lu, P., Cullen, P. J., & Ostrikov, K. (2016b). Atmospheric pressure nonthermal plasma sources. In N. N. Misra, O. Schlüter, & P. J. Cullen (Eds.), *Cold Plasma in Food and Agriculture* (pp. 83-116). Academic Press. <https://doi.org/https://doi.org/10.1016/B978-0-12-801365-6.00004-4>
- Lukes, P., Dolezalova, E., Sisrova, I., & Clupek, M. (2014). Aqueous-phase chemistry and bactericidal effects from an air discharge plasma in contact with water: evidence for the formation of peroxyxynitrite through a pseudo-second-order post-discharge reaction of H₂O₂ and HNO₂. *Plasma Sources Science and Technology*, 23(1), 015019. <https://doi.org/10.1088/0963-0252/23/1/015019>
- Lukes, P., Locke, B. R., & Brisset, J. L. (2012). Aqueous-phase chemistry of electrical discharge plasma in water and in gas-liquid environments. *Plasma Chemistry and Catalysis in Gases and Liquids*, 243-308.
- Lynch, M. F., Tauxe, R. V., & Hedberg, C. W. (2009). The growing burden of foodborne outbreaks due to contaminated fresh produce: risks and opportunities. *Epidemiology and Infection*, 137(3), 307-315. <https://doi.org/10.1017/S0950268808001969>
- Ma, R., Feng, H., Liang, Y., Zhang, Q., Tian, Y., Su, B., . . . Fang, J. (2013). An atmospheric-pressure cold plasma leads to apoptosis in *Saccharomyces cerevisiae* by accumulating intracellular reactive oxygen species and calcium. *Journal of Physics D: Applied Physics*, 46(28), 285401.
- Ma, R., Wang, G., Tian, Y., Wang, K., Zhang, J., & Fang, J. (2015). Non-thermal plasma-activated water inactivation of food-borne pathogen on fresh produce. *Journal of Hazardous Materials*, 300, 643-651. <https://doi.org/10.1016/j.jhazmat.2015.07.061>
- Ma, R., Yu, S., Tian, Y., Wang, K., Sun, C., Li, X., . . . Fang, J. (2016). Effect of non-thermal plasma-activated water on fruit decay and quality in postharvest Chinese bayberries. *Food and Bioprocess Technology*, 9(11), 1825-1834.
- Machado-Moreira, B., Richards, K., Brennan, F., Abram, F., & Burgess, C. M. (2019). Microbial contamination of fresh produce: what, where, and how? *Comprehensive reviews in food science and food safety*, 18(6), 1727-1750. <https://doi.org/10.1111/1541-4337.12487>

- Machala, Z., Tarabová, B., Sersenová, D., Janda, M., & Hensel, K. (2018). Chemical and antibacterial effects of plasma activated water: correlation with gaseous and aqueous reactive oxygen and nitrogen species, plasma sources and air flow conditions. *Journal of Physics D: Applied Physics*, *52*(3), 034002.
- Maguire, P., Mahony, C., Kelsey, C., Bingham, A., Montgomery, E., Bennet, E., . . . Diver, D. (2015). Controlled microdroplet transport in an atmospheric pressure microplasma. *Applied Physics Letters*, *106*(22), 224101.
- Magureanu, M., Mandache, N. B., & Parvulescu, V. I. (2015). Degradation of pharmaceutical compounds in water by non-thermal plasma treatment. *Water Research*, *81*, 124-136. <https://doi.org/10.1016/j.watres.2015.05.037>
- Marković, M., Jović, M., Stanković, D., Kovačević, V., Roglič, G., Gojgić-Cvijović, G., & Manojlović, D. (2015). Application of non-thermal plasma reactor and Fenton reaction for degradation of ibuprofen. *Science of The Total Environment*, *505*, 1148-1155. <https://doi.org/10.1016/j.scitotenv.2014.11.017>
- Matthew, J. T., Matthew, J. P., Sharmin, K., Pritha, H., Yukinori, S., Douglas, S. C., & David, B. G. (2011). Long-term antibacterial efficacy of air plasma-activated water. *Journal of Physics D: Applied Physics*, *44*(47), 472001.
- Mendes, R., Cardoso, C., & Pestana, C. (2009). Measurement of malondialdehyde in fish: A comparison study between HPLC methods and the traditional spectrophotometric test. *Food Chemistry*, *112*(4), 1038-1045.
- Meng, X., Zhang, M., Zhan, Z., & Adhikari, B. (2014). Changes in quality characteristics of fresh-cut cucumbers as affected by pressurized argon treatment. *Food and Bioprocess Technology*, *7*(3), 693-701. <https://doi.org/10.1007/s11947-013-1092-x>
- Meng, Y., Liang, Z., Zhang, C., Hao, S., Han, H., Du, P., . . . Liu, L. (2021). Ultrasonic modification of whey protein isolate: Implications for the structural and functional properties. *LWT*, *152*, 112272. <https://doi.org/10.1016/j.lwt.2021.112272>
- Misra, N., & Jo, C. (2017). Applications of cold plasma technology for microbiological safety in meat industry. *Trends in Food Science & Technology*, *64*, 74-86.
- Misra, N., Pankaj, S., Walsh, T., O'Regan, F., Bourke, P., & Cullen, P. (2014a). In-package nonthermal plasma degradation of pesticides on fresh produce. *Journal of Hazardous Materials*, *271*, 33-40.
- Misra, N., Patil, S., Moiseev, T., Bourke, P., Mosnier, J., Keener, K., & Cullen, P. (2014b). In-package atmospheric pressure cold plasma treatment of strawberries. *Journal of Food Engineering*, *125*, 131-138.
- Misra, N., Schlüter, O., & Cullen, P. J. (2016). *Cold plasma in food and agriculture: fundamentals and applications*. Academic Press.
- Misra, N. N. (2015). The contribution of non-thermal and advanced oxidation technologies towards dissipation of pesticide residues. *Trends in Food Science & Technology*, *45*(2), 229-244. <https://doi.org/10.1016/j.tifs.2015.06.005>
- Misra, N. N., Kaur, S., Tiwari, B. K., Kaur, A., Singh, N., & Cullen, P. J. (2015). Atmospheric pressure cold plasma (ACP) treatment of wheat flour. *Food Hydrocolloids*, *44*(Supplement C), 115-121. <https://doi.org/10.1016/j.foodhyd.2014.08.019>
- Montgomery, D. C. (2017). *Design and analysis of experiments*. John Wiley & sons.
- Moreau, M., Feuilloley, M., Veron, W., Meylheuc, T., Chevalier, S., Brisset, J.-L., & Orange, N. (2007a). Gliding arc discharge in the potato pathogen *Erwinia carotovora* subsp. *atroseptica*: mechanism of

- lethal action and effect on membrane-associated molecules. *Applied and Environmental Microbiology*, 73(18), 5904-5910.
- Moreau, M., Orange, N., & Feuilletoy, M. (2008). Non-thermal plasma technologies: new tools for bio-decontamination. *Biotechnology Advances*, 26(6), 610-617.
- Murray, K., Wu, F., Shi, J., Jun Xue, S., & Warriner, K. (2017). Challenges in the microbiological food safety of fresh produce: Limitations of post-harvest washing and the need for alternative interventions. *Food Quality and Safety*, 1(4), 289-301. <https://doi.org/10.1093/fqsafe/fyx027>
- Naitali, M., Kamgang-Youbi, G., Herry, J.-M., Bellon-Fontaine, M.-N., & Brisset, J.-L. (2010). Combined effects of long-living chemical species during microbial inactivation using atmospheric plasma-treated water. *Applied and Environmental Microbiology*, 76(22), 7662-7664.
- Nehra, V., Kumar, A., & Dwivedi, H. (2008). Atmospheric non-thermal plasma sources. *International Journal of Engineering*, 2(1), 53-68.
- Neretti, G., Taglioli, M., Colonna, G., & Borghi, C. (2016). Characterization of a dielectric barrier discharge in contact with liquid and producing a plasma activated water. *Plasma Sources Science and Technology*, 26(1), 015013.
- Ng, S. W., Lu, P., Rulikowska, A., Boehm, D., O'Neill, G., & Bourke, P. (2021). The effect of atmospheric cold plasma treatment on the antigenic properties of bovine milk casein and whey proteins. *Food Chemistry*, 342, 128283. <https://doi.org/10.1016/j.foodchem.2020.128283>
- Niquet, R., Boehm, D., Schnabel, U., Cullen, P., Bourke, P., & Ehlbeck, J. (2018). Characterising the impact of post-treatment storage on chemistry and antimicrobial properties of plasma treated water derived from microwave and DBD sources. *Plasma Processes and Polymers*, 15(3), 1700127.
- Noriega, E., Shama, G., Laca, A., Diaz, M., & Kong, M. G. (2011). Cold atmospheric gas plasma disinfection of chicken meat and chicken skin contaminated with *Listeria innocua*. *Food Microbiol*, 28(7), 1293-1300. <https://doi.org/10.1016/j.fm.2011.05.007>
- Oehmigen, K., Hähnel, M., Brandenburg, R., Wilke, C., Weltmann, K. D., & von Woedtke, T. (2010). The role of acidification for antimicrobial activity of atmospheric pressure plasma in liquids. *Plasma Processes and Polymers*, 7(3-4), 250-257. <https://doi.org/10.1002/ppap.200900077>
- Oehmigen, K., Hoder, T., Wilke, C., Brandenburg, R., Hahnel, M., Weltmann, K.-D., & von Woedtke, T. (2011a). Volume effects of atmospheric-pressure plasma in liquids. *Ieee Transactions on Plasma Science*, 39(11), 2646-2647.
- Oehmigen, K., Winter, J., Hähnel, M., Wilke, C., Brandenburg, R., Weltmann, K. D., & von Woedtke, T. (2011b). Estimation of possible mechanisms of *Escherichia coli* inactivation by plasma treated sodium chloride solution. *Plasma Processes and Polymers*, 8(10), 904-913.
- Organization, W. H. (2015). WHO estimates of the global burden of foodborne diseases: foodborne disease burden epidemiology reference group 2007-2015.
- Ozen, E., & Singh, R. (2020). Atmospheric cold plasma treatment of fruit juices: A review. *Trends in Food Science Technology*.
- Pan, J., Li, Y., Liu, C., Tian, Y., Yu, S., Wang, K., . . . Fang, J. (2017). Investigation of cold atmospheric plasma-activated water for the dental unit waterline system contamination and safety evaluation in vitro. *Plasma Chemistry and Plasma Processing*, 37(4), 1091-1103.
- Pan, J., Sun, K., Liang, Y., Sun, P., Yang, X., Wang, J., . . . Becker, K. H. (2013). Cold plasma therapy of a tooth root canal infected with *Enterococcus faecalis* biofilms in vitro. *Journal of Endodontics*, 39(1), 105-110. <https://doi.org/10.1016/j.joen.2012.08.017>

- Pankaj, S., Misra, N., & Cullen, P. (2013). Kinetics of tomato peroxidase inactivation by atmospheric pressure cold plasma based on dielectric barrier discharge. *Innovative Food Science Emerging Technologies*, *19*, 153-157.
- Pankaj, S. K., Bueno-Ferrer, C., Misra, N., Milosavljević, V., O'donnell, C., Bourke, P., . . . Cullen, P. (2014). Applications of cold plasma technology in food packaging. *Trends in Food Science & Technology*, *35*(1), 5-17.
- Pankaj, S. K., & Keener, K. M. (2017). Cold plasma: background, applications and current trends. *Current Opinion in Food Science*, *16*, 49-52. <https://doi.org/10.1016/j.cofs.2017.07.008>
- Pankaj, S. K., Wan, Z., Colonna, W., & Keener, K. M. (2017). Effect of high voltage atmospheric cold plasma on white grape juice quality. *Journal of the Science of Food and Agriculture*, *97*(12), 4016-4021. <https://doi.org/10.1002/jsfa.8268>
- Pankaj, S. K., Wan, Z., & Keener, K. M. (2018). Effects of cold plasma on food quality: A review. *Foods*, *7*(1), 4.
- Park, D. P., Davis, K., Gilani, S., Alonzo, C.-A., Dobrynin, D., Friedman, G., . . . Fridman, G. (2013). Reactive nitrogen species produced in water by non-equilibrium plasma increase plant growth rate and nutritional yield. *Current Applied Physics*, *13*, S19-S29.
- Patange, A., Boehm, D., Bueno-Ferrer, C., Cullen, P., & Bourke, P. (2017). Controlling Brochothrix thermosphacta as a spoilage risk using in-package atmospheric cold plasma. *Food Microbiology*, *66*, 48-54.
- Patange, A., Lu, P., Boehm, D., Cullen, P. J., & Bourke, P. (2019). Efficacy of cold plasma functionalised water for improving microbiological safety of fresh produce and wash water recycling. *Food Microbiol*, *84*, 103226. <https://doi.org/10.1016/j.fm.2019.05.010>
- Pathan, A. K., Bond, J., & Gaskin, R. E. (2010). Sample preparation for SEM of plant surfaces. *Materials Today*, *12*, 32-43. [https://doi.org/10.1016/S1369-7021\(10\)70143-7](https://doi.org/10.1016/S1369-7021(10)70143-7)
- Patil, S., Bourke, P., & Cullen, P. (2016). Principles of Nonthermal Plasma Decontamination. In *Cold plasma in food and agriculture* (pp. 143-177). Elsevier.
- Pavlovich, M. J., Chang, H.-W., Sakiyama, Y., Clark, D. S., & Graves, D. B. (2013). Ozone correlates with antibacterial effects from indirect air dielectric barrier discharge treatment of water. *Journal of Physics D: Applied Physics*, *46*(14), 145202.
- Phaephiphat, A., Mahakarnchanakul, W., & Yildiz, F. (2018). Surface decontamination of Salmonella, Typhimurium and Escherichia coli on sweet basil by ozone microbubbles. *Cogent Food & Agriculture*, *4*(1), 1558496. <https://doi.org/10.1080/23311932.2018.1558496>
- Pipa, A. V., Koskulics, J., Brandenburg, R., & Hoder, T. (2012). The simplest equivalent circuit of a pulsed dielectric barrier discharge and the determination of the gas gap charge transfer. *Review of Scientific Instruments*, *83*(11), 115112. <https://doi.org/10.1063/1.4767637>
- Plimpton, S. R., Gołkowski, M., Mitchell, D. G., Austin, C., Eaton, S. S., Eaton, G. R., . . . Voskuil, M. (2013). Remote delivery of hydroxyl radicals via secondary chemistry of a nonthermal plasma effluent. *Biotechnology and Bioengineering*, *110*(7), 1936-1944. <https://doi.org/10.1002/bit.24853>
- Porat, R., Lichter, A., Terry, L. A., Harker, R., & Buzby, J. (2018). Postharvest losses of fruit and vegetables during retail and in consumers' homes: Quantifications, causes, and means of prevention. *Postharvest Biology and Technology*, *139*, 135-149.
- Qi, P. X., & Onwulata, C. I. (2011). Physical properties, molecular structures, and protein quality of texturized whey protein isolate: Effect of extrusion moisture content1. *Journal of dairy science*, *94*(5), 2231-2244. <https://doi.org/10.3168/jds.2010-3942>

- Qi, Z. H., Tian, E. Q., Song, Y., Sosnin, E. A., Skakun, V. S., Li, T. T., . . . Liu, D. P. (2018). Inactivation of *Shewanella putrefaciens* by Plasma Activated Water. *Plasma Chemistry and Plasma Processing*, 38(5), 1035-1050. <https://doi.org/10.1007/s11090-018-9911-5>
- Qian, J., Wang, Y., Zhuang, H., Yan, W., Zhang, J., & Luo, J. (2021). Plasma activated water-induced formation of compact chicken myofibrillar protein gel structures with intrinsically antibacterial activity. *Food Chemistry*, 351, 129278. <https://doi.org/10.1016/j.foodchem.2021.129278>
- Ramazzina, I., Berardinelli, A., Rizzi, F., Tappi, S., Ragni, L., Sacchetti, G., & Rocculi, P. (2015). Effect of cold plasma treatment on physico-chemical parameters and antioxidant activity of minimally processed kiwifruit. *Postharvest Biology and Technology*, 107, 55-65. <https://doi.org/10.1016/j.postharvbio.2015.04.008>
- Rathod, N. B., Kahar, S. P., Ranveer, R. C., & Annapure, U. S. (2021). Cold plasma an emerging nonthermal technology for milk and milk products: A review. *International Journal of Dairy Technology*.
- Rivero Pena, W. C. (2020). Effect of plasma-activated liquids on the growth, quality, and microbiological safety of fresh produce. *North Carolina State University*.
- Rodríguez-López, P., Rodríguez-Herrera, J., Vázquez-Sánchez, D., & Lopez Cabo, M. (2018). Current knowledge on *Listeria monocytogenes* biofilms in food-related environments: Incidence, resistance to biocides, ecology and biocontrol. *Foods*, 7(6), 85.
- Rodriguez, C., Wandell, R. J., Zhang, Z., Neurohr, J. M., Tang, Y., Rhodes, R., . . . Locke, B. R. (2020). *Escherichia coli* survival in plasma-treated water and in a gas-liquid plasma reactor. *Plasma Processes and Polymers*, 17(12), 2000099. <https://doi.org/10.1002/ppap.202000099>
- Royintarat, T., Seesuriyachan, P., Boonyawan, D., Choi, E. H., & Wattanuchariya, W. (2019). Mechanism and optimization of non-thermal plasma-activated water for bacterial inactivation by underwater plasma jet and delivery of reactive species underwater by cylindrical DBD plasma. *Current Applied Physics*, 19(9), 1006-1014.
- Rumbach, P., Bartels, D. M., Sankaran, R. M., & Go, D. B. (2015). The effect of air on solvated electron chemistry at a plasma/liquid interface. *Journal of Physics D: Applied Physics*, 48(42), 424001.
- Sajib, S. A., Billah, M., Mahmud, S., Miah, M., Hossain, F., Omar, F. B., . . . Reza, M. A. (2020). Plasma activated water: the next generation eco-friendly stimulant for enhancing plant seed germination, vigor and increased enzyme activity, a study on black gram (*Vigna mungo* L.). *Plasma Chemistry and Plasma Processing*, 40(1), 119-143. <https://doi.org/10.1007/s11090-019-10028-3>
- Sarangapani, C., Keogh, D. R., Dunne, J., Bourke, P., & Cullen, P. (2017a). Characterisation of cold plasma treated beef and dairy lipids using spectroscopic and chromatographic methods. *Food Chemistry*, 235, 324-333.
- Sarangapani, C., Misra, Milosavljevic, V., Bourke, P., O'Regan, F., & Cullen, P. (2016a). Pesticide degradation in water using atmospheric air cold plasma. *Journal of Water Process Engineering*, 9, 225-232.
- Sarangapani, C., O'Toole, G., Cullen, P. J., & Bourke, P. (2017b). Atmospheric cold plasma dissipation efficiency of agrochemicals on blueberries. *Innovative Food Science & Emerging Technologies*, 44(Supplement C), 235-241. <https://doi.org/10.1016/j.ifset.2017.02.012>
- Sato, M., Ohgiyama, T., & Clements, J. S. (1996). Formation of chemical species and their effects on microorganisms using a pulsed high-voltage discharge in water. *Ieee Transactions on Industry Applications*, 32(1), 106-112.

- Satoh, K., MacGregor, S. J., Anderson, J. G., Woolsey, G. A., & Fouracre, R. A. (2007). Pulsed-plasma disinfection of water containing *Escherichia coli*. *Japanese Journal of Applied Physics*, *46*(3R), 1137.
- Satterfield, C. N., & Bonnell, A. (1955). Interferences in titanium sulfate method for hydrogen peroxide. *Analytical Chemistry*, *27*(7), 1174-1175.
- Scheiner, S., & Kar, T. (2010). Analysis of the reactivities of protein C-H bonds to H atom abstraction by OH radical. *J Am Chem Soc*, *132*(46), 16450-16459. <https://doi.org/10.1021/ja105204v>
- Schnabel, U., Handorf, O., Stachowiak, J., Boehm, D., Weit, C., Weihe, T., . . . Ehlbeck, J. (2021). Plasma-functionalized water: from bench to prototype for fresh-cut lettuce. *Food Engineering Reviews*, *13*(1), 115-135.
- Schnabel, U., Sydow, D., Schlüter, O., Andrasch, M., & Ehlbeck, J. (2015). Decontamination of fresh-cut iceberg lettuce and fresh mung bean sprouts by non-thermal atmospheric pressure plasma processed water (PPW). *Modern Agric. Sci. Technol*, *1*, 23-39.
- Scholtz, V., Julák, J., & Kříha, V. (2010). The microbicidal effect of low-temperature plasma generated by corona discharge: comparison of various microorganisms on an agar surface or in aqueous suspension. *Plasma Processes and Polymers*, *7*(3-4), 237-243.
- Segat, A., Misra, N., Cullen, P., & Innocente, N. (2015). Atmospheric pressure cold plasma (ACP) treatment of whey protein isolate model solution. *Innovative Food Science Emerging Technologies*, *29*, 247-254.
- Segat, A., Misra, N., Fabbro, A., Buchini, F., Lippe, G., Cullen, P. J., & Innocente, N. (2014). Effects of ozone processing on chemical, structural and functional properties of whey protein isolate. *Food Research International*, *66*, 365-372.
- Shah, U., Ranieri, P., Zhou, Y., Schauer, C. L., Miller, V., Fridman, G., & Sekhon, J. K. (2019). Effects of cold plasma treatments on spot-inoculated *Escherichia coli* O157: H7 and quality of baby kale (*Brassica oleracea*) leaves. *Innovative Food Science Emerging Technologies*, *57*, 102104.
- Sharafodin, H., & Soltanizadeh, N. (2022). Potential application of DBD Plasma Technique for modifying structural and physicochemical properties of Soy Protein Isolate. *Food Hydrocolloids*, *122*, 107077. <https://doi.org/10.1016/j.foodhyd.2021.107077>
- Sharma, S. (2020). Cold plasma treatment of dairy proteins in relation to functionality enhancement. *Trends in Food Science Technology*, *102*, 30-36.
- Shaw, P., Kumar, N., Kwak, H. S., Park, J. H., Uhm, H. S., Bogaerts, A., . . . Attri, P. (2018). Bacterial inactivation by plasma treated water enhanced by reactive nitrogen species. *Scientific Reports*, *8*(1), 11268.
- Shen, J., Tian, Y., Li, Y., Ma, R., Zhang, Q., Zhang, J., & Fang, J. (2016). Bactericidal effects against *S. aureus* and physicochemical properties of plasma activated water stored at different temperatures. *Scientific Reports*, *6*, 28505.
- Shen, J., Zhang, H., Xu, Z., Zhang, Z., Cheng, C., Ni, G., . . . Chu, P. K. (2019a). Preferential production of reactive species and bactericidal efficacy of gas-liquid plasma discharge. *Chemical Engineering Journal*, *362*, 402-412. <https://doi.org/10.1016/j.cej.2019.01.018>
- Shen, X., Zhang, M., Devahastin, S., & Guo, Z. (2019b). Effects of pressurized argon and nitrogen treatments in combination with modified atmosphere on quality characteristics of fresh-cut potatoes. *Postharvest Biology and Technology*, *149*, 159-165.
- Shi, X., Zhang, G., Wu, X., Li, Y., Ma, Y., & Shao, X. (2011). Effect of low-temperature plasma on microorganism inactivation and quality of freshly squeezed orange juice. *Ieee Transactions on Plasma Science*, *39*(7), 1591-1597. <https://doi.org/10.1109/TPS.2011.2142012>

- Shinwari, K. J., & Rao, P. S. (2021). Enzyme inactivation and its kinetics in a reduced-calorie sapodilla (Manilkara zapota L.) jam processed by thermal-assisted high hydrostatic pressure. *Food and Bioproducts Processing*, 126, 305-316. <https://doi.org/10.1016/j.fbp.2021.01.013>
- Singleton, V. L., & Rossi, J. A. (1965). Colorimetry of total phenolics with phosphomolybdic-phosphotungstic acid reagents. *American journal of Enology Viticulture*, 16(3), 144-158.
- Sivachandiran, L., & Khacef, A. (2017). Enhanced seed germination and plant growth by atmospheric pressure cold air plasma: combined effect of seed and water treatment. *RSC Advances*, 7(4), 1822-1832. <https://doi.org/10.1039/C6RA24762H>
- Smirnoff, N. (2008). *Antioxidants and reactive oxygen species in plants*. John Wiley & Sons.
- Soheila, M., Amanda, M. L., & Mark, J. K. (2020). Generation of Reactive Species in Water Film Dielectric Barrier Discharges Sustained in Argon, Helium, Air, Oxygen and Nitrogen. *Journal of Physics D: Applied Physics*. 53(43), 435206.
- Soušková, H., Scholtz, V., Julák, J., Kómmová, L., Savická, D., & Pazlarová, J. (2011). The survival of micromycetes and yeasts under the low-temperature plasma generated in electrical discharge. *Folia Microbiologica*, 56(1), 77-79. <https://doi.org/10.1007/s12223-011-0005-5>
- Sruthi, N. U., Josna, K., Pandiselvam, R., Kothakota, A., Gavahian, M., & Mousavi Khaneghah, A. (2022). Impacts of cold plasma treatment on physicochemical, functional, bioactive, textural, and sensory attributes of food: A comprehensive review. *Food Chemistry*, 368, 130809. <https://doi.org/10.1016/j.foodchem.2021.130809>
- Staehelin, J., & Hoigne, J. (1982). Decomposition of ozone in water: rate of initiation by hydroxide ions and hydrogen peroxide. *Environmental science & technology*, 16(10), 676-681. <https://doi.org/10.1021/es00104a009>
- Stoffels, E., Sakiyama, Y., & Graves, D. B. (2008). Cold atmospheric plasma: Charged species and their interactions with cells and tissues. *Ieee Transactions on Plasma Science*, 36(4 PART 2), 1441-1457. <https://doi.org/10.1109/TPS.2008.2001084>
- Su, X., Tian, Y., Zhou, H., Li, Y., Zhang, Z., Jiang, B., . . . Fang, J. (2018). Inactivation efficacy of non-thermal plasma activated solutions against Newcastle disease virus. *Applied and Environmental Microbiology*, AEM. 02836-02817.
- Sun, P., Wu, H., Bai, N., Zhou, H., Wang, R., Feng, H., . . . Fang, J. (2012). Inactivation of Bacillus subtilis spores in water by a direct-current, cold atmospheric-pressure air plasma microjet. *Plasma Processes and Polymers*, 9(2), 157-164. <https://doi.org/10.1002/ppap.201100041>
- Šunka, P. (2001). Pulse electrical discharges in water and their applications. *Physics of Plasmas*, 8(5), 2587-2594.
- Sunka, P., Babický, V., Clupek, M., Lukes, P., Simek, M., Schmidt, J., & Cernak, M. (1999). Generation of chemically active species by electrical discharges in water. *Plasma Sources Science and Technology*, 8(2), 258.
- Surowsky, B., Fischer, A., Schlueter, O., & Knorr, D. (2013). Cold plasma effects on enzyme activity in a model food system. *Innovative Food Science & Emerging Technologies*, 19(Supplement C), 146-152. <https://doi.org/10.1016/j.ifset.2013.04.002>
- Surowsky, B., Fröhling, A., Gottschalk, N., Schlüter, O., & Knorr, D. (2014). Impact of cold plasma on Citrobacter freundii in apple juice: Inactivation kinetics and mechanisms. *International Journal of Food Microbiology*, 174, 63-71. <https://doi.org/10.1016/j.ijfoodmicro.2013.12.031>
- Surowsky, B., Schluter, O., & Knorr, D. (2015). Interactions of non-thermal atmospheric pressure plasma with solid and liquid food systems: A review. *Food Engineering Reviews*, 7(2), 82-108. <https://doi.org/10.1007/s12393-014-9088-5>

- Sutariya, S., & Patel, H. (2017). Effect of hydrogen peroxide on improving the heat stability of whey protein isolate solutions. *Food Chemistry*, 223, 114-120.
- Takai, E., Kitamura, T., Kuwabara, J., Ikawa, S., Yoshizawa, S., Shiraki, K., . . . Kitano, K. (2014). Chemical modification of amino acids by atmospheric-pressure cold plasma in aqueous solution. *Journal of Physics D: Applied Physics*, 47(28), 285403.
- Takai, E., Kitano, K., Kuwabara, J., & Shiraki, K. (2012). Protein inactivation by low-temperature atmospheric pressure plasma in aqueous solution. *Plasma Processes and Polymers*, 9(1), 77-82.
- Talbot, M. J., & White, R. G. (2013). Methanol fixation of plant tissue for Scanning Electron Microscopy improves preservation of tissue morphology and dimensions. *Plant Methods*, 9(1), 36. <https://doi.org/10.1186/1746-4811-9-36>
- Tang, S., Yuan, D., Rao, Y., Zhang, J., Qu, Y., & Gu, J. (2018). Evaluation of antibiotic oxytetracycline removal in water using a gas phase dielectric barrier discharge plasma. *Journal of Environmental Management*, 226, 22-29. <https://doi.org/10.1016/j.jenvman.2018.08.022>
- Tang, Y. Z., Lu, X. P., Laroussi, M., & Dobbs, F. C. (2008). Sublethal and killing effects of atmospheric-pressure, nonthermal plasma on eukaryotic microalgae in aqueous media. *Plasma Processes and Polymers*, 5(6), 552-558.
- Tappi, S., Berardinelli, A., Ragni, L., Dalla Rosa, M., Guarnieri, A., & Rocculi, P. (2014). Atmospheric gas plasma treatment of fresh-cut apples. *Innovative Food Science & Emerging Technologies*, 21(Supplement C), 114-122. <https://doi.org/10.1016/j.ifset.2013.09.012>
- Tendero, C., Tixier, C., Tristant, P., Desmaison, J., & Leprince, P. (2006). Atmospheric pressure plasmas: A review. *Spectrochimica Acta Part B: Atomic Spectroscopy*, 61(1), 2-30. <https://doi.org/10.1016/j.sab.2005.10.003>
- Thagard, S. M., Stratton, G. R., Dai, F., Bellona, C. L., Holsen, T. M., Bohl, D. G., . . . Dickenson, E. R. (2016). Plasma-based water treatment: development of a general mechanistic model to estimate the treatability of different types of contaminants. *Journal of Physics D: Applied Physics*, 50(1), 014003.
- Thirumdas, R., Kadam, D., & Annapure, U. (2017a). Cold plasma: An alternative technology for the starch modification. *Food Biophysics*, 12(1), 129-139.
- Thirumdas, R., Kothakota, A., Annapure, U., Siliveru, K., Blundell, R., Gatt, R., & Valdramidis, V. P. (2018). Plasma activated water (PAW): Chemistry, physico-chemical properties, applications in food and agriculture. *Trends in Food Science & Technology*, 77, 21-31.
- Thirumdas, R., Sarangapani, C., & Annapure, U. S. (2015). Cold Plasma: A novel Non-Thermal Technology for Food Processing. *Food Biophysics*, 10(1), 1-11. <https://doi.org/10.1007/s11483-014-9382-z>
- Thirumdas, R., Trimukhe, A., Deshmukh, R. R., & Annapure, U. S. (2017b). Functional and rheological properties of cold plasma treated rice starch. *Carbohydrate Polymers*, 157(Supplement C), 1723-1731. <https://doi.org/10.1016/j.carbpol.2016.11.050>
- Thiyagarajan, M., Sarani, A., & Gonzales, X. (2013). Atmospheric pressure resistive barrier air plasma jet induced bacterial inactivation in aqueous environment. *Journal of Applied Physics*, 113(9), 093302.
- Thomas, M. K., Murray, R., Flockhart, L., Pintar, K., Pollari, F., Fazil, A., . . . Marshall, B. (2013). Estimates of the burden of foodborne illness in Canada for 30 specified pathogens and unspecified agents, circa 2006. *Foodborne Pathog Dis*, 10(7), 639-648.
- Tian, W., & Kushner, M. J. (2014). Atmospheric pressure dielectric barrier discharges interacting with liquid covered tissue. *Journal of Physics D: Applied Physics*, 47(16), 165201.

- Tian, Y., Guo, J., Wu, D., Wang, K., Zhang, J., & Fang, J. (2017). The potential regulatory effect of nitric oxide in plasma activated water on cell growth of *Saccharomyces cerevisiae*. *Journal of Applied Physics*, *122*(12), 123302. <https://doi.org/10.1063/1.4989501>
- Tian, Y., Ma, R., Zhang, Q., Feng, H., Liang, Y., Zhang, J., & Fang, J. (2015). Assessment of the physicochemical properties and biological effects of water activated by non-thermal plasma above and beneath the water surface. *Plasma Processes and Polymers*, *12*(5), 439-449. <https://doi.org/10.1002/ppap.201400082>
- Tolouie, H., Mohammadifar, M. A., Ghomi, H., & Hashemi, M. (2018). Cold atmospheric plasma manipulation of proteins in food systems. *Crit Rev Food Sci Nutr*, *58*(15), 2583-2597. <https://doi.org/10.1080/10408398.2017.1335689>
- Tomat, D., Balagué, C., Aquili, V., Verdini, R., & Quiberoni, A. (2018). Resistance of phages lytic to pathogenic *Escherichia coli* to sanitisers used by the food industry and in home settings. *International Journal of Food Science & Technology*, *53*(2), 533-540.
- Traylor, M. J., Pavlovich, M. J., Karim, S., Hait, P., Sakiyama, Y., Clark, D. S., & Graves, D. B. (2011). Long-term antibacterial efficacy of air plasma-activated water. *Journal of Physics D: Applied Physics*, *44*(47), 472001.
- Van Boxem, W., Van der Paal, J., Gorbanev, Y., Vanuytsel, S., Smits, E., Dewilde, S., & Bogaerts, A. (2017). Anti-cancer capacity of plasma-treated PBS: effect of chemical composition on cancer cell cytotoxicity. *Scientific Reports*, *7*(1), 16478. <https://doi.org/10.1038/s41598-017-16758-8>
- Van Gils, C., Hofmann, S., Boekema, B., Brandenburg, R., & Bruggeman, P. (2013). Mechanisms of bacterial inactivation in the liquid phase induced by a remote RF cold atmospheric pressure plasma jet. *Journal of Physics D: Applied Physics*, *46*(17), 175203.
- Vandamme, J., Nikiforov, A., De Roose, M., Leys, C., De Cooman, L., & Van Durme, J. (2016). Controlled accelerated oxidation of oleic acid using a DBD plasma: Determination of volatile oxidation compounds. *Food Research International*, *79*, 54-63. <https://doi.org/10.1016/j.foodres.2015.11.028>
- Vanga, S. K., Singh, A., Kalkan, F., Garipey, Y., Orsat, V., & Raghavan, V. (2016). Effect of thermal and high electric fields on secondary structure of peanut protein. *International Journal of Food Properties*, *19*(6), 1259-1271.
- Verlactt, C., Van Boxem, W., & Bogaerts, A. (2018). Transport and accumulation of plasma generated species in aqueous solution. *Physical Chemistry Chemical Physics*, *20*(10), 6845-6859.
- Vlad, I.-E., & Anghel, S. D. (2017). Time stability of water activated by different on-liquid atmospheric pressure plasmas. *Journal of Electrostatics*, *87*, 284-292. <https://doi.org/10.1016/j.elstat.2017.06.002>
- von Woedtke, T., Oehmigen, K., Brandenburg, R., Hoder, T., Wilke, C., Hähnel, M., & Weltmann, K.-D. (2012). Plasma-liquid interactions: chemistry and antimicrobial effects. In *Plasma for Bio-Decontamination, Medicine and Food Security* (pp. 67-78). Springer.
- Waghmare, R. B., & Annapure, U. S. (2017). Effects of hydrogen peroxide, modified atmosphere and their combination on quality of minimally processed cluster beans. *J Food Sci Technol*, *54*(11), 3658-3665. <https://doi.org/10.1007/s13197-017-2827-x>
- Wang, H., Feng, H., Liang, W., Luo, Y., & Malyarchuk, V. (2009). Effect of surface roughness on retention and removal of *Escherichia coli* O157:H7 on surfaces of selected fruits. *74*(1), 8-15. <https://doi.org/10.1111/j.1750-3841.2008.00998.x>

- Wellburn, A. R. (1994). The spectral determination of chlorophylls a and b, as well as total carotenoids, using various solvents with spectrophotometers of different resolution. *Journal of plant physiology*, *144*(3), 307-313.
- Wenske, S., Lackmann, J.-W., Busch, L. M., Bekeschus, S., von Woedtke, T., & Wende, K. (2021). Reactive species driven oxidative modifications of peptides—Tracing physical plasma liquid chemistry. *Journal of Applied Physics*, *129*(19), 193305.
- Wenzheng, L., & Chuanhui, L. (2014). Study on the generation characteristics of dielectric barrier discharge plasmas on water surface. *Plasma Science and Technology*, *16*(1), 26.
- Wibowo, S., Afuape, A. L., De Man, S., Bernaert, N., Van Droogenbroeck, B., Grauwet, T., . . . Technologies, E. (2019). Thermal processing of kale purée: The impact of process intensity and storage on different quality related aspects. *Innovative Food Science & Emerging Technologies*, *58*, 102213.
- Winter, J., Tresp, H., Hammer, M., Iseni, S., Kupsch, S., Schmidt-Bleker, A., . . . Weltmann, K. (2014). Tracking plasma generated H₂O₂ from gas into liquid phase and revealing its dominant impact on human skin cells. *Journal of Physics D: Applied Physics*, *47*(28), 285401.
- Wu, D., Tu, M., Wang, Z., Wu, C., Yu, C., Battino, M., . . . Du, M. (2020). Biological and conventional food processing modifications on food proteins: Structure, functionality, and bioactivity. *Biotechnology Advances*, *40*, 107491. <https://doi.org/10.1016/j.biotechadv.2019.107491>
- Wu, H., Sun, P., Feng, H., Zhou, H., Wang, R., Liang, Y., . . . Fang, J. (2012). Reactive oxygen species in a non-thermal plasma microjet and water system: generation, conversion, and contributions to bacteria inactivation—an analysis by electron spin resonance spectroscopy. *Plasma Processes and Polymers*, *9*(4), 417-424.
- Wu, S., Zhang, Q., Ma, R., Yu, S., Wang, K., Zhang, J., & Fang, J. (2017). Reactive radical-driven bacterial inactivation by hydrogen-peroxide-enhanced plasma-activated-water. *The European Physical Journal Special Topics*, *226*(13), 2887-2899. <https://doi.org/10.1140/epjst/e2016-60330-y>
- Xiang, Q., Fan, L., Li, Y., Dong, S., Li, K., & Bai, Y. (2020). A review on recent advances in plasma-activated water for food safety: current applications and future trends. *Crit Rev Food Sci Nutr*, *1-20*. <https://doi.org/10.1080/10408398.2020.1852173>
- Xiang, Q., Kang, C., Niu, L., Zhao, D., Li, K., & Bai, Y. (2018). Antibacterial activity and a membrane damage mechanism of plasma-activated water against *Pseudomonas deceptionensis* CM2. *LWT*, *96*, 395-401. <https://doi.org/10.1016/j.lwt.2018.05.059>
- Xiang, Q., Kang, C., Zhao, D., Niu, L., Liu, X., & Bai, Y. (2019a). Influence of organic matters on the inactivation efficacy of plasma-activated water against *E. coli* O157: H7 and *S. aureus*. *Food Control*, *99*, 28-33.
- Xiang, Q., Liu, X., Liu, S., Ma, Y., Xu, C., & Bai, Y. (2019b). Effect of plasma-activated water on microbial quality and physicochemical characteristics of mung bean sprouts. *Innovative Food Science & Emerging Technologies*, *52*, 49-56. <https://doi.org/10.1016/j.ifset.2018.11.012>
- Xu, D., Gu, S., Zhou, F., Hu, W., Feng, K., Chen, C., . . . Technology. (2021a). Mechanism underlying sodium isoascorbate inhibition of browning of fresh-cut mushroom (*Agaricus bisporus*). *Postharvest Biology and Technology*, *173*, 111357.
- Xu, L., Hou, H., Farkas, B., Keener, K. M., Garner, A. L., & Tao, B. (2021b). High voltage atmospheric cold plasma modification of bovine serum albumin. *LWT*, *149*, 111995. <https://doi.org/10.1016/j.lwt.2021.111995>

- Xu, R.-G., Chen, Z., Keidar, M., & Leng, Y. (2018). The impact of radicals in cold atmospheric plasma on the structural modification of gap junction: A reactive molecular dynamics study. *International journal of Smart Nano materials*, 10(2), 144-155
- Xu, Y., Tian, Y., Ma, R., Liu, Q., & Zhang, J. (2016). Effect of plasma activated water on the postharvest quality of button mushrooms, *Agaricus bisporus*. *Food Chemistry*, 197, 436-444. <https://doi.org/10.1016/j.foodchem.2015.10.144>
- Yamauchi, N. (2015). Postharvest chlorophyll degradation and oxidative stress. In *Abiotic stress biology in horticultural plants* (pp. 101-113). Springer.
- Yeats, T. H., & Rose, J. K. (2013). The formation and function of plant cuticles. *Plant Physiol*, 163(1), 5-20. <https://doi.org/10.1104/pp.113.222737>
- Yilmaz, C., & Gökmen, V. (2016). Chlorophyll. In B. Caballero, P. M. Finglas, & F. Toldrá (Eds.), *Encyclopedia of Food and Health* (pp. 37-41). Academic Press. <https://doi.org/10.1016/b978-0-12-384947-2.00147-1>
- Yong, H. I., Park, J., Kim, H. J., Jung, S., Park, S., Lee, H. J., . . . Jo, C. (2018). An innovative curing process with plasma-treated water for production of loin ham and for its quality and safety. *Plasma Processes and Polymers*, 15(2), 1700050.
- Yousuf, B., Deshi, V., Ozturk, B., & Siddiqui, M. W. (2020). 1 - Fresh-cut fruits and vegetables: Quality issues and safety concerns. In M. W. Siddiqui (Ed.), *Fresh-Cut Fruits and Vegetables* (pp. 1-15). Academic Press. <https://doi.org/10.1016/B978-0-12-816184-5.00001-X>
- Yusupov, M., Bogaerts, A., Huygh, S., Snoeckx, R., Van Duin, A. C., & Neyts, E. C. (2013a). Plasma-induced destruction of bacterial cell wall components: a reactive molecular dynamics simulation. *The Journal of Physical Chemistry C*, 117(11), 5993-5998.
- Yusupov, M., Neyts, E., Simon, P., Berdiyurov, G., Snoeckx, R., Van Duin, A., & Bogaerts, A. (2013b). Reactive molecular dynamics simulations of oxygen species in a liquid water layer of interest for plasma medicine. *Journal of Physics D: Applied Physics*, 47(2), 025205.
- Zeghioud, H., Nguyen-Tri, P., Khezami, L., Amrane, A., & Assadi, A. A. (2020). Review on discharge Plasma for water treatment: mechanism, reactor geometries, active species and combined processes. *Journal of Water Process Engineering*, 38, 101664.
- Zhang, Q., Liang, Y., Feng, H., Ma, R., Tian, Y., Zhang, J., & Fang, J. (2013). A study of oxidative stress induced by non-thermal plasma-activated water for bacterial damage. *Applied Physics Letters*, 102(20), 203701.
- Zhang, Q., Ma, R., Tian, Y., Su, B., Wang, K., Yu, S., . . . Fang, J. (2016). Sterilization efficiency of a novel electrochemical disinfectant against *Staphylococcus aureus*. *Environmental science & technology*, 50(6), 3184-3192. <https://doi.org/10.1021/acs.est.5b05108>
- Zhang, Q., Sun, P., Feng, H., Wang, R., Liang, Y., Zhu, W., . . . Fang, J. (2012). Assessment of the roles of various inactivation agents in an argon-based direct current atmospheric pressure cold plasma jet. *Journal of Applied Physics*, 111(12), 123305.
- Zhang, Y., Zhang, J., Zhang, Y., Hu, H., Luo, S., Zhang, L., . . . Li, P. (2021). Effects of in-package atmospheric cold plasma treatment on the qualitative, metabolic and microbial stability of fresh-cut pears. *J Sci Food Agric*, 101(11), 4473-4480. <https://doi.org/10.1002/jsfa.11085>
- Zhang, Z., Li, Y., Lee, M. C., Ravanfar, R., Padilla-Zakour, O. I., & Abbaspourrad, A. (2020). The Impact of High-Pressure Processing on the Structure and Sensory Properties of Egg White-Whey Protein Mixture at Acidic Conditions. *Food and Bioprocess Technology*, 13(2), 379-389.

- Zhao, D., Yu, F., Zhou, A., Ma, C., & Dai, B. (2018). High-efficiency removal of NO_x using dielectric barrier discharge nonthermal plasma with water as an outer electrode. *Plasma Science and Technology*, 20(1), 14020-014020.
- Zhao, Y.-M., Patange, A., Sun, D.-W., & Tiwari, B. (2020). Plasma-activated water: Physicochemical properties, microbial inactivation mechanisms, factors influencing antimicrobial effectiveness, and applications in the food industry. *Comprehensive reviews in food science and food safety* 19(6), 3951-3979. <https://doi.org/10.1111/1541-4337.12644>
- Zhao, Y., Chen, R., Liu, D., Wang, W., Niu, J., Xia, Y., . . . Song, Y. (2019). Effect of nonthermal plasma-activated water on quality and antioxidant activity of fresh-cut kiwifruit. *Ieee Transactions on Plasma Science*, 47(11), 4811-4817. <https://doi.org/10.1109/TPS.2019.2904298>
- Zhao, Z., Wang, X., & Ma, T. (2021). Properties of plasma-activated water with different activation time and its effects on the quality of button mushrooms (*Agaricus bisporus*). *LWT*, 147, 111633. <https://doi.org/10.1016/j.lwt.2021.111633>
- Zhou, R., Zhou, R., Prasad, K., Fang, Z., Speight, R., Bazaka, K., & Ostrikov, K. K. (2018). Cold atmospheric plasma activated water as a prospective disinfectant: the crucial role of peroxydinitrite. *Green Chemistry*, 20(23), 5276-5284.
- Zhou, R., Zhou, R., Wang, P., Xian, Y., Mai-Prochnow, A., Lu, X., . . . Bazaka, K. (2020). Plasma-activated water: generation, origin of reactive species and biological applications. *Journal of Physics D: Applied Physics*, 53(30), 303001.
- Zhou, R., Zhou, R., Zhang, X., Zhuang, J., Yang, S., Bazaka, K., & Ostrikov, K. (2016a). Effects of atmospheric-pressure N₂, He, air, and o₂ microplasmas on mung bean seed germination and seedling growth. *Scientific Reports*, 6, 32603. <https://doi.org/10.1038/srep32603>
- Zhou, R., Zhou, R., Zhuang, J., Zong, Z., Zhang, X., Liu, D., . . . Ostrikov, K. (2016b). Interaction of atmospheric-pressure air microplasmas with amino acids as fundamental processes in aqueous solution. *Plos One*, 11(5), e0155584.